DISSERTATION / DOCTORAL THESIS

Titel der Dissertation / Title of the Doctoral Thesis

„Investigation of the ternary Cu-Li-Sn system and its binary subsystems as new anode materials for improved lithium-ion batteries"

verfasst von / submitted by

Mag. Siegfried Fürtauer

angestrebter akademischer Grad / in partial fulfilment of the requirements for the degree of

Doktor der Naturwissenschaften (Dr. rer. nat.)

Wien, 2016 / Vienna, 2016

Acknowledgements

Table of Content

Curriculum Vitae et Studiorum

Name: Siegfried Fürtauer

D.O.B.:   Feb. 3rd, 1984, Wels

Citizenship: Austria

Home address: Sobieskigasse 32/20, 1090 Wien

Contact: s_fuertauer@hotmail.com

Education and career:

From 2015	High-school teacher at BRG 18 Schopenhauerstraße, Vienna
2014-2015	Teachers training (Unterrichtspraktikum) at BRG 18 Schopenhauerstraße, Vienna
2010-2016	PhD studies at the Department of Inorganic Chemistry / Materials Chemistry, Vienna
2009-2010	Diploma thesis at the Department of Inorganic Chemistry / Materials Chemistry, Vienna: Investigation of relevant phase diagrams for high temperature solder materials: The binary systems Cu-Sn and Cu-Sb
2004-2010	Master studies at the University of Vienna Courses: Teachers Profession in Physical Education (PE) Teachers Profession in Chemistry
2003-2004	Basic military service (military top sports centre Linz)
1998-2003	HTBLA in Wels, Upper Austria: College for Chemical Engineering
1994-1998	Junior high school in Lambach, Upper Austria

Preface

The here presented dissertation is written in a cumulative way, which means that several already published articles regarding the dissertation topic are shown in the results and discussion part of this work.

A comprehensive introduction enlightens the necessity of this research and involves cooperation partners and co-workers.

The second part summarizes all methods which have been applied and explains the nature of phase diagrams and their principles of construction to enable a better readability of the following original articles. Since every article has its own introduction and methodical part, some information may be repeated for a better understanding of the context.

The final conclusions condense the main findings of all individual publications and recapitulate improvements for the Cu-Li-Sn system, the binary phase diagrams and thermodynamic data.

1   Introduction

1.1   Why Cu-Li-Sn for lithium ion batteries?

Lithium ion batteries have already been employed successfully for a long time in handheld electronics, like laptops, cameras, mobile phones and many more. Most lithium ion batteries consist of a serial pack of single cells - each cell is constructed by anode, cathode, electrolyte and separator (see Figure 1, example of a common Li-ion battery type). In the charged state, lithium is intercalated in the graphitic anode (Li_XC_6, $x = 0$ - 1), the cathode consists of a transition metal oxide (*e.g.* CoO_2). The electrolyte is a lithium containing complex dissolved in an organic solvent, like $LiPF_6$ in ethyl carbonate or methyl ethyl carbonate. The separator is in many cases a microporous sheet of polyethylene or polypropylene [1]. During discharging, lithium from the electrolyte is incorporated into the crystal lattice of CoO_2 and forms Li_xCoO_2. Li^+ ions, which are accordingly released from the intercalated graphite, assure electroneutrality of $LiPF_6$. The negative graphite affords an electron per lost lithium ion, which finally can do work in an extern load. During charging the process is reversed. New electrodes,
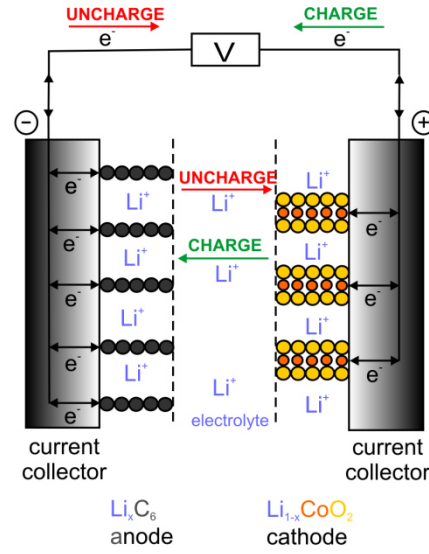
Figure 1: Scheme of common cell of a lithium ion battery
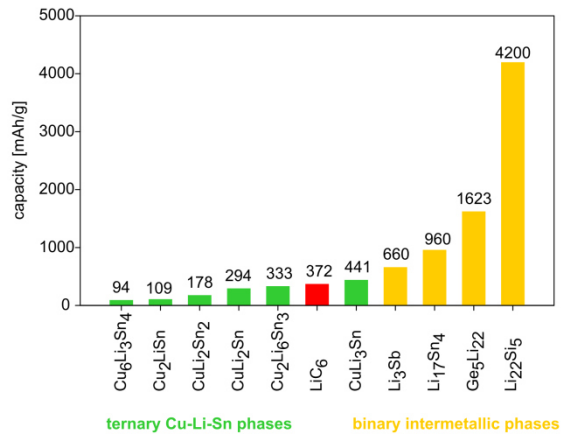
Figure 2: Gravimetric capacities of intermetallic compounds (mAh per gram lithium-free material)

which are able to uptake more lithium, having better cycling behaviour and a longer lifetime and are cheaper and safer than common used ones [2], are mandatory for high-power applications, such as electro mobility or stationary storage systems, *e.g.* for load levelling. Intermetallic anode materials are of special interest, because they benefit of a comparably high storage capacity for lithium. This is for example 960 mAh/g for $Li_{17}Sn_4$, which is the compound with the highest lithium content in the Li-Sn system, compared to 372 mAh/g for LiC_6, which is the maximum what can be obtained by common graphite anodes [3] (see also Figure 2). A main problem with intermetallic anodes, especially binary alloys, is the tremendous volume change during charging and discharging, respectively. This can be 200 vol-% and more and leads to electrode degradation, which results in a loss of electric contact between particles and finally causes a rapid capacity loss [4]. To overcome this problem it is necessary to increase the mechanical stability and reduce the volume expansion during charging, as well as the shrinkage during discharging. This could be achieved by adding materials which are inert against lithium and are able to buffer the volume changes. Another, more sophisticated approach is the application of electrode materials in which an inert phase is precipitated during lithiation. Ternary or higher ordered intermetallic systems whose components have very different compound forming tendencies with lithium are possible candidates. They consist of lithium, a main group metal like Sn or Sb and a transition metal, like Cu, Ni or Co. In the charged state, the anode represents a lithium-rich binary or ternary compound and encapsulates crystals of another phase, *e.g.* the transition metals Cu, Co or Ni, which act as stabilizing matrix. The latter three elements don't form Li-compounds at all. During discharging, pure lithium intercalates into the cathode and a stable binary transition metal compound with Sn or Sb (*e.g.* Cu_6Sn_5, Ni_3Sn_4 or Co_3Sn), or alternatively a ternary compound with low lithium content is formed. Hereby, the ternary system Cu-Li-Sn is of special interest and many investigations of the electrochemical performance of the respective anodes and the lithiation mechanism [5-8] have been performed in the recent years. However, very limited phase diagram and thermodynamic information is available in literature. For a systematic research on such electrode materials these data are indispensable and are topic of the present research work.

1.2 Framework and cooperation

The present work was funded by the FWF-project "Experimental Thermodynamics and Phase Relations of New Electrode Materials for Lithium Ion Batteries" with the project number I559-N19, which is part of the DFG Priority Program SPP 1473 "WeNDeLIB" [9]. This joint project was launched by ao. Univ.-Prof. Dr. Hans Flandorfer, my supervisor, together with two other cooperation partners, Dr. Damian Cupid from KIT Karlsruhe and Prof. Dr.-Ing. Torsten Markus from HS Mannheim, before FZ Jülich. Their respective co-workers were Dr. Dajian Li (KIT Karlsruhe) and Dr. David Henriques (FZ Jülich). Participants of each working group use their expertise to treat the topics of the joint project from different views. The Vienna group is expert in sample preparation, characterisation with XRD and DTA methods and thermochemical methods like *e.g.*, calorimetry. From XRD and DTA data, experimental phase diagrams could be designed. Determined calorimetric data are enthalpies of mixing and formation. The Jülich group offers knowledge in vapour pressure measurements with Knudsen Effusion Mass Spectrometry (KEMS); the direct outputs of this method are activities, which could be used to determine other thermodynamic quantities and finally contribute to Gibbs energy descriptions of intermetallic phases. The KIT group has the expertise to calculate phase diagrams from thermodynamic data, which have been obtained in all three groups. These calculations can be optimized based on literature data and our experimental phase diagrams within the CALPHAD approach [10]. The combination of different expertise in the framework of this cooperation resulted in a conclusive description of interesting material systems, like binary Cu-Sn, Cu-Li and Li-Sn, or ternary Cu-Li-Sn. These data will be summarized in a material data base, similar to that one provided by MSIT [11], and used as a kind of material map for metallurgists and developers of lithium ion batteries.

The very close cooperation with ao. Univ.-Prof. Dr. Herta Effenberger from the Institute of Mineralogy and Crystallography (University of Vienna) has to be mentioned as well here. She performed single crystal XRD measurements and structure refinements which were the basis for the crystallographic description of various ternary phases in the Cu-Li-Sn system.

2   Methods

2.1 Phase diagram work

2.1.1   Sample preparation

Lithium containing intermetallic samples were prepared from pure elements: Cu (99.98 at.%, wire, Goodfellow, Cambridge, UK), Li (99.8 at.%, wire, Alfa Aesar, Karlsruhe, Germany) and Sn (99.95 at.%, ingot, Advent, Oxford, UK). The Cu wire was treated in a H_2-flow (5 hours, 300°C) to remove the oxide layer at the surface before use. The Li wire was stored originally in mineral oil for prevention of oxidation. This coating was removed by n- or cyclohexane in a supersonic bath followed by vacuum evaporation of the solvent. Dark coloured oxidation spots at the surface which occurred during that treatment were removed mechanically with a knife. The metals were stoichiometrically weighed together in thimble-like tantalum crucibles inside a glove box under Ar atmosphere (< 5 ppm O_2 / H_2O). The cylindrical Ta crucibles were made by deep-drawing of a 0.4 mm Ta sheet and had approximately dimensions of 10 mm diameter and 12-14 mm height. Corresponding lids were also prepared by deep drawing. Before use, the Ta crucibles were stored for approximately 30 sec in a highly oxidative acid bath (concentrated acids HF: HNO_3: H_2SO_4 = 1:3:6) to remove the passivizing tantalum oxide layer and finally cleaned with water and acetone. The crucibles were welded in Ar atmosphere; an arc furnace with a tungsten electrode of 1.6 mm was used. During the welding process, the crucibles were chilled by a water cooled copper mount. For melting, the crucibles were heated in an induction furnace at 1100 °C, but only 10 - 20 sec each to prevent high temperature fatigue of the welding seam. The temperature was continuously monitored by an infrared pyrometer. Repetition of the melting process twice with turning the crucible upside down between the heating steps assured homogenous mixing of the liquid alloys. Then the crucibles were sealed in quartz glass tubes under vacuum. All alloys were heat treated consequently in a muffle furnace at 400 °C, but most samples additionally at different temperatures (200, 300, 500, 600, 650, 700 and 750 °C) for several days, weeks or even months (but usually 2 - 4 weeks, depending on the annealing temperature and lithium activity). This annealing process is mandatory to assure thermodynamic equilibrium in the alloys, since they should represent an equilibrium phase diagram. Rapid cooling (quenching) quickly reduces the diffusion rate, which is temperature dependent,

significantly. This is used to "freeze" the equilibrium state of a certain annealing temperature and enables an investigation of these phase relations at ambient temperature. Especially at high temperatures (> 500 °C) and for samples with high lithium content, the tantalum sheet became partially permeable for Li vapour. This was evidenced by a darkening of the surrounding quartz glass, which indicated a reduction of transparent SiO_2 to brown SiO or related lithium containing silicates.

2.1.2   XRD

The phase relations of the samples were characterized with powder XRD. Crucibles were opened with a bolt cutter in the glovebox and a part of each sample was grinded with a tungsten carbide mortar (Durit®). Powder XRD measurements were performed with two different techniques, either with a Bragg-Brentano diffractometer ($\theta/2\theta$-geometry, Bruker AXS) or with the image plate technique (Guinier Camera, Huber). For measurements with the Bragg-Brentano technique, the powder was fixed with petroleum jelly on a flat and disc-shaped sample holder (silicon monocrystal), which rotated during the measurement. Maintaining the protecting gas atmosphere was achieved by an X-ray amorphous cap (polycarbonate) covering the sample. The diffractometer operated with a Cu-radiation source (40 kV/40 mA) and a nickel filter. Diffracted X-ray beams were detected with a strip detector (Lynxeye), which moved with the double angular speed (2θ) along the goniometric circle as the sample was tilted (θ). The Guinier camera, on the other hand, operated with sample holders, in which the powder was fixed with petroleum jelly between two Kapton® foils. The foils were tightened with a metal frame, which oscillated slightly during the measurement. X-Rays were also produced by a copper tube (40 kV/30 mA), but with a monochromator which provides $CuK_{\alpha 1}$ radiation. The diffracted X-rays were simultaneously detected for all angles with an image plate. Obtained patterns from both techniques were evaluated by Full Profile Rietveld-refinements using Topas3® [12] software. By fitting the measured diffraction pattern with calculated patterns of expected phases (structure data from literature and single crystal XRD) an identification of the individual phases of each sample was possible.

The diffraction pattern of several samples showed additional peaks, which could not be explained by literature data. In these cases single crystal XRD was executed, which allowed a crystallographic description of unknown phases. It was necessary to obtain single crystals which have no defects, no crystal intergrowth and a reasonable size (~ 50 – 100 µm in diameter). These single crystals were prepared by fixing small amounts of gritty bulk sample with petroleum jelly between two object plates in the glove box. Slightly pushing and sliding of the object plates crushed the bulk samples into smaller particles and covered them entirely with the grease. Then appropriate crystals under jelly were picked up outside of the glovebox under a binocular microscope (up to 400 fold magnification) with fine acupuncture needles and fixed onto a glass capillary again captured with grease. Single-crystal XRD was performed at 290 K with a four-circle Nonius Kappa diffractometer equipped with a CCD detector, a 300 µm capillary optics collimator and a nitrogen-gas cryostream cooler (OXFORD CryoSystems). Monochromated MoKα radiation was used (graphite monochromator). The continuous stream of dried nitrogen gas enclosed the single-crystals during the measurement; this protected it from both corroding and movement and controlled the isothermal conditions. The unit-cell parameters were obtained by least-squares refinements of the 2θ-values from all collected intensity data. Corrections for Lorentz, polarization and absorption effects (multi-scan method) were applied. Complex scattering functions of Wilson [13] were used for all calculations. For data collection, structure solution and refinements the programs "COLLECT" [14, 15], "SHELXS-97" and "SHELXL-97" [16-18] were used. The crystal structures were displayed by the software "ATOMS" [19].

2.1.3   DTA

Approximately 100-150 mg of sample material, which was annealed at 400 °C, was filled in tantalum crucibles whose bottoms were flattened previously with a hydraulic press. The crucibles were closed with a corresponding lid and welded with an electric arc in an arc furnace. Analysis instrument was a single-point DTA, equipped with small alumina discs put over the welding beads of the S-type thermocouples serving as a base for the crucibles. Reference material was a comparable amount of alumina (NIST standard sapphire) in a second tantalum crucible. By heating both crucibles in a tubular furnace up to a temperature above melting, the sample undergoes usually several phase transitions (at each reaction temperature and at the liquidus temperature). The heat consumption of the sample is compared electronically to that one of the reference – the difference signal is recorded as temperature dependent peak. The furnace program for the measurements was usually as follows: Fast heating to annealing temperature (20 °C / min, usually up to 400 °C) - equilibration for 30 min - heating with 5 °C / min slightly above the estimated liquidus temperature (< 900 °C to prevent leakage of the crucibles) – cooling with 5 °C / min to 100 °C – second heating with 5 °C / min to estimated liquidus temperature – cooling with 5 °C / min to room temperature (see Figure 3).

Temperature calibration was done with pure metals, such as Sn, Ag and Au. Peaks were evaluated with the Netzsch Proteus® software [20], overlapping peaks have been separated by the peak deconvolution tool in the Calisto® software package from Setaram [21]. Peak onsets were identified as thermal effects which occur

Figure 3: Temperature program of DTA analysis

during an invariant phase transformation or at the solidus line – the maximum of the corresponding peak indicates the liquidus temperature.

2.1.4   Construction of a phase diagram

This chapter constitutes a short lecture about how to construct and read phase diagrams. Detailed information about phase diagrams could be found in [22, 23]. A phase diagram is a kind of map of equilibrium states of a chemical system, dependent on temperature, composition and pressure. The Gibbs phase rule at constant pressure

(1) $F' = C - P + 1$

defines the degree of freedom (F') based on the number of phases (P) and the number of components (1 = unary, 2 = binary, 3 = ternary,…). If applied to a binary phase diagram (C = 2), the degree of freedom for a single phase field (P = 1) is 2 (means, that temperature and concentration could vary independently); in a two-phase field P = 2, therefore F' is only 1 (means, that if temperature will be changed, also the concentration of components in phase A or B would change); see also Table 1.

F' = 0 will be reached for three-phase equilibria, which does not allow any change of concentrations of the three equilibrium phases nor a change in temperature. Thus such an equilibrium state is identified as invariant. In binary systems reactions of eutectic and peritectic type could occur. Reactions are usually written as cooling reactions; therefore a eutectic reaction is

	Binary C = 2			Ternary C = 3			
P	1	2	3	1	2	3	4
F'	2	1	0	3	2	1	0

Table 1: Gibbs' phase rule

(2)   Liquid $\rightarrow \alpha + \beta$
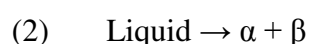
and a peritectic reaction is

(3)   Liquid $+ \alpha \rightarrow \beta$
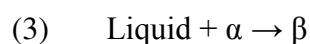
Depending on the involved phases these two types could be classified in three main reactions each (see also Table 2).

eutectic type		peritectic type	
eutectic	Liq. → α + β	peritectic	Liq. + α → β
eutectoid	γ → α + β	peritectoid	α + γ → β
monotectic	Liq. I → α + Liq. II	syntectic	Liq. I + Liq. II → α

Table 2: Eutectic and peritectic reactions

E (type I)	1 → 2 + 3 + 4
U (type II)	1 + 2 → 3 + 4
P (type III)	1 + 2 + 3 → 4

Table 3: Ternary reaction types

For the ternary system is C = 3 and therefore invariant four-phase equilibria can exist at constant temperature and equilibrium phase concentrations. Three-phase equilibria can be found in triangular three-phase spaces, which could be sectioned and visualized as invariant isothermal phase triangles. Two-phase equilibria are three-dimensional spaces which are crossed by isothermal tie-lines and single phase equilibria are irregular spaces with three degrees of freedom (2 compositions + temperature).Ternary reactions could be classified in type E (I), type U (II) and type P (III). Type E has the character of a ternary eutectic and P that one of a ternary peritectic reaction, U is a so-called transformation reaction (*German*: "Umwandlung"); see also Table 3. The isothermal four-phase equilibrium plane of E- and P-type reactions is triangular, that one of the U-type reaction is an irregular rectangle (see Figure 4). A ternary phase diagram with constant *p* and variable *x* and *T* is an equilateral triangular prism. Each of the three sides of the triangle represent the connection to a binary subsystem. The temperature axis is in vertical direction of the prism. It is inappropriate to illustrate such a phase diagram as three-dimensional drawing. Therefore different possibilities of visualization are i) sections at constant temperature (isothermal sections, triangular shape); ii) sections at a constant composition or composition ratio (isopleths, rectangular shape); iii) projection of the liquidus plane along the temperature axis (results in a triangular map of temperature-dependent hypsometric layers). Isothermal sections could be constructed, if phase relations of annealed samples at a certain temperature are known. If the samples contain one, two or three phases, they are allocated to single-, two- or three-phase equilibria. Construction rules are i) no line of any three-phase equilibrium (phase triangle) must intersect another line; ii) three-phase fields are separated by two-phase fields, apices of

Figure 4: Reaction isotherms of four-phase equilibria in ternary systems
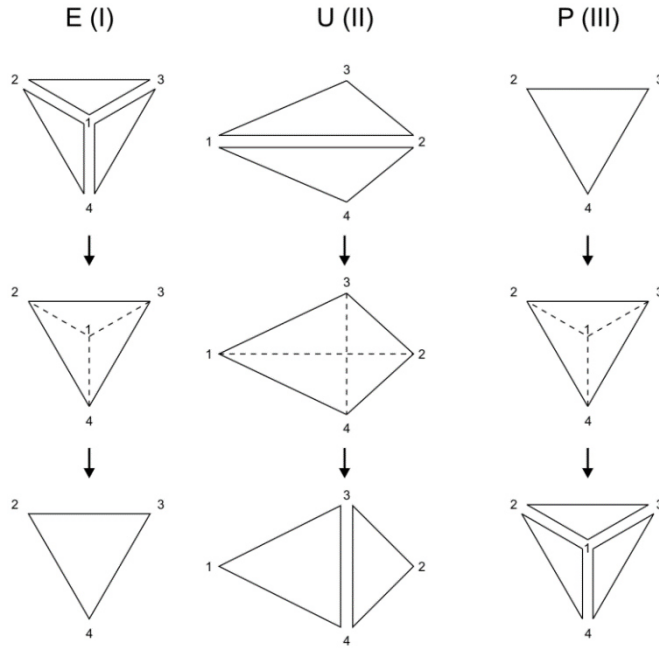
three-phase fields are connected with single-phase fields in one point; iii) extrapolations of the boundaries of the single-phase field (monovariant lines) must fall either both in the adjacent three-phase field or one inside each of the two two-phase fields (Schreinemaker's rule). Usually the positions of the apices of Gibbs triangles are determined by measuring the atomic composition of corresponding single phases in an annealed and quenched sample with three phases in equilibrium, *e.g.* by phase selective spectroscopic methods like SEM-EDX. In samples with two phases in equilibrium the determination of compositions of each phase leads to the isothermal tie-lines in the binary phase fields. Unfortunately, SEM-EDX is no direct quantification method for lithium, because its spectral intensity of X-ray emission is too low. An indirect determination of the lithium concentration from the sum of the concentration of the other elements is highly inaccurate. Therefore Gibbs triangulations shown in this work are estimated from powder-XRD phase analysis of a comparably large number of samples, but apex positions are probably not always exactly expressed.

Based on the constructed isothermal sections, isopleths could be expressed for constant concentration ratios ($x_A : x_B$ = const.) or at fixed concentration of a single component (x_A = const.). Data from thermal analysis are mandatory to determine reaction temperatures. Vicinal samples, which show heat effects at the same temperature, indicate an isothermal ternary reaction (E-, U- or P-type). Further thermal effects explain non-invariant reactions, like phase transitions from single- into two-phase regions or from two- into three-phase regions and *vice versa*. It has to be mentioned, that adjacent phase fields must

be related in terms of occurring phases. The rule for construction of adjacent phase fields was defined by Landau and Palatnik [24]:

(4) $r_1 (\geq 0) = r - d^- - d^+$

(r_1…dimension of boundary between adjacent phase fields; single point = 0, line = 1

r…dimension of plot: two-dimensional = 2 for isopleths or isotherms

d^-…number of disappearing phases

d^+…number of added phases)

 An example should clarify this rule: A ternary isopleth has adjacent phase fields "Liq." and "Liq. + α". The phase α is formally added (1), therefore the phase fields are connected by a monovariant line (1) because $1 = 2 - 0 - 1$. A second example is the transition from phase field "Liq." to "Liq. + α + β". Here phases α and β are formally added (2), therefore both phase fields are connected only by a single point ($0 = 2 - 0 - 2$). The extension of all phase fields in an isopleth has to be identical for the corresponding concentrations in a respective isothermal section. In many cases, narrow or small phase fields have to be assumed in order to be able to draw a consistent isopleth. The liquidus surface could be depicted in a projection and has to correspond with the experimental liquidus
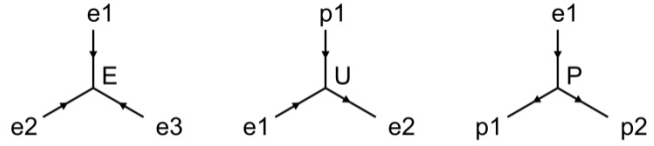
Figure 5: Examples of conjunctions in the liquidus projection (e, p = from binary eutectic, peritectic)

temperatures. Temperature dependent lines (monovariant lines), which are projected grooves, separate primary crystallization fields (projection of "Liq. + crystallizing phase"). Invariant reactions including the liquid phase are shown as conjunctions of always three of such lines. Depending if these lines run towards lower or higher temperatures (respectively towards or off the reaction point), what is indicated by arrows, corresponding ternary reactions as E-, U- and P-type can be distinguished (see Figure 5). With microscopic methods the solidification sequence of identified phases could be found and fields of primary crystallization could be estimated. For Cu-Li-Sn alloys, which are highly sensitive against oxygen and water it was not appropriate to manufacture plain and polished samples which could be used for microscopy. Therefore a consistent liquidus projection was assumed based on the isopleths and additional liquidus temperatures. Possible inaccuracy as a result of this estimation has to be admitted.

2.2   Calorimetry

Calorimetry is an excellent method to determine and quantify heat effects, like enthalpies of solution, formation, phase transition etc. It can be distinguished between isothermal (no temperature difference between calorimeter and surrounding), adiabatic (no heat flow between calorimeter and surrounding) and isoperibolic calorimetry (constant temperature of surrounding, variable temperature of calorimeter). For this work an isoperibolic calorimeter of Tian-Calvet type was used (see Figure 6). One thermopile surrounds the cell where the measurement takes place, the other one the inert reference cell.
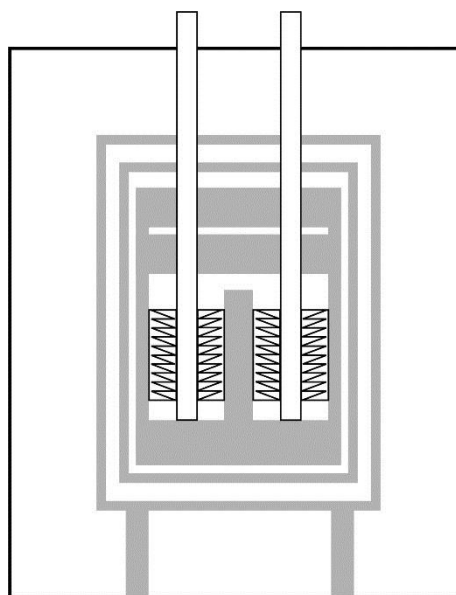
Figure 6: Scheme of a Tian-Calvet calorimeter

Here the voltage between the two identically constructed thermopiles was directly measured and corresponds to a temperature difference between the two cells. Each thermopile is composed of 230 S-type thermocouples (Pt / Pt-10%-Rh) in series which allows a temperature resolution of 10^{-4} K. Both thermopiles are housed in ceramic tubes and fixed on a block of heat resistant Inconel® alloy. The surrounding furnace is optimized to maintain constant temperature. Small variations are compensated using the reference cell. If heat is evolved or consumed in the measurement cell a temperature difference to the surrounding and at the same time to the reference cell occurs which can be detected as a voltage signal. The corresponding heat flow between the measurement cell and its surrounding is proportional to the temperature difference between the two cells and therefore proportional to the thermoelectric voltage:

(5) $\dot{Q} = \frac{Q}{t} = \Delta T \cdot c = \frac{\Delta V}{S} \cdot c$

$\dot{Q}$...heat flow [J / s] Q...heat [J] t...time [s]

ΔT...Temperature difference between measurement and reference cell [K or °C]

c...proportionality factor between temperature and heat flow [J / Ks]

ΔU...thermoelectric voltage between measurement and reference cell [V]

S... proportionality factor (Seebeck coefficient) between temperature and thermoelectric
     voltage [V/K or V/°C]

The measurements were usually performed at several hundred degrees Celsius; therefore Ar as inert gas was necessary to protect the metals from oxidation. To avoid overpressure a constant flow of Ar in an open system was maintained. Via an autosampler up to 30 samples could be dropped in sequence into a crucible, which was surrounded by a quartz glass tube and located at the bottom of the measurement cell. It was usually made of Mo or boron nitride and contained a metal melt, depending on the kind of measurement. Solid metal samples were dropped into the melt – the thermoelectric voltage between the two calorimeter cells was recorded in dependency of time. After the reaction, usually after 10 – 30 min, the thermoelectric voltage returned to the initial value (base line). Measured peaks were integrated mathematically (HiQ software from National Instruments) – their integration result has the unit $V \cdot s$ and is proportional to the heat exchange Q. Pieces of NIST sapphire (National Institute of Standards and Technology) with very well-known heat capacity were dropped for calibration (last 5 – 6 drops) and enabled a calculation of the proportionality factor c_{cal} (= "calorimeter constant"). The heat capacity of NIST sapphire could be calculated according to a temperature dependent polynomial. Thermodynamic quantities for pure elements are also formulated as temperature dependent polynomials, so-called Dinsdale polynomials [25]. For enthalpies they have the format

(6) $H = a - c \cdot T - \sum(n - 1) \cdot d \cdot T^n$

The parameters a, c, d and n are tabulated numbers; T is the temperature in K.

The calorimeter constant c_{cal} [J / Vs] could be calculated as follows:

$$(7) \qquad c_{cal} = \frac{m_{cal}}{M_{cal}} \cdot \frac{H(T_f) - H(T_d)}{A_{cal}}$$

m_{cal}….mass of dropped calibration material (*e.g.* NIST sapphire) [g]

M_{cal}….molar mass of calibration material [g / mol]

A_{cal}…integrated area of measured peak for calibration drop [V s]

$H(T_f) - H(T_d)$…difference of Dinsdale polynomial at furnace temperature (T_f) and

Dinsdale polynomial at drop temperature (T_d); [J / mol]

For each drop the occurred enthalpy $\Delta H_{i;signal}$ dropping substance *i* could be determined:

$$(8) \qquad \Delta H_{i;signal} = \frac{c_{cal} \cdot A_i}{n_i}$$

A_i…. integrated area of measured peak for sample [V s]

n_i….molar amount of sample [mol]

2.2.1   Mixing enthalpy

Mixing enthalpy (*syn.* excess enthalpy) is determined by dropping metal i into melt of metal j. The measured heat effect is the sum of mixing enthalpy and heat increments, which correspond to heating and liquefying the dropped material:

(9) $\Delta H_{ij,signal} = n_i \cdot \left(H_{i(l),f} - H_{i(s),d} \right) + \Delta H_{ij,reaction}$

$H_{i(l),f}$…Enhalpy of drop at furnace temperature (from Dinsdale polynomial) [J / mol]

$H_{i(s),d}$…Enhalpy of drop at dropping temperature (from Dinsdale polynomial) [J / mol]

$\Delta H_{ij,reaction}$…Excess heat of drop [J]

Approximate partial molar enthalpies of mixing were calculated for very small amounts of dropped sample

(10) $\Delta_{mix}\bar{H}_{i,j} \approx \frac{\Delta H_{ij,reaction}}{n_i}$

Extrapolating the graph $\Delta_{mix}\bar{H}_{ij} = f(n_i)$, which is usually nearly linear, to $n_i = 0$, the intercept at the ordinate gives the limiting partial molar enthalpy of mixing $\Delta_{mix}\bar{H}_{ij}^{\infty}$, which could be imagined as the partial molar mixing enthalpy at infinite dilution.

For integral molar mixing enthalpies also the molar amount of the solvent j and the preceding drops i have to be considered:

(11) $\Delta_{mix}H_{ij} = \frac{\sum_{ij} \Delta H_{ij,reaction}}{n_j + \sum_i n_i}$

2.2.2   Formation enthalpy

The molar enthalpy of formation $H_{f,AxBy}^{Td}$ of a compound A_xB_y ($x + y = 1$) at dropping temperature T_d could be determined from the limiting partial molar enthalpy of solution of A in solvent C ($\Delta_{sol}\bar{H}_A^{\infty}$), the limiting partial molar enthalpy of solution of B in solvent C ($\Delta_{sol}\bar{H}_B^{\infty}$) and the limiting partial molar enthalpy of solution of A_xB_y in solvent C ($\Delta_{sol}\bar{H}_{AxBy}^{\infty}$). The enthalpy of solution of a substance in a solvent is identical with the measured enthalpy $\Delta H_{ij;signal}$. Therefore is the limiting partial enthalpy of solution the ordinate intercept of the extrapolation of $\Delta H_{ij;signal} = f(n_i)$ to $n_i = 0$. Following the rule of Hess, the formation enthalpy of A_xB_y at dropping temperature T_d is:

(12) $H_{f,AxBy}^{Td} = x \cdot \Delta_{sol}\bar{H}_A^{\infty} + y \cdot \Delta_{sol}\bar{H}_B^{\infty} - \Delta_{sol}\bar{H}_{AxBy}^{\infty}$

This method works only if the drops are very small and the final concentrations of A or B in C do not exceed a few at.%.

3   Results and Discussion

The quintessence of this thesis persists of 6 scientific publications in well reputed and peer reviewed journals which contribute to the Cu-Li-Sn ternary system and its binary subsystems (Cu-Sn, Cu-Li and Li-Sn).

Table 4Table 4 shows articles, which have already been accepted and published by peer-reviewed journals or are in the review state (grey shadowed). The candidate is first author of all these publications. Table 5 lists further published works of the candidate which are related to phase diagrams or thermodynamics, but are either of minor importance for materials for improved lithium ion batteries, not part of the Cu-Li-Sn system or not mainly the output of the author. The latter came off from cooperation with partners and involved the author only in a little extent. Publications in Table 5 are not discussed in this thesis.

Works in Table 4 and Table 5 are ordered by publication date. Publication #1 describes mixing enthalpies of the Cu-Li, Li-Sn and Cu-Li-Sn system; they were determined by drop calorimetry at 500 and 800 °C. Binary mixing enthalpies were extrapolated with the Chou-model [26, 27] and compared with experimental ternary data. Further thermodynamic properties, namely activities and derived thermodynamics, were published in cooperation with the group in Jülich (#12). They measured KEMS data on samples which have been prepared by the candidate. Three publications, considering the structural characterization of ternary phases in Cu-Li-Sn, were written in cooperation with Prof. Effenberger (Institute of Mineralogy and Crystallography, University of Vienna): #2 (phases T1 & T2), #3 (phases T3 & T4) and #4 (phases T5 & T6). Prepared and characterized samples which contained those phases were selected and respective single crystals were depicted and measured with SC-XRD (program "COLLECT" [14, 15]). Data sets were refined by Prof. Effenberger (programs "SHELXS-97" and "SHELXL-97" [16-18]), structural discussion, relationships to other phases and publication work were the candidate's contribution. Publication #9 is an experimental work in the Cu-Sn system with the question whether the high-temperature phases β and γ, which are not quenchable, are connected by a two-phase field (this would indicate a first-order transition) or not (higher order transition). This problem was treated by means of HT-PXRD, P-XRD and DTA and was base for a succeeding publication where our cooperation partners from KIT Karlsruhe (#10), provided a new thermodynamic description of the phase diagram by the CALPHAD approach [10]. Publication #11 is an assessment of the Li-Sn system. Experimental data, like P-XRD, DTA and enthalpy of

formation measured by calorimetry from our group, are part of an assessment and a thermodynamic optimization (CALPHAD approach) which was performed by the group of KIT Karlsruhe.

Another assessment done by KIT Karlsruhe (#16) describes binary Cu-Li and the liquidus in the ternary Cu-Li-Sn system. Binary data are supported by a few experimental data (P-XRD, DTA), provided from our group. Two successive works contribute to the experimental Cu-Li-Sn phase diagram. Publication #5 shows four isothermal sections from 300 – 600 °C, publication #6 provides nine isopleths, a liquidus projection and recapitulates the Cu-Li-Sn phase diagram by means of a Scheil reaction scheme. These two articles are the key works for the present thesis. Publication #17 is another cooperation paper of KEMS technique with FZ Jülich, recently HS Mannheim. They performed KEMS measurements in Cu-Li-Sn for which our ternary samples and phase diagram knowledge contributed.

Table 4: Articles which are cumulated to this thesis

No.	Co-Authors	Author-ship	Year	Journal	Systems	Methods	Contribution of the candidate	
							%	activity
1	Tse, Yak, Fla	1	2013	JCT	Li-Sn, Cu-Li, Cu-Li-Sn	Calorimetry	80	Calorimentric measurements, supervision, modelling, writing
2	Eff, Fla	1	2014	JSSC	Cu-Li-Sn	SC-XRD, P-XRD	70	Sample preparation, measurement, structural comparison, writing
3	Eff, Fla	1	2015	ZKrist	Cu-Li-Sn	SC-XRD, P-XRD	70	
4	Eff, Fla	1	2015	ZKrist	Cu-Li-Sn	SC-XRD, P-XRD	70	
5	Fla	1	2016	JALCOM	Cu-Li-Sn	P-XRD	90	Sample preparation + characterization, interpretation, phase diagram development, publication
6	Fla	1	2016	Plos One	Cu-Li-Sn	P-XRD, DTA	90	

No.	Co-Authors	Authorship	Year	Journal	Systems	Methods	Contribution of the candidate	
							%	activity
7	Elm, Sab, Fla	2	2012	TA	Ni-Sb-Sn	Calorimetry	10	Measurements, publication
8	Fla	1	2012	MHC	Cu-Sb	P-XRD, DTA, SEM-EDX	80	All experiments, interpretation, publication
9	Li, Cup, Fla	1	2013	Intermet.	Cu-Sn	HT) P-XRD, DTA, SEM-EDX)	80	Sample preparation, analysis and evaluation, writing
10	Li, Fra, Cup, Fla	3	2013	Intermet.	Cu-Sn	Assessment, Optimization	10	publication
11	Li, Fla, Cup	2	2014	CALPHAD	Li-Sn	P-XRD, DTA, calorimetry, assessment, optimization	40	Literature assessment, optimization, phase diagram calculation, writing
12	Hen, Mot, Ben, Mar	4	2014	JALCOM	Li-Sn	KEMS, P-XRD	30	Sample preparation, P-XRD, publication
13	Ple, Yak, Ips, Fla	3	2014	JPED	Ni-Sn-Zn	Calorimetry	5	Assistance for measurements
14	Yak, Elm, Ips, Fla	2	2014	JCT	Co-Sn	Calorimetry	5	Assistance for measurements, publication
15	Yak, Fla, Ips	2	2014	MHC	Co-Li-Sn	Calorimetry	10	Assistance for measurements, publication
16	Li, Fla, Cup	2	2016	CALPHAD	Cu-Li, Cu-Li-Sn	P-XRD, DTA, assessment, optimization	20	Sample preparation, characterization, publication
17	Hen, Mot, Ben, Fla, Mar	4	2016	JALCOM	Cu-Li-Sn	KEMS	20	Sample preparation, publication

3.1   Publication #1

Calorimetric studies of Cu-Li, Li-Sn and Cu-Li-Sn

Siegfried Fürtauer[a], Erdenebat Tserenjav[b], Andriy Yakymovych[a], Hans Flandorfer[a]

[a] Department of Inorganic Chemistry / Materials Chemistry, University of Vienna, Währingerstraße 42, 1090 Vienna, Austria

[b] Centre of Chemistry and Technology for New Materials, National University of Mongolia, P.O. Box 217, University Street, 14201 Ulaanbaatar, Mongolia

Contributions to this paper:

S. Fürtauer:	Calorimentric measurements, supervision, modelling, writing
E. Tserenjav	Calorimentric measurements
A. Yakymovych:	Calorimentric measurements
H. Flandorfer:	General advice and helpful comments, proofreading

Overall contributions of S. Fürtauer to the paper: 80%

Abstract

Integral molar enthalpies of mixing were determined by drop calorimetry for Cu-Li-Sn at 1073 K along five sections $x_{Cu}/x_{Sn} \approx 1{:}1$, $x_{Cu}/x_{Sn} \approx 2{:}3$, $x_{Cu}/x_{Sn} \approx 1{:}4$, $x_{Li}/x_{Sn} \approx 1{:}1$, and $x_{Li}/x_{Sn} \approx 1{:}4$. The integral and partial molar mixing enthalpies of Cu-Li and Li-Sn were measured at the same temperature, for Li-Sn in addition at 773 K. All binary data could be described by Redlich-Kister-polynomials. Cu-Li shows an endothermic mixing effect with a maximum in the integral molar mixing enthalpy of ~5300 J/mol at $x_{Cu} = 0.5$, Li-Sn an exothermic minimum of ~ -37000 J/mol at $x_{Sn} \sim 0.2$. For Li-Sn no significant temperature dependence between 773 K and 1073 K could be deduced. Our measured ternary data were fitted on the basis of an extended Redlich–Kister–Muggianu model for substitutional solutions. Additionally, a comparison of these results to the extrapolation model of Chou is given.

Introduction

The generation of basic kinetic and thermodynamic data of material systems, which could be relevant for the design of new lithium ion batteries, is forced by the DFG priority program 1473 "WeNDeLIB". Within this priority program several joint projects with different experimental and theoretical approaches exist, one of these projects targets on the thermodynamic description of intermetallic anode materials. Such systems, which are able to reversibly uptake lithium, are in discussion as an alternative to the commonly used carbon anodes. Multiphase ternary alloys with selective activity of a certain phase towards lithium exchange promise to overcome the well-known problem of electrode destruction due to large volume changes in the cycling process. The idea is to have a phase with a high lithium activity with the ability to release lithium ions during discharging. Additionally, during discharging a second phase, which acts as a stabilizing matrix, should be formed. This stabilizing phase buffers the destructive volume changes. One promising candidate is the system Cu-Li-Sn, where $Li_{17}Sn_4$ should be the active phase and copper or Cu-Sn-phases form the stabilizing matrix. The challenging experimental handling of lithium and its alloys caused a scarce knowledge of the thermodynamics of these systems, especially of the ternaries. In the scope of a tailored design of new materials for lithium ion batteries, these thermodynamic data are indispensable. Thermodynamic data, *e.g.* molar enthalpies of mixing, are necessary to model ternary and higher ordered phase diagrams with the CALPHAD method and to predict phase relations and thermodynamic properties. This work provides thermodynamic data of the liquid

range, which is another important puzzle piece to fully understand the Cu-Li-Sn phase diagram.

Literature review

Cu-Sn

The determination of thermodynamic data like molar enthalpies of mixing and formation for the Cu-Sn system has started in the middle of the 20th century by several authors (Kawakami [1], Ticknor and Bever [2], Cohen et al. [3] and Kleppa [4; 5]). A critical assessment of thermodynamic data of the Cu-Sn system was first published by Hultgren [6]. Further calorimetric measurements on liquid alloys were done by Itagaki, Yazawa et al. [7; 8], Pool et al. [9] and Lee et al. [10]. The integral molar mixing enthalpies in these works have been measured in the temperature range from 723 K to 1523 K covering the whole composition range. Overall, the curves are S-shaped with a minimum at $x_{Cu} \approx 0.75$, which corresponds to the most stable intermetallic phase Cu_3Sn. Some authors report a slightly positive value at the tin-rich side [4], whereas others find continuous exothermic integral molar mixing enthalpies [7]. No temperature dependence can be determined from a comparison of these works, because the data show no significant tendency. In 2008 Flandorfer et al. [11] systematically investigated the integral molar mixing enthalpies of the Cu–Sn liquid alloys between 773 K and 1523 K and found significant changes in the integral molar mixing enthalpy values between 773 K and 973 K, but they could indicate smaller temperature dependence at higher temperatures. Yassin and Castanet [12] compared the limiting partial molar enthalpies of mixing of copper in tin at different temperatures in their compilation and found a clear temperature dependence $(\frac{\Delta_{mix}\bar{H}_{Cu}^{\infty}}{10^3 J \cdot mol^{-1}} = -13.31 + 0.021 \cdot \frac{T}{K} - 6.3 \cdot 10^{-6} \cdot \frac{T^2}{K^2})$.

Below approximately 823 K the limiting partial molar enthalpies are negatively, at higher temperatures they become positive. This trend was also found by Flandorfer et al. [11], nevertheless the values start to become positive from 773 K. Critical assessments of the phase diagram based on experimental data and thermodynamic calculations were done by Saunders and Miodownik [13], Shim et al. [14] and recently by Li et al. [15].

Cu-Li

This system is one of the less investigated binary systems concerning thermodynamic properties. Nevertheless, DTA, XRD and other methods have been applied to determine the phase diagram. Noteworthy are the works of Pastorello [16] and Klemm and Volavšek [17], who investigated the liquidus by thermal analysis and found the homogeneity range of fcc-(Cu) and bcc-(Li). Pelton [18] assessed the available data to the hitherto known eutectic Cu-Li phase diagram. The first work regarding the thermodynamic data was published by Mikhailovskaya and Sudavtseva [19]. They have measured integral and partial molar mixing enthalpies with a mixing calorimeter at $x_{Li} < 0.3$ and a temperature of 1373 K. They also calculated activities, entropy and Gibbs energy data deduced from the phase diagram [18]. Gąsior et al. [20] performed DTA and EMF- measurements in the temperature range between 633 K and 923 K.

Li-Sn

Wen and Huggins [21] have investigated this system by means of coulometric titration and EMF-measurements in the temperature range of 633-863 K. They confirmed the existence of six intermetallic phases and were able to determine various thermochemical properties. Later on, Moser et al. [22] also performed EMF-measurements on this system, and in addition drop calorimetry at temperatures between 691 K and 938 K, in a composition range of $x_{Li} = 0.01 - 0.5$ and 0.87 - 0.99. Results were integral molar mixing enthalpies, which showed a triangular shaped $\Delta_{mix}H$-curve with an extrapolated minimum of -40000 J/mol at $x_{Li} = 0.77$. According to earlier results from EMF-measurements this integral molar mixing enthalpy minimum can be understood as an ordering phenomenon in the liquid, which supports the theory of associates of Li_4Sn in the melt. In 1999 Gąsior and Moser [23] finalized their EMF-measurements at temperatures between 777 K and 975 K and compositions of $x_{Li} = 0.025 - 0.725$ and 0.91 - 0.954. In this extensive work they published partial and integral thermodynamic properties, which supported the associate theory. Two years later Yassin and Castanet [24] compiled the partial molar limiting enthalpies of mixing of alkali metals in tin and described a slight temperature dependence for the partial molar limiting enthalpy of lithium in tin ($\frac{\Delta_{mix}\bar{H}_{Li}^{\infty}}{10^3 J \cdot mol^{-1}} = -64 + 0.0079 \cdot \frac{T}{K}$). Available assessments, which incorporate thermodynamic as well as crystallographic data, are from Sangster and Bale [25] in 1998, Yin et al. [26] in 2005 and Du et al. [27] in 2006. The later assessments done by Yin et al. [26] and Du et al.

[27] summarize the available thermodynamic data, fit the thermodynamic properties and optimize the Li-Sn phase diagram with the CALPHAD approach.

Cu-Li-Sn

For the ternary system Cu-Li-Sn, to our best knowledge, no thermodynamic description based on experimental data exists. Also no phase diagram or any isothermal section is available, nevertheless two ternary phases have been reported: the phase Li_2CuSn which is fcc [28; 29; 30] and the phase Cu_2LiSn which is hexagonal [31]. Some experiments considering lithiation of Cu_6Sn_5 and its cycling behaviour in lithium ion batteries have been applied recently [32; 33; 34; 35; 36; 37; 38; 39; 40]. However, no information about phase equilibria is given.

Experimental

The calorimetric measurements were performed in a Calvet-type twin calorimeter with two thermopiles with more than 200 thermocouples each. ΔT-values down to 10^{-5}-10^{-4} K could be detected. To enable isoperibolic environment a wire wound resistance furnace was used. Drops were performed using an automated device with a capacity of 30 drops. This device and all measuring facilities are controlled by a user-assembled software in LabVIEW, and the obtained data were evaluated by using HiQ program (for more details see [41]). To prevent oxidation all measurements were carried out under Ar flow (x_{Ar} = 0.99999, flow rate = 30 ml/min, usage of an additional gas purification unit), traces of oxygen were gettered by small slices of titanium next to the crucible. The crucibles (inner diameter 9 mm, length 80 mm) were made of molybdenum for lithium-rich alloys and boron nitride for lithium-poor alloys. Molybdenum is inert against liquid lithium [42], but boron nitride reacts with lithium at higher temperatures (~ 1100 K). Vice versa, boron nitride is inert against liquid tin, but with molybdenum, tin could form intermetallic phases [43]. The boron nitride crucibles were stored in methanol for some days to esterify the boric acid at the surface to volatile methyl esters, which were evaporated in vacuum at 1173 K. Samples were prepared from tin rods (Alfa Aesar, x_{Sn} = 0.999985), lithium wire (Alfa Aesar, x_{Li} = 0.998, stored in mineral oil) and copper wire (Goodfellow, x_{Cu} = 0.9998). The lithium wire was cleaned in a supersonic bath in n-hexane and the solvent removed under vacuum in the glove box antechamber. The copper wire was treated under H_2-flow at 473 K for 5 h to remove oxide layers. Calibration was done by dropping five

pieces of the pure element into the bath of the same element at the start of each measurement. In addition to the calibration with the pure elements also dropping of pieces of NIST standard sapphire was applied. For determining the binary integral and partial molar mixing enthalpies, copper or tin were dropped in liquid lithium and lithium was dropped in liquid tin. The maximum measurement temperature of 1073 K corresponds to the limit of safe handling of liquid lithium. Furthermore, at higher temperatures the lithium melt crept out of the crucible and reacted with the quartz glass wall of our outer tube.

The intervals between the drops were usually 40 min, heat flow acquisition was 0.5 sec. The signals obtained from the thermocouples were recorded, integrated and quantified applying the calorimeter constant, which was determined by the first five calibration drops. To validate the measurements each run was repeated at least one time. The measured enthalpy $\Delta H_{ij;signal}$ is the integrated heat flow at constant pressure and follows this equation:

$$\Delta H_{ij;signal} = n_i \cdot \left[H_{i(l),FT} - H_{i(s),DT}\right] + \Delta H_{ij; reaction} \qquad \text{(Eq.1)}$$

The number of moles of dropped element i is n_i, the furnace temperature is FT and the drop temperature is DT. The furnace temperatures as well as the drop temperatures were recorded for each drop. For the calculation the mean values over all drops were taken because the scattering of the temperature values was low enough to not influence the accuracy of the method. The values for the term $H_{i(l),FT} - H_{i(s),DT}$ were calculated using the polynomials for pure elements in the SGTE unary database [44]. The rather small masses which were added allow the consideration for the partial molar enthalpy of mixing:

$$\Delta_{mix}\overline{H}_{ij} \approx \frac{\Delta H_{ij;reaction}}{n_i} \qquad \text{(Eq. 2)}$$

The integral molar enthalpy of mixing was calculated by summing the respective reaction enthalpies and division by the total molar amount of substance, where n_j stands for the molar amount of substance which was already present in the crucible:

$$\Delta_{mix}H_{ij} = \frac{\sum_{i,j} \Delta H_{ij;reaction}}{n_j + \sum_i n_i} \qquad \text{(Eq. 3)}$$

The respective binary starting value for the sections in the ternary system was calculated from the information listed in Table 1. Random errors as well as systematic errors of calorimetry depend on the construction of the calorimeter, calibration procedure, signal integration and "chemical errors", *e.g.* incomplete reactions, impurities, reactions between the liquid metal and the crucible or evaporation of lithium and reaction of the vapour with the quartz glass wall. Considering many calibration measurements done by dropping NIST standard sapphire, the standard deviation can be estimated to be less than ±1% for the HT-1000. The systematic errors are mainly caused by parasitic heat flows, base line problems at signal integration and mixing problems. One can estimate that the overall error is ±250 J/mol.

Results and discussion

The binary systems Cu-Li and Li-Sn

Due to the lack of information in the binary Cu-Li system, calorimetric studies were necessary. As mentioned in chapter 3 our experiments had to be restricted to 1073 K because lithium and lithium-rich alloys crept out of the crucible at higher temperatures. Thus only the lithium-rich side, where solid copper was dropped into liquid lithium, could be examined. Although the integral molar enthalpy of mixing is endothermic (see Table 2 and Fig. 1) the copper pieces dissolved easily at 1073 K in lithium. Based on our data of two runs until $x_{Cu} \sim 0.28$ we extrapolated the integral molar enthalpies of mixing to $x_{Cu} = 1$ ($\Delta_{mix}H = 0$) with a Redlich-Kister-fit using two interaction parameters [45]:

$$\Delta_{mix}H_{ij} = x_i \cdot x_j \cdot \sum_{\nu} {}^{\nu}L_{i,j}^{H}\left(x_i - x_j\right)^{\nu} \qquad \text{(Eq. 4)}$$

Variables i and j are the binary elements, L is the binary interaction parameter and ν its order. The parameters ${}^{0}L$ and ${}^{1}L$ for Cu-Li are given in Table 1. Our data are quite satisfying matching to the data of Gąsior et al. [20], where integral molar mixing enthalpy values have been derived from EMF-measurements. At estimated $x_{Cu} = 0.5$ there is an endothermic maximum of ~5300 J/mol. Data from Mikhailovskaya and Sudavtseva [19] at the copper-rich side show, however, quite different behaviour. They are slightly exothermic at the copper-rich side and become slightly endothermic at $x_{Li} = 0.23$. It has to be pointed out here that there is obviously a mismatch of measured partial and calculated integral molar enthalpy values in this report. Generally, endothermic behaviour which maximum values significantly higher than 1000-2000

J/mol indicates the occurrence of a miscibility gap in the liquid mixture. This assumption is supported by thermodynamic calculations of Pelton [18], who supposed such a miscibility gap with a maximum at $x_{Li} \sim 0.4$. In order to determine the limiting partial molar enthalpy of copper in liquid lithium ($\Delta_{mix}\overline{H}_{Cu}^{\infty}$), we performed two measurements with all drops within $x_{Cu} = 0 - 0.05$. The obtained values of the partial molar enthalpy of mixing have been extrapolated to pure lithium applying a linear regression. This leads to a highly symmetric mixing curve with endothermic maxima at 23200 and 24300 J/mol (see Table 3). The choice of a first-order extrapolation is supported by Gąsior's calculations from EMF-values [20], which show a very similar tendency to our data, but, nevertheless, with significantly less endothermic values. In addition, no stable intermetallic compounds with a stoichiometry apart from 1:1 are known to this day, therefore no asymmetry in the integral molar mixing enthalpies should be assumed. Measurements in the Li-Sn system at 773 K were mainly dedicated to the validation of our calorimetric method for lithium-containing systems, as most literature data was available around this temperature. Furthermore, no calorimetric determination of $\Delta_{mix}H$ over the entire concentration range was hitherto published. Thus we did further measurements at 1073 K, slightly above the maximum liquidus temperature in this system. Our measured integral molar enthalpy values from the tin- and the lithium-rich side coincided very well (see also Table 4 and Fig. 2). The data were again fitted for each temperature with a Redlich-Kister-polynomial [45], values for ^{0}L, ^{1}L and ^{2}L are listed in Table 1. Graphs are shown in Fig. 2 for 1073 K and Fig. 3 for 773 K. At 773 K there are no experimental data available between $x_{Li} = 0.5$ and 0.98, because the obtained alloys were already partially or completely solid (see Table 5 and Fig. 3). The fit of the data at 1073 K is based on experimental data over the entire concentration range. Our experimental data from both temperatures together with the literature data from EMF- and calorimetric measurements at various temperatures [21; 22] have been as well fitted and are shown Fig. 4. In all cases the integral molar enthalpy of mixing is purely exothermic. The resulting curve which fits all values shows a minimum of ~37000 J/mol at $x_{Sn} = 0.20$ (see Fig. 4). Whereas this curve corresponds very well to that evaluated from our data at 1073 K, the fitted curve for 773 K features a minimum at -33000 J/mol and $x_{Sn} = 0.33$. We believe that this is rather caused by the lack of experimental data in this region than by temperature dependence. In the latter case values at lower temperature should be more exothermic. The pronounced minimum of the integral molar enthalpy of mixing at about Li_4Sn is related to the two most stable intermetallic compounds Li_7Sn_2

[25] and Li$_{17}$Sn$_4$ [46], which melt congruently. This indicates the formation of an associate "Li$_4$Sn", which is already present in the melt close to the liquidus temperature. The associate can be interpreted by an interaction based on the electronic configuration of the two elements. The highly electropositive lithium has a strong tendency to provide one electron per atom ([He] 2s^1), which could be accepted by the remaining free 5p orbitals of tin ([Kr] 4d^{10} 5s^2 5p^2). In the same way as described for Cu-Li, we have determined the limiting partial molar enthalpies from both sides of the binary system at 773 K and 1073 K (see Table 3). Values of lithium in tin ($\Delta_{mix}\overline{H}_{\text{Li}}^{\infty}$) were found to be between -56800 and -59400 J/mol, which is supported by literature data [21; 22; 23; 24], whereas for tin in lithium ($\Delta_{mix}\overline{H}_{\text{Sn}}^{\infty}$) it was found to be between -163100 and -172200 J/mol. No literature data was available for $\Delta_{mix}\overline{H}_{\text{Sn}}^{\infty}$. No significant temperature dependence could be observed.

Measurements and modelling in the ternary system Cu-Li-Sn

Lithium was dropped at 1073 K to liquid mixtures with ratios of $x_{\text{Cu}}/x_{\text{Sn}} \approx 1{:}1$, $x_{\text{Cu}}/x_{\text{Sn}} \approx 2{:}3$, and $x_{\text{Cu}}/x_{\text{Sn}} \approx 1{:}4$, as well as copper was dropped to mixtures of $x_{\text{Li}}/x_{\text{Sn}} \approx 1{:}1$ and $x_{\text{Li}}/x_{\text{Sn}} \approx 1{:}4$, according to the compositions which are shown in Fig. 5. The measured integral and partial molar enthalpies of mixing are listed in Table 6. Plots of the integral molar enthalpies vs. concentration of lithium or copper, respectively, are shown in Fig. 6. Most experiments have been carried out several times to assure reproducibility. The integral molar enthalpy values at all intersection points have been compared (see Table 7), the maximum errors are between ~300 and ~1250 J/mol, what is satisfying regarding the method and the kind of materials used. The integral molar enthalpies of mixing in the ternary system were described with a least square fit, according to a Redlich-Kister-Muggianu-polynomial (Eq. 5):

$$\Delta_{mix}H_{\text{ijk}} = x_{\text{i}} \cdot x_{\text{j}} \cdot \sum_{\text{v}} {}^{\text{v}}L_{\text{ij}}^{H}\left(x_{\text{i}} - x_{\text{j}}\right)^{\text{v}} + x_{\text{j}} \cdot x_{\text{k}} \cdot \sum_{\text{v}} {}^{\text{v}}L_{\text{jk}}^{H}\left(x_{\text{j}} - x_{\text{k}}\right)^{\text{v}}$$

$$+ x_{\text{k}} \cdot x_{\text{i}} \cdot \sum_{\text{v}} {}^{\text{v}}L_{\text{ki}}^{H}(x_{\text{k}} - x_{\text{i}})^{\text{v}} + x_{\text{i}} \cdot x_{\text{j}} \cdot x_{\text{k}} \cdot$$

$$\left({}^{(0)}M_{\text{i,j,k}}^{H} \cdot x_{\text{i}} + {}^{(1)}M_{\text{i,j,k}}^{H} \cdot x_{\text{j}} + {}^{(2)}M_{\text{i,j,k}}^{H} \cdot x_{\text{k}} \right)$$

In this equation the variables i, j, k are copper, lithium and tin and v values are 0, 1 or 2. The *L*-values are the binary interaction parameters for the Redlich-Kister-polynomials, the *M*-values describe the ternary interactions. The resulting ternary *M*-values are listed in Table 1 together with the binary *L*-values applied. For Cu-Sn literature values were

taken from Flandorfer et al. [11]. Based on this equation the integral molar enthalpies of mixing were calculated for the whole ternary composition range. Calculated integral molar enthalpy curves for all sections have been added to the plots, shown in Fig. 6. Isoenthalpy curves across the whole ternary composition range are plotted at a Gibbs triangle in Fig. 7. The values in the plot refer to the solid lines. It is noteworthy to say that the values outside of the fully liquid range at 1073 K, which is shown as a shaded field, have to be considered as integral molar enthalpies of the metastable liquid phase. The liquidus limit was estimated from the constituent binary phase diagrams [18; 47]. In addition the integral molar enthalpies of mixing were calculated without ternary interaction parameters (Eq. 5 without ternary interaction term) along the sections A-E. Generally, the values are significantly less exothermic compared to the calculation with ternary interaction parameters (see Fig. 6). The negative contribution of the ternary interaction term indicates additional ternary interaction of copper, lithium and tin. In order to check, whether an alternative extrapolation model is able to describe our experimental results, the approach of Chou's model [48; 49] was applied. This model describes the integral molar enthalpy of mixing as follows (Eq. 6):

$$\Delta_{mix}H_{ijk} = \quad x_i \cdot x_j \cdot \sum_v \; {}^vL_{ij}^H \big(x_i - x_j\big)^v + x_j \cdot x_k \cdot \sum_v \; {}^vL_{jk}^H \big(x_j - x_k\big)^v$$
$$+ x_k \cdot x_i \cdot \sum_v \; {}^vL_{ki}^H (x_k - x_i)^v + \; x_i \cdot x_j \cdot x_k \cdot f$$

The factor f represents the ternary interaction coefficient and can be expressed as (Eq. 7)

$$f = \big(2 \cdot \xi_{ij} - 1\big) \cdot \left[\Big({}^2L_{ij}^H \cdot \big(2 \cdot \xi_{ij} - 1\big) \cdot x_k + 2 \cdot \big(x_i - x_j\big) \Big) + {}^1L_{ij}^H \right] +$$
$$\big(2 \cdot \xi_{jk} - 1\big) \cdot \left[\Big({}^2L_{jk}^H \cdot \big(2 \cdot \xi_{jk} - 1\big) \cdot x_i + 2 \cdot \big(x_j - x_k\big) \Big) + {}^1L_{jk}^H \right] +$$
$$\big(2 \cdot \xi_{ki} - 1\big) \cdot \left[\Big({}^2L_{ki}^H \cdot (2 \cdot \xi_{ki} - 1) \cdot x_j + 2 \cdot (x_k - x_i) \Big) + {}^1L_{ki}^H \right]$$

The factors ξ_{ij}, ξ_{jk} and ξ_{ki} are similarity coefficients of i, j and k and are a relation of the "deviation sums of squares" η_I, η_{II} and η_{III} (Eq. 8):

$$\xi_{ij} = \frac{\eta_I}{\eta_I + \eta_{II}} \quad ; \xi_{jk} = \frac{\eta_{II}}{\eta_{II} + \eta_{III}} \quad \text{and } \xi_{ki} = \frac{\eta_{III}}{\eta_{III} + \eta_I}$$

η_{I}, η_{II} and η_{III} are integral values of the square of the difference between the binary integral molar enthalpies of mixing as follows: (Eq. 9):

$$\eta_{\mathrm{I}} = \int_0^1 \left(\Delta_{mix}H_{\mathrm{ij}} - \Delta_{mix}H_{\mathrm{ik}}\right)^2 \mathrm{d}X_{\mathrm{i}}\ ;$$

$$\eta_{\mathrm{II}} = \int_0^1 \left(\Delta_{mix}H_{\mathrm{ji}} - \Delta_{mix}H_{\mathrm{jk}}\right)^2 \mathrm{d}X_{\mathrm{j}}\ ;$$

$$\eta_{\mathrm{III}} = \int_0^1 \left(\Delta_{mix}H_{\mathrm{ki}} - \Delta_{mix}H_{\mathrm{kj}}\right)^2 \mathrm{d}X_{\mathrm{k}}$$

In our case i, j and k are copper, lithium and tin, respectively. Capital X is the binary concentration of copper, lithium or tin, lower-case x is the concentration in the ternary system. The similarity coefficients and the deviation sums of squares for Cu-Li, Sn-Cu and Li-Sn are listed in Table 8.

From the resulting ξ-values we can conclude that the integral molar mixing enthalpies of Cu-Li and Cu-Sn are more similar to each other than to Li-Sn, respectively. According to the shape of the curves this is obvious because Cu-Li shows relatively low endothermic, Cu-Sn low exothermic values, whereas Li-Sn has a pronounced exothermic behaviour. As we can see in Fig. 6, Chou's model, however, is not able to describe our experimental data better than the Muggianu model without ternary interaction parameters. For all sections, the two models result in very similar values. Considering that Chou's model would provide the best extrapolation from the asymmetric binaries, we can conclude that additional ternary interactions exist in this system. Fig. 7 shows a comparison between fitted experimental data and those ones calculated with the Chou-model in an isoenthalpy plot. For Cu-Sn an associate "Cu_3Sn" was postulated in Flandorfer et al. [11], and we have indications for the occurrence of an associate "Li_4Sn" in Li-Sn. Regarding the isoenthalpy plot in Fig. 7 one can see an exothermic integral molar enthalpy of mixing valley which connects those two associates. Compared to the extrapolation data the valley according to the experimental results is shifted towards more exothermic values and slightly lower tin content. The assumption of an additional ternary interaction between the two associates is supported by the formation of two ternary intermetallic compounds along this valley, Cu_2LiSn and $CuLi_2Sn$ [28; 29; 30; 31].

Acknowledgements

References

[1]   M. Kawakami, Sci. Rep. Tohoku Imp. Univ. 19 (1930) 521.

[2]   L.B. Ticknor, M.B. Bever, Trans. Am. Inst. Min. Metal. Eng. 194 (1952) 941-945.

[3]   J.B. Cohen, J.S.L. Leach, M.B. Bever, Trans. Am. Inst. Min. Metal. Eng. 200 (1954) 1257-1258.

[4]   O.J. Kleppa, J. Phys. Chem. 60 (1956) 842-846.

[5]   O.J. Kleppa, J. Phys. Chem. 60 (1956) 852-858.

[6]   R.R. Hultgren, P.D. Desai, D.T. Hawkins, M. Gleiser, K.K. Kelley, Selected values of the thermodynamic properties of the elements, American Society for Metals (Metals Park, Ohio) 1973.

[7]   K. Itagaki, A. Yazawa, Trans. Jpn. Inst. Met. 16 (1975) 679-686.

[8]   A. Yazawa, K. Itagaki, T. Azakami, Trans. Jpn. Inst. Met. 16 (1975) 687-695.

[9]   M.J. Pool, B. Predel, E. Schultheiss, Thermochim. Acta 28 (1979) 349-358.

[10]   J.J. Lee, B.J. Kim, W.S. Min, J. Alloys and Compd. 202 (1993) 237-242.

[11]   H. Flandorfer, C. Luef, U. Saeed, J. Non-Cryst. Solids 354 (2008) 2953-2972.

[12]   A. Yassin, R. Castanet, J. Alloys and Compd. 307 (2000) 191-198.

[13]   N. Saunders, A.P. Miodownik, Bull. Alloy Phase Diagrams 11 (1990) 278-287.

[14]   J.H. Shim, C.S. Oh, B.J. Lee, D.N. Lee, Z. Metallkd. 87 (1996) 205-212.

[15]   D. Li, P. Franke, S. Fürtauer, D. Cupid, H. Flandorfer, Intermetallics 34 (2013) 148-158.

[16]   S. Pastorello, W. Klemm, B. Volavsek, Gazz. Chim. Ital. 60 (1930) 988-992.

[17]   W. Klemm, B. Volavšek, Z. Anorg. Allg. Chem. 296 (1958) 184-187.

[18]   A.D. Pelton, Bull. Alloy Phase Diagrams 7 (1986) 142-144.

[19]   M.V. Mikhailovskaya, V.S. Sudavtseva, Ukr. Khim. Zh. 55 (1989) 1106-1108.

[20]   W. Gąsior, B. Onderka, Z. Moser, A. Dębski, T. Gancarz, CALPHAD: Comput. Coupl. Phase Diagrams Thermochem. 33 (2009) 215-220.

[21]   C.J. Wen, R.A. Huggins, J. Electrochem. Soc. 128 (1981) 1181-1187.

[22]   Z. Moser, W. Gąsior, F. Sommer, G. Schwitzgebel, B. Predel, Metall. Trans. B 17 (1986) 791-796.

[23]   W. Gąsior, Z. Moser, Arch. Metall. 44 (1999) 83-92.

[24]   A. Yassin, R. Castanet, J. Alloys and Compd. 314 (2001) 160-166.

[25]   J. Sangster, C.W. Bale, J. Phase Equilib. 19 (1998) 70-75.

[26]   F. Yin, X. Su, Z. Li, J. Wang, J. Alloys and Compd. 393 (2005) 105-108.

[27]   Z.M. Du, Z.Q. Jiang, C.P. Guo, Z. Metallkd. 97 (2006) 10-16.

[28]   H.U. Schuster, Die Naturwiss. 53 (1966) 360-361.

[29]   H. Pauly, A. Weiss, H. Witte, Z. Metallkd. 59 (1968) 47-58.

[30]   H.U. Schuster, D. Thiedemann, H. Schönemann, Z. Anorg. Allg. Chem. 370 (1969) 160-170.

[31]   P.I. Kripyakevich, G.I. Oleksiv, Dopov. Akad. Nauk Ukr. RSR A (1970) 63-65.

[32]   K.D. Kepler, J.T. Vaughey, M.M. Thackeray, Electrochem. Solid State Lett. 2 (1999) 307-309.

[33]   G.X. Wang, L. Sun, D.H. Bradhurst, S.X. Dou, H.K. Liu, J. Alloys and Compd. 299 (2000) L12-L15.

[34]   S. Sharma, L. Fransson, E. Sjostedt, L. Nordstrom, B. Johansson, K. Edstrom, J. Electrochem. Soc. 150 (2003) A330-A334.

[35]   W. Choi, J.Y. Lee, H.S. Lim, Electrochem. Commun. 6 (2004) 816-820.

[36]   H.C. Shin, M.L. Liu, Adv. Funct. Mater. 15 (2005) 582-586.

[37]   A.H. Reshak, D.A.O. Ortiz, J. Phys. Chem. B 113 (2009) 13208-13215.

[38]   S. Zhang, Y. Xing, T. Jiang, Z. Du, F. Li, L. He, W. Liu, J. Power Sources (2010).

[39]   A. Jansen, J. Clevenger, A. Baebler, J. Vaughey, Variable Temperature Performance of Intermetallic Lithium-Ion Battery Anode Materials, J. Alloys and Compd., 2011.

[40]   Y.S. Lin, J.G. Duh, H.S. Sheu, J. Alloys and Compd. 509 (2011) 123-127.

[41]   H. Flandorfer, F. Gehringer, E. Hayer, Thermochim. Acta 382 (2002) 77-87.

[42]   T.B. Massalski, H. Okamoto, P.R. Subramanian, L. Kacprzak, (Eds.), Li-Mo (Lithium-Molybdenum), The Materials Information Society, Ohio, 1990.

[43]   L. Brewer, R.H. Lamoreaux, (Eds.), Mo-Sn (Molybdenum-Tin), The Materials Information Society, Ohio, 1990.

[44]   A.T. Dinsdale, SGTE Data for Pure Elements, updated version 5.0 (2009), CALPHAD: Comput. Coupl. Phase Diagrams Thermochem. 1991, pp. 317-425.

[45]   O. Redlich, A.T. Kister, Ind. Eng. Chem. 40 (1948) 345-348.

[46]   C. Lupu, J.G. Mao, J.W. Rabalais, A.M. Guloy, J.W.J. Richardson, Inorg. Chem. 42 (2003) 3765-3771.

[47]   S. Fürtauer, D. Li, D. Cupid, H. Flandorfer, Intermetallics 34 (2013) 142-147.

[48]   K.C. Chou, CALPHAD: Comput. Coupl. Phase Diagrams Thermochem. 19 (1995) 315-325.

[49]   K.C. Chou, W.C. Li, F.S. Li, M.H. He, CALPHAD: Comput. Coupl. Phase Diagrams Thermochem. 20 (1996) 395-406.

Table 1: Binary and ternary interaction parameters in Cu-Li-Sn (1073 K)

System	Reference	$\dfrac{^{\nu}L_{i,j}^{H}}{J \cdot mol^{-1}}$ or $\dfrac{^{\nu}M_{i,j}^{H}}{J \cdot mol^{-1}}$		
Cu-Sn	[11]	^{0}L = -10232	^{1}L = -22098	^{2}L = -13216
Cu-Li	This work	^{0}L = 21165	^{1}L = -1681	
Li-Sn	This work	^{0}L = -111137	^{1}L = -124601	^{2}L = -89726
Cu-Li-Sn	This work	^{0}M = -388766	^{1}M = -501989	^{2}M = 134799

$^{\nu}L_{i,j}^{H}$ or $^{\nu}M_{i,j}^{H}$ ….. binary or ternary interaction parameters

ν…………….…....order

i, j………….….…elements in binary system

Table 2: Partial and integral molar enthalpies of mixing of liquid Cu-Li alloys at 1073 K; standard states: pure liquid metals.

Dropped mole $\dfrac{n_{Cu}}{10^{-3}\,mol}$	Drop enthalpy $\dfrac{\Delta H_{signal}}{J}$	Partial molar enthalpy		Integral molar enthalpy	
		x_{Cu}[a]	$\dfrac{\Delta_{mix}\overline{H}_{Cu}}{J\cdot mol^{-1}}$	x_{Cu}[b]	$\dfrac{\Delta_{mix}H}{J\cdot mol^{-1}}$
Starting amount: $n_{Li} = 54.2732 \cdot 10^{-3}$ mol, calibration: 5 pieces Li, calibration constant $k = (0.52995 \pm 0.0055)$ J/(μV·s)					
0.4709	20763	0.0043	23124 ± 458	0.0086	199 ± 4
0.5173	22534	0.0132	22588 ± 452	0.0179	408 ± 8
0.5343	22843	0.0226	21779 ± 444	0.0273	613 ± 12
0.5626	23644	0.0321	21056 ± 436	0.0370	817 ± 17
0.5993	24554	0.0421	20002 ± 426	0.0471	1019 ± 21
0.6317	25494	0.0524	19381 ± 419	0.0576	1220 ± 25
0.6621	26551	0.0629	19131 ± 416	0.0683	1424 ± 30
0.6948	27296	0.0738	18311 ± 408	0.0793	1623 ± 34
0.7190	28020	0.0848	17998 ± 405	0.0904	1820 ± 39
0.7517	28790	0.0960	17330 ± 398	0.1017	2013 ± 43
0.7984	30488	0.1075	17213 ± 397	0.1134	2212 ± 48
0.8229	31602	0.1193	17430 ± 399	0.1252	2413 ± 52
0.8478	32076	0.1311	16864 ± 393	0.1370	2608 ± 57

0.8909	33371	0.1430	16486	±	389	0.1490	2802	± 62
0.9247	33883	0.1551	15668	±	381	0.1612	2986	± 66
0.9534	35120	0.1673	15864	±	383	0.1734	3173	± 71
0.9800	35111	0.1794	14854	±	372	0.1855	3345	± 75
1.0182	35823	0.1916	14209	±	365	0.1978	3508	± 80
1.0414	36356	0.2039	13939	±	363	0.2099	3666	± 84
1.0708	36841	0.2160	13431	±	357	0.2221	3816	± 88
1.1006	37054	0.2281	12693	±	350	0.2341	3954	± 92
1.1487	38406	0.2403	12460	±	347	0.2464	4090	± 96
1.1753	38869	0.2524	12098	±	343	0.2585	4219	± 100
1.2077	39784	0.2645	11969	±	342	0.2705	4344	± 104
1.2366	41009	0.2765	12191	±	344	0.2824	4473	± 108

[a] Average of x_{Cu} before and after the drop

[b] Per mole of binary mixture

Table 3: Limiting partial molar enthalpies in Cu-Li and Li-Sn, comparison of measured and literature data

System	T/K		Run No			Literature, at T/K			
			1	2	3	[19] 1373	[20][c] 1373		
Cu-Li	1073	$\Delta_{mix}\overline{H}_{Cu}^{\infty}$ / J·mol^{-1}	23200 (± 400)	24300 (± 200)			13500		
Cu-Li		$\Delta_{mix}\overline{H}_{Li}^{\infty}$ / J·mol^{-1}				-30900	18500		
						[21][c] 688	[22] 807	[23][c]	[24][c] 773
Li-Sn	773	$\Delta_{mix}\overline{H}_{Sn}^{\infty}$ / J·mol^{-1}	-163100 (± 1100)	-172200 (± 2700)					
Li-Sn	773	$\Delta_{mix}\overline{H}_{Li}^{\infty}$ / J·mol^{-1}	-57900 (± 800)	-57800 (± 700)		-55500	-57400	-56500	-57900
						[22] 938	[24][c] 1073		
Li-Sn	1073	$\Delta_{mix}\overline{H}_{Sn}^{\infty}$ / J·mol^{-1}	-170200 (± 1400)	-168600 (± 4100)					
Li-Sn	1073	$\Delta_{mix}\overline{H}_{Li}^{\infty}$ / J·mol^{-1}	-59400 (± 400)	-56800 (± 300)	-58600 (± 400)	-56700	-55500		

$\Delta_{mix}\overline{H}_{i}^{\infty}$…..Limiting partial molar enthalpy
[c] calculated

Table 4: Partial and integral molar enthalpies of mixing of liquid Li-Sn alloys at 1073 K; standard states: pure liquid metals.

A: Li in liquid Sn

Dropped mole	Drop enthalpy	Partial molar enthalpy		Integral molar enthalpy	
$\dfrac{n_{Li}}{10^{-3}\,mol}$	$\dfrac{\Delta H_{signal}}{J}$	$x_{Li}{}^{a}$	$\dfrac{\Delta_{mix}\overline{H}_{Li}}{J \cdot mol^{-1}}$	$x_{Li}{}^{b}$	$\dfrac{\Delta_{mix}H}{J \cdot mol^{-1}}$

Starting amount: $n_{Sn} = 19.2055 \cdot 10^{-3}$ mol, calibration: 5 pieces Sn, calibration constant $k = (0.56048 \pm 0.0040)$ J/(μV·s)

0.3256	-11578	0.0083	-60939 ± 254	0.0167	-1016 ± 4
0.3688	-12468	0.0258	-59184 ± 242	0.0349	-2094 ± 9
0.4250	-14240	0.0450	-58886 ± 240	0.0551	-3282 ± 13
0.4913	-15746	0.0662	-57431 ± 229	0.0774	-4560 ± 19
0.6109	-20134	0.0905	-58340 ± 236	0.1037	-6093 ± 25
0.6454	-20212	0.1168	-56696 ± 224	0.1299	-7572 ± 31
0.7535	-23242	0.1443	-56225 ± 221	0.1586	-9179 ± 37
0.8284	-27165	0.1733	-58172 ± 234	0.1881	-10894 ± 44
0.8558	-25650	0.2023	-55353 ± 214	0.2164	-12447 ± 50
0.9408	-29308	0.2309	-56534 ± 223	0.2454	-14076 ± 56
0.9840	-29576	0.2594	-55437 ± 215	0.2735	-15616 ± 62
1.0647	-31703	0.2875	-55158 ± 213	0.3016	-17147 ± 68
1.1482	-35602	0.3156	-56386 ± 222	0.3296	-18720 ± 74
1.2577	-38134	0.3437	-55700 ± 217	0.3578	-20275 ± 80
1.3269	-40114	0.3714	-55612 ± 216	0.3851	-21776 ± 86
1.3802	-41241	0.3981	-55261 ± 214	0.4111	-23193 ± 91
1.4249	-41710	0.4234	-54654 ± 209	0.4358	-24510 ± 96

1.5099	-43965	0.4477	-54499 ± 208	0.4597	-25784 ± 101
1.6251	-46986	0.4715	-54293 ± 207	0.4833	-27030 ± 106
1.6727	-47799	0.4945	-53957 ± 204	0.5056	-28190 ± 110
1.7505	-50261	0.5162	-54093 ± 205	0.5269	-29307 ± 114
1.8182	-49586	0.5370	-52653 ± 195	0.5472	-30308 ± 117
1.8744	-48911	0.5568	-51475 ± 187	0.5664	-31203 ± 120
1.9378	-49175	0.5754	-50758 ± 181	0.5845	-32023 ± 123
2.0141	-49755	0.5932	-50084 ± 177	0.6019	-32777 ± 125

B: Sn in liquid Li

Dropped mole	Drop enthalpy	Partial molar enthalpy		Integral molar enthalpy	
$\dfrac{n_{Sn}}{10^{-3}\,mol}$	$\dfrac{\Delta H_{signal}}{J}$	$x_{Sn}{}^{a}$	$\dfrac{\Delta_{mix}\overline{H}_{Sn}}{J \cdot mol^{-1}}$	$x_{Sn}{}^{b}$	$\dfrac{\Delta_{mix}H}{J \cdot mol^{-1}}$

Starting amount: $n_{Li} = 28.2874 \cdot 10^{-3}$ mol, calibration: 5 pieces Li, calibration constant $k = (0.64430 \pm 0.0168)$ J/(µV·s)

0.8476	-130494	0.0145	-183228 ± 4025	0.0291	-5330 ± 117
0.8778	-140136	0.0433	-188916 ± 4174	0.0575	-10700 ± 236
0.9260	-154635	0.0716	-196260 ± 4366	0.0857	-16254 ± 359
0.9671	-168763	0.0996	-203778 ± 4562	0.1134	-21937 ± 487
2.0686	-380843	0.1404	-213376 ± 4813	0.1674	-33594 ± 750
1.0982	-120392	0.1804	-138899 ± 2866	0.1935	-36891 ± 816
2.3200	-33766	0.2185	-43822 ± 380	0.2435	-37321 ± 789
1.2179	-12091	0.2554	-39196 ± 260	0.2674	-37380 ± 773

1.2674	-2548	0.2790	-31279	±	53	0.2906	-37186	±	750
1.3092	6985	0.3019	-23932	±	139	0.3132	-36765	±	722
1.3458	14436	0.3241	-18542	±	280	0.3349	-36188	±	690
1.3900	21541	0.3455	-13771	±	405	0.3560	-35479	±	655
1.4303	27439	0.3661	-10084	±	502	0.3763	-34678	±	619
1.4728	32727	0.3861	-7048	±	581	0.3959	-33809	±	581
1.5011	37382	0.4053	-4366	±	651	0.4147	-32894	±	543
1.5579	40971	0.4238	-2970	±	688	0.4329	-31960	±	504
1.5628	44193	0.4416	-991	±	739	0.4502	-31019	±	466
1.6465	48418	0.4587	139	±	769	0.4672	-30053	±	428
1.6929	50830	0.4755	758	±	785	0.4837	-29101	±	391
1.7374	54300	0.4916	1985	±	817	0.4996	-28145	±	354
1.7470	55722	0.5071	2628	±	834	0.5146	-27223	±	318
1.8094	58645	0.5219	3143	±	847	0.5292	-26308	±	283
1.8587	61125	0.5362	3617	±	860	0.5433	-25410	±	249

[a] Average of x_i before and after the drop

[b] Per mole of binary mixture

Table 5: Partial and integral molar enthalpies of mixing of liquid Li-Sn alloys at 773 K; standard states: pure liquid metals.

A: Li in liquid Sn

Dropped mole $\dfrac{n_{Li}}{10^{-3}\,mol}$	Drop enthalpy $\dfrac{\Delta H_{signal}}{J}$	Partial molar enthalpy		Integral molar enthalpy	
		$x_{Li}{}^{a}$	$\dfrac{\Delta_{mix}\overline{H}_{Li}}{J \cdot mol^{-1}}$	$x_{Li}{}^{b}$	$\dfrac{\Delta_{mix}H}{J \cdot mol^{-1}}$
Starting amount: $n_{Sn} = 16.8847 \cdot 10^{-3}$ mol, calibration: 5 pieces Sn, calibration constant $k = (0.46792 \pm 0.0057)$ J/(μV·s)					
0.2651	-14777	0.0077	-72564 ± 678	0.0155	-1122 ± 10
0.3760	-13977	0.0260	-53992 ± 452	0.0366	-2256 ± 20
0.4481	-19607	0.0486	-60580 ± 532	0.0606	-3710 ± 33
0.5143	-21885	0.0737	-59373 ± 517	0.0867	-5258 ± 46
0.5806	-24864	0.1006	-59647 ± 521	0.1145	-6914 ± 61
0.6627	-27856	0.1294	-58855 ± 511	0.1443	-8659 ± 76
0.7362	-31359	0.1597	-59418 ± 518	0.1751	-10485 ± 92
0.7881	-32648	0.1904	-58250 ± 504	0.2056	-12256 ± 107
0.8716	-35190	0.2213	-57195 ± 491	0.2369	-14026 ± 122
0.9393	-39206	0.2525	-58560 ± 507	0.2680	-15839 ± 138
1.0200	-43151	0.2835	-59125 ± 514	0.2990	-17673 ± 154
1.1036	-46197	0.3144	-58682 ± 509	0.3297	-19469 ± 169
1.1598	-48637	0.3445	-58759 ± 510	0.3592	-21198 ± 184
1.2477	-52358	0.3737	-58787 ± 510	0.3882	-22898 ± 199
1.3024	-54054	0.4020	-58325 ± 505	0.4158	-24494 ± 213
1.3687	-56302	0.4290	-57958 ± 500	0.4422	-26008 ± 226
1.4436	-57078	0.4549	-56361 ± 481	0.4676	-27389 ± 237

1.5243	-55867	0.4798	-53474 ± 446	0.4920	-28585 ± 247
1.5891	8857	0.5036	-11249 ± 68	0.5152	-27794 ± 233
1.6424	-75724	0.5261	-62927 ± 561	0.5370	-29377 ± 247
1.7101	-68630	0.5474	-56953 ± 488	0.5577	-30612 ± 258
1.8095	28000	0.5677	-1349 ± 188	0.5778	-29288 ± 238
1.8715	-399	0.5872	-17035 ± 3	0.5966	-28740 ± 227
1.9478	34401	0.6056	839 ± 215	0.6146	-27425 ± 208
2.0098	-54946	0.6230	-44161 ± 332	0.6315	-28159 ± 213

B: Sn in liquid Li

Dropped mole	Drop enthalpy	Partial molar enthalpy		Integral molar enthalpy	
$\dfrac{n_{Sn}}{10^{-3}\,mol}$	$\dfrac{\Delta H_{signal}}{J}$	x_{Sn}^{a}	$\dfrac{\Delta_{mix}\overline{H}_{Sn}}{J \cdot mol^{-1}}$	x_{Sn}^{b}	$\dfrac{\Delta_{mix}H}{J \cdot mol^{-1}}$
Starting amount: $n_{Li} = 79.8948 \cdot 10^{-3}\,mol$, calibration: 5 pieces Li, calibration constant $k = (0.44009 \pm 0.0035)\ J/(\mu V \cdot s)$					
0.0836	-12187	0.0005	-166064 ± 1164	0.0010	-174 ± 1
0.1013	-14213	0.0017	-160562 ± 1120	0.0023	-376 ± 3
0.1209	-17031	0.0031	-161082 ± 1124	0.0038	-619 ± 4
0.1315	-19127	0.0046	-165738 ± 1162	0.0054	-889 ± 6
0.1517	-21819	0.0064	-164103 ± 1149	0.0073	-1196 ± 8
0.1698	-24380	0.0084	-163851 ± 1147	0.0094	-1539 ± 11

0.1853	-29547	0.0105	-179660	±	1273	0.0117	-1947	±	14
0.2037	-35023	0.0129	-192031	±	1373	0.0142	-2425	±	17
0.2210	-39343	0.0155	-198148	±	1422	0.0168	-2957	±	21
0.2316	-41064	0.0182	-197431	±	1416	0.0196	-3509	±	25
0.2528	-49782	0.0212	-216908	±	1572	0.0227	-4169	±	30
0.2674	-52712	0.0243	-217154	±	1574	0.0259	-4864	±	35
0.2860	-57918	0.0275	-222543	±	1617	0.0292	-5620	±	40
0.3044	-60017	0.0310	-217164	±	1574	0.0328	-6399	±	46
0.3221	-67882	0.0347	-230724	±	1683	0.0366	-7270	±	52
0.3361	-70680	0.0385	-230230	±	1679	0.0405	-8170	±	59
0.3569	-75234	0.0425	-230775	±	1683	0.0446	-9120	±	66
0.3661	-77203	0.0466	-230860	±	1684	0.0487	-10086	±	73
0.3868	-80975	0.0509	-229312	±	1672	0.0531	-11091	±	80
0.4064	-85745	0.0554	-230952	±	1685	0.0576	-12145	±	88
0.4202	-88539	0.0599	-230656	±	1682	0.0623	-13223	±	96
0.4401	-92875	0.0647	-231002	±	1685	0.0671	-14341	±	104
0.4570	-96418	0.0696	-230944	±	1685	0.0720	-15491	±	112
0.4726	-100081	0.0746	-231718	±	1691	0.0771	-16671	±	121
0.4878	-102871	0.0797	-230846	±	1684	0.0823	-17871	±	130

[a] Average of x_i before and after the drop

[b] Per mole of binary mixture

Beyond the liquidus

Table 6: Partial and integral molar enthalpies of mixing of liquid Cu-Li-Sn alloys at 1073 K; standard states: pure liquid metals.

Dropped mole	Drop enthalpy	Partial molar enthalpy		Integral molar enthalpy	
$\dfrac{n_i}{10^{-3}\,\text{mol}}$	$\dfrac{\Delta H_{signal}}{J}$	$x_i^{\,a}$	$\dfrac{\Delta_{mix}\overline{H}_i}{J \cdot \text{mol}^{-1}}$	$x_i^{\,b}$	$\dfrac{\Delta_{mix}H}{J \cdot \text{mol}^{-1}}$
		^{a} Average of x_i before and after the drop		^{b} Per mole of ternary mixture	

Section A: $x_{Cu}/x_{Sn} \approx 1{:}1$; i = Li; starting amounts: $n_{Cu} = 7.9212 \cdot 10^{-3}$ mol; $n_{Sn} = 7.8768 \cdot 10^{-3}$ mol, calibration: 5 pieces of NIST-sapphire, calibration constant $k = (1.2364 \pm 0.0272)$ J/(µV·s)

n_i	ΔH_{signal}	$x_i^{\,a}$	$\Delta_{mix}\overline{H}_i$	$x_i^{\,b}$	$\Delta_{mix}H$
0.0000		0.0000		0.0000	-2577
0.2953	-12205	0.0092	-66515 ± 910	0.0184	-3750 ± 17
0.3991	-15628	0.0302	-64350 ± 862	0.0421	-5217 ± 37
0.4682	-18114	0.0553	-63875 ± 852	0.0686	-6836 ± 60
0.5115	-18044	0.0822	-60469 ± 777	0.0958	-8406 ± 81
0.5748	-19458	0.1102	-59037 ± 745	0.1246	-10019 ± 102
0.6584	-22593	0.1400	-59504 ± 755	0.1554	-11760 ± 125
0.7492	-23356	0.1717	-56365 ± 686	0.1880	-13478 ± 146
0.7665	-21602	0.2033	-53373 ± 620	0.2187	-14990 ± 164
0.8860	-26976	0.2351	-55635 ± 670	0.2515	-16697 ± 186
0.9566	-26353	0.2678	-52737 ± 606	0.2840	-18259 ± 204
1.0373	-27459	0.3001	-51660 ± 583	0.3161	-19759 ± 221
1.1151	-25769	0.3319	-48298 ± 509	0.3476	-21073 ± 234
1.1699	-24262	0.3627	-45929 ± 457	0.3777	-22219 ± 244
1.2030	-22020	0.3918	-43493 ± 403	0.4058	-23181 ± 252
1.2952	-21685	0.4196	-41932 ± 369	0.4334	-24052 ± 257

1.3600	-18755	0.4466	-38979	±	304	0.4598	-24746	±	259
1.4450	-17743	0.4725	-37468	±	270	0.4852	-25345	±	260
1.4839	-15426	0.4971	-35584	±	229	0.5090	-25818	±	258
1.6179	-12806	0.5207	-33104	±	174	0.5325	-26166	±	254
1.6554	-8819	0.5434	-30516	±	117	0.5543	-26370	±	248
1.7548	-4099	0.5648	-27525	±	51	0.5753	-26424	±	239
1.8167	1571	0.5852	-24324	±	19	0.5951	-26326	±	227
1.8571	5796	0.6043	-22068	±	69	0.6135	-26133	±	213
1.9579	14022	0.6223	-18027	±	158	0.6312	-25762	±	196
2.0112	20855	0.6394	-14820	±	228	0.6477	-25272	±	177

Section B: $x_{Cu}/x_{Sn} \approx 2:3$; i = Li; starting amounts: $n_{Cu} = 7.5713 \cdot 10^{-3}$ mol; $n_{Sn} = 10.8901 \cdot 10^{-3}$ mol, starting alloy made from dropping Sn in Cu; calibration: 5 pieces Cu, calibration constant $k = (0.8934 \pm 0.0147)$ J/(µV·s)

0.0000		0.0000				0.0000	-1618		
0.7276	-27306	0.0190	-62861	±	616	0.0379	-3940	±	23
0.8140	-31736	0.0575	-64318	±	640	0.0771	-6397	±	48
0.8817	-31264	0.0965	-60788	±	582	0.1160	-8693	±	71
0.9437	-32647	0.1351	-59927	±	568	0.1542	-10908	±	93
1.0243	-33987	0.1732	-58509	±	545	0.1922	-13042	±	113
1.0877	-38198	0.2105	-60447	±	577	0.2289	-15196	±	134
1.1713	-36427	0.2468	-56430	±	511	0.2648	-17119	±	151
1.2088	-35395	0.2817	-54612	±	481	0.2986	-18841	±	167
1.3125	-37116	0.3153	-53610	±	464	0.3319	-20492	±	181

1.3615	-36309	0.3476	-52000	± 438	0.3633	-21972	± 193
1.4594	-36445	0.3785	-50302	± 410	0.3938	-23329	± 203
1.5358	-38013	0.4083	-50082	± 407	0.4229	-24614	± 213
1.5833	-34829	0.4365	-47328	± 361	0.4501	-25685	± 220
1.6611	-33335	0.4631	-45398	± 330	0.4760	-26614	± 225
1.7548	-30275	0.4885	-42583	± 283	0.5009	-27372	± 228
1.8196	-28228	0.5126	-40844	± 255	0.5243	-28004	± 229
1.8484	-25064	0.5351	-38890	± 223	0.5459	-28499	± 229
1.9867	-23403	0.5565	-37110	± 193	0.5671	-28900	± 227

Section C: $x_{Cu}/x_{Sn} \approx 1{:}4$; i = Li; starting amounts: $n_{Cu} = 1.6002 \cdot 10^{-3}$ mol; $n_{Sn} = 6.3727 \cdot 10^{-3}$ mol, calibration: 5 pieces of NIST-sapphire, calibration constant $k = (0.6523 \pm 0.0049)$ J/(µV·s)

0.0000		0.0000			0.0000	-280	
0.4697	-16767	0.0278	-16767	± 271	0.0556	-3654	± 15
0.5446	-17187	0.0842	-17187	± 239	0.1129	-6873	± 29
0.5849	-18316	0.1400	-18316	± 237	0.1671	-9907	± 41
0.6973	-22344	0.1953	-22344	± 243	0.2236	-13123	± 55
0.7103	-22180	0.2487	-22180	± 237	0.2739	-15925	± 67
0.7693	-23855	0.2976	-23855	± 235	0.3214	-18564	± 78
0.8054	-24003	0.3432	-24003	± 226	0.3649	-20903	± 87
0.9581	-27015	0.3874	-27015	± 214	0.4100	-23208	± 96
1.0287	-27994	0.4308	-27994	± 206	0.4517	-25275	± 104
1.1094	-29437	0.4711	-29437	± 201	0.4906	-27152	± 111

1.1655	-28330	0.5082	-28330	±	184	0.5259	-28703	±	116
1.2102	-27545	0.5418	-27545	±	172	0.5577	-29997	±	120
1.3082	-27066	0.5727	-27066	±	157	0.5876	-31073	±	122
1.3413	-24990	0.6010	-24990	±	141	0.6144	-31902	±	124
1.4825	-24271	0.6273	-24271	±	124	0.6402	-32550	±	124
1.5012	-21950	0.6516	-21950	±	111	0.6630	-33013	±	123
1.5963	-20274	0.6737	-20274	±	96	0.6843	-33323	±	121
1.6467	-18137	0.6940	-18137	±	83	0.7036	-33501	±	119
1.7577	-15471	0.7127	-15471	±	67	0.7218	-33533	±	116
1.8239	-13375	0.7301	-13375	±	56	0.7385	-33474	±	112
1.8917	-6487	0.7461	-6487	±	26	0.7537	-33192	±	107
1.9738	3026	0.7608	3026	±	12	0.7679	-32646	±	100
2.0156	17570	0.7743	17570	±	66	0.7808	-31751	±	91
2.1611	28626	0.7869	28626	±	100	0.7931	-30641	±	80
2.2072	38862	0.7987	38862	±	133	0.8043	-29393	±	69

Section D: $x_{Li}/x_{Sn} \approx 1:4$; i = Cu; starting amounts: $n_{Li} = 3.0269 \cdot 10^{-3}$ mol; $n_{Sn} = 12.0795 \cdot 10^{-3}$ mol, starting alloy made from dropping Li in Sn, calibration: 5 pieces of Sn, calibration constant $k = (0.7834 \pm 0.0027)$ J/(μV·s)

0.0000		0.0000				0.0000	-11006		
1.2644	43171	0.0386	248	±	116	0.0772	-10137	±	9
1.3169	43050	0.1116	-1206	±	111	0.1459	-9472	±	17
1.4439	45717	0.1782	-2234	±	108	0.2104	-8926	±	23
1.5464	48188	0.2399	-2734	±	106	0.2694	-8463	±	30

1.6243	46888	0.2960	-5029 ± 98	0.3226	-8212 ± 35
1.7292	48241	0.3470	-5999 ± 95	0.3714	-8053 ± 39
1.8275	50044	0.3936	-6512 ± 93	0.4158	-7944 ± 43
1.9228	51516	0.4360	-7104 ± 91	0.4562	-7886 ± 46
1.9834	51792	0.4744	-7783 ± 89	0.4925	-7879 ± 49
2.0895	54042	0.5091	-8032 ± 88	0.5258	-7889 ± 51
2.1442	54949	0.5407	-8269 ± 87	0.5557	-7913 ± 54
2.2464	56918	0.5694	-8559 ± 86	0.5832	-7953 ± 56
2.3173	57863	0.5957	-8926 ± 85	0.6083	-8012 ± 57
2.3726	60934	0.6196	-8214 ± 87	0.6310	-8023 ± 59
2.4413	62437	0.6414	-8321 ± 87	0.6517	-8040 ± 61
2.5132	66124	0.6613	-7585 ± 89	0.6708	-8015 ± 62
2.5773	69533	0.6796	-6917 ± 92	0.6883	-7957 ± 64
2.6678	73454	0.6964	-6363 ± 94	0.7046	-7874 ± 65
2.7556	78629	0.7121	-5362 ± 97	0.7197	-7745 ± 67
2.8442	82386	0.7267	-4930 ± 98	0.7337	-7604 ± 69
2.9341	88256	0.7403	-3817 ± 116	0.7468	-7418 ± 9

Section E: $x_{Li}/x_{Sn} \approx 1:1$; i = Cu; starting amounts: $n_{Li} = 8.6616 \cdot 10^{-3}$ mol; $n_{Sn} = 8.6560 \cdot 10^{-3}$ mol, starting alloy made from dropping Li in Sn, calibration: 5 pieces of Sn, calibration constant $k = (0.5944 \pm 0.0032)$ J/(µV·s)

0.0000		0.0000		0.0000	-27794
0.8344	26253	0.0230	-2428 ± 169	0.0460	-26628 ± 8
0.8771	26726	0.0680	-3419 ± 164	0.0899	-25559 ± 15

0.9703	29099	0.1120	-3902	±	161	0.1341	-24508	±	22
1.0236	30438	0.1552	-4155	±	160	0.1763	-23517	±	29
1.1607	34291	0.1978	-4347	±	159	0.2194	-22514	±	36
1.2203	35711	0.2397	-4626	±	157	0.2601	-21581	±	42
1.2772	37121	0.2792	-4827	±	156	0.2983	-20714	±	48
1.3640	39735	0.3167	-4761	±	157	0.3351	-19879	±	54
1.4049	41363	0.3521	-4450	±	158	0.3691	-19089	±	59
1.4926	44352	0.3854	-4176	±	160	0.4017	-18320	±	64
1.5719	47377	0.4171	-3752	±	162	0.4325	-17570	±	69
1.6144	49679	0.4467	-3120	±	166	0.4610	-16843	±	74
1.7203	53488	0.4747	-2799	±	167	0.4884	-16130	±	79
1.7802	57425	0.5012	-1634	±	174	0.5140	-15405	±	83
1.9103	62046	0.5263	-1411	±	175	0.5387	-14693	±	88
1.9504	64351	0.5501	-898	±	177	0.5615	-14012	±	93
2.0330	67970	0.5722	-458	±	180	0.5829	-13348	±	97
2.1217	71384	0.5931	-247	±	181	0.6032	-12711	±	101
2.2138	74828	0.6128	-90	±	182	0.6224	-12102	±	105
2.2200	74350	0.6311	-400	±	180	0.6398	-11562	±	108

Table 7: Experimental values of the integral molar enthalpy of mixing at the intersection points a, b, c, d, e and f

Intersection	Composition			Integral molar enthalpy of mixing $\Delta_{mix}H$ / J $\cdot$ mol^{-1}				
				A	B	C	D	E
	x_{Cu}	x_{Li}	x_{Sn}	$Cu_{0.5}Sn_{0.5}$ + Li	$Cu_{0.4}Sn_{0.6}$ + Li	$Cu_{0.2}Sn_{0.8}$ + Li	$Li_{0.2}Sn_{0.8}$ + Cu	$Li_{0.5}Sn_{0.5}$ + Cu
a	0.443	0.114	0.443	-8800			-7900	
b	0.351	0.133	0.516		-9350		-8100	
c	0.161	0.173	0.666			-10300	-9300	
d	0.333	0.334	0.333	-20200				-19900
e	0.250	0.375	0.375		-22800			-21800
f	0.112	0.444	0.444			-24700		-24800

Table 8: Similarity coefficients and deviation sum of squares for Chou's model [48; 49] applied on Cu-Li-Sn

Deviation sum of squares	$\frac{\eta_I}{J^2/mol^2} = 39{,}312{,}253$		$\frac{\eta_{II}}{J^2/mol^2} = 785{,}249{,}940$		$\frac{\eta_{III}}{J^2/mol^2} = 471{,}413{,}453$	
Interaction of	Cu-Li	Cu-Sn	Li-Cu	Li-Sn	Sn-Cu	Sn-Li
			$\eta_{II} > \eta_{III} \gg \eta_I$			
Similarity coeff.	$\xi_{CuLi} = 0.0477$		$\xi_{LiSn} = 0.6247$		$\xi_{SnCu} = 0.9230$	
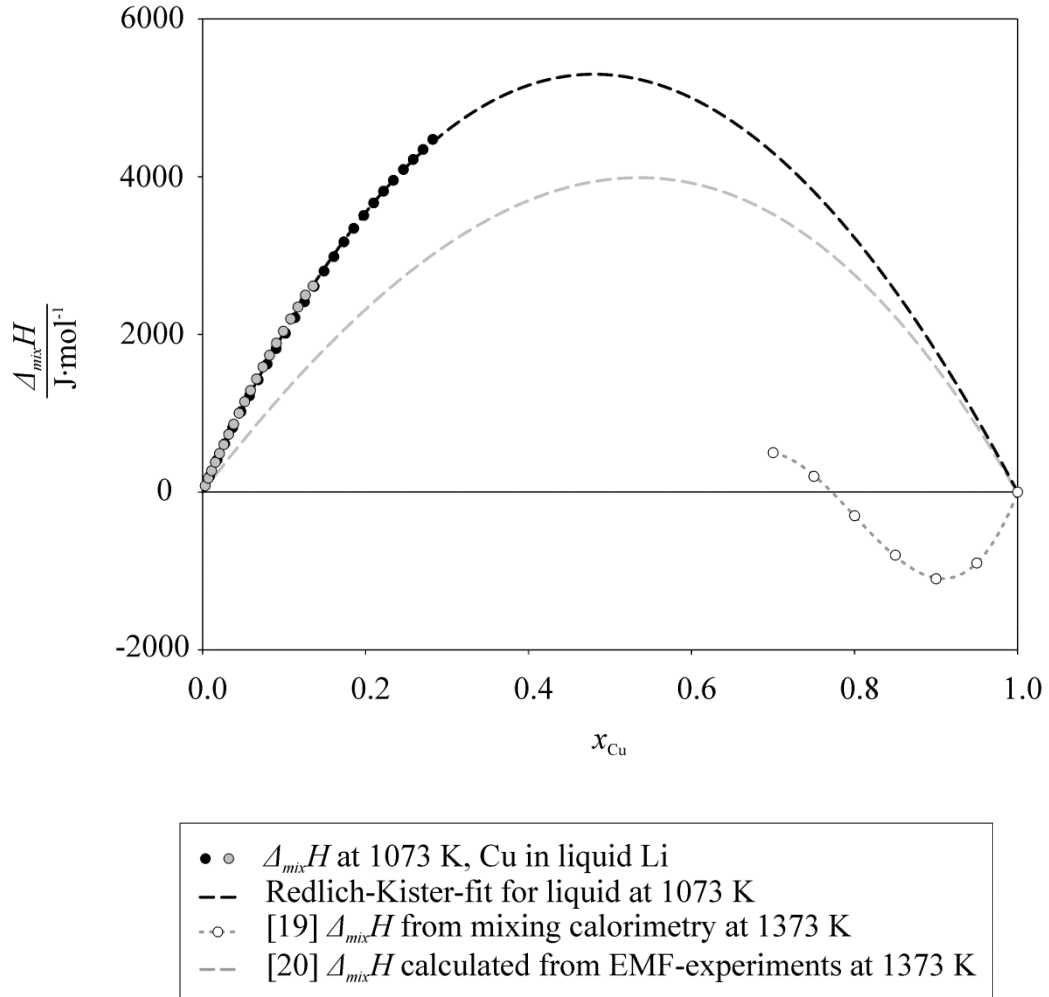
Fig. 1: Integral molar enthalpies of mixing of liquid Cu-Li alloys at 1073 K; comparison with literature values
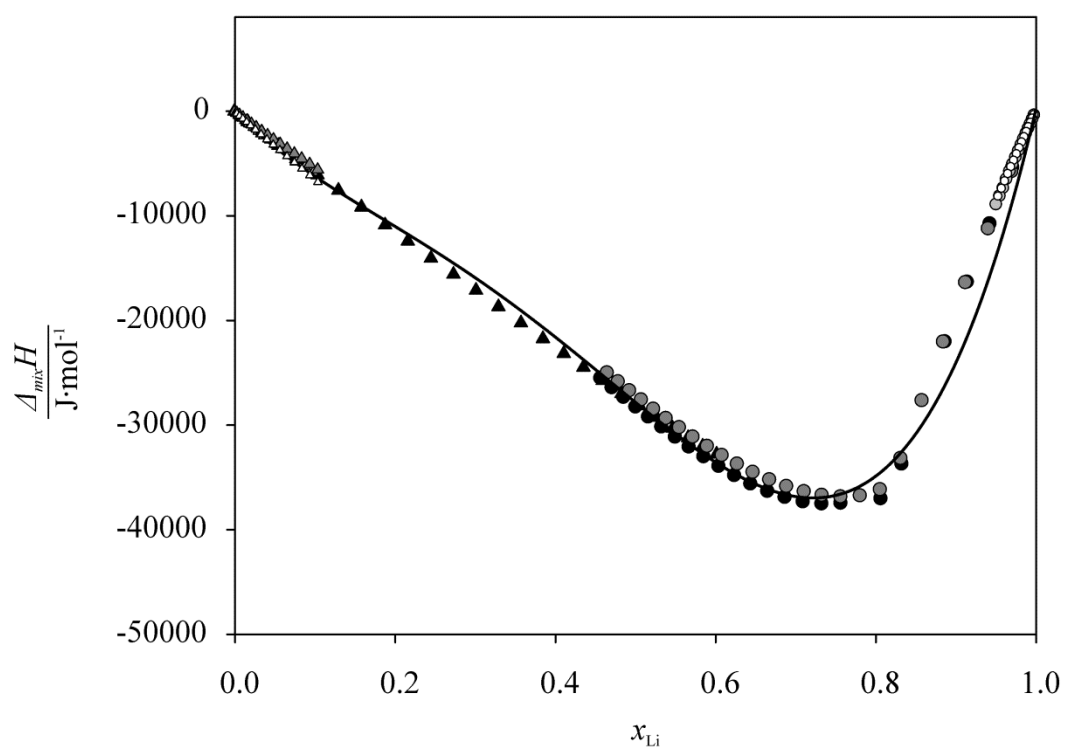
Fig. 2: Integral molar enthalpies of mixing of liquid Li-Sn alloys at 1073 K
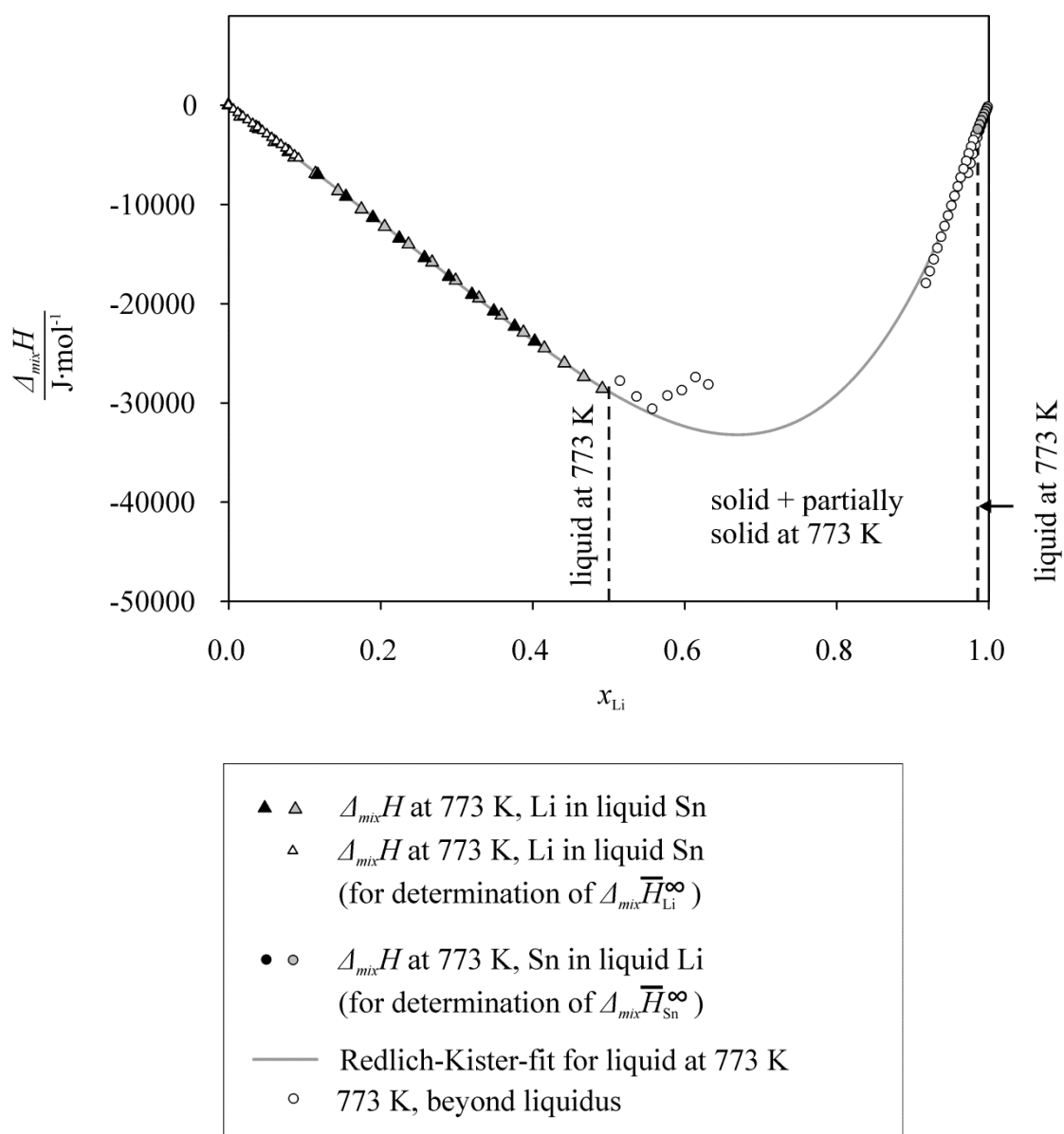
Fig. 3: Integral molar enthalpies of mixing of liquid Li-Sn alloys at 773 K
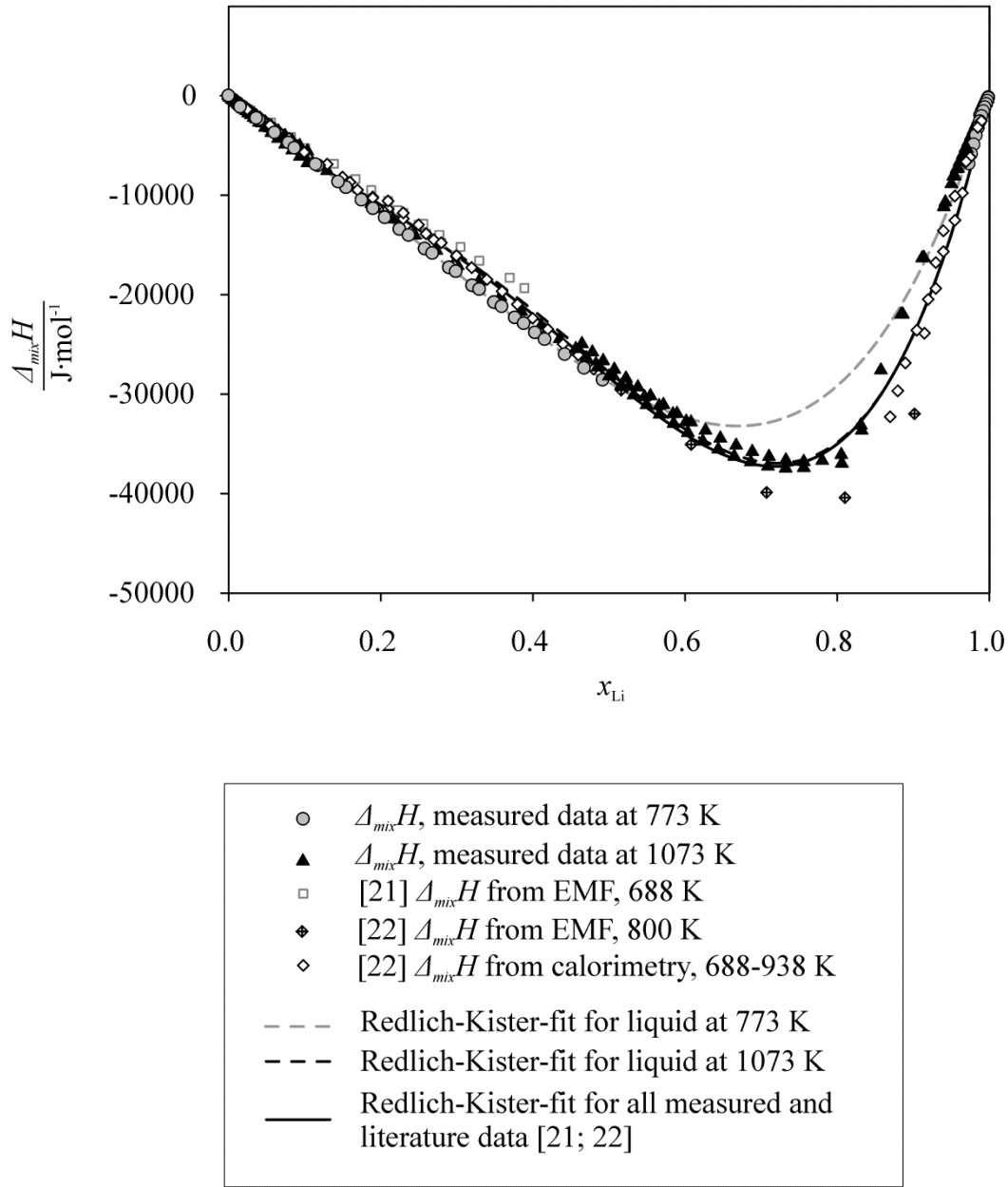
Fig. 4: Integral molar enthalpies of mixing of liquid Li-Sn alloys at 773 K and 1073 K; comparison with literature values
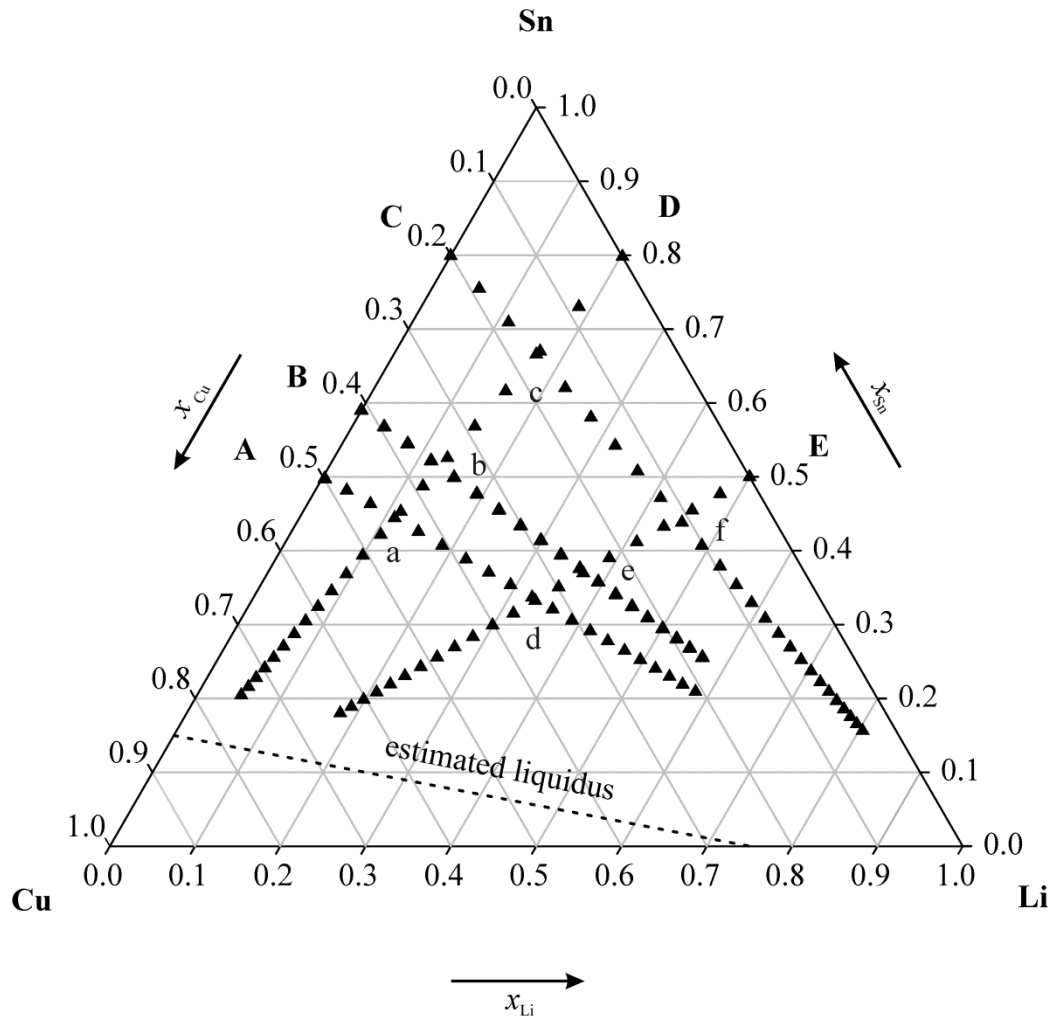
Fig. 5: Measured sections (A, B, C, D, E) and alloy compositions in the ternary Cu-Li-Sn system at 1073 K
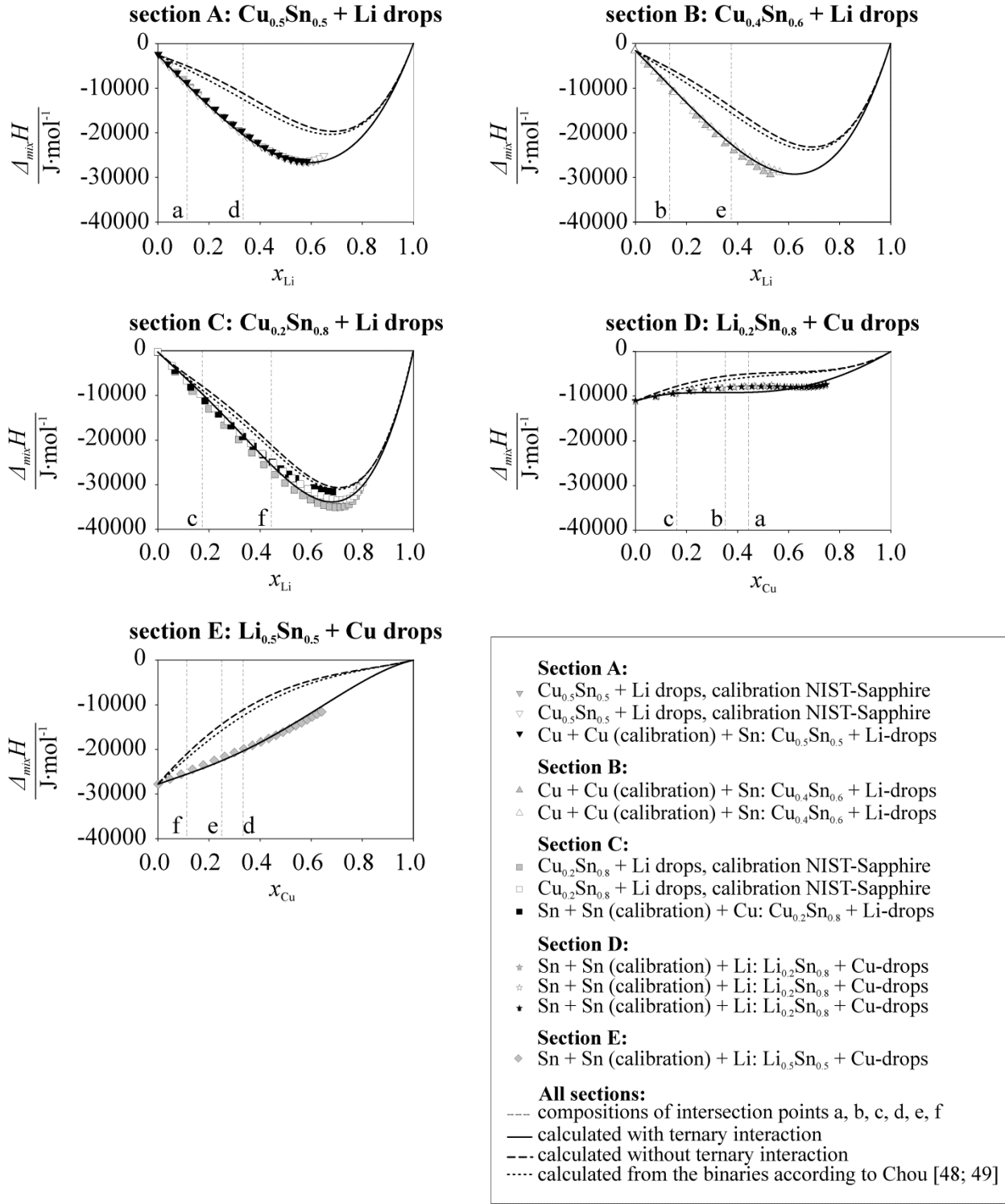
Fig. 6: Integral molar enthalpies of mixing of liquid Cu-Li-Sn alloys at 1073 K for the sections: (A) Cu$_{0.5}$Sn$_{0.5}$ + Li-drops; (B) Cu$_{0.4}$Sn$_{0.6}$ + Li-drops; (C) Cu$_{0.2}$Sn$_{0.8}$ + Li-drops; (D) Li$_{0.2}$Sn$_{0.8}$ + Cu-drops; (E) Li$_{0.5}$Sn$_{0.5}$ + Cu-drops; standard states: pure liquid metals. Comparison between fit with ternary interactions, fit without ternary interactions and extrapolation from binary data [48; 49]
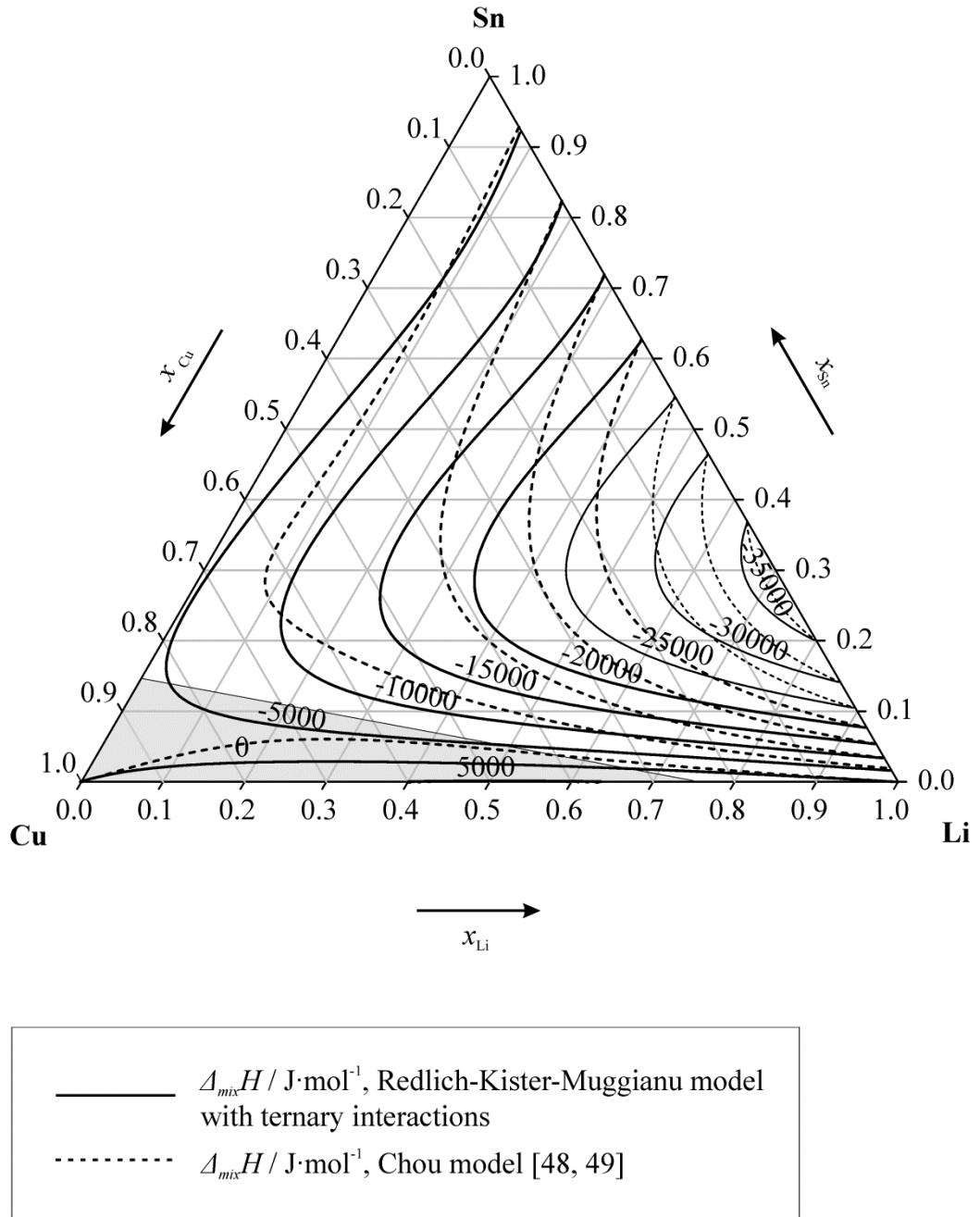
Fig. 7: Isoenthalpy curves of liquid Cu-Li–Sn alloys at 1073 K; standard states: pure liquid metals; metastable liquid region is indicated by shadowed field.

3.2 Publication #2

CuLi$_2$Sn and Cu$_2$LiSn: Characterization by single crystal XRD and structural discussion towards new anode materials for Li-ion batteries.

Siegfried Fürtauer[†], Herta S. Effenberger[‡], Hans Flandorfer[†]

[†]Institute of Inorganic Chemistry (Materials Chemistry), University of Vienna, Währingerstraße 42, A-1090 Wien, Vienna

[‡]Institute of Mineralogy und Crystallography, University of Vienna, Althanstraße 14, A-1090 Wien, Vienna

Contributions to this paper:

|	
S. Fürtauer:	Sample preparation, measurement, structural comparison, writing
H. Effenberger	Measurement and data refinement, writing, proofreading
H. Flandorfer:	General advice and helpful comments, proofreading

Overall contributions of S. Fürtauer to the paper: 70%

Abstract

The stannides $CuLi_2Sn$ (CSD-427095) and Cu_2LiSn (CSD-427096) were synthesized by induction melting of the pure elements and annealing at 400 °C. The phases were reinvestigated by X-ray powder and single-crystal X-ray diffractometry. Within both crystal structures the ordered CuSn and Cu_2Sn lattices form channels which host Cu and Li atoms at partly mixed occupied positions exhibiting extensive vacancies. For $CuLi_2Sn$, the space group $F\bar{4}3m$ was verified (structure type $CuHg_2Ti$; $a = 6.295(2)$ Å; $wR_2(F^2) = 0.0355$ for 78 unique reflections). The 4(c) and 4(d) positions are occupied by Cu atoms and Cu + Li atoms, respectively. For Cu_2LiSn, the space group $P6_3/mmc$ was confirmed (structure type $InPt_2Gd$; $a = 4.3022(15)$ Å, $c = 7.618(3)$ Å; $wR_2(F^2) = 0.060$ for 199 unique reflections). The Cu and Li atoms exhibit extensive disorder; they are distributed over the partly occupied positions 2(a), 2(b) and 4(e). Both phases seem to be interesting in terms of application of Cu-Sn alloys as anode materials for Li-ion batteries.

Introduction

Intermetallic compounds in Li-containing systems are in focus of research due to the promising application of intermetallic alloy electrodes in enhanced Li-ion batteries [1-3]. Special interest has been drawn to Sn containing systems. The binary compound $Li_{17}Sn_4$ offers, for example, a theoretical energy density of 960 mAh/g, compared to a theoretical energy density of 372 mAh/g for LiC_6, which is formed in currently commercially used graphite anodes [4]. The pronounced volume change by reversible insertion of Li atoms into the Sn containing compound, however, is a main obstacle for practical application of such alloys at room temperature. Cu-Li-Sn compounds are a promising prospective material system for improved anode materials. Cu probably acts as a buffer to overcome the mechanical stress and electrode destruction during cycling. Based on electrochemical insertion experiments, various authors [5-8] proposed the reaction mechanisms

$$Cu_6Sn_5 + 10\ Li \rightarrow 5\ CuLi_2Sn + Cu$$

$$5\ CuLi_2Sn + 11.25\ Li \rightarrow 5\ Li_{4.25}Sn + 5\ Cu.$$
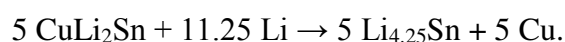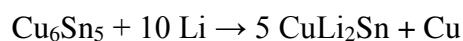
According to this mechanisms the insertion of Li atoms into the compound Cu_6Sn_5 [9] (related to the structure type NiAs) results - besides the formation of a solid solution between Sn and Li in Cu - in the formation of the ternary intermetallic phase $CuLi_2Sn$. Continuing the insertion of Li atoms into $CuLi_2Sn$, again Cu precipitates and the binary

compound $Li_{4.25}Sn$ (= $Li_{17}Sn_4$ [10]), exhibiting the highest known Li content, forms. Despite such electrochemical studies there is still scarce knowledge about the fundamentals of the ternary system Cu-Li-Sn with respect to phase relations, crystallographic and thermochemical data [11]. In contrast, the binary systems Cu−Sn [12, 13], Cu−Li [14] and Li−Sn [15, 16] and their constituting phases have been extensively investigated. For tentative applications of the Cu-Li-Sn system in competitive battery systems, phase relations and knowledge of ternary intermetallic compounds is mandatory. Though the reliable prediction of the formation of ternary compounds based on calculations is limited to some extent, complementary experimental studies are indispensable. The ternary compound $CuLi_2Sn$ was first synthesized by Pauly et al. [17] in the 1960's; they found the structure type $CuHg_2Ti$ for this phase based on X-ray powder diffraction data, a *fcc* atomic arrangement exhibiting the acentric space-group symmetry $F\bar{4}3m$. Later on, Schuster et al. [18, 19] refined this crystal structure again with powder X-ray techniques, but they found the centric space group $Fm\bar{3}m$. The two structure models are essentially the same but differ with respect to an order–disorder phenomenon. In the acentric structure model Li and Cu are ordered to a large extent occupying the 4(c) and 4(d) position whereas in the centric structure model these two atoms are allocated randomly forming the 8(c) mixed occupied site (see Table 1). The ternary compound Cu_2LiSn was only described by Kripyakevich et al. [20]. They found hexagonal symmetry (space group $P6_3/mmc$) from powder-diffraction data (see also Table 1). Even the structure types could be characterized by these authors, details about mixed and/or partly occupied sites as well as the chemical variability and the formation of solid solutions maintained undetected in those days. The actual work aims at an improved and detailed description of the crystal structures of both phases by single-crystal X-ray diffraction and a clarification of the contradicting literature data. Furthermore, the possibility of a mutual substitution of Li and Cu atoms was of interest for the Li insertion mechanisms required for batteries. Although the resulting nomenclature of both compounds, considering occupation ratios of Cu and Li atoms, would be $Cu_{1+x}Li_{2-x}Sn$ for $CuLi_2Sn$ and $Cu_{2+x}Li_{1-y}Sn$ for Cu_2LiSn, the designations with integer values are preferred for easier readability throughout this paper.

Materials and Methods

Sample Preparation

As inserts for sample preparations served the pure elements Cu (99.98 at.%, wire, Goodfellow, Cambridge, UK), Li (99.8 at.%, wire, Alfa Aesar, Karlsruhe, Germany) and Sn (99.95 at.%, ingot, Advent, Oxford, UK). The Cu wire was treated in a H_2-flow for 5 hours at 300°C to remove the oxide layer at the surface. The Li wire was stored originally in mineral oil, which was removed by n-hexane in a supersonic bath followed by vacuum evaporation of the solvent. Visible oxidation spots occurring partially at the surface were removed mechanically with a scalpel. Inside a glove box under Ar atmosphere (< 5 ppm O_2 / H_2O), the metal pieces were assembled in tantalum crucibles, which were made by deep-drawing of a 0.4 mm tantalum sheet. For welding the crucibles in argon atmosphere, an arc furnace with a tungsten electrode of 1.6 mm was used. During the welding process, the crucibles were chilled by a water cooled Cu mount. The filled crucibles were put into an induction furnace at 1100°C for only 10-20 sec to prevent high temperature fatigue of the welding seam. This procedure allowed melting of the input. Repetition of the melting process twice with turning the crucible upside down between the heating steps assured homogenous mixing. After that, the crucibles were sealed in quartz glass tubes under vacuum and annealed at 400°C in a muffle furnace. After 35 days the samples were quenched in cold water and opened in the glove box with a bolt cutter. The obtained alloys were very brittle and had a coloured tint ($CuLi_2Sn$: metallic pink; Cu_2LiSn: metallic violet).

Powder XRD

In a glove box small amounts of the samples were grinded with a Durit® mortar. The obtained powder had a particle size < 25µm, therefore sieving was not necessary. For powder XRD measurements a Bragg-Brentano diffractometer ($\Theta/2\Theta$-geometry) with a Cu radiation source (40 kV / 40 mA) and a Ni filter were used. Signals were detected by a strip detector. A silicon mono-crystal was used as sample holder. The powdered sample was fixed by petroleum jelly on the sample holder in the glove box. Oxidation was prevented by an X-ray amorphous cap of polycarbonate, which maintained the protection gas atmosphere on the sample. The obtained patterns were evaluated by Rietveld-refinements using Topas3® [21] software.

Single-crystal XRD

The models of the atomic arrangement published so far [17-19] are based on X-ray investigations by Debye-Scherrer and Straumanis exposures in combination with powder-diffractometer measurements. These methods gave rough information about the structure type only. However, the tentative application for Li-ion batteries requires a detailed knowledge about possible substitution mechanisms which is available only by single-crystal XRD investigations. Samples again had to be protected from interactions with atmosphere. Small amounts of gritty bulk samples were fixed in the glove box with amorphous petroleum jelly between two object plates. Slightly pushing and sliding of the object plates crushed the bulk samples into smaller particles and covered it entirely with the grease. Crystal chips suitable for the X-ray investigations were selected outside the glove box under a binocular microscope (up to 400 fold magnification) and handled with fine acupuncture needles. The respective crystals were approximately 50 µm in diameter; they were fixed onto a glass capillary. During this procedure the samples were kept under petroleum jelly which protected them from altering due to interaction with moisture from the air. Single-crystal XRD was performed with a four-circle Nonius Kappa diffractometer with a CCD detector and a 300 µm capillary optics collimator (MoK$_\alpha$ radiation, graphite monochromator). Isothermal conditions at 290 K were enabled by a continuous stream of nitrogen enclosing the single crystal, which protected the sample from corrosion due to moisture in the atmosphere. After data collection, the unit cell parameters were obtained from least-square refinements of all observed 2ϑ values. Corrections for Lorentz, polarization and absorption effects (multi-scan method) were applied. Complex scattering functions from Wilson [22] and the programs "Collect" [23, 24], "SHELXL-97" [25-27] as well as "PLATON" [28] were used.

Results

Powder XRD measurements were applied to check phase homogeneity of the synthesized samples. Observed diffractograms and refinement results are given in Figs. 1 and 2, respectively. No impurities or any additional phases could be detected. The wide peak at low angles originates from the protection cap. Details of the data collection of single-crystal X-ray investigations and structure refinements are compiled in Table 2, and fractional coordinates and interatomic bond distances are given in Table 3 and Table 4, respectively. For both cases the atomic coordinates from literature [17-20] served in the starting set of the structure refinement. The space-group symmetries agreed with the

extinction rules. Successive Fourier and difference Fourier summations revealed details of the atomic arrangements. The chemical compositions found from structure investigations are in accordance with the atomic fractions of the input for syntheses. Structural parameters including anisotropic displacements were refined (Table 3). In $CuLi_2Sn$, the atomic sites were considered as fully but partly mixed occupied according to the chemical formula $Cu_{1+x}Li_{2-x}Sn$ including occupation ratios (see also Table 3). The highest peaks in the electron densities found in the final difference Fourier maps are located close to Sn or Cu sites. In Cu_2LiSn occurs an extensive atomic dislocation going along with partial occupied sites (see discussion).

Discussion

$CuLi_2Sn$

All atoms occupy special positions. Besides changed point symmetries in the two proposed space groups $Fm\overline{3}m$ and $F\overline{4}3m$ the sites 4(a) and 4(b) are identical and occupied by Sn and Li atoms, respectively, corresponding to the NaCl structure type. All cubic eightfold coordinated voids are occupied by further Li atoms and by the Cu atoms. The acentric space group $F\overline{4}3m$ allows order between the sites 4(c) (¼ ¼ ¼) and 4(d) (¾ ¾ ¾), whereas in $Fm\overline{3}m$ these two sites are crystallographically identical - site 8(c) - resulting in a statistical occupation by Cu and Li atoms. Different syntheses methods are quoted as tentative reasons for the distinct distribution of the Li and Cu atoms. Already Schuster et al. [19] discussed these differences and mentioned that some of the intensities in the powder pattern vary significantly. Actual refinements were performed for both structure models. As an example, the reflections 111, 200, 220 and 311 have structure-factor ratios of 52:32:100:84 in the centrosymmetric and 72:32:100:66 in the acentric space group if the ideal composition $CuLi_2Sn$ is considered [29]; single-crystal data clearly correspond better with the latter one: 72:20:100:54. After a few cycles of the least-squares refinement in the acentric space group $F\overline{4}3m$ a satisfactory result could be observed. Especially the difference Fourier summation calculated with the three sites 4(a)-Sn, 4(c)- and 4(d)-(Cu,Li) clearly showed the highest residual density at the site 4(b) which could be refined considering full occupation by Li atoms successfully (see Table 3 and Fig. 3). In contrast, refinements in space group $Fm\overline{3}m$ with the Sn atoms at the site 4(a) and (Cu,Li) at 8(c) astonishingly didn't show further residual densities at the site 4(b). Trials to refine this latter position occupied by Li atoms failed (either the occupation factor dropped down to zero or the displacement parameter increased to a physically

unrealistic value) suggesting the chemical composition CuLiSn which contradicts the expectations from syntheses. A centrosymmetric structure model for CuLiSn exhibits an unusual fourfold coordination polyhedron around the atoms Sn and Cu/Li which is not in agreement with crystal chemical expectations. Also the volume per atom is too large for a formula CuLiSn (20.8 Å³) whereas it is in the expected range for $CuLi_2Sn$ (15.6 Å³). However, the *R* values are practically the same (R_1 = 0.014 and wR_2 = 0.038 for 46 reflections and 6 variable parameters; chemical formula CuLiSn; space group $Fm\overline{3}m$) as compared with the refinements in space group $F\overline{4}3m$ (R_1 = 0.013 and wR_2 = 0.036 for 78 reflections and 9 variable parameters; chemical composition $CuLi_2Sn$). Finally, the structural data for $CuLi_2Sn$ are given in the acentric space group due to crystal chemical reasons. The larger displacement parameter observed for the Cu/Li site (0.034 Å²) is to be mentioned; it might be an artefact of some systematic errors in the data set and high correlation terms. Refinements without a partial substitution of Cu at the site 4(*d*) increase the *R* value and the refinement tends not being stable. The crystal structure of the $CuLi_2Sn$ phase is similar to the γ-Cu_3Sn [13, 30] phase in the Cu-Sn binary system, which is BiF_3-isotype. In γ-Cu_3Sn the Sn and Cu atoms form a NaCl lattice and all cubic holes are filled consequently by further Cu atoms. Each interstitial Cu atom is quasi surrounded by four further Cu atoms and four Sn atoms. The cubic holes can be considered as a two-tetrahedral coordination of Cu by Cu and Sn, respectively. In $CuLi_2Sn$, in contrast, Sn and Li atoms form the NaCl-lattice, interstitial cubic positions are split into 4(*c*)-(¼ ¼ ¼) occupied solely by Cu atoms and 4(*d*)-(¾ ¾ ¾) mainly occupied with Li atoms. Here each interstitial Cu or Li atom is quasi surrounded by four Li atoms and four Sn atoms. Analogue to γ-Cu_3Sn, the cubic holes can be considered as a two-tetrahedral coordination of Cu or Li by Li and Sn, respectively. Tetrahedral fillings with same chemical environment are located on furthermost positions, corresponding to a distance of 4.4512(6) Å (half-length of face diagonal). In such an arrangement distances between atoms of the same kind are larger than in γ-Cu_3Sn [30] (4.3258(6) Å). This effect is accompanied by the expansion of the lattice compared to γ-Cu_3Sn. The refined crystal structure is closely related to the ferromagnetic Heusler phases [31, 32] (space group $Fm\overline{3}m$, $AlCu_2Mn$ type), which have the general formula XY_2Z. X is a main group element (group 13-15) at the 4(*a*) site 000 (*e.g.* Al), Y is a transition element at the 8(*c*) site ¼ ¼ ¼ (*e.g.* Cu), and Z is a transition element at the 4(*b*) site ½ ½ ½ (*e.g.* Mn). This means that Al and Mn atoms form a NaCl lattice and all cubic holes are filled with atoms of one kind, namely Cu. In the $CuLi_2Sn$ structure, as already mentioned, the NaCl-like lattice is formed of Sn atoms, which is a group 13-15 element, and from Li, which is an alkali

element. Furthermore the cubic holes are not filled solely by Cu atoms, but by Cu and by positions mixed occupied by both Li and Cu atoms. These two differences to the Heusler phase result in a non-ferromagnetic, but as reported weak diamagnetic behavior [19]. Along the [110] direction (face diagonal), chair-shaped CuSn-hexagons show up which are condensed *via* adjacent edges and show a honeycomb-like structure in the projection (see Fig. 4a). The corners of the chair-shaped hexagons consist of shifted stacks of Cu and Sn atoms, respectively. The shifting vector between atoms of the Cu and Sn stacks is 2.2256(3) Å, which is a quarter of the unit cell's face diagonal. The formed hexagonal CuSn channel contains two piles with Li and mixed Cu/Li atoms each, which are also shifted to each other by a shifting vector of 2.2256(3) Å. Fig. 5a shows the vertical section of such a channel according to the shaded area in Fig. 4a. The atoms could be considered as ideal spheres with purely atomic radii [33]. However, this only approximates the real relations in the crystal lattice, because polarisation effects due to different electronegativity values between the Cu, Li and Sn atoms, respectively, would modify the atomic radii significantly (*e.g.* Li: r_{atom} = 1.520 Å, $r_{covalent}$ = 1.230 Å, r_{ionic} = 0.780 Å, values taken from Emsley [33]). The open diameter of the Li-conducting channel is 2.537(4) Å, which would allow an atom with a radius of 1.268(2) Å to penetrate. This is somewhere between the atomic and the covalent radius of Li and raises hope that this material could be interesting for technical applications.

Cu₂LiSn

The refinement was started from the atomic coordinates given by Kripyakevich and Oleksiv [20]. In addition to the sites 2(*c*), 4(*f*) and 2(*a*) given by the former authors, the difference Fourier summation showed a significant electron density also at 4(*e*) and 2(*b*) (Fig. 6). Site 2(*c*) is occupied by Sn atoms and site 4(*f*) by Cu atoms. The Cu atoms located at the 4(*f*) site form six-membered rings with chair configuration. Mirror inverted pairs of chair-shaped Cu rings are stacked in the [001] direction and centred in z = 0.09/ 0.91 and z = 0.41/0.59, respectively. The Sn atoms at 2(*c*) are located within the Cu chains forming the channels along [001]. Two Cu atoms are separated by one Sn atom. Considering its coordination sphere it is surrounded by eight Cu atoms forming a *di*capped trigonal prismatic coordination polyhedron (Fig. 7). The three additional sites labelled Cu/Li1 to Cu/Li3 require further discussion due to (1) too short contacts between these positions, (2) excess of electrons as compared to a full occupation of any of these three sites with Li atoms and (3) stoichiometry. In total there are eight atom positions for the Cu/Li atoms in the unit cell, all located at (00z). Full site occupation can be realised

solely either on 2(a) or 2(b). An occupation of the site 4(e) only requires half occupation; ordering requires a reduction of space-group symmetry to $P6_3mc$. If either site 2(a) or 2(b) is fully occupied, two atoms per unit cell are possible. If the sites 2(a), 2(b) and 4(e) are partially occupied, the maximum filling level per unit cell is 2.5 atoms to avoid too close atom-atom contacts. This can be achieved either by a combination of the partially occupied positions 2(a) and 4(e) or by 2(a), 2(b) and 4(e) (for possible combinations of partially occupied positions see Fig. 8). It could be assumed, that the mixed Cu/Li atoms at the 2(b), 4(e) and 2(a) sites are somehow mobile along the (00z) axis and migrate along channels (Fig. 4b), built up from the eightfold coordination polyhedron (Fig. 7). Due to the mixed occupations of the 2(b), 4(e) and 2(a) sites, including the occupation ratios, the chemical formula in this case has two variable parameters: $Cu_{2+x}Li_{1-y}Sn$. Despite a full occupation of none of the three Cu/Li sites is possible considering all of them, the electron density exceeds the expected scattering power of two Li atoms per unit cell; the refinement converges for 4.8 Li atoms per unit cell. Consequently a mixed occupation is considered. Due to crystal chemical experiences, a partial substitution by Cu atoms seems most probable. Trials refining the structure model with variable Cu:Li ratios failed; therefore a refinement with the scattering power of Li alone and allowing an excess of atoms was performed (see Table 3, footnote[1]). The occupation of the sites 2(a), 2(b) and 4(e) is not completely statistical but exhibits some order mechanisms. It is verified by a significant elongation of the X-ray scattering reflections parallel to c (see Table 3, footnote[2]). In a few cases it was possible to resolve them as satellite reflections. However, most of the main and their satellite reflections are overlapping and a separate measurement was not possible; a **q** vector could not at all be determined. Anyhow, the crystal structure of this phase has to be considered as incommensurate with an extended portion of disorder. The before mentioned channels in this phase are, similar to the $CuLi_2Sn$ phase, probably wide enough to allow a migration of Li and Cu atoms, respectively. Fig. 5b shows a vertical section of the channels according to the shaded area in Fig. 4b. The open diameter of the Li-conducting channels is 2.434(5) Å. This is less than in the $CuLi_2Sn$ phase, but in the Cu_2LiSn phase the channels are filled only with one pile of Cu/Li atoms. This leads to shorter diffusion paths along the channel, what could be beneficially for the Li-"ion" migration. The structural relationship between the binary phase ε-Cu_3Sn [34] and the corresponding Cu_2LiSn phase are not obvious on the first glance, but astonishingly close. Considering the half unit cell of the ε-Cu_3Sn phase, it consists of parallel zigzag layers of Cu_2Sn subunits. A third Cu atom that corresponds to

each Sn atom is opposed to the Cu atoms belonging to the Cu_2Sn subunits, forming a ridge along the Sn atoms (see Fig. 9). By aligning the Sn atoms into the centre of the Cu_2Sn subunits and removing the opposing Cu atom on the ridge, the hexagonal backbone of the Cu_2LiSn phase is formed. The Cu atoms of one layer are now located in a shorter distance to the closest Sn atom of another layer (d_{Cu-Sn} = 2.5825(6) Å) than to that one within the same layer (d_{Cu-Sn} = 2.7702(7) Å). During this alignment of the Cu_2Sn layers the previous mentioned honeycomb-shaped (Cu/Li)-channels open up and Li atoms may be inserted (compare Fig. 4b).

Conclusions

The compounds $CuLi_2Sn$ and Cu_2LiSn have been re-investigated by powder and single-crystal diffractometry. For $CuLi_2Sn$ and Cu_2LiSn ordered CuSn and Cu_2Sn lattices, respectively, were found. Extensive Cu-Li substitutions were proofed from structure refinements. This is in accordance with the variable chemical composition and the extension in both phase fields towards higher Cu concentrations at constant Sn content. Both structures could be relevant for the application of Cu-Sn alloys as anodes in Li-ion batteries. The theoretical capacity of $CuLi_2Sn$ is 273 mAh/g, that one of Cu_2LiSn is 106 mAh/g. Besides beneficial gravimetric capacities also sufficient kinetic properties are mandatory. Several studies have investigated the electrochemical performance of the $CuLi_2Sn$ phase [6, 8, 35, 36], one in particular which measured the kinetic properties [37]. On the other hand, the kinetic properties of Cu_2LiSn have not been treated by literature and are therefore still unknown. These would be of great interest hence the Cu-Sn main body of Cu_2LiSn shows very close structural relationship to ε-Cu_3Sn. A direct equilibrium of both phases caused by lithiation can be assumed. Generally, the mechanism of Li insertion and the reaction schemes are still widely unknown. The elucidation of these questions will be substantial for further works. Further details on the structure refinement are available from FIZ Karlsruhe [38] by quoting the registry numbers CSD-427095 ($CuLi_2Sn$) and CSD-427096 (Cu_2LiSn).

References

[1]   M. S. Whittingham, MRS Bull. 33 (2008) 411-419.

[2]   C. Daniel, JOM 60 (2008) 43-48.

[3]   H. J. Seifert; Materials with New Design for Improved Lithium Ion Batteries. http://www.spp1473.kit.edu/ (April 2014),

[4]   A. K. Shukla; T. P. Kumar, Curr. Sci. India 94 (2008) 314-331.

[5]   A. Jansen; J. Clevenger; A. Baebler; J. Vaughey, J. Alloys Compd. (2011) 4457–4461.

[6]   W. Choi; J. Y. Lee; H. S. Lim, Electrochem. Commun. 6 (2004) 816-820.

[7]   S. Sharma; L. Fransson; E. Sjostedt; L. Nordstrom; B. Johansson; K. Edstrom, J. Electrochem. Soc. 150 (2003) A330-A334.

[8]   K. D. Kepler; J. T. Vaughey; M. M. Thackeray, Electrochem. Solid St. 2 (1999) 307-309.

[9]   A. Gangulee; G. C. Das; M. B. Bever, Metall. Trans. 4 (1973) 2063-2066.

[10]   C. Lupu; J. G. Mao; J. W. Rabalais; A. M. Guloy; J. W. J. Richardson, Inorg. Chem. 42 (2003) 3765-3771.

[11]   S. Fürtauer; E. Tserenjav; A. Yakymovych; H. Flandorfer, J. Chem. Thermodyn. 61 (2013) 105-116.

[12]   D. Li; P. Franke; S. Fürtauer; D. Cupid; H. Flandorfer, Intermetallics 34 (2013) 148-158.

[13]   S. Fürtauer; D. Li; D. Cupid; H. Flandorfer, Intermetallics 34 (2013) 142-147.

[14]   A. D. Pelton, Bull. Alloy Phase Diagr. 7 (1986) 142-144.

[15]   D. Li; S. Fürtauer; H. Flandorfer; D. M. Cupid, CALPHAD 47 (2014) 181-195.

[16]   J. Sangster; C. W. Bale, J. Phase Equilib. 19 (1998) 70-75.

[17]   H. Pauly; A. Weiss; H. Witte, Z. Metallkd. 59 (1968) 47-58.

[18]   H. U. Schuster, Naturwissenschaften 53 (1966) 360-361.

[19]   H. U. Schuster; D. Thiedemann; H. Schönemann, Z. Anorg. Allg. Chem. 370 (1969) 160-170.

[20]   P. I. Kripyakevich; G. I. Oleksiv, Dopov. Akad. Nauk Ukr. RSR A (1970) 63-65.

[21]   Bruker-AXS Topas, Version 3; Billerica / MA, 1999 / 2000.

[22] A. J. C. Wilson, *International tables for crystallography*. Kluwer: Dordrecht / NL, 1992.

[23] Z. Otwinowski; W. Minor, Method. Enzymol. 276 (1997) 307-326.

[24] B. V. Nonius Collect - data collection software, Delft / Netherlands, 1999.

[25] G. M. Sheldrick, Acta Crystallogr. A 64 (2008) 112-122.

[26] G. M. Sheldrick SHELXS 97 - a program for the solution of crystal structures, Göttingen, 1997.

[27] G. M. Sheldrick SHELXL 97 - a program for crystal structure refinement, Göttingen, 1997.

[28] A. L. Spek, Acta Crystallogr. Sect D - Biol. Crystallogr. 65 (2009) 148-155.

[29] K. Yvon; W. Jeitschko; E. Parthe, J. Appl. Crystallogr. 10 (1977) 73-74.

[30] H. Knödler, Metall 20 (1966) 823-829.

[31] F. Heusler; W. Starck; E. Haupt, Verh. Dtsch. Phys. Ges. 5 (1903) 219-223.

[32] O. Heusler, Ann. Phys. 19 (1934) 155-201.

[33] J. Emsley, The Elements. Clarendon Press: Oxford, 1989.

[34] Y. Watanabe; Y. Fujinaga; H. Iwasaki, Acta Crystallogr. B - Struct. Sci. 39 (1983) 306-311.

[35] G. X. Wang; L. Sun; D. H. Bradhurst; S. X. Dou; H. K. Liu, J. Alloys Compd. 299 (2000) L12-L15.

[36] Y. S. Lin; J. G. Duh; H. S. Sheu, J. Alloys Compd. 509 (2011) 123-127.

[37] J. J. Zhang; P. He; Y. Y. Xia, Electroanal. Chem. 624 (2008) 161-166.

[38] ICSD, Inorganic Crystal Structure Database, FIZ Karlsruhe - Leibniz-Institut für Informationsinfrastruktur, Hermann-von-Helmholtz-Platz 1, 76344 Eggenstein-Leopoldshafen, 2013.

Table 1: Literature crystal structures for CuLi$_2$Sn and Cu$_2$LiSn

phase	isotype	Pearson symbol	space group	SG No	a (Å)	c (Å)	Atom	site	x	y	z	occ.	Ref.
CuLi₂Sn	CuHg₂Ti	cF16	$F\bar{4}3m$	216	6.282(3)	-	Sn	4a	0	0	0	1.0	[17]
							Li1	4b	0.5	0.5	0.5	1.0	
							Li2	4c	0.25	0.25	0.25	1.0	
							Cu	4d	0.75	0.75	0.75	1.0	
CuLi₂Sn	AlCu₂Mn	cF16	$Fm\bar{3}m$	225	6.263	-	Sn	4a	0	0	0	1.0	[18,19]
							Li1	4b	0.5	0.5	0.5	1.0	
							Li2	8c	0.25	0.25	0.25	0.5	
							Cu	8c	0.25	0.25	0.25	0.5	
Cu₂LiSn	InPt₂Gd	hP8	*P63/mmc*	194	4.303	7.637	Li	2a	0	0	0	1.0	[20]
							Sn	2c	1/3	2/3	0.25	1.0	
							Cu	4f	1/3	2/3	0.583	1.0	

Table 2: Single-crystal X-ray data-collection and crystal structure refinements of CuLi$_2$Sn and Cu$_2$LiSn. Cell parameters determined from PXRD are given in square brackets.

	CuLi$_2$Sn	Cu$_2$LiSn
(ideal) chemical formula	CuLi$_2$Sn	Cu$_2$LiSn
nominal composition of sample preparation	Cu$_{0.25}$Li$_{0.50}$Sn$_{0.25}$	Cu$_{0.50}$Li$_{0.25}$Sn$_{0.25}$
chemical formula including occupation ratios	Cu$_{1+x}$Li$_{2-x}$Sn	Cu$_{2+x}$Li$_{1-y}$Sn
a (Å)	6.295(2)	4.3022(15)
	[6.27922(8)]	[4.30711(8)]
c (Å)	—	7.618(3)
		[7.6198(1)]
space group (no.)	$F\bar{4}3m$ (216)	$P6_3/mmc$ (194)
V (Å^3)	249.5	122.1
Pearson symbol	$cF16$	$hP8$
Z	4	2
ρ_{calc} (g cm^{-3}) / μ(Mo$K\alpha$) (mm^{-1})	5.22 / 18.1	6.87 / 27.0
crystal dimensions (μm)	75×95×120	35×60×60
range of data collection ($\pm h \pm k \pm l$) (°)	$3 < 2\vartheta < 70$	$3 < 2\vartheta < 70$
number of images / rotation angle per image (°)	431 / 2.0	603 / 2.0
scan mode (φ-scans at distinct ω-angles)	9 φ-scans	10 φ-scans
scan time (s/°) / frame size 621×576 pixels (binned mode)	20	140
detector-to-sample distance (mm)	30	30
measured reflections	1,018	2,015
unique reflections (n) / observed reflections ($F_o > 4\sigma(F_o)$)	78 / 78	199 / 125
$R_{int} = \Sigma\left| F_o^2 - F_o^2(\text{mean})\right|/\Sigma F_o^2$	0.035	0.034
extinction parameter k:		
$F_c^* = F_c \cdot k(1+0.001\cdot F_c^2\lambda^3/\sin(2\vartheta))^{-1/4}$	0.0086(16)	0.022(5)
$R_1 = \Sigma(\left|\left|F_o\right| - \left|F_c\right|\right|) / \Sigma F_o$ (all / observed reflections)	0.013 / 0.013	0.020 / 0.022
$wR_2 = (\Sigma w(F_o^2 - F_c^2)^2 / \Sigma\left|wF_o^4\right|)^{1/2}$	0.0355	0.060
GooF = $\{\Sigma(w(F_o^2-F_c^2)^2) / (n-p)\}^{0.5}$	1.32	1.03
max Δ/σ; number of variable parameters (p)	< 0.001; 9	< 0.001; 14
final difference Fourier map (eÅ^{-3})	-0.35 to +0.57	-1.26 to +1.01
parameters a / b for weighting scheme	0.022 / 0.19	0.039 / 0.50
racemic twin component	0.09(9)	—
volume per atom (Å^3)	15.6	15.3

Table 3. Fractional atomic coordinates and displacement parameters for CuLi₂Sn and Cu₂LiSn

The anisotropic displacement parameters are defined as: exp (-2π^2 $\Sigma^3_{i=1}$ $\Sigma^3_{j=1}$ U_{ij} a^*_i a^*_j h_i h_j)

	occupation	Wyckoff letter	Site symmetry	x	y	z	U_{equiv} / U_{iso}	U_{11}	U_{22}	U_{33}	U_{23}	U_{13}	U_{12}
CuLi₂Sn													
Sn	Sn$_{1.00}$	4(a)	$\overline{4}3m$	0	0	0	0.0178(3)	0.0178(3)	$= U_{11}$	$= U_{11}$	0	0	0
Cu	Cu$_{1.00}$	4(c)	$\overline{4}3m$	¼	¼	¼	0.0189(12)	0.0189(12)	$= U_{11}$	$= U_{11}$	0	0	0
Li	Li$_{1.00}$	4(b)	$\overline{4}3m$	0	0	½	0.016(7)	0.016(7)	$= U_{11}$	$= U_{11}$	0	0	0
Li/Cu	Li$_{0.846(15)}$Cu$_{0.154}$	4(d)	$\overline{4}3m$	¾	¾	¾	0.034(9)	0.034(9)	$= U_{11}$	$= U_{11}$	0	0	0
Cu₂LiSn													
Sn	Sn$_{1.00}$	2(c)	$\overline{6}m2$	⅓	⅔	¼	0.0174(3)	0.0180(3)	$= U_{11}$	0.0161(3)	0	0	$= ½*U_{11}$
Cu	Cu$_{1.00}$	4(f)	$3m$	⅓	⅔	0.58905(9)	0.0191(3)	0.0200(3)	$= U_{11}$	0.0172(4)	0	0	$= ½*U_{11}$
Li/Cu1	Li$_{0.8(6)}$ [1]	2(a)	$\overline{3}m$	0	0	0	0.028(6) [2]	0.019(5) [2]	$= U_{11}$	0.045(15) [2]	0	0	$= ½*U_{11}$
Li/Cu2	Li$_{0.5(6)}$ [1]	4(e)	$3m$	0	0	0.090(5)	0.028(6) [2]	0.019(5) [2]	$= U_{11}$	0.045(15) [2]	0	0	$= ½*U_{11}$
Li/Cu3	Li$_{0.6(6)}$ [1]	2(b)	$\overline{6}m2$	0	0	¼	0.021(9)						

[1] Excess of Li-atoms was allowed due to electron density

[2] The displacement parameters for the atoms Li/Cu1 and Li/Cu2 in Cu₂LiSn were constrained

Table 4. Interatomic bond lengths (Å) of CuLi₂Sn and Cu₂LiSn

CuLi$_2$Sn

Sn—Cu[0, iii, viii, xiii]	2.7258(10)	Li—Li/Cu[xiii, xvi, xvii, xviii]	2.7258(10)
Sn—Li/Cu[xvii, xviii, xix, xx]	2.7258(10)	Li—Cu[0, v, x xiii]	2.7258(10)
Cu—Li[0, iv, ix, xiv]	2.7258(10)	Li/Cu—Li[i, vii, xii, xiv]	2.7258(10)
Cu—Sn[0, vi, xi, xiv]	2.7258(10)	Li/Cu—Sn[ii, vii, xii, xv]	2.7258(10)

Symmetry code: not specified and [0] x,y,z; [i] x+1, y+1, z; [ii] x+1, y+1, z+1; [iii] x, y-1/2, z-1/2;

[iv] x, y+1/2, z-1/2; [v] x, y-1/2, z+1/2; [vi] x, y+1/2, z+1/2; [vii] x+1, y+1/2, z+1/2; [viii] x-1/2, y, z-1/2; [ix] x+1/2, y, z-1/2; [x] x-1/2, y, z+1/2; [xi] x+1/2, y, z+1/2; [xii] x+1/2, y+1, z+1/2; [xiii] x-1/2, y-1/2, z; [xiv] x+1/2, y+1/2, z; [xv] x+1/2, y+1/2, z+1; [xvi] x-1, y-1, z; [xvii] x-1, y-1/2, z-1/2; [xviii] x-1/2, y-1, z-1/2; [xix] x-1/2, y-1/2, z-1; [xx] x-1, y-1, z-1

Cu$_2$LiSn

Sn—Li3[0, iii, iv]	2.4839(9)	Li2···Li1[0]	0.69(4)
Sn—Cu[0, xiv]	2.5829(12)	Li2···Li3[0]	1.22(4)
Sn—Cu[ix, x, xi, xviii, xix, xx]	2.7700(9)	Li2···Li2[v]	1.37(8)
Sn—Li2[0, iii, xiv, xv]	2.767(17)	Li2—Li2[xiii]	2.44(8)
		Li2—Cu[xvii, xviii, xix]	2.4839(9)
Cu—Cu[xvi]	2.4523(17)	Li2—Li3[v]	2.59(4)
Cu—Li2[xxi, xxii, xxiii]	2.4839(9)	Li2—Sn[0, i, ii]	2.77(2)
Cu—Li1[xiii, xiv, xv]	2.5748(9)	Li2—Cu[xii, xiii, xiv]	2.83(2)
Cu—Sn[0]	2.5829(12)		
Cu—Sn[ix, x, xi]	2.7700(9)	Li3···Li2[0, xiii]	1.22(0.04)
Cu—Li3[viii, ix, x]	2.7700(9)	Li3···Li1[0, xiii]	1.9045(7)
Cu—Li2[xiv]	2.834(18)	Li3—Sn[0, i, ii]	2.4839(9)
		Li3—Li2[v, xxi]	2.59(4)
Li1···Li2[0, v]	0.69(4)	Li3—Cu[viii, ix, x, xvii, xviii, xix]	2.7700(9)
Li1···Li3[0, v]	1.9045(7)		
Li1—Cu[xii, xiii, xiv, xvii, xviii, xix]	2.5748(9)		

Symmetry code: not specified and ^{0} x,y,z; ^{i} x-1, y-1, z; ^{ii} x, y-1, z; ^{iii} x, y+1, z; ^{iv} x+1, y+1, z; ^{v} -x, -y, -z; ^{vi} -x, -y+1, -z; ^{vii} -x+1, -y+1, -z; ^{viii} -x, -y, -z+1; ^{ix} -x, -y+1, -z+1; ^{x} -x+1, -y+1, -z+1; ^{xi} -x+1, -y+2, -z+1; ^{xii} x-1, x-y, -z+1/2; ^{xiii} x, x-y, -z+1/2; ^{xiv} x, x-y+1, -z+1/2; ^{xv} x+1, x-y+1, -z+1/2; ^{xvi} x, x-y+1, -z+3/2; ^{xvii} -x, -x+y-1, z-1/2; ^{xviii} -x, -x+y, z-1/2; ^{xix} -x+1, -x+y, z-1/2; ^{xx} -x+1, -x+y+1, z-1/2; ^{xxi} -x, -x+y, z+1/2; ^{xxii} -x, -x+y+1, z+1/2; ^{xxiii} -x+1, -x+y+1, z+1/2
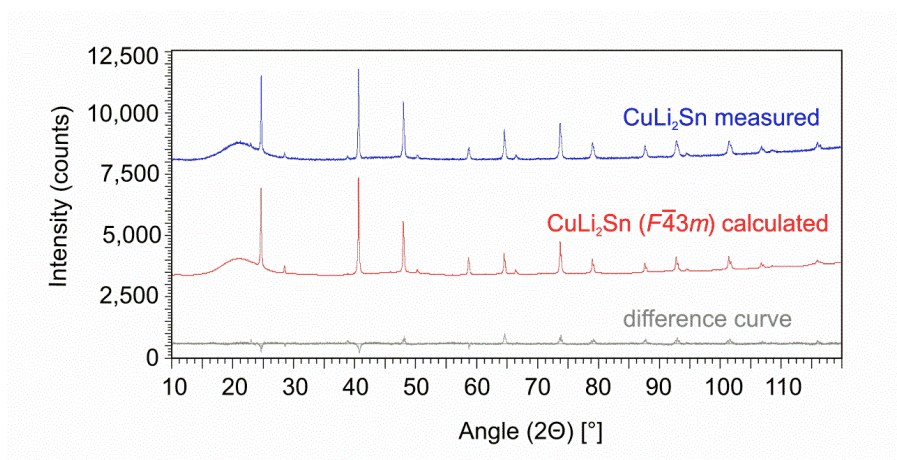
Fig. 1: Powder diffractogram of CuLi$_2$Sn: measured, calculated and difference patterns.
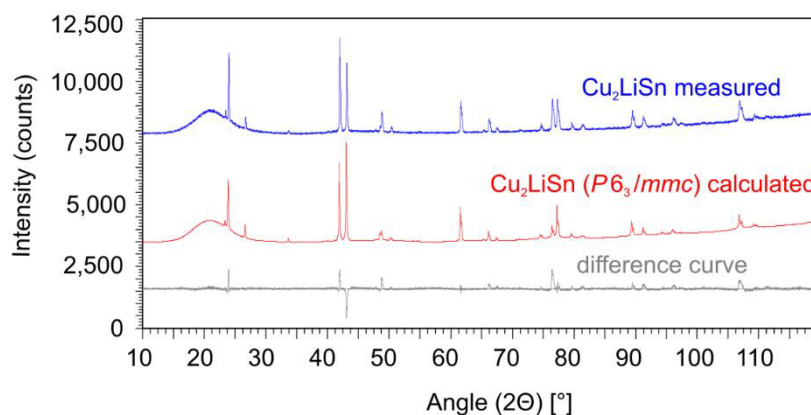
Fig. 2: Powder diffractogram of Cu$_2$LiSn: measured, calculated and difference patterns.
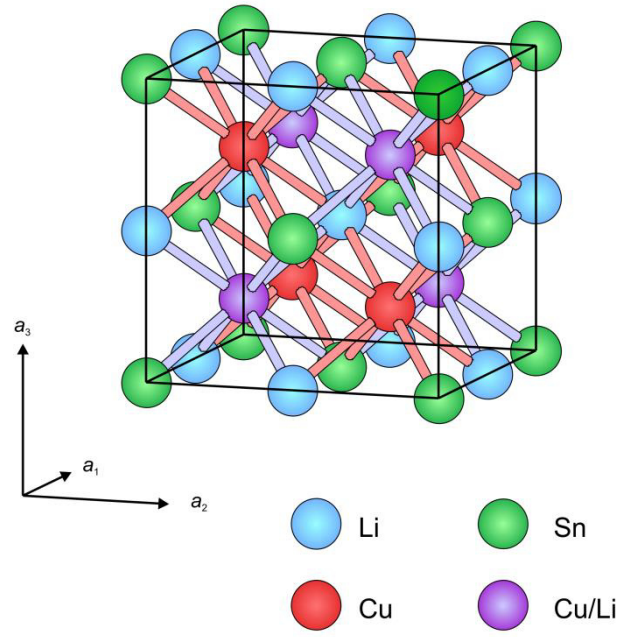
Fig. 3: Unit cell of CuLi₂Sn phase; Sn atoms at 4(*a*)-site, Li atoms at 4(*b*)-site, Cu atoms at 4(*c*)-site, mixed occupation of Cu/Li atoms at 4(*d*)-site.
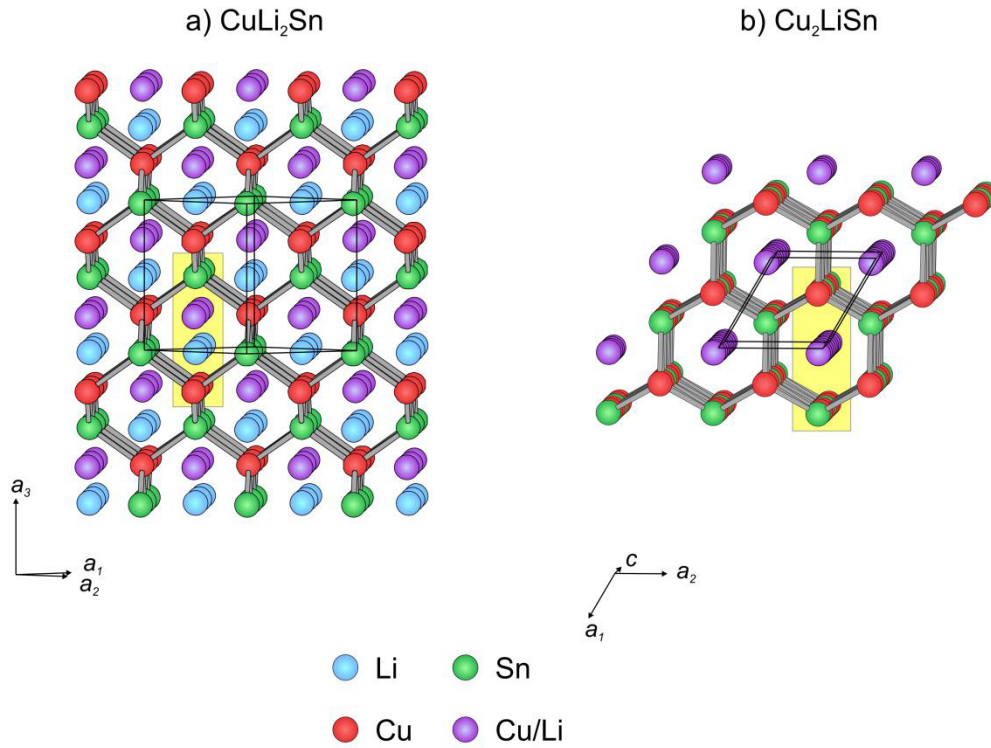
a) CuLi$_2$Sn

b) Cu$_2$LiSn

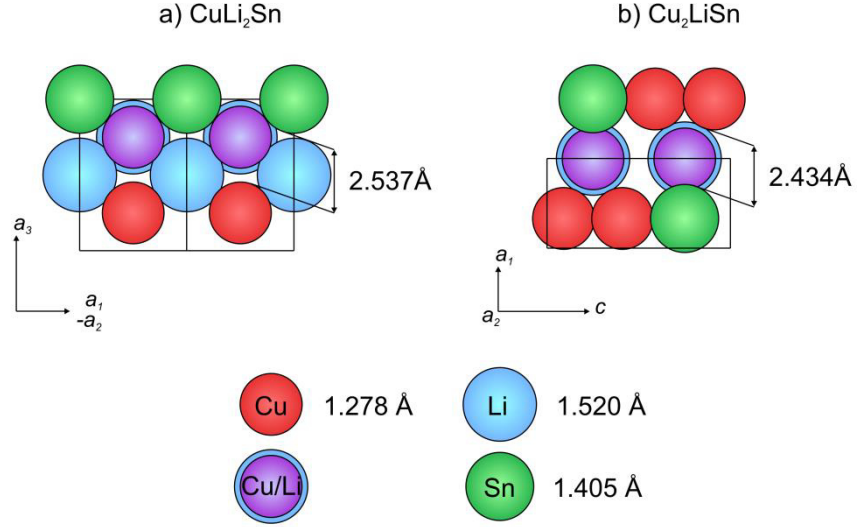**Fig. 4: Comparison of channel structure of CuLi₂Sn and Cu₂LiSn.**

Fig. 5: Comparison of vertical sections of channels in CuLi₂Sn and Cu₂LiSn according to shaded area in Figs. 4a and 4b; mixed Cu/Li-sites in Cu₂LiSn are only shown for 2(a)- and 2(b)-positions.
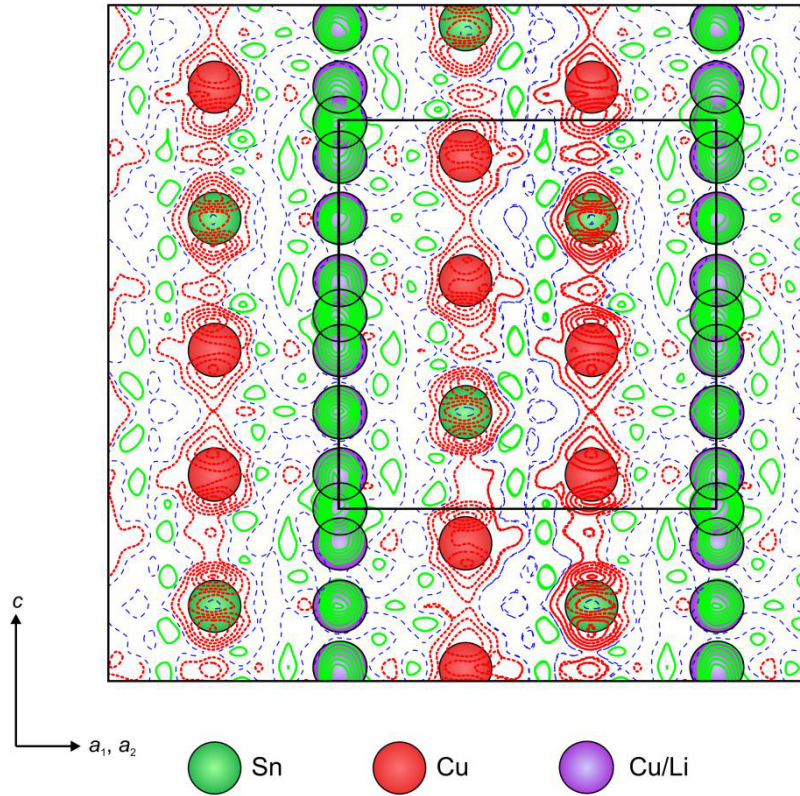

Fig. 6: Cu₂LiSn: Difference electron densities between measured and calculated pattern in [-110] direction, considering only 2(c)-Sn and 4(f)-Cu atoms in calculation. Negative, positive and no electron density differences are indicated with bold dashed, bold solid and normal dashed lines, respectively. Contour lines are graduated in steps of 0.5 e⁻/Å³. Excess electron clouds (solid lines) on 2(a)-, 2(b) and 4(e)-sites can be described by Cu/Li mixed occupations.
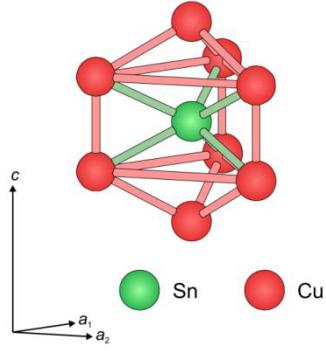
Fig. 7: *Di*capped trigonal prismatic coordination polyhedron as backbone structure of Cu$_2$LiSn, only 2(*c*)-Sn and 4(*f*)-Cu atoms are shown. Cu/Li atoms in channels are neglected in drawing.
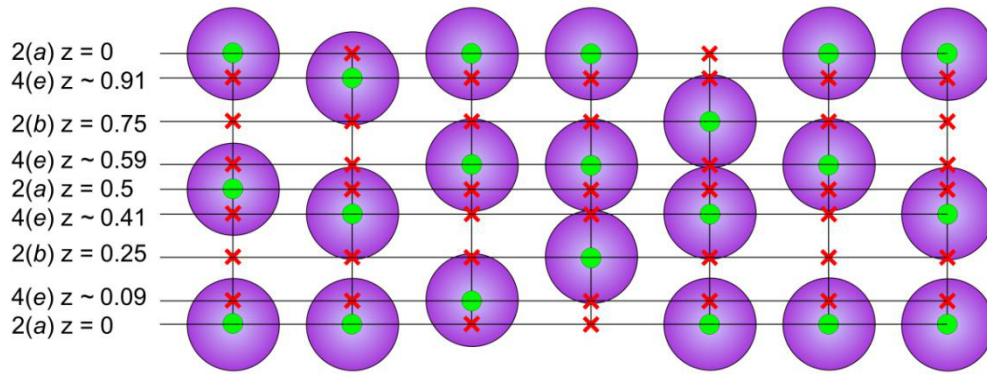

Fig. 8: The seven possible models for the partially occupied (Cu/Li)-positions in the Cu$_2$LiSn phase (possible (•) with corresponding impossible (x) positions, each vertical axis shows one channel along one unit cell).
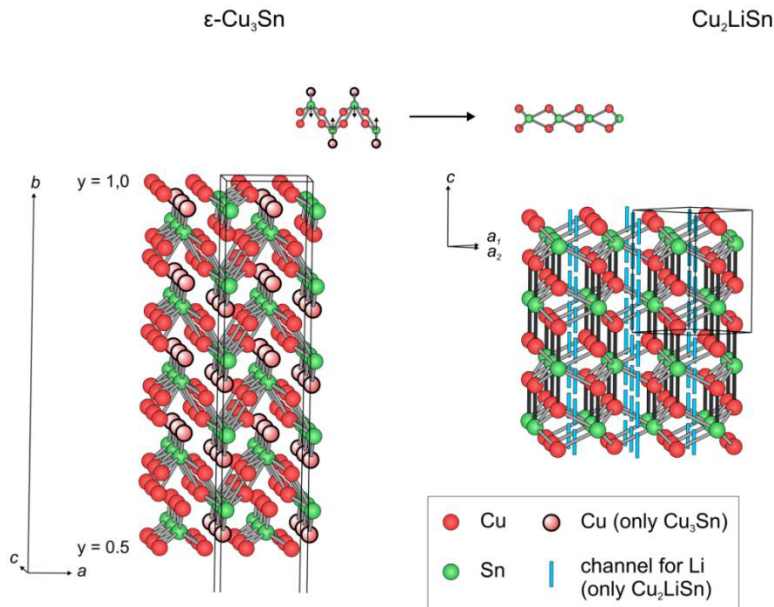

Fig. 9: Relations between ε-Cu$_3$Sn and Cu$_2$LiSn. Shorter Cu-Sn bonds in Cu$_2$LiSn are shown in dark grey.

3.3 Publication #3

The tin-rich copper-lithium stannides:

$Li_3Cu_6Sn_4$ and Li_2CuSn_2

Siegfried Fürtauer[†], Herta S. Effenberger[‡], Hans Flandorfer[†]

[†]Institute of Inorganic Chemistry (Materials Chemistry), University of Vienna, Währingerstraße 42, A-1090 Wien, Vienna

[‡]Institute of Mineralogy and Crystallography, University of Vienna, Althanstraße 14, A-1090 Wien, Vienna

Contributions to this paper:

S. Fürtauer:	Sample preparation, measurement, structural comparison, writing
H. Effenberger	Measurement and data refinement, writing, proofreading
H. Flandorfer:	General advice and helpful comments, proofreading

Overall contributions of S. Fürtauer to the paper: 70%

Abstract

The Sn rich ternary intermetallic compounds $Li_3Cu_6Sn_4$ (CSD-427097) and Li_2CuSn_2 (CSD-427098) were synthesized from the pure elements by induction melting and annealing at 400°C. Structural investigations were performed by powder- and single-crystal XRD. $Li_3Cu_6Sn_4$ crystallizes in space group *P6/mmm*; it is structurally related to but not isotypic with $MgFe_6Ge_6$ ($a = 5.095(2)$ Å, $c = 9.524(3)$ Å; $wR_2 = 0.059$; 239 unique F^2-values, 17 free variables). $Li_3Cu_6Sn_4$ is characterized by two sites with a mixed Cu:Sn occupation. In contrast to all other Cu-Li-Sn compounds known so far, any mixed occupation was found for Cu-Li pairs only. In addition, one Li site is only half occupied. The second Sn rich phase is Li_2CuSn_2 (space group *I4₁/amd*, $a = 4.4281(15)$ Å, $c = 19.416(4)$ Å; $wR_2 = 0.033$; 213 unique F^2-values, 12 atom free variables); it is the only phase in the Cu-Li-Sn system which is noted for full ordering. Both crystal structures exhibit 3D-networks which host Li atoms in channels. They are important for understanding the lithiation mechanism in Cu-Sn electrodes for Li-ion batteries.

Introduction

Ternary phases in the Cu-Li-Sn system are on general interest because Cu-Sn alloys are promising candidates as electrode materials in Li-ion batteries [1-4]. The mass charge capacities of interacting binary phases like $Li_{17}Sn_4$ are of higher efficiency than that of *e.g.* graphite [5, 6]. To verify possible mechanisms of Li insertion into binary Cu-Sn phases and to describe the formation of intermetallic ternary phases, new insights into the phase diagram are provided. So far, the only known ternary compounds are Li_2CuSn [7-9], $LiCu_2Sn$ [10], Li_2CuSn_2 [11] and $LiCu_3Sn_2$ [12]. However, any structural mechanisms for the possibility of exchange reactions and substitution paths remained unclear because all these papers are based on stoichiometric Cu-Li-Sn compounds. During ongoing experimental phase-diagram investigations of the Cu-Li-Sn system, several new intermetallic ternary phases were obtained besides those known already. They were structurally characterized and the variability in their chemical composition was investigated. Single-crystal investigations of Li_2CuSn and $LiCu_2Sn$ were reported recently [13]. For both these compounds extensive substitution between Cu and Li atoms was observed. The results of our structure refinements on stannides in the Cu-Li-Sn system (among them Li_2CuSn_2 and $Li_3Cu_6Sn_4$) were presented at the TMS conference in March 2013 in San Antonio, Texas, USA [14]. Later on, Winter et al. [11] described the crystal structure of Li_2CuSn_2 in their systematic study on tetragonal Li_2TSn_2 phases (T =

Ag, Au, Cu; space group $I4_1/amd$, Pearson symbol tI20). $Li_3Cu_6Sn_4$ crystallizes in space group $P6/mmm$; it is closely related to the structure type of $MgFe_6Ge_6$ (*cf.* Buchholz and Schuster [15, 16], Mazet et al. [17]). In the review paper on lithium- transition metal-tetrelides from Pöttgen et.al [12], a phase $LiCu_3Sn_2$ with the same space group and similar lattice parameters like $Li_3Cu_6Sn_4$ is mentioned. However, hence the crystal structure is referred only to an internal communication and neither to a peer-reviewed article nor to a data base entry, no further information of this phase is available. Both, $Li_3Cu_6Sn_4$ and Li_2CuSn_2, exhibit the highest Sn contents in the Cu-Li-Sn system and show some topological similarities to the NiAs-structure type and to the related compound η-Cu_6Sn_5 [18].

Materials and Methods

Sample Preparation

The inserts for sample preparations were the pure elements Cu (99.98 at.%, wire, Goodfellow, Cambridge, UK), Li (99.8 at.%, wire, Alfa Aesar, Karlsruhe, Germany) and Sn (99.95 at.%, ingot, Advent, Oxford, UK). The Cu wire was treated in a H_2-flow (5 hours, 300°C) to remove the oxide layer at the surface. The Li wire was stored originally in mineral oil, which was removed by n-hexane in a supersonic bath followed by vacuum evaporation of the solvent. Visible oxidation spots occurring partially at the surface were removed mechanically with a knife. Inside a glove box under Ar atmosphere (< 5 ppm O_2 / H_2O), the metal pieces were assembled in Ta crucibles, which were made by deep-drawing of a 0.4 mm tantalum sheet. For welding the crucibles in argon atmosphere, an arc furnace with a W electrode of 1.6 mm was used. During the welding process, the crucibles were chilled by a water cooled Cu mount. For melting, the crucibles were put into an induction furnace at 1100°C (but only 10-20 sec to prevent high temperature fatigue of the welding seam). Repetition of the melting process twice with turning the crucible upside down between the heating steps assured homogenous mixing. Then the crucibles were sealed in quartz glass tubes under vacuum. The alloys were annealed at 400°C in a muffle furnace (various durations, see Table 1) and quenched in cold water. After annealing of a sample with the composition Cu_6Sn_5:Li = 7:3 (input $Cu_{0.38}Li_{0.30}Sn_{0.32}$) three phases were obtained: $Li_3Cu_6Sn_4$, Li_2CuSn_2, and traces of (Sn); see Table 1 and Fig. 1. It is assumed that both compounds $Li_3Cu_6Sn_4$ and Li_2CuSn_2 coexist at 400°C as solid phases, whereas the pure Sn originates from quenched and solidified

liquid. To verify the stoichiometry of $Li_3Cu_6Sn_4$, another sample in the estimated single-phase field was prepared ($Cu_{0.46}Li_{0.23}Sn_{0.31}$). Besides traces of Li_2CuSn_2 this sample was nearly homogeneous. The sample obtained from an input with the ratio Cu:Li:Sn = 1:2:2 showed after quenching of the annealed sample mostly Li_2CuSn_2 besides traces of both η-Cu_6Sn_5 and (Sn); see Table 1 and Fig. 2. It is reasonable that at 400°C the sample consists of solid Li_2CuSn_2 and some amount of liquid, which solidifies during quenching to η-Cu_6Sn_5 + (Sn).

Powder XRD

Powdered samples were exposed to Cu-$K_α$ X-ray radiation (40 kV / 40 mA) in a diffractometer with Bragg-Brentano geometry and a Ni filter. Signals were detected by a strip detector. The powder was fixed with petroleum jelly on a silicon monocrystal and protected by argon atmosphere under a polycarbonate cap to prevent oxidation during measurements. Rietveld refinements were applied for phase analyses. In addition, the lattice parameters were refined. They are in good agreement with those obtained from single-crystal investigations.

Single crystal XRD

Single crystals were mounted with petroleum jelly on a glass capillary and measured at 290 K (in thermostatic nitrogen gas stream to prevent decomposition of the sample) with a four-circle Nonius Kappa diffractometer (CCD detector, 300 µm capillary optics collimator, Mo-X-ray tube, monochromated $K_α$ radiation). The unit-cell parameters were obtained from least-square refinements of the 2ϑ values from the position of the measured reflections; they were used for calculation of the interatomic bond distances and angles. Corrections for Lorentz, polarization and absorption effects (multi-scan method) were applied, complex scattering functions of Wilson were used [19]. For data collection, structure solution and refinements the programs "Collect" [20, 21], "SHELXS-97" and "SHELXL-97" [22-24] and for displaying the crystal structures the software "ATOMS" [25] were used. Laue- and space-group symmetries were found from the extinction rules and structure refinements. The location of (parts) of the Sn and Cu atom positions were obtained by direct methods in combination with a Patterson summation. Successive Fourier and difference Fourier summations revealed the remaining atom sites. Finally, the chemical compositions found from single-crystal refinements agreed with the nominal compositions. Details of the single crystal-data collection and structure refinement are

compiled in Table 2, fractional coordinates and interatomic bond distances are given in Tables 3 and 4, respectively. Structural parameters including anisotropic displacement parameters for all atoms but the half occupied Li2 site in $Li_3Cu_6Sn_4$ were refined. In general, the highest peaks in the final difference Fourier maps are located close to Sn or Cu sites.

Results and Discussion

$Li_3Cu_6Sn_4$

Considering η-Cu_6Sn_5 as a tentative material for Li-ion batteries requires the knowledge about the possibility of a substitution by or even an incorporation of Li atoms. Syntheses experiments were applied for alloying Li to the binary η-Cu_6Sn_5; as a result the compound $Li_3Cu_6Sn_4$ was formed. The crystal structure was solved in space group *P*6/*mmm*; during the final stage of refinement, a difference Fourier summation showed the Li2 atom at site 1(*b*) 0 0 ½. Least-squares refinements of the atomic parameters derived a U_{iso} value of 0.12(4) Å², a succeeding anisotropic refinement yielded r.m.s. amplitudes of 0.384 Å² parallel [001] and 0.034 Å² parallel to (0001). Consequently a split model was considered with the Li2 atom at a half occupied site 2(*e*) 00*z* resulting in a Li2···Li2 distance of 0.70(14) Å. This site was refined with an isotropic displacement parameter only; for all the other atoms, anisotropic displacement parameters were considered. Trials to refine the crystal structure in any subgroup of *P*6/*mmm* to obtain an ordered model failed. Only two atomic sites are solely and fully occupied by one kind of atoms - site 2(*e*) by Sn and site 2(*c*) by Li atoms. Two further sites - 2(*d*) and 6(*i*) - exhibit an extensive substitution of Sn and Cu atoms. Whereas the Sn atoms predominantly occupy the site 2(*d*), site 6(*i*) is mainly occupied by Cu atoms ($Cu_{0.179}Sn_{0.821(5)}$, $Cu_{0.938}Sn_{0.062(3)}$). The principal mean square atomic displacement parameters reflect the mixed occupation of the Cu/Sn sites: Whereas the ratio longest : shortest axis is 1.03 for the Sn site, it is 2.36 and 2.96 for the Cu/Sn1 and Cu/Sn2 site due to the different space requirement of the two kind of atoms. Considering the occupation ratios of the mixed occupied positions 2(*d*) and 6(*i*), the experimental composition is $Cu_{5.99}Li_3Sn_{4.01}$. These values induce integer numbers within the accuracy of structure refinements. However, the same composition $Li_3Cu_6Sn_4$ represents also the ordered end member with the sites 2(*d*) and 6(*i*) occupied by Sn and Cu only. This was the starting composition for further syntheses runs; a verification of phase purity by powder XRD (see Table 1) revealed nearly phase homogeneity. Due to the presence of only minor amounts of Li_2CuSn_2 an ideal composition close to the boarder

to a two-phase equilibrium of both phases is expected. Topologically, the crystal structure of $Li_3Cu_6Sn_4$ (Fig. 3) is formed by 3 different structural motifs: These are linked to layers which are stacked along the c-direction. The structural motifs are I) trigonal pyramids with 6(i)-Cu/Sn2 atoms at the base and a 2(d)-Cu/Sn1 atom at the apex. Two such pyramids are connected via their apices; the six 6(i)-Cu/Sn2 atoms of the two pyramids form a trigonal prism to adopt $\overline{6}m2$ symmetry; II) hexagonal pyramids with a 2(e)-Sn atom at the top and six 6(i)-Cu/Sn2 atoms at the base; III) hexagonal bipyramids with 2(c)-Li1 atoms forming the equatorial plane and 2(e)-Sn atoms at the apices. These three structural units are stacked along the c-direction in the order ...-I-II-III-II-... sharing common atom corners and edges (Fig 3). They form a 3D-framework with channels in the a-direction (symmetrically equal to the [110] direction), which are occupied by 2(e)-Li2 atoms. If the crystal structure is considered to be built from layers, there are superimposed graphite-like arrangements of 2(c)-Li1 and 2(d)-Cu/Sn1 atoms, respectively. The interatomic distances within both layers (Li1—Li1 and Cu/Sn1—Cu/Sn1) are equivalent (2.9416(12) Å). The two different layers are separated by a layer of 6(i)-Cu/Sn2 atoms, which form a 2D network of corner-linked hexagons, with triangles between three hexagons. The hexagons formed by Li1 and Cu/Sn1 atoms, respectively, and these formed by 6(i)-Cu/Sn2 atoms are twisted with respect to each other by 30°. The stacking order of the layers is ...-Li-Cu-Sn-Cu-... (Fig. 3), assuming that the Cu/Sn1 site is predominantly occupied by Sn, and the Cu/Sn2 predominantly by Cu atoms, respectively. The crystal structure exhibits channels along [001], which are filled with Li2 and Sn atoms: Their order is ...-Sn-Li-Sn-...; the ratio Li:Sn is 1:2. The crystal structure of $Li_3Cu_6Sn_4$ is closely related to that of $MgFe_6Ge_6$ [15-17]. They have the same space-group symmetry and the same Pearson symbol. By shifting the origin of the unit cell of $Li_3Cu_6Sn_4$ by 0 0 ½, the close structural relationship to $MgFe_6Ge_6$ becomes obvious (Fig. 4). The positions of the atoms Ge1, Ge3, Fe, Ge2 and Mg in $MgFe_6Ge_6$ correspond with the sites Sn, Cu/Sn1, Cu/Sn2, Li1 and Li2 in $Li_3Cu_6Sn_4$. However, in the title compound the cell parameter a is enlarged by only 0.55% whereas that of c by 15.53%, which is contributed to the larger atomic radii of Cu (1.278 Å) and Sn (1.405 Å) compared to that of Fe (1.241 Å) and Ge (1.225 Å) (atomic radii from Emsley [26]). The atomic radius of Mg (1.60 Å) is slightly increased to that one of Li (1.52 Å) and has only minor influence on the cell dimensions. The main difference between both crystal structures is related to the site 1(a)-Mg and the corresponding split and only half occupied site 2(e)-Li2. The structural relationship of the binary phase η-Cu_6Sn_5 and the ternary phase $Li_3Cu_6Sn_4$ is shown in Fig. 5. The phase η-Cu_6Sn_5 (space-group $P6_3/mmc$) is

isotypic to Ni_2In (filled NiAs-type); the unit cell contains two Cu atoms (at 000, etc.) and two Sn atoms (at ⅓ ⅔ ¼, etc.); the position (⅓ ⅔ ¾, etc.) is partially filled by Cu atoms. The arrows in Fig. 5 indicate the structural reorganization paths of the atoms to obtain the Cu-Sn sublattice of $Li_3Cu_6Sn_4$ from that of η-Cu_6Sn_5. Both crystal structures have a primitive hexagonal lattice. An evident difference between both structures is, besides the presence of Li atoms, that structural motifs in η-Cu_6Sn_5 are puckered, whereas plane in $Li_3Cu_6Sn_4$. In both structures condensed rings with sixfold coordinated Sn atoms form planes. In $Li_3Cu_6Sn_4$ these planes are parallel to (000z), flat (graphite-like) and consisting mainly by Sn atoms (site 2(d)-Cu/Sn1, Fig. 3), whereas in η-Cu_6Sn_5 they are arranged parallel to ($10\overline{1}0$), bowl shaped and formed solely by Sn atoms. A further Sn atom is located in the centre of these bowl-shaped rings (with identical crystal site as other Sn atoms). The corresponding 2(e)-Sn atoms in $Li_3Cu_6Sn_4$ are shifted by $z = ±0.35$ with respect to the main layer of the Sn atoms (Fig. 3). Consequently, the main difference between η-Cu_6Sn_5 and $Li_3Cu_6Sn_4$ is that the bowl-shaped hexagons formed by Sn atoms align and the centred Sn atoms shift perpendicular to the Sn-atom plane. Besides this, the Cu1 and Cu2 atoms of η-Cu_6Sn_5 separate perpendicular to the Sn-atom plane as well and form two corresponding layers, which are located on opposing sides of this Sn layer (see arrows in Fig. 5 and planes in Fig. 3). In addition, during this change both Cu1 and Cu2 atoms migrate parallel to [001] to the centre of the Sn-Sn bond of the Sn layer ($Li_3Cu_6Sn_4$: $x = 0$, $y = ½$, $z = 0.25920$). In the ternary compound this Cu/Sn2 site is occupied by Cu atoms which are partly substituted by Sn atoms. Further Li atoms form both superimposed graphite-like layers (Li1) and fillings with neighboured Sn atoms in the hexagonal channels (Li2), as described above (see also Fig. 3). For consideration of stereochemical aspects of the mobility of Li atoms at the 2(c) and 2(e) sites *cf.* Fig. 6. Li1 atoms at the 2(c) site build up the graphite-like layers. They are easily moveable within the (0001) plane along channels (diameter = 3.032 Å) formed by Sn atoms at 2(e). They are not hindered by Sn atoms at the Sn-2(e) position but are inhibited by the adjacent Cu/Sn2-layers (shortest distance between layers = 2.387 Å). The Li2 atoms at the half occupied 2(e) site are trapped by rings of mainly Sn atoms (Cu/Sn1 site) and planes of mainly Cu atoms (Cu/Sn2 site) in the c-direction. The Li2 atoms are located in holes within layers formed by the Cu/Sn2 atoms (smallest hole diameter = 2.545 Å). However, neighbouring Sn atoms at the Sn-2(e) site would inhibit and limit the migration in the [001] direction. As a conclusion we suppose higher mobility of the Li atoms at the 2(c) site as compared to the Li atoms at the 2(e) site.

Li$_2$CuSn$_2$

So far, Li$_2$CuSn$_2$ is the only phase investigated in the Cu-Li-Sn system which exhibits an ordered atomic arrangement without mixed occupied positions. It is isotypic to the Li$_2$AuSn$_2$ structure of Wu et al. [27]. Before published by Winter et al. [11], it was experimentally found by powder and single-crystal XRD. The main features of the crystal structure were outlined by [11]; this paper focuses on some additional topological aspects. The crystal structure consists of a network of CuSn$_4$ tetrahedra linked by common corners (see Fig. 7). They are arranged in a 3D-network of condensed rings with (CuSn$_2$)-subunits, forming distorted honeycomb-shaped channels. These channels occur along the *a*-direction and host the Li atoms. A section of such a channel is shown in Fig. 8. The channel diameter is controlled by the position of the Sn atoms. Centre-to-centre distances between Li and Sn atoms are between 2.918 and 2.941 Å, which is approximately the sum of both the atomic radii (r_{Li} + r_{Sn} = 2.925 Å). The Cu atoms do not limit the channel diameter. According to Winter et al. [11], Li atoms in Li$_2$CuSn$_2$ possess considerable mobility, which is reproducible from these stereoscopic considerations. A close structural relationship between tetragonal Li$_2$CuSn$_2$ and cubic Li$_2$CuSn [13] is evident. Both structures represent stacking sequences of two different kinds of layers. Layer 1 consists of Li and Sn atoms with chess board topology (see Fig. 9 a, c). Interatomic distances between Li and Sn atoms are d_{Li-Sn} = 3.1475 Å for Li$_2$CuSn and d_{Li-Sn} = 3.1313 Å for Li$_2$CuSn$_2$. Layer 2 consists of a net of Cu atoms (see Fig. 9 d). In Li$_2$CuSn the latter is decorated by an additional site that is mixed occupied by Cu and Li atoms located in the centre of the basic squares formed by the Cu atoms (see Fig. 9 b). The crystal structures are characterized by an alternate stacking of layers 1 (Fig. 9 a) and layers 2 (Fig. 9 b). Cu or Cu/Li atoms of layer 2 fill the gaps between the Li and Sn atoms of layer 1 and *vice versa* (see also Figs. 9 a-d: Yellow shaded areas represent the unit cells which overlap in both figures). In Li$_2$CuSn$_2$ each two layers 1 succeed each other; they are shifted by a_1/2 (see Fig. 9 c). Pairs of layer 1 are separated by one layer 2. In both crystal structures succeeding layers 1 and 2, respectively, are twisted by 90° with respect to each other. For Li$_2$CuSn this arrangement results in a cubic symmetry ($F\bar{4}3m$) whereas Li$_2$CuSn$_2$ is tetragonal ($I4_1/amd$). The unit-cell parameter parallel to the stacking direction reflects the distinct sequences of two layers in Li$_2$CuSn (a_3 = 6.295 Å = 2 · 3.148 Å) and Li$_2$CuSn$_2$ (c = 19.416 Å = 6 · 3.236 Å). For a topological comparison of the structural similarities between η-Cu$_6$Sn$_5$ and Li$_2$CuSn$_2$ *cf.* Fig. 10: The partially filled Cu-2(*d*) position of η-Cu$_6$Sn$_5$ is entirely filled by Li atoms. In addition, the hexagonal lattice is distorted along distinct directions by various amounts (depicted by different lengths of arrows in Fig. 10);

consequently, the angle γ of the hexagonal lattice is reduced astonishingly to 71.38°, whereas the angle of 60° in the base of the hexagonal unit cell is increased to 108.62°. These distinct arrangements cause a significant change of the distances between the Cu atoms. The Cu-Cu distance along a in η-Cu_6Sn_5 is 4.1920 Å, which changes drastically to 4.4281 Å and 6.9334 Å, respectively, in Li_2CuSn_2. These differences are caused by incorporated Li atoms. The lattice parameter c of η-Cu_6Sn_5 (6.0370 Å) corresponds with the slightly enlarged d_{110} distance by ~3% to 6.2622 Å only. It is caused by the simultaneous elimination of the Cu-atoms at (00½) and incorporation of the Li atoms. In case of a phase transformation from η-Cu_6Sn_5 to Li_2CuSn_2 the remaining Cu atoms from the former compound form a phase richer in Cu, probably $Li_3Cu_6Sn_4$. Uptake of Li atoms and exclusion of Cu atoms finally leads to a stoichiometry of two Sn atoms, two Li atoms and one remaining Cu atom per distorted unit cell.

Conclusions

Two phases in the Cu-Li-Sn system have been synthesized, identified by powder and single crystal X-ray diffraction techniques and topologically characterized: $Li_3Cu_6Sn_4$ and Li_2CuSn_2. Both crystal structures exhibit channels in a 3D-framework which are filled with Li atoms. If satisfying mobility of Li atoms is provided, both compounds could be of interest for application as electrode materials in Li-ion batteries. The crystallographic relationship of both ternary phases to the binary η-Cu_6Sn_5 phase was presented; evidences of their formation during Li insertion are outlined. Similarities between Li_2CuSn_2 and another ternary phase, Li_2CuSn, are discussed. Further details on the structure refinement of the discussed phases are available from Fachinformationszentrum Karlsruhe, 76344 Eggenstein-Leopoldshafen, Germany, by quoting the Registry No's CSD-427097 ($Li_3Cu_6Sn_4$) and CSD-427098 (Li_2CuSn_2).

References

[1]   A.N. Jansen, J.A. Clevenger, A.M. Baebler, J.T. Vaughey, Variable temperature performance of intermetallic lithium-ion battery anode materials. *J. Alloys Compd.* **2011,** *509*, 4457.

[2]   W. Choi, J.Y. Lee, H.S. Lim, Electrochemical lithiation reactions of Cu_6Sn_5 and their reaction products. *Electrochem. Commun.* **2004,** *6*, 816.

[3]   S. Sharma, L. Fransson, E. Sjostedt, L. Nordstrom, B. Johansson, K. Edstrom, A theoretical and experimental study of the lithiation of η'-Cu_6Sn_5 in a lithium-ion battery. *J. Electrochem. Soc.* **2003,** *150*, A330.

[4]   K.D. Kepler, J.T. Vaughey, M.M. Thackeray, $Li_xCu_6Sn_5$ (0 < x < 13): An intermetallic insertion electrode for rechargeable lithium batteries. *Electrochem. Solid St.* **1999,** *2*, 307.

[5]   A.K. Shukla, T.P. Kumar, Materials for next-generation lithium batteries. *Curr. Sci. India* **2008,** *94*, 314.

[6]   W.J. Zhang, A review of the electrochemical performance of alloy anodes for lithium-ion batteries. *J. Power Sources* **2011,** *196*, 13.

[7]   H.U. Schuster, Ternäre Lithium-Verbindungen mit Elementen der 4. Hauptgruppe. *Naturwissenschaften* **1966,** *53*, 360.

[8]   H. Pauly, A. Weiss, H. Witte, Crystal structure of ternary intermetallic phases Li_2EX (E = Cu, Ag, Au; X = Al, Ga, In, Tl, Si, Ge, Sn, Pb, Sb, Bi). *Z. Metallkd.* **1968,** *59*, 47.

[9]   H.U. Schuster, D. Thiedemann, H. Schönemann, Ternary lithium compounds with formulas of $LiMe_2X$ and Li_2MeX (Me = Cu, Ag or Au; X = Si, Ge or Sn). *Z. Anorg. Allg. Chem.* **1969,** *370*, 160.

[10]   P.I. Kripyakevich, G.I. Oleksiv, Crystal structure of the compound $LiCu_2Sn$. *Dopov. Akad. Nauk Ukr. RSR* **1970,** *A*, 63.

[11]   F. Winter, S. Dupke, H. Eckert, U.C. Rodewald, R. Pöttgen, Lithium mobility in the stannides Li_2CuSn_2 and Li_2AgSn_2. *Z. Anorg. Allg. Chem.* **2013,** *639*, 2790.

[12]   R. Pöttgen, T. Dinges, H. Eckert, P. Sreeraj, H.D. Wiemhöfer, Lithium-Transition Metal-Tetrelides - Structure and Lithium Mobility. *Z. Phys. Chem.* **2010,** *224*, 1475.

[13]   S. Fürtauer, H.S. Effenberger, H. Flandorfer, $CuLi_2Sn$ and Cu_2LiSn: Characterization by single crystal XRD and structural discussion towards new anode materials for Li-ion batteries. *J. Solid State Chem.* **2014,** *220*, 198.

[14]   S. Fürtauer, A. Yakymovych, E. Tserenjav, H. Flandorfer, "Phase relations and thermodynamic data in the system Cu-Li-Sn and the binary constituent systems". TMS 2013: Annual Meeting & Exhibition. San Antonio / Texas, **2013**.

[15]   W. Buchholz, H.U. Schuster, Compounds $MgFe_6Ge_6$ and $LiCo_6Ge_6$. *Z. Naturforsch. B* **1978,** *33*, 877.

[16]   W. Buchholz, H.U. Schuster, Intermetallic phases with B35-superstructure and relationship to $LiFe_6Ge_6$. *Z. Anorg. Allg. Chem.* **1981,** *482*, 40.

[17]   T. Mazet, V. Ban, R. Sibille, S. Capelli, B. Malaman, Magnetic properties of $MgFe_6Ge_6$. *Solid State Commun.* **2013,** *159*, 79.

[18]   A. Gangulee, G.C. Das, M.B. Bever, X-ray diffraction and calorimetric investigation of compound Cu_6Sn_5. *Metall. Trans.* **1973,** *4*, 2063.

[19]   A.J.C. Wilson, (Ed.), International Tables for Crystallography, Kluwer, Dordrecht / NL **1992**.

[20]   Z. Otwinowski, W. Minor, Processing of X-ray diffraction data collected in oscillation mode. *Method. Enzymol.* **1997,** *276*, 307.

[21]   B.V. Nonius, *Collect - Data Collection Software*. Delft / Netherlands **1999**.

[22]   G.M. Sheldrick, A short history of SHELX. *Acta Crystallogr. A* **2008,** *64*, 112.

[23]   G.M. Sheldrick, *SHELXS 97 - A Program for the Solution of Crystal Structures*. Göttingen **1997**.

[24]   G.M. Sheldrick, *SHELXL 97 - A Program for Crystal Structure Refinement*. Göttingen **1997**.

[25]   E. Dowty, *Atoms - A Computer Program for Displaying Atomic Structures*. Version 6.2, Shape Software, Kingsport / TN **2004**.

[26]   J. Emsley, The Elements. Clarendon Press, Oxford, **1989**.

[27]   Z.Y. Wu, B.D. Mosel, H. Eckert, R.D. Hoffmann, R. Pöttgen, Structure and lithium dynamics of Li_2AuSn_2 - A ternary stannide with condensed $AuSn_{4/2}$ tetrahedra. *Chem. - Eur. J.* **2004,** *10*, 1558.

Table 1: Composition, heat treatment and powder XRD data

Nominal composition	Heat treatment	Phases	Space group	Lattice Parameter (Å)	Comments
$Cu_{0.38}Li_{0.30}Sn_{0.32}$	42d / 400°C	$Li_3Cu_6Sn_4$	$P6/mmm$	$a = 5.08612(9)$ $c = 9.5063(3)$	minor amount of Li_2CuSn_2, traces of (Sn)
		Li_2CuSn_2	$I4_1/amd$	$a = 4.4188(3)$ $c = 19.361(2)$	
		(Sn)	$I4_1/amd$	$a = 5.901(2)$ $c = 3.160(2)$	
$Cu_{0.46}Li_{0.23}Sn_{0.31}$ ($= Li_3Cu_6Sn_4$)	70d / 400°C	$Li_3Cu_6Sn_4$	$P6/mmm$	$a = 5.08676(5)$ $c = 9.5064(2)$	traces of Li_2CuSn_2
		Li_2CuSn_2	$I4_1/amd$	$a = 4.422(11)$ $c = 19.27(11)$	
$Cu_{0.20}Li_{0.40}Sn_{0.40}$	9d / 400°C	Li_2CuSn_2	$I4_1/amd$	$a = 4.42496(4)$ $c = 19.4092(3)$	traces of η-Cu_6Sn_5 and (Sn)
		η-Cu_6Sn_5	$P6_3/mmc$	$a = 4.1999(3)$ $c = 5.0917(6)$	
		(Sn)	$I4_1/amd$	$a = 5.8314(2)$ $c = 3.1817(2)$	

Table 2: Single-crystal X-ray data-collection and crystal structure refinements of $Li_3Cu_6Sn_4$ and Li_2CuSn_2.

Sample composition	$Cu_{0.38}Li_{0.3}Sn_{0.32}$	$Cu_{0.2}Li_{0.4}Sn_{0.4}$
(ideal) chemical formula	$Li_3Cu_6Sn_4$	Li_2CuSn_2
a (Å)	5.095(2)	4.4281(15)
c (Å)	9.524(3)	19.416(4)
Space group	$P6/mmm$ (191)	$I4_1/amd$ (141)
V (Å³)	214.1	380.7
Z	1	4
ρ_{calc} (g cm^{-3}) / μ(Mo$K\alpha$) (mm^{-1})	6.80 / 25.9	5.49 / 18.3
crystal dimensions (μm)	43×60×85	50×85×120
Range of data collection ($\pm h \pm k \pm l$) (°)	3 < 2ϑ < 70	3 < 2ϑ < 70
Number of images / rotation angle per image (°)	448 / 2.0	437 / 2.0
Scan mode (φ-scans at distinct ω-angles)	9 φ-scans	9 φ-scans
Scan time (s/°) / frame size 621×576 pixels (binned mode)	105	60
Detector-to-sample distance (mm)	30	30
Measured reflections	3,034	2,902
Unique reflections (n) / observed reflections ($F_o > 4\sigma(F_o)$)	239 / 231	213 / 251
$R_{int} = \Sigma\,\lvert F_o^2 - F_o^2(\text{mean})\rvert\,/\Sigma F_o^2$	0.042	0.054
Extinction parameter k:		
$F_c^* = F_c \cdot k(1+0.001 \cdot F_c^2\lambda^3/\sin(2\vartheta))^{-1/4}$	0.063(4)	0.0073(4)
$R_1 = \Sigma(\lvert\,\lvert F_o\rvert - \lvert F_c\rvert\,\rvert) / \Sigma F_o$ (all / observed reflections)	0.022 / 0.023	0.014 / 0.018
$wR_2 = (\Sigma w(F_o^2 - F_c^2)^2 / \Sigma\lvert wF_o^4)^{1/2}$	0.059	0.033
GooF = $\{\Sigma(w(F_o^2 - F_c^2)^2) / (n-p)\}^{0.5}$	1.15	1.24
max Δ/σ; number of variable parameters (p)	< 0.001; 17	< 0.001; 12
Final difference Fourier map (eÅ^{-3})	-1.81 to +2.39	-1.44 to +0.67
Parameters a / b for weighting scheme $w = 1 / \{\,\sigma^2(F_o^2) + [a \times P]^2 + b \times P\}$; $P = ([\max(0,F_o^2)] + 2 \times F_c^2) / 3]$	0.027 / 1.57	0.000 / 1.21
Volume per atom (Å³)	16.5	19.0

Table 3: Fractional atomic coordinates and displacement parameters;
The anisotropic displacement parameters are defined as: exp ($-2\pi^2 \Sigma^3_{i=1} \Sigma^3_{j=1} U_{ij} a_i^* a_j^* h_i h_j$); $U_{23} = U_{13} = 0$

	occupation	Wyckoff letter	Site symm.	x	y	z	U_{equiv} / U_{iso}	U_{11}	U_{22}	U_{33}
Li$_3$Cu$_6$Sn$_4$										
Sn	Sn$_{1.00}$	2(e)	$6mm$	0	0	0.15005(7)	0.0132(2)	0.0133(3)	= U_{11}	0.0129(3)
Cu/Sn1	Cu$_{0.179}$Sn$_{0.821(5)}$	2(d)	$\bar{6}m2$	2/3	1/3	1/2	0.0141(3)	0.0182(3)	= U_{11}	0.0077(3)
Cu/Sn2	Cu$_{0.938}$Sn$_{0.062(3)}$	6(i)	$2mm$	0	1/2	0.25920(7)	0.0138(3)	0.0076(3)	0.0103(3)	0.0225(4)
Li1	Li$_{1.00}$	2(c)	$\bar{6}m2$	2/3	1/3	0.0000	0.019(4)	0.015(4)	= U_{11}	0.027(9)
Li2	Li$_{0.50}$	2(e)	$6mm$	0	0	0.463(8)	0.06(2)			
Li$_2$CuSn$_2$ *										
Sn	Sn$_{1.00}$	8(e)	$2mm$.	0	1/4	0.050537(12)	0.01242(11)	0.01079(14)	0.01422(15)	0.01225(14)
Cu	Cu$_{1.00}$	4(b)	$\bar{4}m2$	0	1/4	3/8	0.01327(14)	0.01179(19)	= U_{11}	0.0162(3)
Li	Li$_{1.00}$	8(e)	$2mm$	0	1/4	0.5492(3)	0.0188(15)	0.022(4)	0.019(4)	0.016(3)

* origin at 2/m

Table 4. Interatomic bond lengths (Å) of $Li_3Cu_6Sn_4$ and Li_2CuSn_2

$Li_3Cu_6Sn_4$

Sn—Cu2[0, ii, xiv, xvi, xix, xx]	2.7514(10)	Cu/Sn2—Cu/Sn2[xv, xvi, xix, xxi]	2.5475(10)
Sn—Sn[vi]	2.8582(16)	Cu/Sn2—Cu/Sn1[iii, xi]	2.7245(9)
Sn—Li2[0]	2.98(7)	Cu/Sn2—Sn[0,]	2.7514(10)
		Cu/Sn2—Li1[iii, viii]	2.8735(9)
Cu/Sn1—Cu/Sn2[iv, xi, xvi, xviii, xx, xxiii]	2.7245(9)		
Cu/Sn1—Cu/Sn1[x, xi, xiii]	2.9416(12)		
Cu/Sn1—Li2[0, iv, ix, x, xi,, xxiv]	2.963(9)		
		Li2···Li2[ix]	0.70(14)
Li1—Cu/Sn2[iv, viii, xx, xvi, xviii, xxii]	2.8735(9)	Li2—Cu/Sn1[0, i, iii, , ix, x, xi]	2.963(9)
Li1—Li1[vii, viii, xii]	2.9416(12)	Li2—Sn[0]	2.98(7)

Symmetry code: not specified and [0] x,y,z; [i] x-1, y-1, z; [ii] x, y-1, z; [iii] x-1, y, z;
[iv] x+1, y, z; [v] x, y+1, z; [vi] -x, -y, -z; [vii] -x+1, -y, -z; [viii] -x+1, -y+1, -z;
[ix] -x, -y, -z+1; [x] -x+1, -y, -z+1; [xi] -x+1, -y+1, -z+1; [xii] -x+2, -y+1, -z; [xiii] -x+2, -y+1, -z+1;
[xiv] -y, x-y, z; [xv] -y, x-y+1, z; [xvi] -y+1, x-y+1, z; [xvii] y, -x+y, -z; [xviii] y, -x+y, -z+1;
[xix] -x+y-1, -x, z; [xx] -x+y, -x, z; [xxi] -x+y, -x+1, z; [xxii] x-y+1, x, -z; [xxiii] x-y+1, x, -z+1 z; [xxiv] x+1, y, z

Li_2CuSn_2

Sn—Cu[iii, iv]	2.6443(5)	Li—Cu[i, ii]	2.658(4)
Sn—Li[v]	2.917(7)	Li—Sn[v]	2.917(7)
Sn—Li[iii, iv]	2.942(5)	Li—Li[i, ii]	2.925(9)
Sn—Sn[x, xi]	2.9586(6)	Li—Sn[iii, iv]	2.942(5)
Cu—Sn[iii, iv, viii, ix]	2.6443(5)		
Cu—Li[i, ii, vi, vii]	2.658(4)		

Symmetry code:
not specified and [0] x,y,z; [i] -x, -y, -z+1; [ii] -x, -y+1, -z+1; [iii] -x-1/2, -y+1/2, -z+1/2;
[iv] -x+1/2, -y+1/2, -z+1/2; [v] y-1/4, x+1/4, -z+3/4; [vi] -y-1/4, -x+1/4, z-1/4; [vii] -y+3/4, -x+1/4, z-1/4;
[viii] -y+1/4, -x-1/4, z+1/4; [ix] -y+1/4, -x+3/4, z+1/4; [x] -x, -y, -z; [xi] -x, -y+1, -z
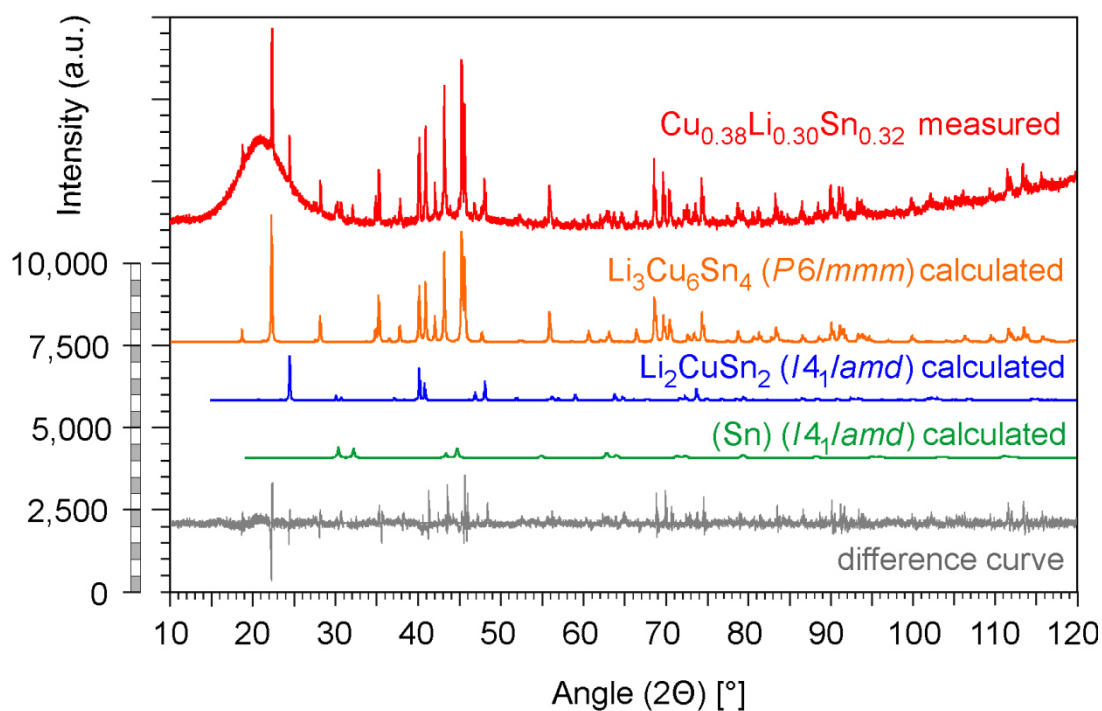
Fig. 1: Powder diffractogram of the sample Cu₀.₃₈Li₀.₃Sn₀.₃₂: Measured, calculated and difference patterns.
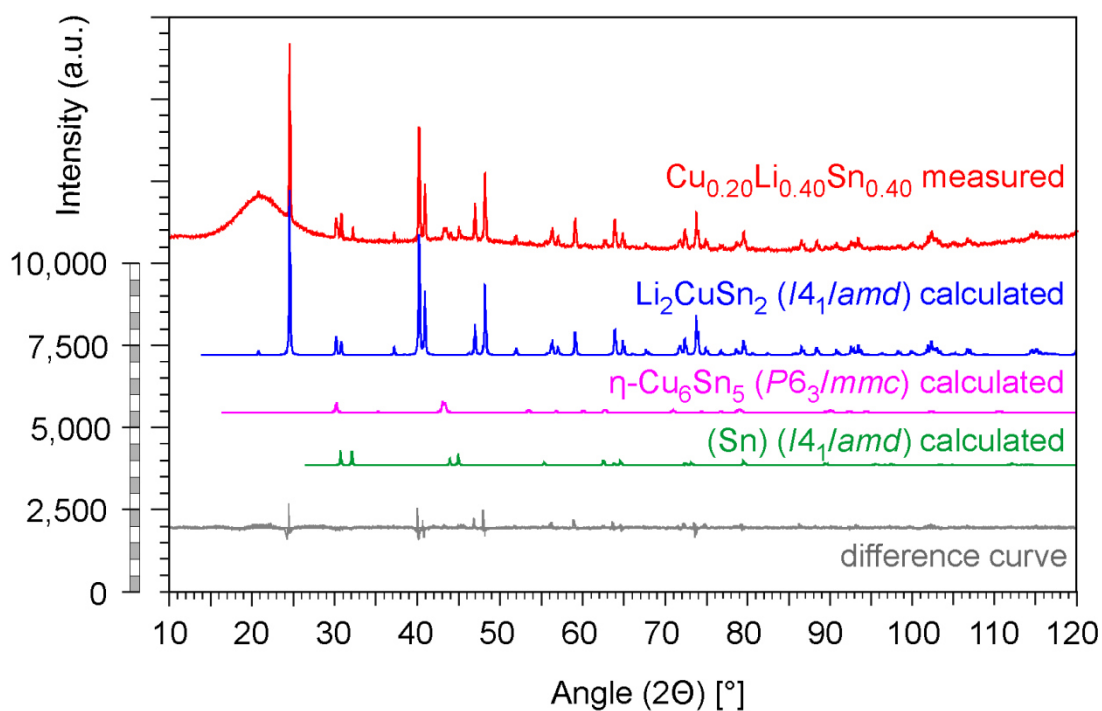
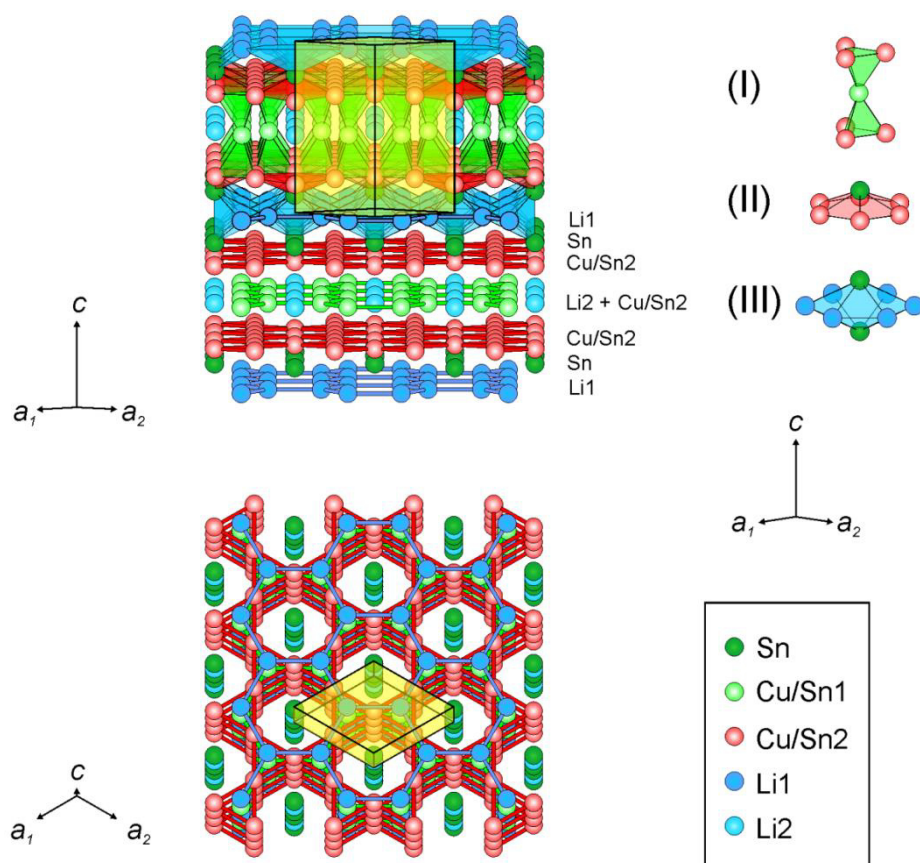**Fig. 2: Powder diffractogram of the sample Cu₀.₂₀Li₀.₄₀Sn₀.₄₀: Measured, calculated and difference patterns.**

94

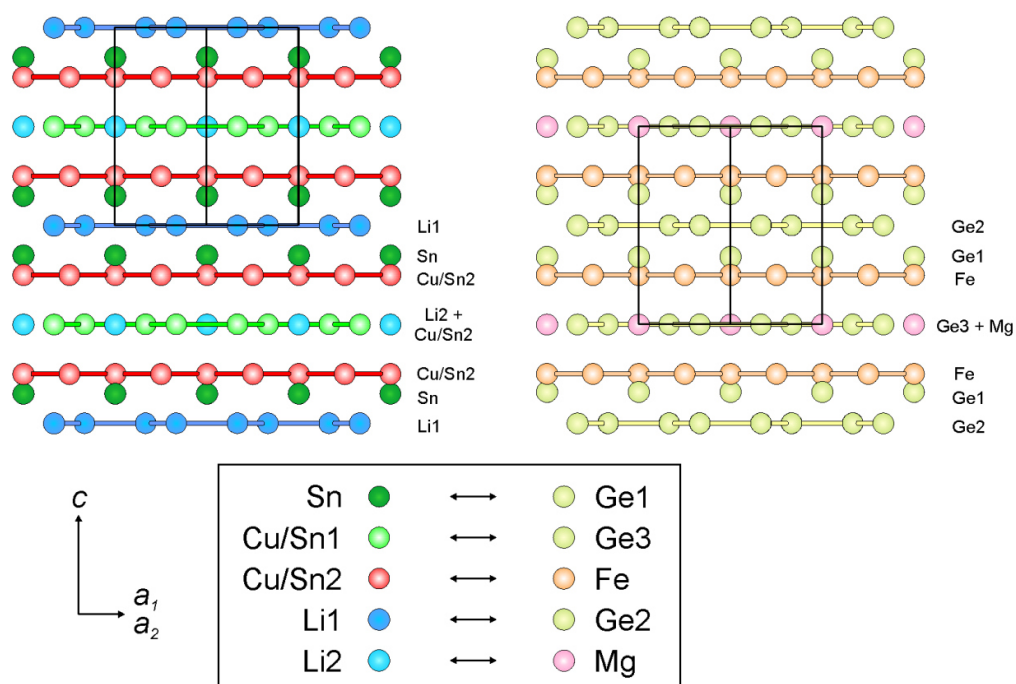**Fig. 3: Li₃Cu₆Sn₄: Presentation of structural motifs and layers; unit cell is yellow shaded**

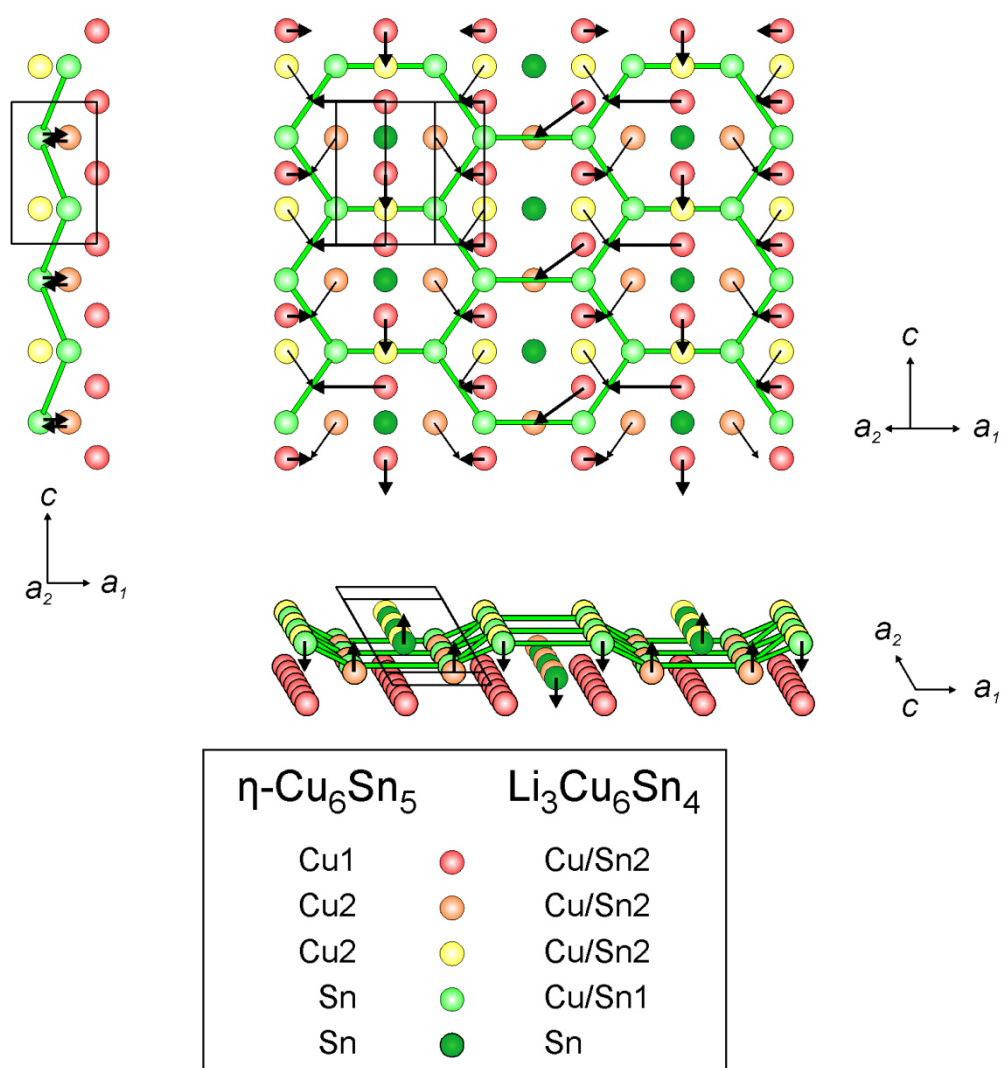**Fig. 4: Structural relationship between Li₃Cu₆Sn₄ and MgFe₆Ge₆**

95

Fig. 5: The crystal structure of η-Cu$_6$Sn$_5$ and the shifting vectors of the atoms Cu1, Cu2 and Sn to form the virtual Cu-Sn sublattice of the Li$_3$Cu$_6$Sn$_4$ structure; bold arrows indicate shifts of the Cu1 atoms and narrow lines shifts of Cu2 atoms (form separate layers in the ternary phase Li$_3$Cu$_6$Sn$_4$).
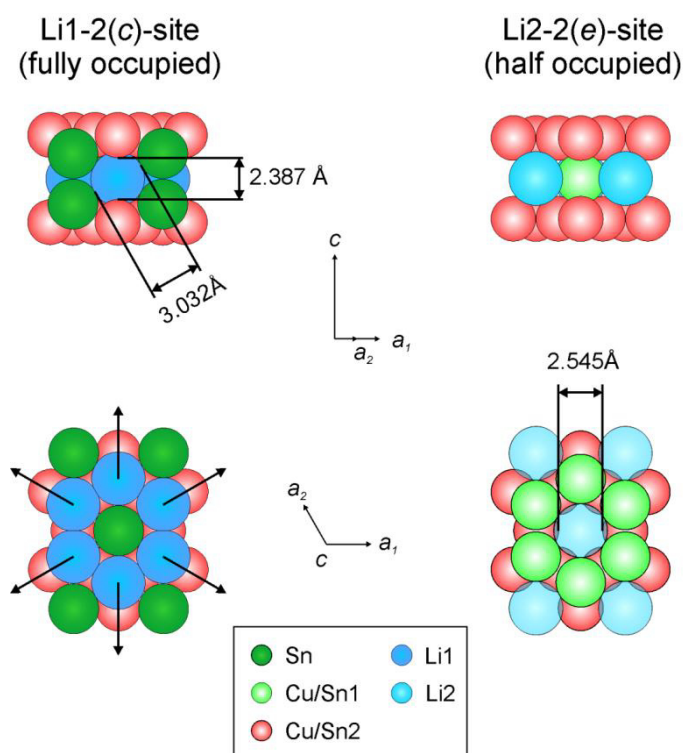
Fig. 6: Li-conducting channels and dimensions in $Li_3Cu_6Sn_4$; Li2 atoms are transparent for visibility of channels in [001].
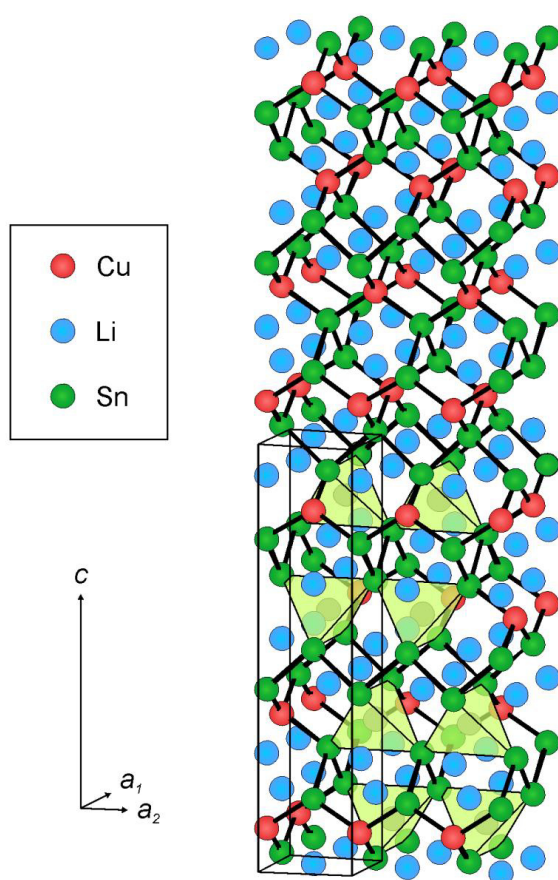
Fig. 7: Li_2CuSn_2: Tetrahedra of $CuSn_4$ and distorted rings of $(CuSn_2)$ subunits are shown.
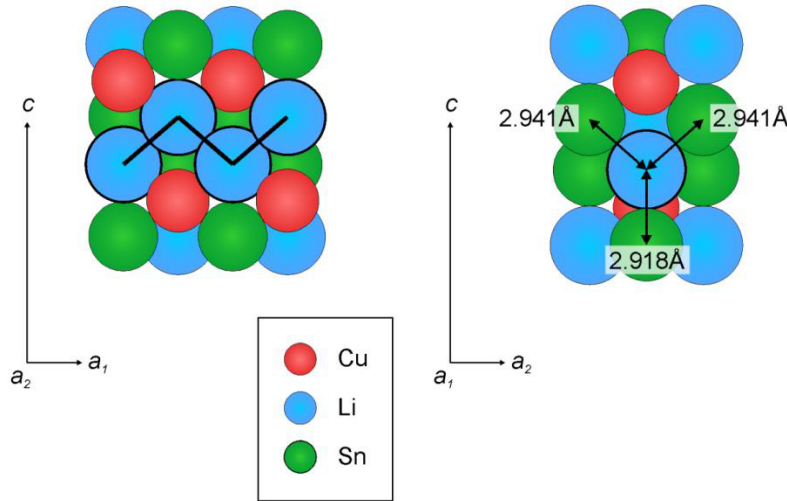
Fig. 8: Li-conducting channels and dimensions in Li₂CuSn₂; Li atoms are arranged in zigzag line inside channel.
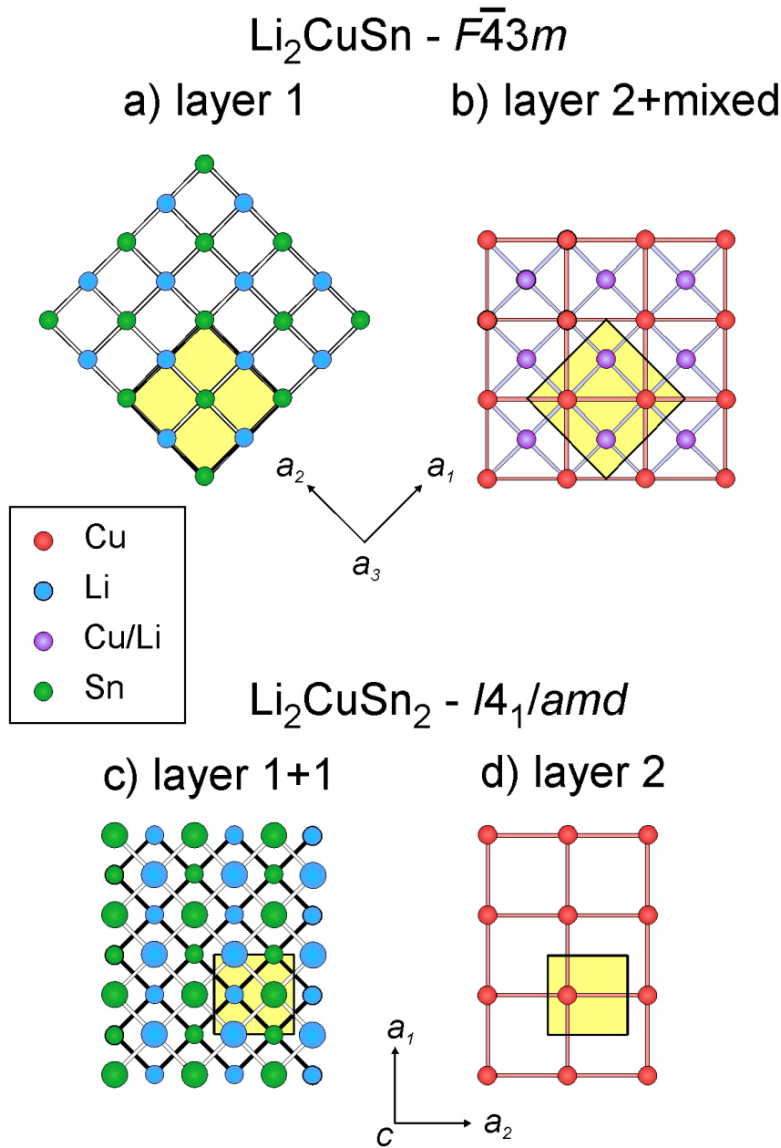
Fig. 9: Relationship between Li₂CuSn (a, b) and Li₂CuSn₂ (c, d): a) single layer of chess patterned Li and Sn atoms; b) squared Cu atom layer with mixed Cu/Li positions in face diagonal centre; c) double layer of Li and Sn atoms, chess pattern; different layers are plotted with different atom size for better visibility; d) squared primitive Cu atom layer.
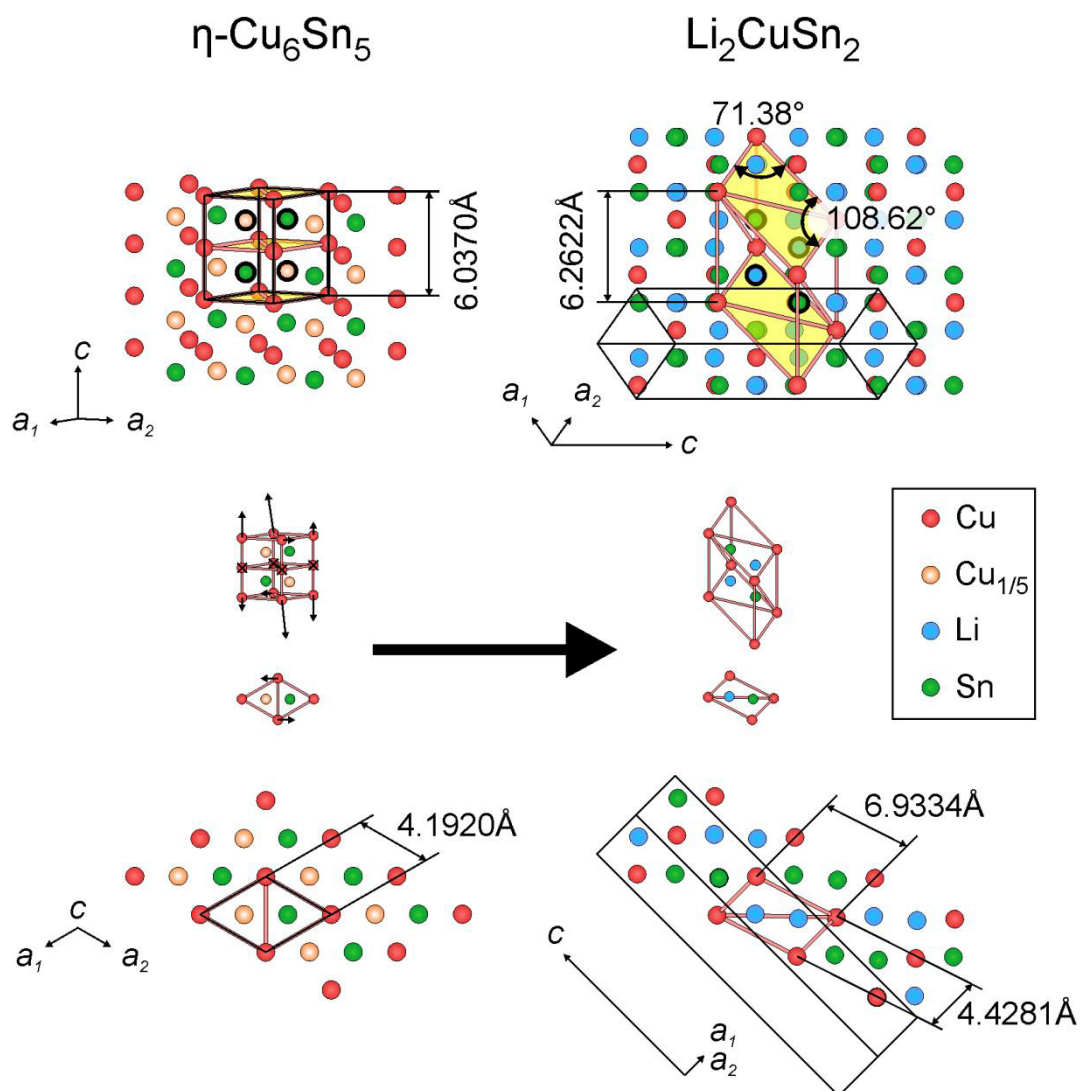
Fig. 10: Structural relationship between η-Cu₆Sn₅ and Li₂CuSn₂; atoms with bold rims are inside the unit cell.

3.4   Publication #4

New intermetallic phases in the Cu-Li-Sn system: The lithium-rich phases Li$_3$CuSn and Li$_6$Cu$_2$Sn$_3$

Siegfried Fürtauer[†], Herta S. Effenberger[‡], Hans Flandorfer[†]

[†]Institut für Anorganische Chemie (Materialchemie), University of Vienna, Währingerstraße 42, A-1090 Wien, Austria

[‡]Institut für Mineralogie und Kristallographie, University of Vienna, Althanstraße 14, A-1090 Wien, Austria

Contributions to this paper:

S. Fürtauer:	Sample preparation, measurement, structural comparison, writing
H. Effenberger	Measurement and data refinement, writing, proofreading
H. Flandorfer:	General advice and helpful comments, proofreading

Overall contributions of S. Fürtauer to the paper: 70%

Abstract

The Li-rich ternary intermetallic compounds with the idealized end-member compositions Li_3CuSn (CSD-427099) and $Li_6Cu_2Sn_3$ (CSD-427100) were synthesized from the pure elements by induction melting in Ta crucibles and annealing at 400 °C. Both powder and single-crystal XRD investigations were performed. Li_3CuSn crystallizes in space group $P6/mmm$ ($a = 4.5769(2)$, $c = 8.461(2)$ Å; $wR_2 = 0.073$ for 180 unique F^2-values and 25 free variables). All atoms are located along [00z], [1/3 2/3 z] and [2/3 1/3 $z$]; individual sites are arranged in layers parallel to (00.1). One site is fully, one partially occupied by Sn atoms. Fully but mixed occupation with Cu and Li atoms was found for one site. The remaining electron-density distribution resulting from the strong anisotropic displacement parallel to the c axis is considered in four further sites, which are mixed occupied with (Li, Cu, □), but modelled solely by Li atoms. The crystal structure exhibits analogies with that of Li_2CuSn ($F\bar{4}3m$); comparable layers occur parallel to {111} but the stacking sequence and packing density differs adopting cubic symmetry.

In $Li_6Cu_2Sn_3$ (space group $R\bar{3}2/m$, $a = 4.5900(2)$, $c = 30.910(6)$ Å; $wR_2 = 0.039$ for 253 unique F^2-values for 25 free variables) all atoms are arranged again at (00z), (1/3 2/3 z) and (2/3 1/3 z). Three sites are fully occupied (two by Sn atoms, a further one by Li atoms). Three additional positions are mixed occupied by Cu and Li atoms. The crystal structure is closely related to that of the binary phases $Li_{13}Sn_5$ and Li_5Sn_2; the substitution of Li by Cu atoms and *vice versa* is evident. The structural relationship to $Li_{13}Ag_5Si_6$, which is permeable for Li ions, makes the title compound interesting as anode material in Li-ion batteries.

Introduction

Li-ion batteries were already employed successfully in handheld electronics for a long time. However, for high-power applications such as electro mobility or stationary storage systems satisfactory cells based on Li-ion technique are not available up to now. Several research centres worldwide aim at developing new materials to be used as electrodes; aspired are improved properties such as an increased capacity based on an enlarged exchange of Li, revised cycling behaviour, longer lifetime, better economics, and higher reliability as compared to those Li anode materials available now [1]. Currently anodes based on graphitic materials have Li storage capacities of approximately 372 mAh/g [2]. An increase of the storage capacity seems possible using intermetallic anode materials. So far, the compound with the highest Li content in the binary system Li−Sn, *i.e.*, $Li_{17}Sn_4$, offers a capacity of 960 mAh/g. The main problem using intermetallic anode materials is

102

the tremendous volume change during charging and discharging; this holds especially for binary alloys. The volume change can reach more than 200 vol.-% and results in an electrode crumbling, which finally causes a loss of the electronic contact between the individual particles and ends up in a rapid capacity loss [3]. To overcome this problem, an increase of the mechanical stability and, in parallel, a reduction of the volume changes during charging and discharging is required. For an improvement, compounds belonging to a ternary or even a higher ordered intermetallic system are considered. A promising candidate is the Cu-Li-Sn system. In the charged state, the anode might consist of a Li-rich (Cu-)Li-Sn compound, which is encapsulated in an inert phase like (Cu) acting as a stabilizing matrix [4]. Discharging transforms the anode material to a binary or even ternary phase with reduced Li content. Based on electrochemical insertion experiments, various authors [5-10] proposed the two-step reaction mechanism

(1) $Cu_6Sn_5 + 10\ Li \rightarrow 5\ Li_2CuSn + (Cu)$

(2) $5\ Li_2CuSn + 11.25\ Li \rightarrow 5\ Li_{4.25}Sn + 5\ (Cu)$.
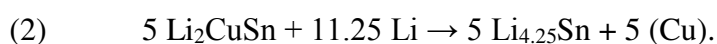
According to this reaction scheme the insertion of Li atoms into the compound Cu_6Sn_5 [11] results in the formation of the ternary intermetallic phase Li_2CuSn, besides the formation of (Cu) (1). The continuation of the insertion of Li atoms into Li_2CuSn causes again the precipitation of Cu (*i.e.*, a solid solution of Sn and Li in Cu) and forms the binary compound $Li_{4.25}Sn$ (= $Li_{17}Sn_4$ [12]) (2). However, at the time this reaction mechanism was proposed, only two ternary compounds in the system Cu−Li−Sn were known: Li_2CuSn [13-15] and $LiCu_2Sn$ [16]; furthermore these compounds were considered as stoichiometric. Deviations from stoichiometry suggesting exchange mechanisms were detected based on improved powder and single-crystal X-ray experiment techniques by the present authors recently [17]. Structural refinements of these two compounds gave evidence for extensive solid solutions. Li_2CuSn_2 [18, 19] was described later, again with moderate deviations from stoichiometry. Ongoing systematic researches in the Cu-Li-Sn system revealed further ternary intermetallic compounds. The Sn-rich compound $Li_3Cu_6Sn_4$ [18] is located in the proposed three-phase field (Cu)−Cu_6Sn_5−Li_2CuSn and rather indicates a more complex reaction scheme. Ongoing investigations in the Li-rich section of the Cu−Li−Sn system yielded two further compounds unknown so far; they have the ideal end-member formulas Li_3CuSn and $Li_6Cu_2Sn_3$. The present paper characterizes these compounds structurally and crystal chemically; in addition, topological relations to $Li_{13}Sn_5$, Li_5Sn_2, and $Li_{13}Ag_5Si_6$ are discussed. The development

of improved electrode materials requires detailed knowledge of the respective phase diagrams as well as of the occurring phases as a basis to understand thermodynamics of the relevant phase reactions.

Materials and Methods

Sample Preparation

For sample preparations the pure elements Cu (99.98 at.%, wire, Goodfellow, Cambridge, UK), Li (99.8 at.%, wire, Alfa Aesar, Karlsruhe, Germany) and Sn (99.95 at.%, ingot, Advent, Oxford, UK) were inserted. The thin oxide layer on the Cu wire was removed by reduction in an H_2-flow for 5 hours at 300 °C. The Li wire was stored originally in mineral oil, which was removed by n-hexane in a supersonic bath followed by vacuum evaporation of the solvent. The required amounts of metal pieces were assembled in Ta crucibles. All operations with Li were done in a glove box under Ar atmosphere (< 5 ppm O_2 / H_2O). Afterwards the crucibles were welded again in Ar atmosphere using an arc furnace. For melting of the inserted metals, the crucibles were put into an induction furnace at 1100 °C. Repetition of the melting process twice (only 10-20 sec. each to prevent high temperature fatigue of the welding seam) with turning the crucible upside down between the heating steps assured homogenous mixing of the liquid alloys. Then the crucibles were sealed in quartz-glass tubes under vacuum. The alloys were annealed at 400 °C in a muffle furnace (various durations, see Table 1) and finally quenched in cold water.

Powder-XRD investigations

All preparation steps for the powder investigations were performed in a glove box. The samples were grinded with a Durit® mortar. The powder was fixed with petroleum jelly on the sample holder (Si monocrystal). Maintaining the protecting gas atmosphere was achieved by an X-ray amorphous cap (polycarbonate) covering the sample. Powder-XRD measurements were performed on a Bragg-Brentano diffractometer ($\theta/2\theta$-geometry) operated with a Cu radiation source (40 kV / 40 mA) and a Ni filter. Signals were detected with a strip detector. The obtained patterns were evaluated by Rietveld-refinements using Topas3® [20] software. Powder XRD allowed the identification of the individual phases and their relative amounts occuring in the investigated Cu−Li−Sn system. Unknown phases could be identified. Characteristic powder patterns for syntheses products rich in Li_3CuSn and $Li_6Cu_2Sn_3$ are given in Figs. 1 and 2, respectively.

Single-crystal XRD investigations

For selection and preparation of the single-crystals used for XRD, small amounts of gritty bulk samples were fixed in the glovebox with amorphous petroleum jelly between two object plates. Slightly pushing and sliding of the object plates crushed the bulk samples into smaller particles and covered them entirely with the grease. Then appropriate crystals under jelly were picked up outside of the glovebox under a binocular microscope (up to 400 fold magnification) with fine acupuncture needles and fixed onto a glass capillary again captured with grease. The respective crystals have a diameter of approx. 50 to 100 µm. Single-crystal XRD was performed at 290 K with a four-circle Nonius Kappa diffractometer equipped with a CCD detector, a 300 µm capillary optics collimator and a N_2-gas cryostream cooler from OXFORD CryoSystems. Monochromated MoKα radiation was used (graphite monochromator). The continuous stream of dried N_2 gas enclosed the single-crystal during the measurement protecting it from corroding and, in addition, controlled the isothermal conditions. The unit-cell parameters were obtained by least-squares refinements of the 2ϑ values from all collected intensity data. Corrections for Lorentz, polarization and absorption effects (multi-scan method) were applied. Complex scattering functions of Wilson [21] were used for all calculations. For data collection, structure solution and refinements the programs "COLLECT" [22, 23], "SHELXS-97" and "SHELXL-97" [24-26] were employed. The crystal structures were displayed by the software "ATOMS" [27]. The extinction symbols and space-group symmetries were found from the extinction rules and the structure refinements, respectively. Direct methods in combination with Patterson summations yielded a first set of positions occupied by Sn and Cu atoms. Successive difference Fourier summations and least-squares refinements revealed the remaining atom sites and their occupations. The high correlation between the distinct scattering functions considering mixed occupation together with the expected vacancies caused large uncertainties of the occupation refinements. Details of the single-crystal data-collection and structure refinements are compiled in Table 2, fractional coordinates and interatomic bond distances are given in Tables 3 and 4, respectively.

Results and Discussion

Li₃CuSn

The powder XRD obtained from reaction products of syntheses runs, with the nominal composition $Li_{0.60}Cu_{0.20}Sn_{0.20}$, showed Li_3CuSn besides minor amounts of (Cu) (see Table 1 and Fig. 1). The latter probably results from non-stoichiometry of the phase, either at annealing temperature or at lower temperatures for the case that equilibrium freezing is not fully possible. Small deviations from the 3:1 occupation of Li and Cu are probable because of mixed and partial occupation of the respective sites. However, because Li has the atomic number three only, the instability of the phase in the electron beam and in air, the composition cannot be determined by single-crystal refinements nor by analytical methods including EPMA with certain. At least the average atomic arrangement of Li_3CuSn crystallizes in space group *P6/mmm*. At the beginning of the refinement, the positions 1(*a*) and 2(*d*) were considered as fully occupied by Sn and Cu atoms, respectively. Partial and mixed occupation by Cu and Li atoms was assumed for further positions detected in the difference Fourier summation. However, this allocation resulted in an unacceptable discrepancy between the chemical composition recalculated from structure refinements and the synthesis input (recalculated: $Li_{0.45}Cu_{0.41}Sn_{0.14}$ = $Li_{3.16}Cu_{2.84}Sn$; nominal: $Li_{0.60}Cu_{0.20}Sn_{0.20}$ = Li_3CuSn). The phase Li_3CuSn was also identified in samples of several syntheses in the surrounding of the nominal composition. Extensive investigations of the phase diagram Cu−Li−Sn contradicted the Cu:Sn ratio of about 3:1 found in the first step of structure refinement. Therefore, an allocation of Sn atoms also at the site 2(*d*) is considered, the occupation factor decreased according to the larger scattering power of 29 and 50 electrons, respectively. It has to be mentioned, that the *R* values are influenced insignificantly considering the different occupations at site 2(*d*); from refinements a decision between a full occupation by Cu atoms or a partial occupation by Sn±Cu±Li atoms is impossible. However, succeeding structure investigations on samples from further syntheses runs improved the crystals' quality and further weak occupied sites at (1/3 2/3 *z*) could be seen in the difference Fourier summation contradicting with a fully occupied site 2(*d*). Even many efforts were made finding a sample with sharp reflection profiles, also the finally used crystal exhibited a relatively broad reflection profile. It has to be mentioned that no relations with respect to the reciprocal lattice could be observed. Only slight relicts from Debye rings close to the Bragg reflections were evident indicating some powdery admixture with a preferred orientation with respect to the main crystal. Especially neither streaks nor diffuse

scattering that might result from distinct disorder phenomena could be detected with the CCD area detector; especially the direction along c^* was checked carefully. Furthermore, some trials to refine the crystal structure in subgroups of $P6/mmm$ and considering (merohedral) twinning were not successful; they failed due to the limited quality of the sample or due to the verified disorder. From powder X-ray diffraction patterns a (111) twinning of the $F\bar{4}3m$-structure type (Li_2CuSn) could be excluded. The site $M1$ has distances to neighbouring atoms > 2.60 Å; it was considered as fully occupied. The atomic ratio of Li and Cu atoms was allowed to vary during the structure refinement. Between several sites short distances (0.56 to 1.81 Å) occur – requiring vacancies at the positions Sn2, $M2$, $M3$, $M4$ and $M5$. These sites model the electron density distribution resulting from the strong anisotropic displacement mainly but not only parallel to the $\boldsymbol{c}$ axis. All these sites are located at (1/3 2/3 z) indicating enabling an extensive exchange mechanism. The similar space requirements of the atoms Cu and Li as compared to the somewhat larger Sn atom (covalent radii of 1.17, 1.23 and 1.40 Å [28]) suggest an exchange mechanism mainly between the atoms Li and Cu. The composition resulting from this model agrees with the expectations from syntheses experiments. Mixed occupied (Li,Cu, □) sites are well known from literature and were earlier found also in Li_2CuSn as well as in $LiCu_2Sn$ (*cf.* [17]); they are evident also in $Li_6Cu_2Sn_3$ (see below) whereas $Li_3Cu_6Sn_4$ [18] exhibits substitutions of Sn by Cu atoms and *vice versa*. The large (anisotropic) displacement parameters going along with partial and mixed occupations were considered as a hint for a possible reduction of the space group and perhaps Laue symmetry. To check a tentative multiplication of the cell volume the reciprocal lattice was carefully investigated for weak *super*-structure reflections. However, all trials to reduce the space-group symmetry or increase the cell volume failed; consequently $P6/mmm$ has to be considered as the most probable and applicable solution.

Topologically, the crystal structure of Li_3CuSn exhibits layers parallel to (0001). Neglecting the sites $M3$, $M4$ and $M5$ which model the elongated displacement of the sites Sn2 and $M2$, six distinct layers are evidently arranged according to the sequence […−Sn1−$M2$−$M1$−Sn2−$M1$−$M2$−…] (Fig. 3a). Each of the sites Sn1 and $M1$ has six neighbours in a distance of $a = 4.52$ Å (within this layer A) whereas the sites Sn2 and $M2$ form honeycomb nets with interatomic distances of $a\sqrt{3}/3 = 2.61$ Å) (layer B). The stacking sequence is [−A−B−A−B−A−B−]. Structural similarities between the phases Li_3CuSn and Li_2CuSn (space group $F\bar{4}3m$) [17] are evident. Whereas Li_3CuSn exhibits mixed and only partially occupied sites, Li_2CuSn has a fully ordered atomic arrangement.

The projection of the crystal structure of Li_3CuSn parallel to [001] appears as identical with that of Li_2CuSn parallel to <111>. Topologically Li_2CuSn consists of *pseudo*hexagonal layers perpendicular to <111> (Fig. 3b), each formed by one of the four distinct atom sites (Wyckoff sites 4(*a*), 4(*b*), 4(*c*) and 4(*d*), respectively). Within these layers the interatomic distance between atoms is 4.451 Å, *i.e.* $a\sqrt{2}/2$. Succeeding layers are separated by a quarter of the unit-cell's space diagonal, *i.e.*, 2.726 Å. Within all layers, the atoms have six neighbours and a topological stacking sequence [−A−A−A−A−]. The allocation of the atoms at these layers is [−*M*−Li−Cu−Sn−]. It is noteworthy that the Li_3CuSn phase contains two additional *M*-layers per unit cell as compared to that of Li_2CuSn. Despite the different stoichiometry of the layers A and B as well as different occupation ratios at the distinct sites, these structural analogies probably might be an indication for a formation mechanism of Li_3CuSn from Li_2CuSn by introduction of Li atoms.

$Li_6Cu_2Sn_3$

In the samples resulting from a synthesis input with the nominal composition $Li_{0.63}Cu_{0.10}Sn_{0.27}$ a two-phase equilibrium between the binary phase $Li_{13}Sn_5$ [29] and the new ternary phase $Li_6Cu_2Sn_3$ was found. However, $Li_{13}Sn_5$ is present in smaller amounts only (see Table 1 and Fig. 2). A close structural relationship of $Li_6Cu_2Sn_3$ with Li_5NaSn_4 (space group $R3m$, [30]) and $Li_5Na_2Sn_4$ (space group $R\bar{3}m$, [31]) was expected from the similarities of the cell metrics and the X-ray powder patterns. Whereas the cell parameter *a* of the title compound compares quite well with those ones of Li_5NaSn_4 and $Li_5Na_2Sn_4$ (4.590, 4.710, 4.723 Å), comparable values for *c* were only found for Li_5NaSn_4 (31.725 Å; title compound: $c = 30.910$ Å); *c* is more than twice as large in $Li_5Na_2Sn_4$ (71.78 Å). Several trials using the atomic coordinates of Li_5NaSn_4 in the starting set for structure refinements of $Li_6Cu_2Sn_3$ failed. Based on Patterson maps the close structural relations between these compounds estimated from powder X-ray experiments could be verified. From both, successive difference Fourier summations and crystal chemical considerations, the crystal structure of the title compound was solved and finally refined successively in space group $R\bar{3}2/m$. The calculated composition of the $Li_6Cu_2Sn_3$ phase obtained from single-crystal XRD refinements ($Li_{0.57}Cu_{0.16}Sn_{0.27}$) is very close to the composition estimated from the synthesis input ($Li_{0.55}Cu_{0.18}Sn_{0.27}$), considering the formation of $Li_{13}Sn_5$ besides the title compound.

The common feature of the crystal structures of $Li_6Cu_2Sn_3$, Li_5NaSn_4 and $Li_5Na_2Sn_4$ is the arrangement of all atoms at $(00z)$ [and at $(1/3\ 2/3\ z)$ and $(2/3\ 1/3\ z)$ due to R centring]. It is worthy to note that the z-parameters along [001] in the title compound feature differences between 0.0896 and 0.0937 only. Accounting to the R centring, the atoms are arranged in 33 layers parallel to (0001). Their distances amount 0.881 to 0.937 Å and 1.020 to 1.060 Å, respectively. The stacking sequence with an alternation of one large and two small gaps is interrupted three times within the unit cell by one short interval only. In Li_5NaSn_4 only 30 layers parallel to (0001) exist per unit cell. Three different distances along [001] between the layers occur: short (0.465 Å), medium (0.719 to 1.000 Å) and long (1.046 to 1.529Å); the stacking sequence is: long (3x), medium (2x), long (2x), short (1), long (1x) and medium (1x) with a threefold repetition within the unit cell. These distinct differences were responsible for the impossibility to use the atomic coordinates of Li_5NaSn_4 in the starting set for structure solution of $Li_6Cu_2Sn_3$. In addition, the only occupation of special sites - one atom at $3(a)$ (000) and all the other atoms at $6(c)$ $(00z)$ - hindered a smooth refinement of the crystal structure. $Li_5Na_2Sn_4$ features in total 66 distinct layers with a distinct succession of gaps between the layers. The structural similarity between $Li_6Cu_2Sn_3$ and several other phases ($Li_{13}Sn_5$ [29], Li_5Sn_2 [32], Li_5NaSn_4 [30] and $Li_{13}Ag_5Si_6$ [33]) is demonstrated in Fig. 4 and Table 5. Structural and topological relations between $Li_6Cu_2Sn_3$ and the binary Li-Sn phases are of interest for understanding the Cu-Li-Sn phase diagram and possible lithiation and delithiation pathways. $Li_{13}Ag_5Si_6$ is considered as a promising candidate for anode materials in Li-ion batteries; in electrochemical lithiation experiments, the reversible capacity was found to be 800 mAh/g [33]. The structural similarities of $Li_{13}Ag_5Si_6$ with $Li_6Cu_2Sn_3$ suggest that the latter compound may be considered as a prospective anode material. The crystal structures of the five compounds mentioned in the last paragraph are topologically described as formed by three kinds of polyhedra around the atoms Li, Li/Cu, Ag/Li or Na: trigonal prisms, tetrahedra, and octahedra. In $Li_{13}Ag_5Si_6$ the strongly distorted tetrahedra and octahedra are rather trigonal pyramids and trigonal antiprisms, respectively. Mostly atoms of group-4 elements (Sn or Si atoms) are located at the corners of each of these polyhedra (see Table 5). The trigonal antiprism is formed around two (Ag,Li)1 sites (separation 3.104 Å). Because of their linkage parallel to (0001), the tetrahedra are elongated parallel [001] forming trigonal pyramids. The linkage of these polyhedra among each other form three distinct kinds of layers parallel to (0001): A_1) distorted tetrahedra fill the interstices between the respective octahedra and *vice versa*; A_2) similarly the layers are formed by trigonal pyramids, distorted tetra- and octahedra;

A$_3$) formed by tetrahedra and trigonal antiprisms, respectively. B) face-sharing trigonal prisms fill the space completely; C) trigonal prisms share edges only, half of the central positions are vacant. Two, three or four succeeding layers form building blocks. The three compounds Li$_6$Cu$_2$Sn$_3$, Li$_5$Sn$_2$ and Li$_{13}$Ag$_5$Si$_6$ crystallize in space group $R\overline{3}2/m$ with the building block sequences −A$_1$−B−A$_1$−, −A$_1$−B−, and −A$_2$−B−A$_2$−A$_3$−, respectively; these units are stacked according to the R centring. In the crystal structure of Li$_{13}$Sn$_5$ (space group $P\overline{3}m1$) the layer stacking sequence is [−A$_1$−B−A$_1$−B−A$_1$−]; $i.e.,$ as compared to an alternating arrangement of A$_1$ and B layers, each third B-layer is missing. The formation of Li$_6$Cu$_2$Sn$_3$ by insertion of Cu atoms substituting for Li atoms is evident. At the same time, Sn atoms stabilize the ternary phase and contribute to the stacking sequence [−A$_1$−B−A$_1$−]. In most cases, the individual layers are connected by sharing their group-4 atom corners. However, in Li$_5$NaSn$_4$ (space group $R3m$) the building block sequences [−C−A$_1$−B−] are separated, they are not linked by sharing any atoms at the top and bottom face: Two adjacent Sn atom layers are separated by 1.0 Å. As mentioned above, the coordination polyhedra formed around the group-4 atoms with interstitial atoms of various kinds are distorted. Due to the site symmetries $\overline{3}m$ and $3m$, respectively, an elongation or even a compression of the polyhedra is observed parallel to [00z]. Interatomic attraction and repulsion forces as well as different sizes of atoms cause the deviation from the ideal hexagonal close packing.

Conclusions

In two earlier papers, the authors reported on the crystal chemistry of crystal structures of ternary phases in the Cu-Li-Sn system: Li$_2$CuSn ($F\overline{4}3m$), LiCu$_2$Sn ($P6_3/mmc$), Li$_2$CuSn$_2$ ($I4_1/amd$) and Li$_3$Cu$_6$Sn$_4$ ($P6/mmm$) [17, 18]. Now this series is supplemented by the description of the Li-rich compounds Li$_3$CuSn and Li$_6$Cu$_2$Sn$_3$. The Li$_3$CuSn phase crystallizes in space group $P6/mmm$ with the unit cell parameters $a = 4.5769(2)$ and $c = 8.461(2)$ Å. It exhibits some similarities to the Li$_2$CuSn phase [17]; different stacking order and a distinct atom distribution at the layers are evident. The Li$_6$Cu$_2$Sn$_3$ phase crystallizes in space group $R\overline{3}2/m$. The lattice parameters are $a = 4.5900(2)$ and $c = 30.910(6)$ Å. All atoms are located at (00z), z of neighbouring atoms differs between 0.0896 and 0.0937 only. The crystal structure is topologically related to that of Li$_{13}$Sn$_5$ ($P\overline{3}m1$) and Li$_5$Sn$_2$ ($R\overline{3}2/m$); differences are evident by partial substitutions of Li by Cu atoms and distinct stacking of layers along [001]. Structural similarity to both Li$_5$NaSn$_4$ ($R3m$) and Li$_{13}$Ag$_5$Si$_6$ ($R\overline{3}2/m$) are also evident. The latter one is permeable for Li ions [33, 34]; similar electric behaviour has to be tested for Li$_6$Cu$_2$Sn$_3$. Further investigations

like solid-state [6]Li-NMR have to be applied to validate the compound as appropriate Li storage material. The occurrence of both title compounds, Li_3CuSn and $Li_6Cu_2Sn_3$, contradicts the earlier assumed phase relations [5-10]. They have been deduced only from ternary phases (Li_2CuSn and $LiCu_2Sn$) thitherto known without doing respective investigation on phase relations. In-situ XRD reported in several works during lithiation process of binary Cu_6Sn_5 alloys [6-10] revealed a pattern similar to Li_2CuSn, which however, can also be allocated to Li_2CuSn_2 - a phase that was described years later [18, 19]. A serious evaluation of such mechanisms efforts the knowledge of all existing compounds in the respective alloy systems as well as kinetic and electrochemical investigations. Thus, the investigation of phase equilibria under consideration of all ternary phases in the Cu-Li-Sn system aims at further work.

Acknowledgements

References

[1]   C. Daniel, Materials and processing for lithium-ion batteries. *JOM* **2008,** *60*, 43.

[2]   A.K. Shukla, T.P. Kumar, Materials for next-generation lithium batteries. *Curr. Sci. India* **2008,** *94*, 314.

[3]   M.S. Whittingham, Materials challenges facing electrical energy storage. *MRS Bull.* **2008,** *33*, 411.

[4]   M. Winter, J.O. Besenhard, Electrochemical lithiation of tin and tin-based intermetallics and composites. *Electrochim. Acta* **1999,** *45*, 31.

[5]   A.N. Jansen, J.A. Clevenger, A.M. Baebler, J.T. Vaughey, Variable temperature performance of intermetallic lithium-ion battery anode materials. *J. Alloys Compd.* **2011,** *509*, 4457.

[6]   W. Choi, J.Y. Lee, H.S. Lim, Electrochemical lithiation reactions of Cu_6Sn_5 and their reaction products. *Electrochem. Commun.* **2004,** *6*, 816.

[7]   S. Sharma, L. Fransson, E. Sjostedt, L. Nordstrom, B. Johansson, K. Edstrom, A theoretical and experimental study of the lithiation of η'-Cu_6Sn_5 in a lithium-ion battery. *J. Electrochem. Soc.* **2003,** *150*, A330.

[8]   G.X. Wang, L. Sun, D.H. Bradhurst, S.X. Dou, H.K. Liu, Lithium storage properties of nanocrystalline η-Cu_6Sn_5 alloys prepared by ball-milling. *J. Alloys Compd.* **2000,** *299*, L12.

[9]   J.T. Vaughey, K.D. Kepler, R. Benedek, M.M. Thackeray, NiAs- versus zinc-blende-type intermetallic insertion electrodes for lithium batteries: lithium extraction from Li_2CuSn. *Electrochem. Commun.* **1999,** *1*, 517.

[10]   K.D. Kepler, J.T. Vaughey, M.M. Thackeray, $Li_xCu_6Sn_5$ (0 < x < 13): An intermetallic insertion electrode for rechargeable lithium batteries. *Electrochem. Solid St.* **1999,** *2*, 307.

[11]   A. Gangulee, G.C. Das, M.B. Bever, X-ray diffraction and calorimetric investigation of compound Cu_6Sn_5. *Metall. Trans.* **1973,** *4*, 2063.

[12]   C. Lupu, J.G. Mao, J.W. Rabalais, A.M. Guloy, J.W.J. Richardson, X-ray and neutron diffraction studies on "$Li_{4.4}Sn$". *Inorg. Chem.* **2003,** *42*, 3765.

[13]   H.U. Schuster, Ternäre Lithium-Verbindungen mit Elementen der 4. Hauptgruppe. *Naturwissenschaften* **1966,** *53*, 360.

[14]   H. Pauly, A. Weiss, H. Witte, Crystal structure of ternary intermetallic phases Li_2EX (E = Cu, Ag, Au; X = Al, Ga, In, Tl, Si, Ge, Sn, Pb, Sb, Bi). *Z. Metallkd.* **1968,** *59*, 47.

[15]   H.U. Schuster, D. Thiedemann, H. Schönemann, Ternary lithium compounds with formulas of $LiMe_2X$ and Li_2MeX (Me = Cu, Ag or Au; X = Si, Ge or Sn). *Z. Anorg. Allg. Chem.* **1969,** *370*, 160.

[16]   P.I. Kripyakevich, G.I. Oleksiv, Crystal structure of the compound $LiCu_2Sn$. *Dopov. Akad. Nauk Ukr. RSR* **1970,** *A*, 63.

[17]   S. Fürtauer, H.S. Effenberger, H. Flandorfer, $CuLi_2Sn$ and Cu_2LiSn: Characterization by single crystal XRD and structural discussion towards new anode materials for Li-ion batteries. *J. Solid State Chem.* **2014,** *220*, 198.

[18]   S. Fürtauer, H.S. Effenberger, H. Flandorfer, The tin-rich copper lithium stannides: $Li_3Cu_6Sn_4$ and Li_2CuSn_2. *Z. Kristallogr.* **2015,** *230*, 97.

[19]   F. Winter, S. Dupke, H. Eckert, U.C. Rodewald, R. Pöttgen, Lithium mobility in the stannides Li_2CuSn_2 and Li_2AgSn_2. *Z. Anorg. Allg. Chem.* **2013,** *639*, 2790.

[20]   Bruker-AXS, *Topas*. Version 3, Billerica / MA **1999 / 2000**.

[21]   A.J.C. Wilson, (Ed.), International Tables for Crystallography, Kluwer, Dordrecht / NL **1992**.

[22]   Z. Otwinowski, W. Minor, Processing of X-ray diffraction data collected in oscillation mode. *Method. Enzymol.* **1997,** *276*, 307.

[23]   B.V. Nonius, *Collect - Data Collection Software*. Delft / Netherlands **1999**.

[24]   G.M. Sheldrick, A short history of SHELX. *Acta Crystallogr. A* **2008,** *64*, 112.

[25]   G.M. Sheldrick, *SHELXS 97 - A Program for the Solution of Crystal Structures*. Göttingen **1997**.

[26]   G.M. Sheldrick, *SHELXL 97 - A Program for Crystal Structure Refinement*. Göttingen **1997**.

[27]   E. Dowty, *Atoms - A Computer Program for Displaying Atomic Structures*. Version 6.2, Shape Software, Kingsport / TN **2004**.

[28]   J. Emsley, The Elements. Clarendon Press, Oxford, **1989**.

[29]   U. Frank, W. Müller, Darstellung und Struktur der Phase $Li_{13}Sn_5$ und die strukturelle Verwandtschaft der Phasen in den Systemen Li-Sn und Li-Pb. *Z. Naturforsch. B* **1975,** *30*, 316.

[30]   K. Volk, W. Müller, Li_5NaSn_4 - Eine Phase mit gewellten Sn-Sechsecknetzen. *Z. Naturforsch. B* **1978,** *33*, 593.

[31]   K. Volk, W. Müller, Darstellung und Struktur der Phase $Li_5Na_2Sn_4$. *Z. Naturforsch. B* **1978,** *33*, 823.

[32]   U. Frank, W. Müller, H. Schäfer, Die Kristallstruktur der Phase Li_5Sn_2. *Z. Naturforsch. B* **1975,** *30*, 1.

[33]   L. Lacroix-Orio, M. Tillard, C. Belin, Synthesis, crystal and electronic structure of $Li_{13}Ag_5Si_6$, a potential anode for Li-ion batteries. *Solid State Sci.* **2008,** *10*, 5.

[34]   R. Pöttgen, T. Dinges, H. Eckert, P. Sreeraj, H.D. Wiemhöfer, Lithium-Transition Metal-Tetrelides - Structure and Lithium Mobility. *Z. Phys. Chem.* **2010,** *224*, 1475.

Table 1: Composition, heat treatment and cell metrics determined from powder XRD data.

Nominal Composition	Heat treatment	Phases	Space group	Lattice parameter (Å)	
$Li_{0.60}Cu_{0.20}Sn_{0.20}$	27d / 400°C	Li_3CuSn (Cu)	*P6/mmm* *Fm$\overline{3}$m*	$a = 4.558(4)$ $a = 3.615(3)$	$c = 8.467(8)$
$Li_{0.63}Cu_{0.10}Sn_{0.27}$	7d / 400°C	$Li_6Cu_2Sn_3$ $Li_{13}Sn_5$	*R$\overline{3}$2/m* *P$\overline{3}$m1*	$a = 4.58366(8)$ $a = 4.6482(2)$	$c = 30.830(11)$ $c = 16.913(13)$

Table 2: Single-crystal X-ray data-collection and crystal structure refinements of Li$_3$CuSn and Li$_6$Cu$_2$Sn$_3$.

Sample composition	Li$_{0.60}$Cu$_{0.20}$Sn$_{0.20}$	Li$_{0.63}$Cu$_{0.10}$Sn$_{0.27}$
(ideal) chemical formula	Li$_3$CuSn	Li$_6$Cu$_2$Sn$_3$
a (Å)	4.5769(2)	4.5900(2)
c (Å)	8.461(2)	30.910(6)
space group	$P6/mmm$ (191)	$R\bar{3}2/m$ (166)
V (Å^3)	151.1	564.0
Z	2	3
ρ_{calc} (g cm^{-3}) / μ(Mo$K\alpha$) (mm^{-1})	4.39 / 14.7	4.64 / 15.3
crystal dimensions (μm)	70×90×100	50×70×85
range of data collection ($\pm h \pm k \pm l$) (°)	3 < 2ϑ < 70	3 < 2ϑ < 70
number of images / rotation angle per image (°)	561 / 2	1082 / 1
scan mode (φ-scans at distinct ω-angles)	11 φ-scans	10 φ-scans
scan time (s/°); frame size 621×576 pixels (binned mode)	200	180
detector-to-sample distance (mm)	30	30
measured reflections	2,551	1,949
unique reflections (n) / observed reflections ($F_o > 4\sigma(F_o)$)	180 / 164	253 / 227
$R_{int} = \Sigma\left\vert F_o{}^2 - F_o{}^2(\text{mean})\right\vert / \Sigma F_o{}^2$	0.0938	0.0292
extinction parameter x: $F_c{}^* = F_c \cdot k \cdot (1 + 0.001 \cdot F_c{}^2 \cdot \lambda^3 \cdot x/\sin(2\vartheta))^{-1/4}$	0.16(2)	0.00032(19)
$R_1 = \Sigma(\left\vert\left\vert F_o\right\vert - \left\vert F_c\right\vert\right\vert) / \Sigma F_o$ (all / observed reflections)	0.034 / 0.030	0.016 / 0.021
$wR_2 = (\Sigma w(F_o{}^2 - F_c{}^2)^2 / \Sigma\left\vert wF_o{}^4\right\vert)^{1/2}$	0.073	0.039
GooF = $\{\Sigma(w(F_o{}^2 - F_c{}^2)^2) / (n-p)\}^{0.5}$	1.20	1.19
max Δ/σ; number of variable parameters (p)	< 0.001; 25	< 0.001; 25
final difference Fourier map (eÅ^{-3})	-1.57 to +1.42	-0.55 to +0.89
parameters a / b for weighting scheme $w = 1 / \{\sigma^2(F_o{}^2) + [a \times P]^2 + b \times P\}$; $P = ([\max(0, F_o{}^2)] + 2 \times F_c{}^2) / 3]$	0.027 / 0.35	0.019 / 0.49
volume per atom (Å^3)	15.1	17.1

Table 3: Fractional atomic coordinates and displacement parameters;

The anisotropic displacement parameters are defined as: exp $(-2\pi^2 \Sigma^3_{i=1} \Sigma^3_{j=1} U_{ij} a_i a_j h_i h_j)$; $U_{11} = U_{22}$; $U_{23} = U_{13} = 0$; $U_{12} = \frac{1}{2}*U_{11}$

	occupation	Wyckoff letter	Site symmetry	x	y	z	U_{equiv} U_{iso}	U_{11}	U_{33}
Li$_3$CuSn									
Sn1	Sn$_{1.00}$	1(a)	6/mmm	0	0	0	0.0266(4)	0.0275(4)	0.0247(5)
Sn2	Sn$_{0.57(2)}$	2(d)	$\bar{6}m2$	1/3	2/3	1/2	0.0346(15)	0.0308(7)	0.042(4)
M1	Li$_{0.922(17)}$Cu$_{0.078(13)}$	2(e)	6mm	0	0	0.3390(15)	0.057(5)	0.063(7)	0.045(6)
M2	Li$_{2.0(2)}$	4(h)	3m	1/3	2/3	0.120(4)	0.084(12)	0.043(5)	0.16(3)
M3	Li$_{1.0(2)}$	4(h)	3m	1/3	2/3	0.432(6)	0.048(7)	0.065(13)	0.015(11)
M4	Li$_{0.30(18)}$	4(h)	3m	1/3	2/3	0.218(13)	0.07(3)		
M5	Li$_{0.97(14)}$	2(c)	$\bar{6}m2$	1/3	2/3	0	0.026(7)		
Li$_6$Cu$_2$Sn$_3$									
Sn1	Sn$_{1.00}$	3(a)	$\bar{3}m$	0	0	0	0.0214(2)	0.0193(2)	0.0254(3)
Sn2	Sn$_{1.00}$	6(c)	3m	0	0	0.453169(12)	0.0205(2)	0.0209(2)	0.0196(3)
Li	Li$_{1.00}$	6(c)	3m	0	0	0.2705(3)	0.022(2)	0.026(3)	0.012(4)
Li/Cu1	Li$_{0.407(5)}$Cu$_{0.593}$	6(c)	3m	0	0	0.08955(4)	0.0234(5)	0.0225(5)	0.0253(7)
Li/Cu2	Li$_{0.935(4)}$Cu$_{0.065}$	6(c)	3m	0	0	0.1805(2)	0.037(2)	0.024(2)	0.062(5)
Li/Cu3	Li$_{0.810(5)}$Cu$_{0.190}$	6(c)	3m	0	0	0.36184(11)	0.0291(12)	0.0250(13)	0.037(2)

Table 4. Interatomic bond lengths (Å) of Li₃CuSn and Li₆Cu₂Sn₃

Li₃CuSn

Sn1—*M5*	2.6425(9)	6×	*M3*···Sn2, *M3*, *M4*	≤ 1.81(12)		
Sn1—*M2*	2.830(11)	12×	*M3*—*M2*	2.64(6)		
Sn1—*M1*	2.802(5)	2×	*M3*—*M3*	2.6425(9)	3×
			M3—Sn2	2.704(11)	3×
Sn2···*M3*, *M4*	≤ 2.38(11)		*M3*—*M1*	2.757(15)	3×
Sn2—Sn2	2.6425(9)	3×	*M3*—*M3*	2.88(4)	3×
Sn2—*M3*	2.704(11)	6×			
Sn2—*M1*	2.973(6)	6×	*M4*···*M2*, *M3*, *M5*, Sn2	≤ 2.38(11)	
			M4—*M4*	2.6425(9)	3×
M1—*M1*	2.73(2)		*M4*—*M2*	2.77(3)	3×
M1—*M3*	2.757(15)	6×	*M4*—*M1*	2.83(4)	3×
M1—*M4*	2.83(4)	6×	*M4*—*M2*	2.86(14)	
M1—Sn1	2.868(12)		*M4*—*M3*	2.96(12)	
M1—Sn2	2.973(6)	6×			
			M5···*M2*, *M4*	≤ 1.85(11)	
M2···*M4*, *M5*, *M2*	≤ 2.03(6)		*M5*—*M5*	2.643(9)	3×
M2—*M2*	2.6425(9)	3×	*M5*—Sn1	2.643(9)	3×
M2—*M3*	2.64(6)		*M5*—*M2*	2.830(11)	6×
M2—*M4*	2.77(3)	3×			
M2—*M5*	2.830(11)	3×			
M2—Sn1	2.830(11)	3×			
M2—*M4*	2.86(14)				

Li$_6$Cu$_2$Sn$_3$

Sn1—Li/Cu1	2.7679(13)	2×	Li/Cu1—Sn1	2.7679(13)		
Sn1—Li/Cu3	2.7927(11)	6×	Li/Cu1—Li	2.775(2)	3×	
			Li/Cu1—Sn	2.8105(5)	3×	
Sn2—Li/Cu1	2.8105(5)	3×	Li/Cu1—Li/Cu2	2.812(7)		
Sn2—Li/Cu3	2.823(3)					
Sn2—Li/Cu2	2.839(2)	3×	Li/Cu2—Li3	2.780(11)		
Sn2—Sn2	2.8951(8)		Li/Cu2—Li/Cu2	2.785(4)	3×	
			Li/Cu2—Li/Cu1	2.812(7)		
Li—Li/Cu1	2.775(2)	3×	Li/Cu2—Sn2	2.839(2)	3×	
Li—Li/Cu2	2.780(11)					
Li—Li/Cu3	2.824(9)		Li/Cu3—Sn1	2.7927(11)	3×	
Li—Li/Cu3	2.855(4)	3×	Li/Cu3—Sn2	2.823(3)		
			Li/Cu3—Li	2.824(9)		
			Li/Cu3—Li	2.855(4)	3×	

Table 5. Structural relationship between $Li_6Cu_2Sn_3$, $Li_{13}Sn_5$ [29], Li_5Sn_2 [32], Li_5NaSn_4 [30], and $Li_{13}Ag_5Si_6$ [33]: stacking sequence of the individual polyhedra to building blocks.

compound	trigonal prism	tetrahedron	trigonal pyramid	octahedron	trigonal antiprism	A_1	A_2	A_3	B	C	stacking sequence
$Li_6Cu_2Sn_3$	$(Li,Cu)Sn_6$	$(Li,Cu)Sn_4$	-	$(Li,Cu)Sn_6$	-	x	-	-	x	-	$[-A_1-B-A_1-]$
$Li_{13}Sn_5$	$LiSn_6$	$LiSn_4$	-	$LiSn_6$	-	x	-	-	x	-	$[-A_1-B-A_1-B-A_1-]$
Li_5Sn_2	$LiSn_6$	$LiSn_4$	-	$LiSn_6$	-	x	-	-	x	-	$[-A_1-B-]$
Li_5NaSn_4	$LiSn_6$	$LiSn_4$	-	$NaSn_6$	-	x	-	-	x	x	$[-C-A_1-B-]$
$Li_{13}Ag_5Si_6$	$LiSi_6$	$LiSi_4$	$(Ag,Li)Si_4$	$LiSi_6$	$(Ag,Li)_2Si_6$	-	x	x	x	-	$[-A_2-B-A_2-A_3-]$

A_1…. tetrahedra + octahedra (2:1)

A_2…. tetrahedra + trigonal pyramids + octahedra (1:1:1)

A_3…. tetrahedra + trigonal antiprisms (2:1)

B…. trigonal prisms

C…. trigonal prisms + vacancies (1:1)
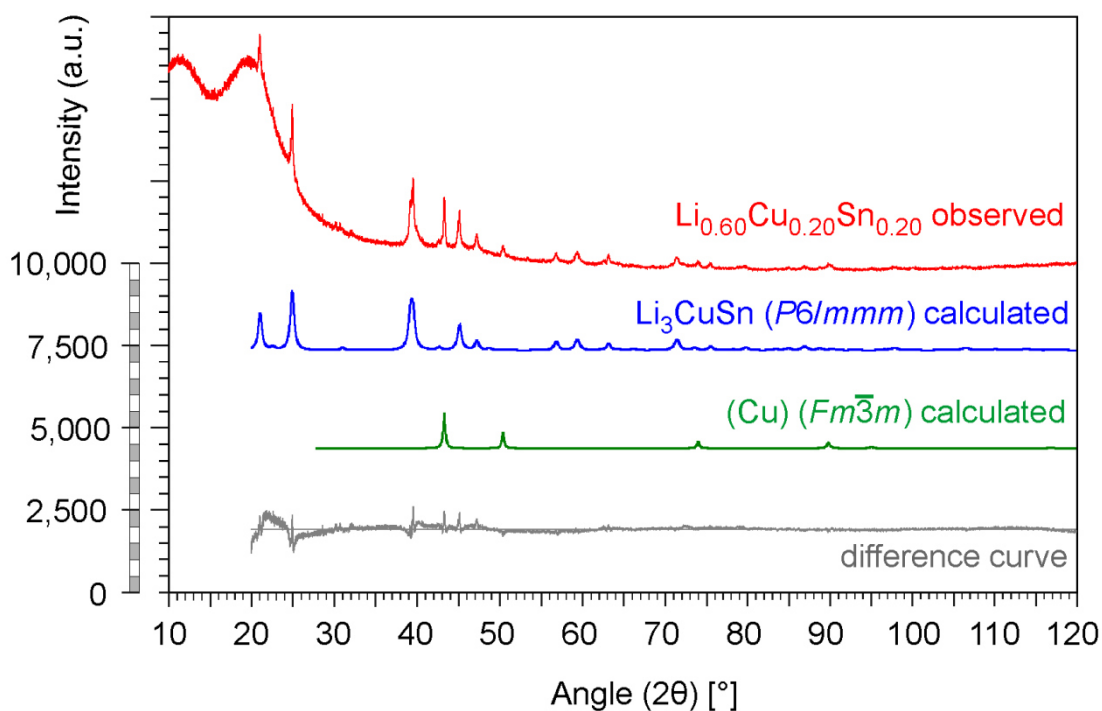
Fig. 1: Powder X-ray pattern of the sample synthesized from an input Li$_{0.60}$Cu$_{0.20}$Sn$_{0.20}$: observed, calculated and difference pattern.
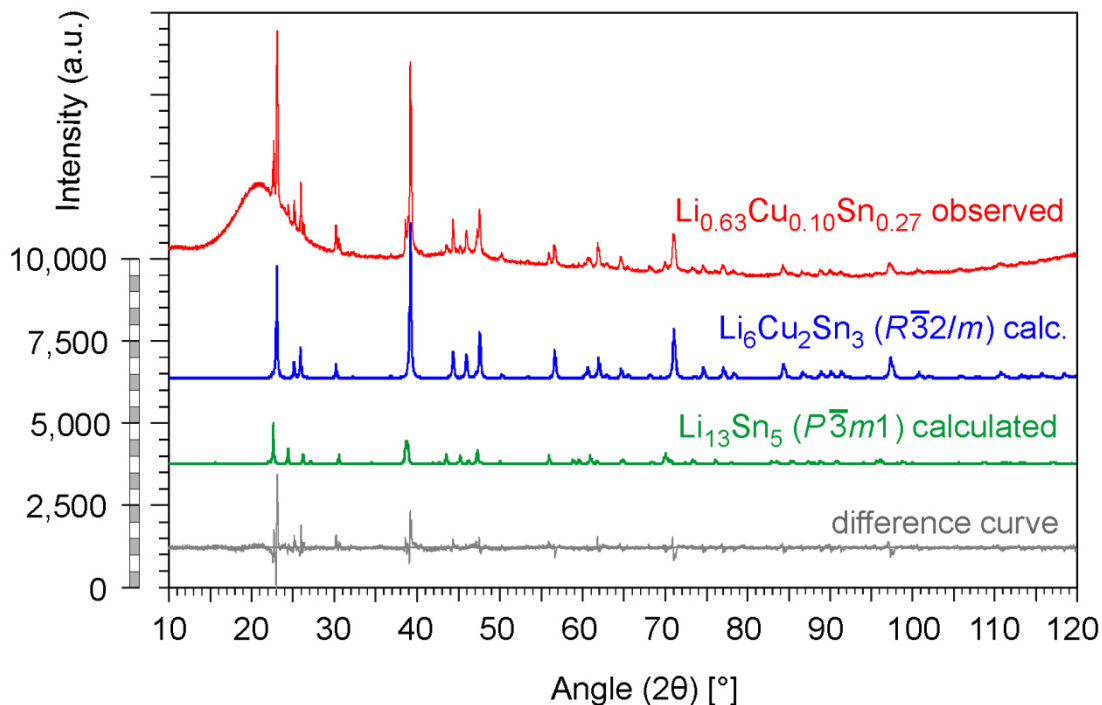
Fig. 2: Powder X-ray pattern of the sample synthesized from an input Li$_{0.63}$Cu$_{0.10}$Sn$_{0.27}$: observed, calculated and difference pattern.
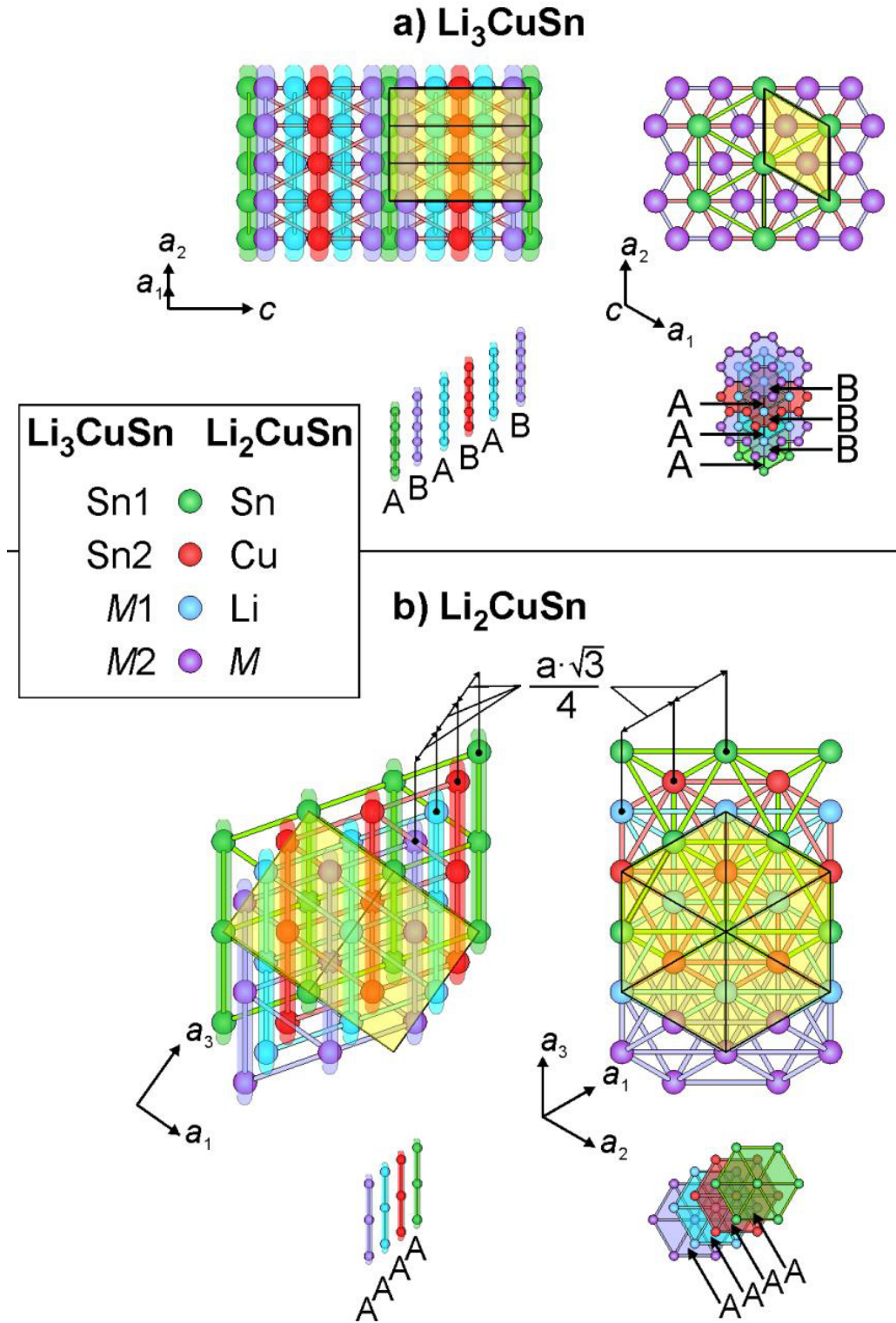
Fig. 3: Crystallographic relationship and layer sequences of a) Li₃CuSn and b) Li₂CuSn. Sites *M*3, *M*4 and *M*5 in structure Li₃CuSn are not shown. Unit cells are highlighted (yellow).
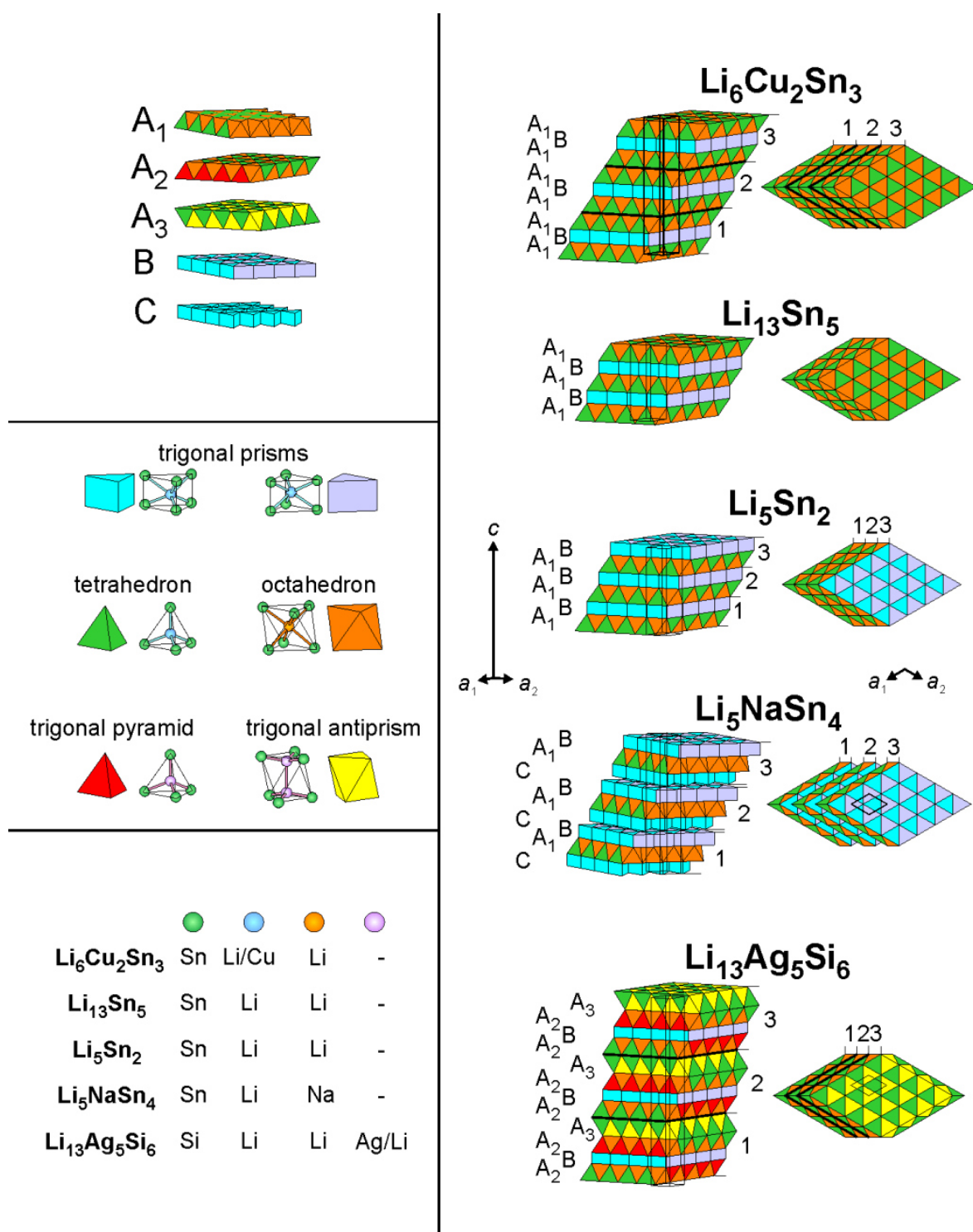
Fig. 4: Layers and building blocks formed by distinct (Li,Cu,Ag)(Si,Sn)₄ or (Li,Cu,Ag)(Si,Sn)₆ polyhedra: Topological comparison of Li₆Cu₂Sn₃ with Li₁₃Sn₅, Li₅Sn₂, Li₅NaSn₄ and Li₁₃Ag₅Si₆.

3.5 Publication #5

The Cu-Li-Sn phase diagram: Isothermal sections

Siegfried Fürtauer[†], Hans Flandorfer[†]

[†]Institute of Inorganic Chemistry – Functional Materials, University of Vienna, Währingerstraße 42, A-1090 Wien

Contributions to this paper:

S. Fürtauer:	Sample preparation and characterization, interpretation, phase diagram development, publication
H. Flandorfer:	General advice and helpful comments, publication and proofreading

Overall contributions of S. Fürtauer to the paper: 90%

Abstract

Four isothermal sections in the Cu-Li-Sn phase diagram at 300 °C, 400 °C, 500 °C and 600 °C have been investigated by powder XRD of 108 samples, which are based on 60 alloy compositions annealed at different temperatures and quenched in cold water. Altogether 47 three-phase equilibria have been allocated experimentally to the isotherms. Besides the established two ternary compounds Li_2CuSn (T1) and $LiCu_2Sn$ (T2), allocated in the hitherto known phase diagrams, four further ternary compounds could be proved. Their compositions are $Li_3Cu_6Sn_4$ (T3), Li_2CuSn_2 (T4), Li_3CuSn (T5) and $Li_6Cu_2Sn_3$ (T6). There are hints to the existence of two additional ones with the estimated compositions $Cu_{0.12}Li_{0.66}Sn_{0.22}$ (T7) and $Cu_{0.11}Li_{0.65}Sn_{0.24}$ (T8). A new lithiation path of $\eta´-Cu_6Sn_5$ at room temperature was suggested, based on the appearance of ternary phases and phase equilibria along the section from $\eta´-Cu_6Sn_5$ to (Li): $(\eta´-Cu_6Sn_5) \rightarrow (\eta´-Cu_6Sn_5 + T3) \rightarrow (T3) \rightarrow (T3 + T4) \rightarrow (T2 + T3 + T4) \rightarrow (T2 + T4) \rightarrow (T1 + T2 + T4) \rightarrow (T1 + T4) \rightarrow (T1) \rightarrow ((Cu) + T1) \rightarrow ((Cu) + T1 + T5) \rightarrow ((Cu) + T5) \rightarrow ((Cu) + T5 + Li_{17}Sn_4) \rightarrow ((Cu) + Li_{17}Sn_4) \rightarrow ((Cu) + (Li) + Li_{17}Sn_4) \rightarrow ((Li) + Li_{17}Sn_4) \rightarrow (Li)$.

Introduction

Li-ion batteries have already been employed successfully for a long time in handheld electronics. High-power cells for electro mobility or stationary storage systems based on Li-ion technique are not available yet. Improved cell design using well established materials will not be sufficient for the necessary enhancement of energy and power density, and thus new materials have to be found. There are different approaches to develop new electrodes, which are able to uptake more Li, have better cycling behavior and a longer lifetime, and which are cheaper and safer than commonly used ones [1]. Intermetallic anodes have the major benefit of comparably high storage capacity for Li. This corresponds to a charge capacity of *e.g.*, 960 mAh/g for $Li_{17}Sn_4$, which is the compound with the highest Li content in the Li-Sn system, compared to 372 mAh/g for LiC_6, which is the maximum what can be obtained by common graphite anodes [2]. A main problem with intermetallic anodes, especially those based on binary alloy systems, is the tremendous volume change during charging and discharging. This can be 200 vol.% or even more, and leads to electrode crumbling, which results in a loss of electronic contact between particles and finally causes a rapid capacity loss after few cycles [3]. To overcome this problem, it is necessary to increase the mechanical stability and reduce the overall volume change during insertion and release of Li. This could be achieved by

particular structural features *e.g.*, nano-powders or additions of materials which are suitable to buffer the mechanical stress and avoid degradation of the electrodes *e.g.*, conducting polymers [4]. However, a much finer distribution of the buffer matrix can be achieved by precipitation of the buffer phase during lithiation of the metal electrode. Probable candidates are binary starting alloys, leading to ternary systems consisting of Li, a main-group metal like Sn or Sb and a transition metal, like Cu, Ni or Co. Whereas the main-group elements form stable compounds with Li, *e.g.* $Li_{17}Sn_4$ or Li_3Sb, the transition metals are practically inert against Li [5-7]. Accordingly, lithiation of a binary compound, *e.g.* Cu_6Sn_5, leads to the precipitation of copper metal and a binary or ternary Li compound. As a result, we have an admixture of a so-called inactive and an active phase, which contains Li. The inactive phase acts to buffer volume changes and stabilizes the electrode material. For instance in the case of Cu_6Sn_5, various authors [8-11] proposed the following reaction mechanism for the insertion of Li:

(1) $Cu_6Sn_5 + 10\ Li \rightarrow 5\ Li_2CuSn + (Cu)$

(2) $4\ Li_2CuSn + 9\ Li \rightarrow Li_{17}Sn_4 + 4\ (Cu)$
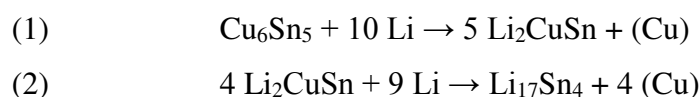
These reactions have been proposed based on a tentative ternary phase diagram showing the two well-known ternary intermetallic compounds Li_2CuSn [12, 13] and $LiCu_2Sn$ [14]. During our systematic investigation of the Cu-Li-Sn phase diagram, these phases have been reprocessed [15] and further ternary intermetallic compounds have been discovered ($Li_3Cu_6Sn_4$ and Li_2CuSn_2 [16, 17], Li_3CuSn and $Li_6Cu_2Sn_3$ [18]). From these findings and the resulting new phase relations a new evaluation of the lithiation process arises. Generally, for a systematic design of new materials beyond trial and error methods, knowledge of thermodynamic and kinetic data of respective material systems is indispensable. To provide this is the scope of the priority program 1473 "WeNDeLIB" (German abbreviation for "materials for a new design of Li-ion batteries), which was funded by the DFG (German Research Association) and involves several joint projects. The present work aims to establish phase relations in the system Cu-Li-Sn at different temperatures in order to provide thermodynamic information necessary for a comprehensive assessment and optimization of the respective phase diagram. Furthermore, assumptions to the lithiation mechanisms of different intermetallic Cu-Sn compounds based on thermodynamic considerations should be possible.

Experimental procedure

Sample preparation

Intermetallic samples with 60 different compositions (Table 1 and Fig. 1) have been prepared from pure elements Cu (99.98 wt.%, wire, Goodfellow, Cambridge, UK), Li (99.8 wt.%, wire, Alfa Aesar, Karlsruhe, Germany) and Sn (99.95 wt.%, ingot, Advent, Oxford, UK). Before use, the Cu wire was treated in an H_2 flow (5 hours, 300 °C) to remove the oxide layer at the surface. The Li wire was stored originally in mineral oil, which was removed by *n*-hexane in a supersonic bath followed by vacuum evaporation of the solvent. Visible, black oxidation spots occurring at the surface were removed mechanically with a knife. Sn was used as purchased. Weighing and assembling of the metal pieces in Ta crucibles was performed inside a glove box under an Ar atmosphere (< 5 ppm O_2 / H_2O). The cylindrical Ta crucibles were made by deep-drawing of a 0.4 mm Ta sheet and had an approximate size of 10 mm diameter and 12-14 mm height. The corresponding lids were also prepared by deep drawing. Before use, the Ta crucibles were stored for maximum 30 s in a highly oxidative acid bath (with volume fractions of concentrated acids $HF : HNO_3 : H_2SO_4 = 1:3:6$) to remove the passivizing Ta-oxide layer and cleaned with water and acetone afterwards. The crucibles were sealed under an Ar atmosphere by using an arc furnace with a W electrode of 1.6 mm diameter. During the welding process, the crucibles were chilled by a water cooled Cu mount. In order to melt the components together, the crucibles were put into an induction furnace at 1100 °C, but only for 10-20 s to prevent high temperature fatigue of the welding seam. The temperature was continuously monitored by an infrared pyrometer. Repetition of the melting process twice with turning the crucible upside down between the heating steps assured homogenous mixing. Then the crucibles were sealed in quartz glass tubes under vacuum. All alloy compositions were annealed consequently in a muffle furnace at 400 °C for several weeks; most compositions were also annealed at other temperatures (300, 500 and 600 °C, Table 1). Especially at high temperatures (500 and 600 °C) and for samples with high Li content, the Ta sheet became partially permeable for Li vapour. This was evidenced by a darkening of the surrounding quartz glass, which could be explained by a reduction of transparent SiO_2 to brown SiO or related Li-containing silicates. After the heat treatment, all samples were quenched in cold water and checked for mass loss. In most cases, it was negligible with respect to the extension of the respective phase fields (see Figs. 2-5).

Analytical method: Powder XRD

Ta crucibles were opened in the glove box with a bolt cutter; afterwards the alloys were extracted. The samples were powdered with a Durit® mortar. The powder was fixed with water-free petroleum jelly on a specimen holder consisting of a Si monocrystal. It was covered with a gastight polycarbonate cap, which prevented oxidation, before being shuttled out of the glove box. Samples were exposed to Cu-Kα X-ray radiation (40 kV / 40 mA) in a diffractometer with Bragg-Brentano geometry and a Ni filter. Signals were detected by a strip detector. Full profile Rietveld refinements were subsequently performed for phase analyses. XRD results of samples are reported in Table 1 and structure data of binary and ternary phases are listed in Table 2.

Results and discussion

60 alloys with different compositions were annealed at various temperatures and finally 108 samples with different phase equilibria were gained (Table 1). Based on these comprehensive data, four isothermal sections at 300, 400, 500 and 600 °C could be well established (Figs. 2-5). The major three phase fields are supported by results of several samples within their range of existence (Table 1). Only a few particular regions of the experimental phase diagram, *e.g.* the Li-rich corner, had to be left as tentative. Limiting factors especially attributed to this system are i) the very limited application of metallographic methods like LOM, SEM and X-ray spectroscopic analysis: Polishing of Cu-Li-Sn alloys is extremely difficult because they are brittle and immediately react with traces of water; methods, like *e.g.* SEM-EDX, are not accessible to Li because of its low atomic number. Conclusions from the Cu and Sn concentrations to the Li content are highly inaccurate because of the high difference in electron densities between both electron-rich Cu and Sn atoms and the electron-poor Li atom. EDX measurements result in a relative low quantity of emitted X-rays for Li compared to the quantity of emitted X-rays of Cu and Sn and therefore in an insignificant quantification of Li. As a consequence the apices of the phase triangles which correspond to the solubility of unary, binary and ternary phases had to be approximated. Nevertheless, their representation is reliable because of the interplay of information by manifold samples. ii) In nearly half of the samples liquid phase was present at the respective annealing temperature. Therefore, not all phases which were finally found at room temperature are equilibrium phases, because they formed during quenching. A critical evaluation including also the binary subsystems allowed us to construct respective phase relations in an iterative process. A further

limiting factor is iii) that the binary Cu-Sn high temperature phases A2-β and D0₃-γ cannot be quenched and transform into low temperature phases δ, ε, ζ and η (Ref. [35] and Table 2). To establish high temperature equilibria their appearance and sequence of formation had to be considered. The last restriction (iv) concerns the expansion of narrow binary Li-Sn two-phase fields at the Li-rich edge into the ternary. The width of the resulting three-phase fields are often well below one at.%. It is practically impossible to prepare high Li samples with sufficiently accurate stoichiometry. Despite the mass losses caused by evaporation of Li being negligible, it is likely that in some cases, especially in the Li-rich samples, Li was lost by diffusion into the Ta-crucible wall. In addition, at temperatures well above 1000 °C, liquid Li creeps up due to its reduced density and concentrates at the upper side of the crucible wall, so that complete alloying with the other elements is hindered.

As binary subsystems, the recent works on Cu-Sn [35, 36] and Li-Sn [37] were employed. The Cu-Li subsystem origins from an earlier work [5]. Additional XRD measurements of several binary Cu-Li samples were performed [38] to verify whether the Cu-Li system possess the intermetallic compound claimed by Gąsior et al. [39], which is in contradiction to the phase diagram shown by Pelton [5]. The investigations of Li et al. [38] did not reveal the presence of the proposed Cu_2Li_3 phase, which was neither seen from XRD analysis nor indicated by thermal analysis by Gąsior et al. [39]. They only observed trends in their EMF measurements against temperature for various compositions. In addition, the compound-forming tendency of Li with transition metals is generally low and the mixing enthalpy of Cu and Li [40] is clearly endothermic. Thus Cu_2Li_3 was not included and is not listed in Table 2.

Table 1 shows in addition the composition and heat treatment of all samples, the phases which could be identified by powder XRD and the corresponding phase fields. Table 3 summarises the 47 three-phase fields which were established at different annealing temperatures. It has to be emphasized that XRD results of most samples distinctly indicated two- and three-phase equilibria. Whenever liquid was present at the annealing temperature, one or more non-equilibrium phases (mostly (Sn), η or T4) were formed during quenching as indicated in the column ''formed during quenching'' in Table 1. In the same column, low temperature phases formed by quenching of D0₃-γ are listed. Three further samples (#5 at 600 °C, #49 at 400 °C and #50 at 400 °C), which were annealed very closely below the solidus temperatures, showed more than three phases in XRD;

additional phases supposed to originate from minor amounts of liquid present at the respective annealing temperatures.

Li-rich corner

Sample #56, annealed at 400 and 600 °C should show (Li) solid solution as an equilibrium phase after quenching. However, this phase could not be proved by XRD because of its low scattering factor. For two samples in the Li-rich corner of the phase diagram (#54 and #55, annealed at 400 °C), several strong peaks in the XRD patterns were found, which could not be allocated to any hitherto known binary or ternary phase. Because additional peaks in both XRD patterns were at different positions, it is suggested that probably two further ternary phases (namely T7 and T8) exist. However, both phases T7 and T8 could neither be prepared as pure compounds nor described by single crystal XRD. From positions of adjacent phase triangles, it could be assumed that samples #54 and #55 are located very closely to the supposed phases T8 and T7, respectively. According to the XRD pattern sample #55 at 400 °C mainly contains (Sn); Fig. 6. The additional phase T7 could not be accurately indexed from powder XRD data but seems to be hexagonal. A Rietveld refinement of the XRD pattern of sample #54 at 400 °C shows phases (Sn), T6 and T1, but also with peaks which are still unexplained. They are considered to belong to the previously unknown phase T8 (Fig. 7). Trials to index the XRD pattern also suggest a hexagonal lattice, although it cannot be excluded that the T8 phase reveals a superstructure of T1. Attributed to very narrow phase fields in the Li-rich corner and slightly loss of Li during sample preparation, phase triangles in this region could not be fully determined and are drawn mostly with dashed lines; see also above. Small amounts of (Sn) and/or η phase were found in several samples as indicated in Table 1. It is supposed that during XRD measurements, even traces of water reacted with the highly moisture-sensitive samples. High Li phases decomposed to LiOH (which cannot be detected in XRD) and phases of the Cu-Li-Sn system which do not contain Li, *e.g.* the η phase. However, this was only observed at long exposure times and to a very small extent; therefore it is supposed that phase relations are not affected significantly.

Cu-rich corner

In the binary Cu-Sn system, the ζ phase exists between 589 and 641 °C [35] and the δ phase between ~350 and 603 °C. Sample #2 annealed at 600 °C showed both phases, together with T2 after quenching. The ζ phase, however originated from the bulk transformation of the non-quenchable high temperature phase $D0_3$-γ and thus the latter was attributed to the corresponding three-phase field; Table 1.

Although at 400 °C, δ phase is in equilibrium with (Cu), the ζ phase was found in samples #2 and #3 at this temperature, which is much below its eutectoid decomposition. However, the two phases are structurally related to a high extent, and thus difficult to differentiate. Even so, the quality of the full powder refinements were slightly better based on ζ phase, so samples #2 and #3 are suggested to contribute to the (Cu) + δ + T2 phase field in order to be consistent with the binary Cu-Sn.

Common features of the system's ternary crystal structures

Relationships of the Cu/Sn matrices in binary Cu-Sn and ternary alloys, as well as similarities in the distribution of Li among ternary Cu-Li-Sn phases can be expected. This has been discussed in more detail in three articles of Fürtauer et al. [15, 16, 18] and illustrated in Fig. 8. The figure shows which crystal structures are directly related to each other. The fcc-Cu structure can serve as a starting point for all considerations. Substitution of Cu by Sn covers three different phases, the solid solution (Cu), the bcc A2-β phase (approx. $Cu_{17}Sn_3$) and finally the $D0_3$-γ phase. In the latter phase, Cu and Sn atoms are ordered and located at different atomic sites [41]. Further site-selective substitution of Cu atoms by Li leads to the structure of T1 phase. The T1 phase has a wide solubility range at constant Sn amount, which is attributed to partial substitution at one distinct Cu-position (Cu/Li site). This structure is further related to the ternary phases T2, T4 and T5. Both T1 and T2 phases form honeycomb-shaped structures of Cu and Sn atoms in the [110] and [001] directions, respectively [15]. Perpendicular to these layers, piles of Cu/Li atoms fill these channel-like structures. Both T1 and T4 phase could be described by different succeeding atom layers, which show significant similarities [16]. The phase T5 viewed in the [001] direction can be compared with the T1 phase viewed in [111] direction. However, T5 comprises further mixed Cu/Li layers per structural unit and shows a slightly different sequence of layers compared to the T1 phase [18]. A further structural relation exists between η-Cu_6Sn_5, T3 and T4. By consecutive shifts of Cu and Sn atoms based on η-Cu_6Sn_5 and additional insertion of Li atoms, the T3 phase is formed,

which consists of planar atom layers [16]. The tetragonal T4 phase is formed from η-Cu_6Sn_5 by asymmetric distortion of the hexagonal unit cell along *c*-direction and substitution of certain Cu atoms by Li [16]. The formation of the T2 phase from ε-Cu_3Sn can be considered by substitution of one Cu atom by one Li atom per formula unit and alignment of the remaining Cu_2Sn-subunits to hexagonal symmetry [15]. The Li-rich T6 phase is structurally related to both Li_5Sn_2 and $Li_{13}Sn_5$ phases. Two types of layers, which are originated from polyhedral subunits, form different sequences of 9 (T6), 6 (Li_5Sn_2) or 5 ($Li_{13}Sn_5$) succeeding layers [18].

Summary and Conclusions

By annealing at various temperatures and quenching of 108 ternary intermetallic samples at 60 different alloy compositions and identification of equilibrium phases, isothermal sections at 300, 400, 500 and 600 °C could be established. There are, however, several general experimental restrictions with this system, *e.g.* the impossibility of measuring the Li-content of phases by SEM-EDX. In those parts of the isotherms where phase relations could not be clearly proved, tie-lines are drawn as dotted lines. Surprisingly, the Cu-Li-Sn phase diagram exhibits at least six ternary compounds. There are hints to the existence of two more ternary phases. It is much more complex than supposed, and was before thought to have only two ternary compounds [8-11]. This is highly relevant for a systematic development of related electrode materials based on thermodynamic and kinetic data. Li-ion batteries with alloy anodes are targeted to operate at temperatures between room temperature and well below 100 °C. Therefore, knowledge of the Cu-Li-Sn phase diagram at lower temperatures is crucial. Naturally, experimental work on a phase diagram mostly requires elevated annealing temperatures for diffusion into equilibrium state in reasonable time. A reliable extrapolation to lower temperatures would become possible if directly measured thermodynamic data [40], and phase diagram data from this work are unified in a CALPHAD optimization and assessment. Together with kinetic data, this would also allow the prediction of reaction paths of Cu-Sn anodes during lithiation. According to literature [8-11], the most promising Cu-Sn anode material is the low temperature phase η´-Cu_6Sn_5 [25, 42], which is structurally similar to the NiAs-type η-Cu_6Sn_5 [25, 42] and stable at temperatures up to 189 °C. The lithiation path of η´-Cu_6Sn_5 [8-11] can be revised based on our findings and assumptions for low temperature phase relations, *e.g.* the ternary phases present at 300 °C are stable down to room temperature. From the thermodynamic point of view the lithiation path, considering all

crossing phase equilibria, can be estimated as follows: $(\eta'\text{-}Cu_6Sn_5) \rightarrow (\eta'\text{-}Cu_6Sn_5 + T3)$ $\rightarrow (T3) \rightarrow (T3 + T4) \rightarrow (T2 + T3 + T4) \rightarrow (T2 + T4) \rightarrow (T1 + T2 + T4) \rightarrow (T1 + T4)$ $\rightarrow (T1) \rightarrow ((Cu) + T1) \rightarrow ((Cu) + T1 + T5) \rightarrow ((Cu) + T5) \rightarrow ((Cu) + T5 + Li_{17}Sn_4) \rightarrow$ $((Cu) + Li_{17}Sn_4) \rightarrow ((Cu) + (Li) + Li_{17}Sn_4) \rightarrow ((Li) + Li_{17}Sn_4) \rightarrow (Li)$. Despite electrochemical lithiation for technical purposes being usually a non-equilibrium process, which is controlled by kinetic properties of the material, the suggested lithiation pathway at equilibrium conditions is fundamental to understand phase formations and reactions. Further experimental work on the Cu-Li-Sn phase diagram in respect to the construction of vertical sections and solidification behavior is currently being done. The knowledge of the ternary system at equilibrium conditions is a base for the design of new anode materials and a good example for the necessity of fundamental research in the framework of applied science, which is done within the DFG WeNDeLIB priority program SPP 1473.

References

[1]   C. Daniel, Materials and processing for lithium-ion batteries, JOM - The Journal of The Minerals, Metals & Materials Society, 60 (2008) 43-48.

[2]   A.K. Shukla, T.P. Kumar, Materials for next-generation lithium batteries, Current Science, 94 (2008) 314-331.

[3]   M.S. Whittingham, Materials challenges facing electrical energy storage, MRS Bulletin, 33 (2008) 411-419.

[4]   D.L. Ma, Z.Y. Cao, A.M. Hu, Si-Based Anode Materials for Li-Ion Batteries: A Mini Review, Nano-Micro Letters, 6 (2014) 347-358.

[5]   A.D. Pelton, The Cu-Li (Copper-Lithium) system, Bulletin of Alloy Phase Diagrams, 7 (1986) 142-144.

[6]   J. Sangster, A.D. Pelton, The Co-Li (Cobalt-Lithium) system, Bulletin of Alloy Phase Diagrams, 11 (1990) 440-441.

[7]   K.J. Lee, S.Y. Lee, P. Nash, Li-Ni (Lithium-Nickel), in: T.B. Massalski, H. Okamoto, P.R. Subramanian, L. Kacprzak (Eds.) Binary Alloy Phase Diagrams. The Materials Information Society, Ohio, 1990, pp. 2450-2453.

[8]   A. Jansen, J. Clevenger, A. Baebler, J. Vaughey, Variable temperature performance of intermetallic lithium-ion battery anode materials, Journal of Alloys and Compounds, (2011) 4457–4461.

[9]   W. Choi, J.Y. Lee, H.S. Lim, Electrochemical lithiation reactions of Cu_6Sn_5 and their reaction products, Electrochemistry Communications, 6 (2004) 816-820.

[10]   S. Sharma, L. Fransson, E. Sjostedt, L. Nordstrom, B. Johansson, K. Edstrom, A theoretical and experimental study of the lithiation of $\eta´\text{-}Cu_6Sn_5$ in a lithium-ion battery, Journal of the Electrochemical Society, 150 (2003) A330-A334.

[11]   K.D. Kepler, J.T. Vaughey, M.M. Thackeray, $Li_xCu_6Sn_5$ (0 < x < 13): An intermetallic insertion electrode for rechargeable lithium batteries, Electrochemical and Solid State Letters, 2 (1999) 307-309.

[12]   H.U. Schuster, Ternäre Lithium-Verbindungen mit Elementen der 4. Hauptgruppe, Die Naturwissenschaften, 53 (1966) 360-361.

[13]   H. Pauly, A. Weiss, H. Witte, Crystal structure of ternary intermetallic phases Li_2EX (E = Cu, Ag, Au; X = Al, Ga, In, Tl, Si, Ge, Sn, Pb, Sb, Bi), Zeitschrift für Metallkunde, 59 (1968) 47-58.

[14]   P.I. Kripyakevich, G.I. Oleksiv, Crystal structure of the compound $LiCu_2Sn$, Dopovidi Akademiï Nauk Ukraïns'koï RSR, A (1970) 63-65.

[15]   S. Fürtauer, H.S. Effenberger, H. Flandorfer, $CuLi_2Sn$ and Cu_2LiSn: Characterization by single crystal XRD and structural discussion towards new anode materials for Li-ion batteries, Journal of Solid State Chemistry, 220 (2014) 198-205.

[16]   S. Fürtauer, H.S. Effenberger, H. Flandorfer, The tin-rich copper lithium stannides: $Li_3Cu_6Sn_4$ and Li_2CuSn_2, Zeitschrift für Kristallographie, 230 (2015) 97-105.

[17]   F. Winter, S. Dupke, H. Eckert, U.C. Rodewald, R. Pöttgen, Lithium mobility in the stannides Li_2CuSn_2 and Li_2AgSn_2, Zeitschrift für Anorganische und Allgemeine Chemie, 639 (2013) 2790-2795.

[18]   S. Fürtauer, H.S. Effenberger, H. Flandorfer, New intermetallic phases in the Cu-Li-Sn system: The lithium rich phases Li_3CuSn and $Li_6Cu_2Sn_3$, Zeitschrift für Kristallographie - Crystalline Materials, 231 (2016) 79-87.

[19] M. Kantola, E. Tokola, X-ray studies on the thermal expansion of copper-nickel alloys, Annales Academiæ Scientiarum Fennicæ, 223 (1967) 1–10.

[20] H. Knödler, Über Kristallstruktur und strukturellen Zusammenhang der Phasen gamma und epsilon im System Kupfer-Zinn, Metall, 20 (1966) 823-829.

[21] M.H. Booth, J.K. Brandon, R.Y. Brizard, C. Chieh, W.B. Pearson, Gamma-brasses with F cells, Acta Crystallographica Section B-Structural Science, 33 (1977) 30-36.

[22] Y. Watanabe, Y. Fujinaga, H. Iwasaki, Lattice Modulation in the Long-Period Superstructure of Cu_3Sn, Acta Crystallographica Section B-Structural Science, 39 (1983) 306-311.

[23] J.K. Brandon, W.B. Pearson, D.J.N. Tozer, A single-crystal X-ray diffraction study of the zeta bronze structure, $Cu_{20}Sn_6$, Acta Crystallographica Section B-Structural Science, 31 (1975) 774-779.

[24] A. Gangulee, G.C. Das, M.B. Bever, X-ray diffraction and calorimetric investigation of compound Cu_6Sn_5, Metallurgical Transactions, 4 (1973) 2063-2066.

[25] A.K. Larsson, L. Stenberg, S. Lidin, The superstructure of domain-twinned eta´-Cu_6Sn_5, Acta Crystallographica Section B-Structural Science, 50 (1994) 636-643.

[26] W.J. Helfrich, R.A. Dodd, Densities and lattice parameters of tin (indium) solid solutions, Acta Metallurgica, 12 (1964) 667-669.

[27] R. Berliner, O. Fajen, H.G. Smith, R.L. Hitterman, Neutron powder-diffraction studies of lithium, sodium, and potassium metal, Physical Review B, 40 (1989) 12086-12097.

[28] C. Lupu, J.G. Mao, J.W. Rabalais, A.M. Guloy, J.W.J. Richardson, X-ray and neutron diffraction studies on "$Li_{4.4}Sn$", Inorganic Chemistry 42 (2003) 3765-3771.

[29] U. Frank, W. Müller, H. Schäfer, Die Kristallstruktur der Phase Li_7Sn_2, Zeitschrift für Naturforschung - Teil B, 30 (1975) 6-9.

[30] U. Frank, W. Müller, Darstellung und Struktur der Phase $Li_{13}Sn_5$ und die strukturelle Verwandtschaft der Phasen in den Systemen Li-Sn und Li-Pb, Zeitschrift für Naturforschung - Teil B, 30 (1975) 316-322.

[31] U. Frank, W. Müller, H. Schäfer, Die Kristallstruktur der Phase Li_5Sn_2, Zeitschrift für Naturforschung - Teil B, 30 (1975) 1-5.

[32]   W. Müller, Darstellung und Struktur der Phase Li_7Sn_3, Zeitschrift für Naturforschung - Teil B, 29 (1974) 304-307.

[33]   W. Müller, H. Schäfer, Die Kristallstruktur der Phase LiSn, Zeitschrift für Naturforschung - Teil B, 28 (1973) 246-248.

[34]   D.A. Hansen, L.J. Chang, Crystal structure of Li_2Sn_5, Acta Crystallographica B, 25 (1969) 2392-2395.

[35]   S. Fürtauer, D. Li, D. Cupid, H. Flandorfer, The Cu-Sn phase diagram, Part I: New experimental results, Intermetallics, 34 (2013) 142-147.

[36]   D. Li, P. Franke, S. Fürtauer, D. Cupid, H. Flandorfer, The Cu-Sn phase diagram part II: New thermodynamic assessment, Intermetallics, 34 (2013) 148-158.

[37]   D. Li, S. Fürtauer, H. Flandorfer, D.M. Cupid, Thermodynamic assessment and experimental investigation of the Li-Sn system, CALPHAD - Computer Coupling of Phase Diagrams and Thermochemistry, 47 (2014) 181-195.

[38]   D. Li, S. Fürtauer, H. Flandorfer, D.M. Cupid, Thermodynamic Assessment of the Cu-Li System and Prediction of Enthalpy of Mixing of Cu-Li-Sn Liquid Alloys, CALPHAD - Computer Coupling of Phase Diagrams and Thermochemistry, 53 (2016) 105-115.

[39]   W. Gąsior, B. Onderka, Z. Moser, A. Dębski, T. Gancarz, Thermodynamic evaluation of Cu-Li phase diagram from EMF measurements and DTA study, CALPHAD - Computer Coupling of Phase Diagrams and Thermochemistry, 33 (2009) 215-220.

[40]   S. Fürtauer, E. Tserenjav, A. Yakymovych, H. Flandorfer, Calorimetric studies of Li-Sn, Cu-Li and Cu-Li-Sn, Journal of Chemical Thermodynamics, 61 (2013) 105-116.

[41]   H. Knödler, Die Überstruktur der gamma-Hochtemperaturphase im System Kupfer-Zinn, Acta Crystallographica, 9 (1956) 1036-1036.

[42]   N. Saunders, A.P. Miodownik, Cu-Sn (Copper-Tin), in: T.B. Massalski (Ed.) Binary Alloy Phase Diagrams. The Materials Information Society, Ohio, 1990, pp. 1481-1483.

Table 1: Heat treatment and quenched phases of Cu-Li-Sn samples

[1] Samples are ordered with decreasing Cu and increasing Li concentration;

[2] Identified phases are ordered with decreasing amount, approximated from Rietveld refinements;

[3] Corresponding phases are ordered systematically (Liq – unary – binary – ternary phases);

* denotes phases, which were only present in traces.

x(Cu)	x(Li)	x(Sn)	Sample No	Heat treatment	Identified phases [2]	Corresponding phase field [3]	Formed during quenching	Formed during hydrolysis	Comments
0.80	0.10	0.10	1	400 °C / 27d	(Cu), T2, T1*	(Cu), T1, T2			
0.78	0.02	0.20	2	400 °C / 65d	ζ, T2, (Cu)*	(Cu), δ, T2			ζ and δ very similar in XRD
0.78	0.02	0.20	2	600 °C / 91d	ζ, δ, T2*	D0$_3$-γ, δ, T2	ζ (from D0$_3$-γ)		
0.70	0.10	0.20	3	400 °C / 9d	ζ, T2, (Cu)	(Cu), δ, T2			ζ and δ very similar in XRD
0.70	0.20	0.10	4	400 °C / 27d	(Cu), T1	(Cu), T1			
0.70	0.20	0.10	4	600 °C / 3d	(Cu), T1	(Cu), T1			
0.65	0.10	0.25	5	400 °C / 27d	ε, T3, T2*	ε, T2, T3			
0.65	0.10	0.25	5	500 °C / 100d	ε, T3, T2*	Liq, ε, T2	T3		
0.65	0.10	0.25	5	600 °C / 100d	ε, T2, ζ*, T4*	ε, ζ, T2	T4*		T4 from quenched liquid (minor amount)
0.60	0.10	0.30	6	300 °C / 105d	ε, T3, η	ε, η, T3			
0.60	0.10	0.30	6	400 °C / 70d	T3, ε, η, (Sn)*, T2*	Liq, ε, T3	(Sn), η, T2		
0.60	0.10	0.30	6	500 °C / 65d	ε, T3, η*, (Sn)*	Liq, ε, T2	(Sn), η, T3		Composition shifted to Liq + ε
0.60	0.10	0.30	6	600 °C / 65d	ε, T3, η, (Sn)*	Liq, ε, T2	(Sn), η, T3		Composition shifted to Liq + ε

0.60	0.20	0.20	7	400 °C / 21d	T2, (Cu)	T2, (Cu)		
0.60	0.30	0.10	8	400 °C / 9d	(Cu), T5, T1	(Cu), T1, T5		
0.60	0.30	0.10	8	500 °C / 7d	(Cu), T5, T1	(Cu), T1, T5		
0.57	0.16	0.27	9	400 °C / 65d	T2, T3, ε	ε, T2, T3		
0.57	0.16	0.27	9	600 °C / 91d	T2, ζ, ε, η*, T3*, T4*, (Sn)*	Liq, ε, T2	(Sn), ζ, η, T3, T4	
0.55	0.25	0.20	10	400 °C / 70d	T1, T2, (Cu)	(Cu), T1, T2		
0.54	0.20	0.26	11	500 °C / 35d	T2, T3*	Liq, T2	T3	
0.52	0.20	0.28	12	400 °C / 21d	T3, T2, ε	ε, T2, T3		
0.52	0.20	0.28	12	500 °C / 35d	T2, δ, T3*, T4*, (Sn)*, η*	Liq, T2	(Sn)*, δ, η*, T3*, T4*	
0.51	0.10	0.40	13	300 °C / 122d	η, T3, ε	ε, η, T3		
0.51	0.10	0.40	13	400 °C / 21d	ε, T3, T4*, T2*, η*, (Sn)*	Liq, ε, T3	T4*, T2*, η*, (Sn)*	
0.51	0.10	0.40	13	500 °C / 35d	ε, η, (Sn), T4*	Liq, ε	(Sn), η, T4*	
0.51	0.10	0.40	13	600 °C / 35d	ε, η, T3, (Sn)	Liq, ε	(Sn), η, T3	
0.50	0.18	0.33	14	300 °C / 105d	T3, ε, η, (Sn)*	ε, η, T3		(Sn)*
0.50	0.18	0.33	14	400 °C / 70d	T3, ε, η, T2*, (Sn)*	Liq, ε, T3	(Sn)*, η, T2*	
0.50	0.18	0.33	14	500 °C / 65d	T2, δ, ε, T3, η, (Sn)	Liq, ε, T2	(Sn), δ, η, T3	
0.50	0.25	0.25	15	300 °C / 84d	T2	T2		
0.50	0.25	0.25	15	400 °C / 35d	T2	T2		
0.50	0.25	0.25	15	600 °C / 84d	T2	T2		
0.47	0.25	0.28	16	400 °C / 21d	T2, T3, T4, (Sn)*	T2, T3, T4		(Sn)*

3 Results and Discussion

0.47	0.25	0.28	16	500 °C / 27d	T2, η, (Sn), T4*	Liq, T2	(Sn), η, T4*		
0.47	0.25	0.28	16	600 °C / 35d	T2, T4, η*, (Sn)*	Liq, T2	(Sn)*, η*, T4		
0.46	0.23	0.31	17	400 °C / 70d	T3, T4*	T3, T4			
0.46	0.23	0.31	17	500 °C / 65d	T2, δ, (Sn)*, η*	Liq, T2	(Sn)*, δ, η*		
0.45	0.10	0.45	18	300 °C / 100d	η, T4, (Sn)	Liq, η, T4	(Sn)		
0.45	0.10	0.45	18	400 °C / 27d	ε, T3, (Sn), η	Liq, ε, T3	(Sn), η		
0.45	0.45	0.10	19	400 °C / 27d	(Cu), Li$_{17}$Sn$_4$, (Sn)*	(Cu), Li$_{17}$Sn$_4$		(Sn)*	
0.43	0.43	0.15	20	400 °C / 27d	T5, (Cu), T1	(Cu), T1, T5			
0.40	0.20	0.40	21	300 °C / 100d	T4, η, T3, (Sn)*	η, T3, T4		(Sn)*	
0.40	0.20	0.40	21	400 °C / 27d	T3, η, (Sn), ε*, T4*	Liq, ε, T3	(Sn), η, T4*		
0.40	0.20	0.40	21	500 °C / 100d	T2, T4, η, T3*, (Sn)*	Liq, T2	(Sn)*, η, T3*, T4		
0.40	0.40	0.20	22	400 °C / 56d	T1, (Cu)	(Cu), T1			
0.40	0.40	0.20	22	600 °C / 3d	T1, (Cu)	(Cu), T1			
0.40	0.50	0.10	23	400 °C / 9d	(Cu), Li$_{17}$Sn$_4$, T5, (Sn)*	Liq, (Cu), Li$_{17}$Sn$_4$	(Sn)*, T5		
0.38	0.30	0.32	24	400 °C / 42d	T3, T4, (Sn)*	T3, T4		(Sn)*	
0.38	0.30	0.32	24	500 °C / 77d	T2, T4, (Sn)*	Liq, T2, T4	(Sn)*		
0.38	0.30	0.32	24	600 °C / 77d	T2, T4, η, (Sn)	Liq, T2	(Sn), η, T4		
0.36	0.36	0.29	25	400 °C / 21d	T1, T4, η*, T2*, (Sn)*	T1, T2, T4,		(Sn)*, η*	
0.35	0.40	0.25	26	400 °C / 70d	T1	T1			

0.33	0.33	0.33	27	400 °C / 70d	T4, T2, T3	T2, T3, T4			
0.33	0.33	0.33	27	500 °C / 65d	T2, T4, η, (Sn)	Liq, T2, T4	(Sn), η		
0.33	0.33	0.33	27	600 °C / 65d	T2, η, (Sn), T4, T1*	Liq, T1, T2	(Sn), η, T4		
0.30	0.20	0.50	28	300 °C / 77d	η, T4, (Sn)	Liq, η, T4	(Sn)		
0.30	0.20	0.50	28	400 °C / 9d	T3, η, (Sn), ε*	Liq, ε, T3	(Sn), η		
0.27	0.43	0.30	29	400 °C / 70d	T4, T1	T1, T4			
0.27	0.50	0.23	30	400 °C / 42d	T1, T5, (Cu)	(Cu), T1, T5			
0.25	0.50	0.25	31	400 °C / 35d	T1	T1			
0.25	0.50	0.25	31	600 °C / 4d	T1, T6, T4	T1, T6	T4		Composition shifted to Liq + T1 + T6
0.25	0.60	0.15	32	400 °C / 56d	(Cu), Li$_{17}$Sn$_4$, T5	(Cu), Li$_{17}$Sn$_4$, T5			
0.22	0.56	0.22	33	400 °C / 54d	T5, T1, (Cu)	(Cu), T1, T5			
0.22	0.56	0.22	33	600 °C / 2d	T5, T1, η, (Sn)*, (Cu)*	(Cu), T1, T5		(Sn)*, η	
0.20	0.10	0.70	34	300 °C / 100d	(Sn), η, T4	Liq, η, T4	(Sn)		
0.20	0.10	0.70	34	400 °C / 27d	(Sn), η, T4	Liq	(Sn), η, T4		
0.20	0.20	0.60	35	300 °C / 100d	T4, η, (Sn)	Liq, η, T4	(Sn)		
0.20	0.20	0.60	35	400 °C / 27d	T3, T4, η, (Sn), ε*	Liq, ε, T3	(Sn), η, T4		
0.20	0.30	0.50	36	300 °C / 105d	T4, η, (Sn)	Liq, η, T4	(Sn)		
0.20	0.30	0.50	36	400 °C / 70d	T4, T3, η*, (Sn)*	Liq, T3, T4	(Sn)*, η*		
0.20	0.30	0.50	36	500 °C / 65d	T4, (Sn), η	Liq, T4	(Sn), η		
0.20	0.40	0.40	37	300 °C / 77d	T4, η, (Sn)	Liq, T4	(Sn), η		
0.20	0.40	0.40	37	400 °C / 70d	T4, η, (Sn)	Liq, T4	(Sn), η		
0.20	0.40	0.40	37	500 °C / 77d	T4, η, (Sn)	Liq, T4	(Sn), η		
0.20	0.53	0.27	38	400 °C / 65d	T6, T1	T6, T7, T8			Composition shifted to T1 + T6

0.20	0.55	0.25	39	400 °C / 27d	T1, T6, η, (Sn)*	T1, T6, T7	(Sn)*, η		Composition shifted to Liq + T1 + T6
0.20	0.55	0.25	39	600 °C / 3d	T1, T6, η, (Sn)*	T1, T6, T7	(Sn)*, η		Composition shifted to Liq + T1 + T6
0.20	0.60	0.20	40	400 °C / 27d	T5, (Cu)	T5, (Cu)			
0.20	0.70	0.10	41	400 °C / 9d	$Li_{17}Sn_4$, (Cu), (Li)	Liq, (Cu), $Li_{17}Sn_4$	(Li)		
0.20	0.70	0.10	41	600 °C / 2d	(Li), $Li_{17}Sn_4$, (Cu)	Liq, (Cu), $Li_{17}Sn_4$	(Li)		
0.18	0.55	0.27	42	400 °C / 65d	T1, T6, $Li_{13}Sn_5$*, (Sn)*	$Li_{13}Sn_5$, T6, T8		(Sn)*	Composition shifted to $Li_{13}Sn_5$ + T1 + T6
0.17	0.67	0.17	43	400 °C / 21d	$Li_{17}Sn_4$, (Cu), T5	(Cu), $Li_{17}Sn_4$, T5			
0.10	0.20	0.70	46	300 °C / 100d	T4, (Sn), η	Liq, η, T4	(Sn)		
0.10	0.20	0.70	46	400 °C / 27d	(Sn), η, T4	Liq	(Sn), η, T4		
0.10	0.30	0.60	47	300 °C / 77d	T4, (Sn), Li_2Sn_5, η	Liq, Li_2Sn_5, T4	(Sn), η		
0.10	0.30	0.60	47	400 °C / 9d	T4, (Sn), Li_2Sn_5, η	Liq, T4	(Sn), η, Li_2Sn_5		
0.10	0.45	0.45	48	300 °C / 100d	T4, LiSn, Li_2Sn_5*, η*, (Sn)*	LiSn, Li_2Sn_5, T4		(Sn)*, η*	
0.10	0.45	0.45	48	400 °C / 27d	T4, η, (Sn), LiSn, Li_2Sn_5*, Li_7Sn_3*, T1*	Liq, LiSn, T4	(Sn), η, Li_2Sn_5*, Li_7Sn_3*, T1*		
0.10	0.45	0.45	48	500 °C / 100d	T4, LiSn, eta*, Li_2Sn_5*, (Sn)*	Liq, Li_7Sn_3, T6	LiSn, eta*, Li_2Sn_5*, (Sn)*		Composition shifted to Liq + T4
0.10	0.50	0.40	49	400 °C / 9d	T1, LiSn, (Sn), η, Li_7Sn_3	LiSn, Li_7Sn_3, T1	(Sn), η		(Sn), η from quenched liquid (minor amount)

0.10	0.50	0.40	49	500 °C / 22d	T4, (Sn), Li_7Sn_3, T6*	Liq, Li_7Sn_3, T6	(Sn), T4		
0.10	0.60	0.30	50	400 °C / 65d	T1, Li_7Sn_3, $Li_{13}Sn_5$, (Sn)*	Li_7Sn_3, T1	(Sn)*, $Li_{13}Sn_5$		(Sn)*, $Li_{13}Sn_5$ from quenched liquid (minor amount)
0.10	0.60	0.30	50	600 °C / 5d	Li_7Sn_3, T1, T4	Liq, Li_5Sn_2, T6	Li_7Sn_3, T4		Composition shifted to Liq + T1
0.10	0.62	0.28	51	400 °C / 21d	$Li_{13}Sn_5$, T1, Li_5Sn_2	Li_5Sn_2, $Li_{13}Sn_5$, T1			
0.10	0.63	0.27	52	400 °C / 7d	T6, $Li_{13}Sn_5$	$Li_{13}Sn_5$, T6, T8			Composition shifted to $Li_{13}Sn_5$ + T6 + T8
0.10	0.65	0.25	53	400 °C / 34d	T6, T1, $Li_{13}Sn_5$*, (Sn)*	$Li_{13}Sn_5$, T6, T8	(Sn)*, T1		Composition shifted to $Li_{13}Sn_5$ + T1 + T6
0.10	0.65	0.25	53	600 °C / 2d	T6, T4, T1, (Sn)*	$Li_{13}Sn_5$, T6, T8	(Sn)*, T1, T4		Composition shifted to Liq + T1 + T6
0.10	0.66	0.24	54	400 °C / 21d	T6, T1, T8, (Sn)*	$Li_{13}Sn_5$, T8			Composition shifted to $Li_{13}Sn_5$ + T8
0.10	0.66	0.24	54	600 °C / 2d	T6, T1, T8, (Sn)*	Li_7Sn_2, $Li_{13}Sn_5$, T8			Composition shifted to Li_7Sn_2 + $Li_{13}Sn_5$ + T8
0.10	0.70	0.20	55	400 °C / 9d	(Sn), T7	Li_7Sn_2, $Li_{17}Sn_4$, T5			Composition shifted to Li_7Sn_2 + $Li_{17}Sn_4$ + T5
0.10	0.80	0.10	56	400 °C / 9d	$Li_{17}Sn_4$, (Cu)	Liq, (Cu), $Li_{17}Sn_4$	(Li)		(Li) hardly visible in XRD
0.10	0.80	0.10	56	600 °C / 2d	$Li_{17}Sn_4$, (Cu)	Liq, (Cu), $Li_{17}Sn_4$	(Li)		(Li) hardly visible in XRD
0.05	0.72	0.23	58	400 °C / 21d	Li_7Sn_2, $Li_{17}Sn_4$, T1	Li_7Sn_2, T7	T1, T4*, T5		Composition shifted to Li_7Sn_2 + $Li_{17}Sn_4$ + T1
0.05	0.75	0.20	59	400 °C / 14d	T5, $Li_{17}Sn_4$	$Li_{17}Sn_4$, T5			
0.02	0.49	0.49	60	300 °C / 91d	LiSn, T4, Li_2Sn_5, (Sn)*	LiSn, Li_2Sn_5, T4		(Sn)*	
0.02	0.49	0.49	60	400 °C / 65d	LiSn, Li_2Sn_5, (Sn), η*, T4*	Liq, LiSn, T4	(Sn), η*, Li_2Sn_5		

Table 2: Crystallographic data of unary, binary and ternary phases in Cu-Li-Sn

	Phase	Stochio-metry	Type	Pearson symbol	Space group	No.	a (pm)	b (pm)	c (pm)	β (°)	Ref.
Cu-Sn	(Cu)	Cu	Cu	$cF4$	$Fm\bar{3}m$	225	361.443	-	-	90	[19]
	A2-β	$Cu_{17}Sn_3$	W	$cI2$	$Im\bar{3}m$	229	302.61	-	-	90	[20]
	D0$_3$-γ	Cu_3Sn	BiF$_3$	$cF16$	$Fm\bar{3}m$	225	611.76	-	-	90	[20]
	δ	$Cu_{41}Sn_{11}$	$Cu_{41}Sn_{11}$	$cF416$	$F\bar{4}3m$	216	1798	-	-	90	[21]
	ε	Cu_3Sn	Cu_3Ti	$oC80$	$Cmcm$	63	552.9	4775	432.3	90	[22]
	ζ	$Cu_{10}Sn_3$	ζ-AgZn	$hP26$	$P6_3$	173	733.0	-	786.4	90	[23]
	η	Cu_6Sn_5	AsNi	$hP4$	$P6_3/mmc$	194	419.2	-	503.7	90	[24]
	η´	Cu_6Sn_5	η´-Cu_6Sn_5	$mC44$	$C2/c$	15	1102.2	728.2	982.7	98.84	[25]
	(Sn)	Sn	Sn	$tI4$	$I4_1/amd$	141	579.98	-	316.42	90	[26]
Li-Sn	(Li)	Li	W	$cI2$	$Im\bar{3}m$	229	347.85	-	-	90	[27]
	$Li_{17}Sn_4$	$Li_{17}Sn_4$	$Li_{17}Sn_4$	$cF420$	$F\bar{4}3m$	216	1969.07	-	-	90	[28]
	Li_7Sn_2	Li_7Sn_2	Ge_2Li_7	$oC36$	$Cmmm$	65	980	1380	475	90	[29]
	$Li_{13}Sn_5$	$Li_{13}Sn_5$	$Li_{13}Sn_5$	$hP18$	$P\bar{3}m1$	164	470	-	1712	90	[30]
	Li_5Sn_2	Li_5Sn_2	Li_5Sn_2	$hR7$	$R\bar{3}2/m$	166	474	-	1983	90	[31]
	Li_7Sn_3	Li_7Sn_3	Li_7Sn_3	$mP20$	$P2_1/m$	11	856	472	945	105.95	[32]
	LiSn	LiSn	LiSn	$mP6$	$P2/m$	10	517	318	774	104.5	[33]
	Li_2Sn_5	Li_2Sn_5	Hg_5Mn_2	$tP14$	$P4/mbm$	127	1027.4	-	312.5	90	[34]
Cu-Li-Sn	T1	Li_2CuSn	$CuHg_2Ti$	$cF16$	$F\bar{4}3m$	216	629.5	-	-	90	[15]
	T2	$LiCu_2Sn$	$InPt_2Gd$	$hP8$	$P6_3/mmc$	194	430.22	-	761.8	90	[15]
	T3	$Li_3Cu_6Sn_4$	$Li_3Cu_6Sn_4$	$hP13$	$P6/mmm$	191	509.5	-	952.4	90	[16]
	T4	Li_2CuSn_2	Li_2AuSn_2	$tI20$	$I4_1/amd$	141	442.81	-	1941.6	90	[16]
	T5	Li_3CuSn	Li_3CuSn	$hP10$	$P6/mmm$	191	457.69	-	846.1	90	[18]
	T6	$Li_6Cu_2Sn_3$	$Li_6Cu_2Sn_3$	$hR33$	$R\bar{3}2/m$	166	459.00	-	3091.0	90	[18]

142

Table 3: Three-phase equilibria shown in isothermal sections from 300 to 600 °C

			300 °C	400 °C	500 °C	600 °C
Liq	(Cu)	$Li_{17}Sn_4$	x	x	x	x
Liq	ε	T2			x	x
Liq	ε	T3		x		
Liq	ε	η		x		
Liq	η	T4	x			
Liq	Li_2Sn_5	T4	x			
Liq	Li_5Sn_2	T6				x
Liq	Li_7Sn_3	T6			x	
Liq	LiSn	T4		x		
Liq	T1	T2				x
Liq	T1	T6				x
Liq	T2	T4			x	
Liq	T3	T4		x		
Liq	T4	T6			x	
(Cu)	A2-β	T2				x
(Cu)	δ	T2		x	x	
(Cu)	ε	T2	x			
(Cu)	$Li_{17}Sn_4$	T5	x	x	x	x
(Cu)	T1	T2	x	x	x	x
(Cu)	T1	T5	x	x	x	x
A2-β	D0$_3$-γ	T2				x
D0$_3$-γ	δ	T2				x
δ	ε	T2		x	x	
δ	ζ	T2				x
ε	ζ	T2				x
ε	η	T3	x			
ε	T2	T3	x	x		
η	T3	T4	x			
$Li_{13}Sn_5$	T1	T6	x	x		
$Li_{13}Sn_5$	T6	T8	x	x	x	x
Li_5Sn_2	$Li_{13}Sn_5$	T1	x	x		
Li_5Sn_2	$Li_{13}Sn_5$	T6			x	x
Li_5Sn_2	Li_7Sn_3	T1	x	x		
Li_5Sn_2	Li_7Sn_3	T6			x	
Li_7Sn_2	$Li_{13}Sn_5$	T8	x	x	x	x
Li_7Sn_2	$Li_{17}Sn_4$	T5	x	x	x	x
Li_7Sn_2	T5	T7	x	x	x	x
Li_7Sn_2	T7	T8	x	x	x	x
LiSn	Li_2Sn_5	T4	x			
LiSn	Li_7Sn_3	T1	x	x		
LiSn	T1	T4	x	x		
T1	T2	T4	x	x	x	
T1	T4	T6			x	
T1	T5	T7	x	x	x	x
T1	T6	T7	x	x	x	x
T2	T3	T4	x	x		
T6	T7	T8	x	x	x	x
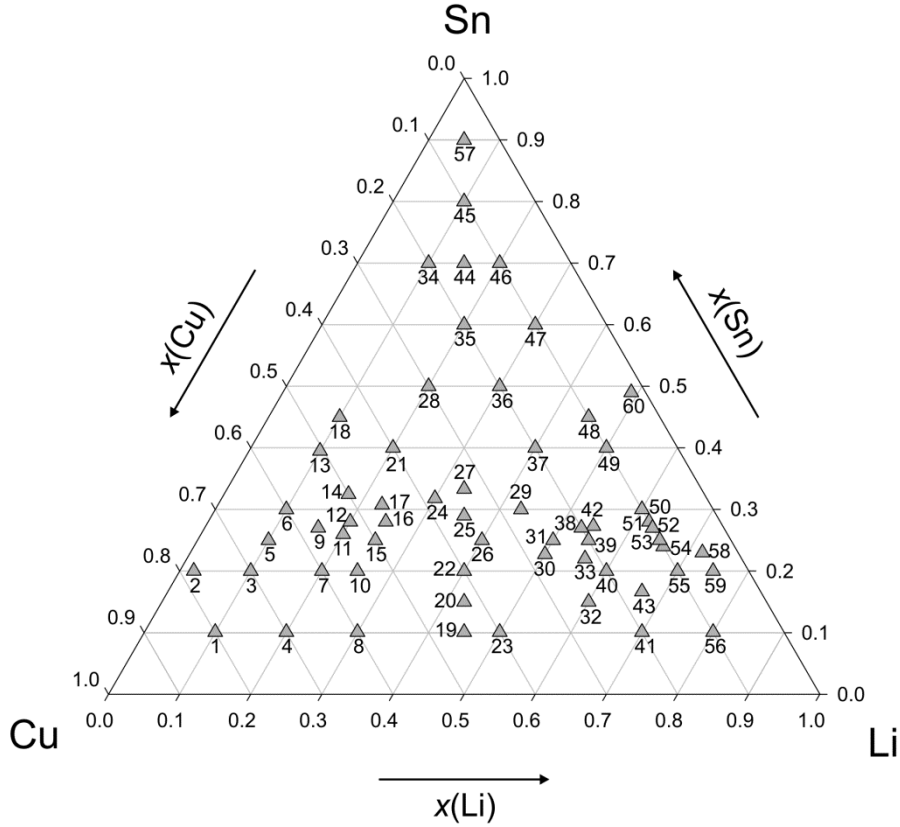
Fig. 1: 60 sample compositions in the Cu-Li-Sn system
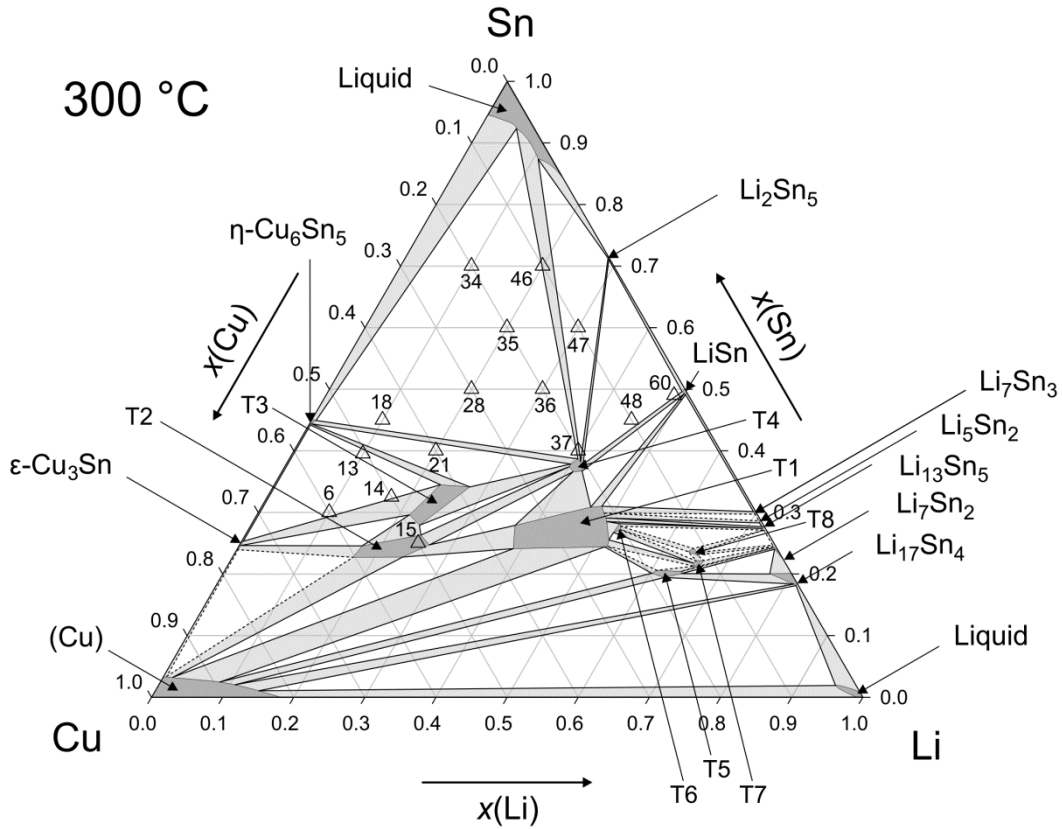
Fig. 2: Isothermal section at 300 °C with annealed samples: Dotted tie lines are tentative; dark grey, light grey and white areas are single-, two- and three-phase fields, respectively.
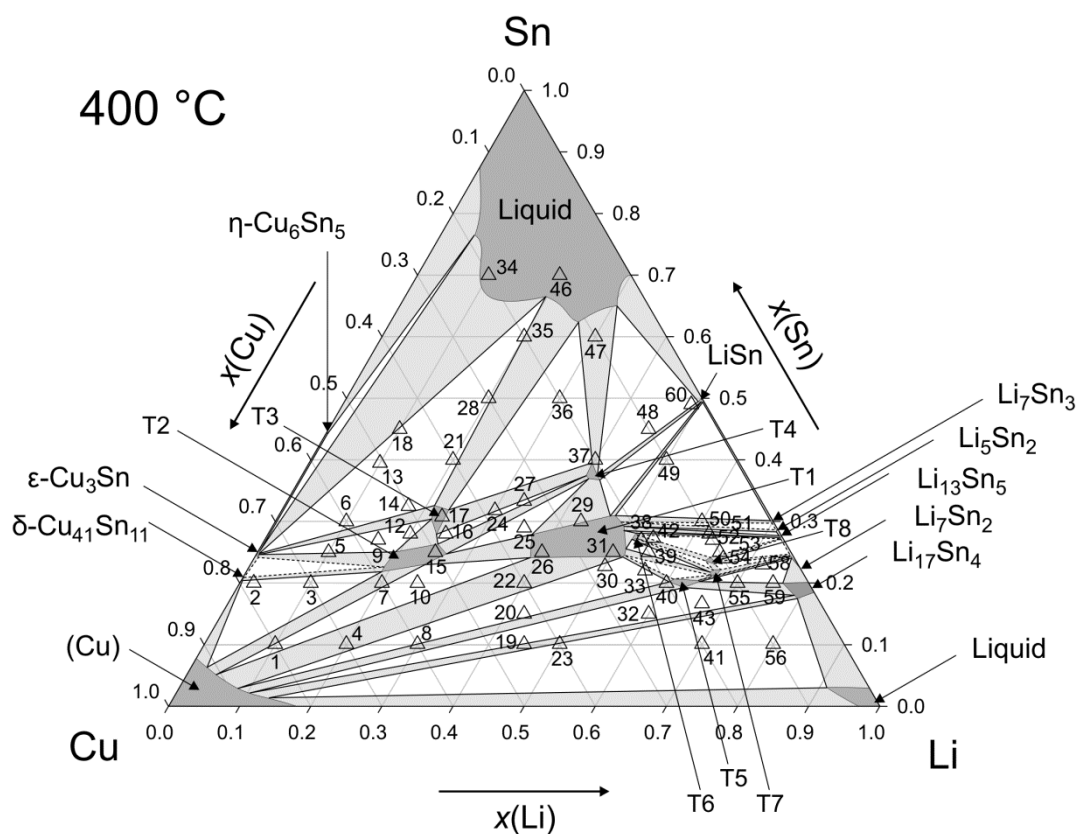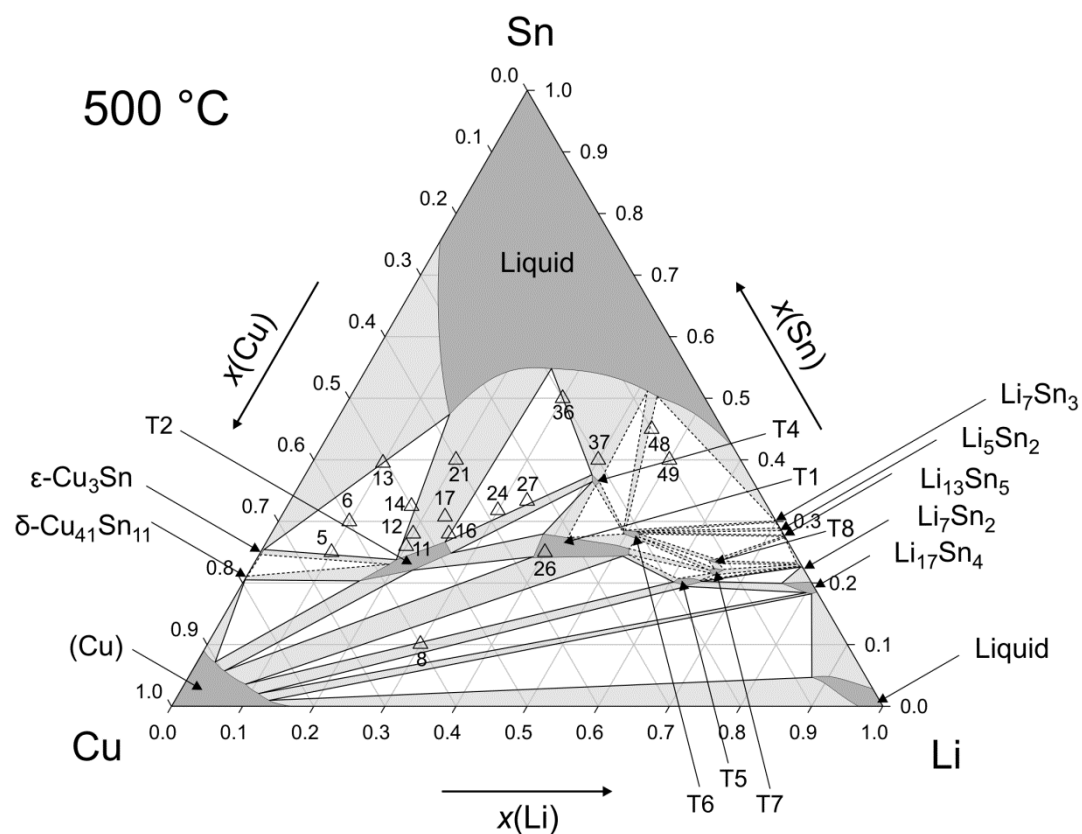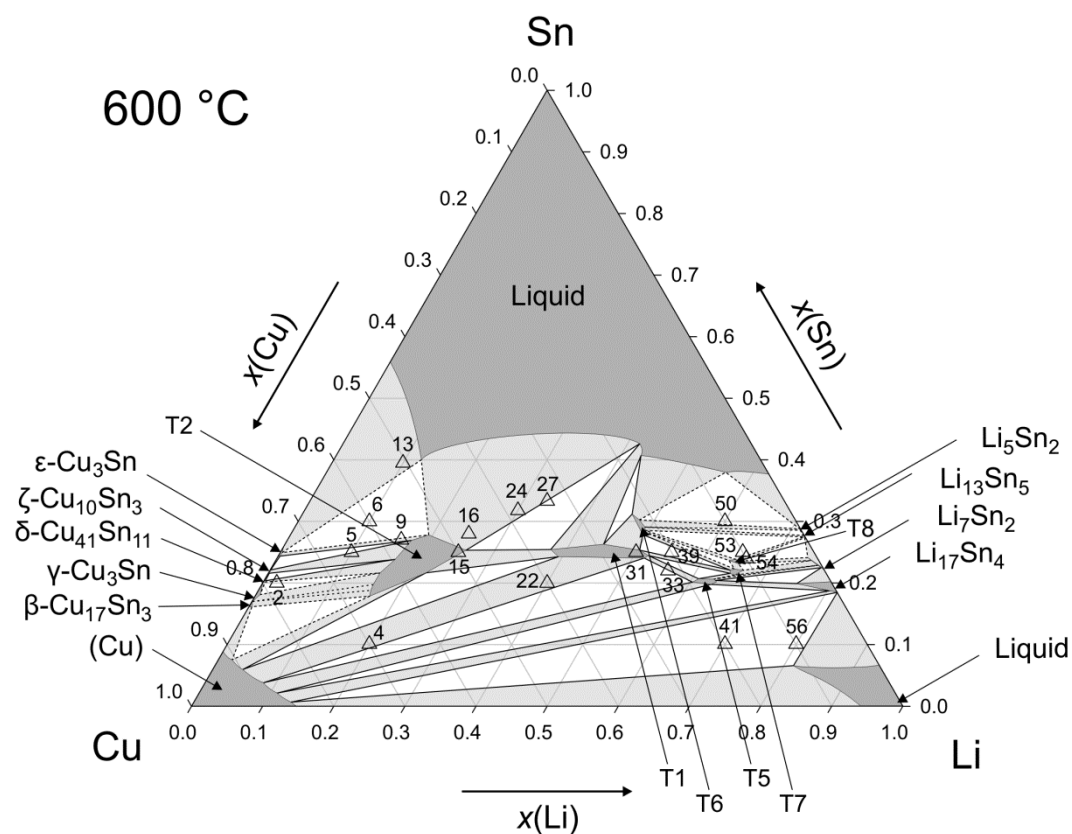
Fig. 3: Isothermal section at 400 °C with annealed samples: Dotted tie lines are tentative; dark grey, light grey and white areas are single-, two- and three-phase fields, respectively.

Fig. 4: Isothermal section at 500 °C with annealed samples: Dotted tie lines are tentative; dark grey, light grey and white areas are single-, two- and three-phase fields, respectively.

Fig. 5: Isothermal section at 600 °C with annealed samples: Dotted tie lines are tentative; dark grey, light grey and white areas are single-, two- and three-phase fields, respectively.
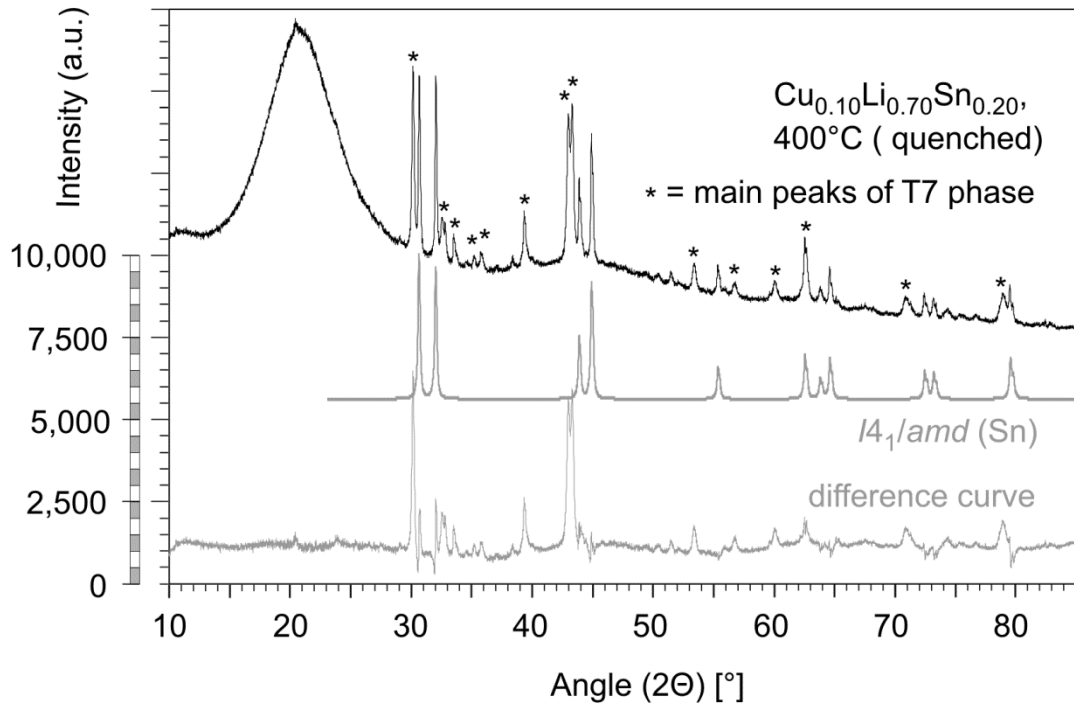
Fig. 6: XRD of sample Cu$_{0.10}$Li$_{0.70}$Sn$_{0.20}$ (# 55), annealed at 400 °C: estimated T7 phase (indicated by *) with (Sn)
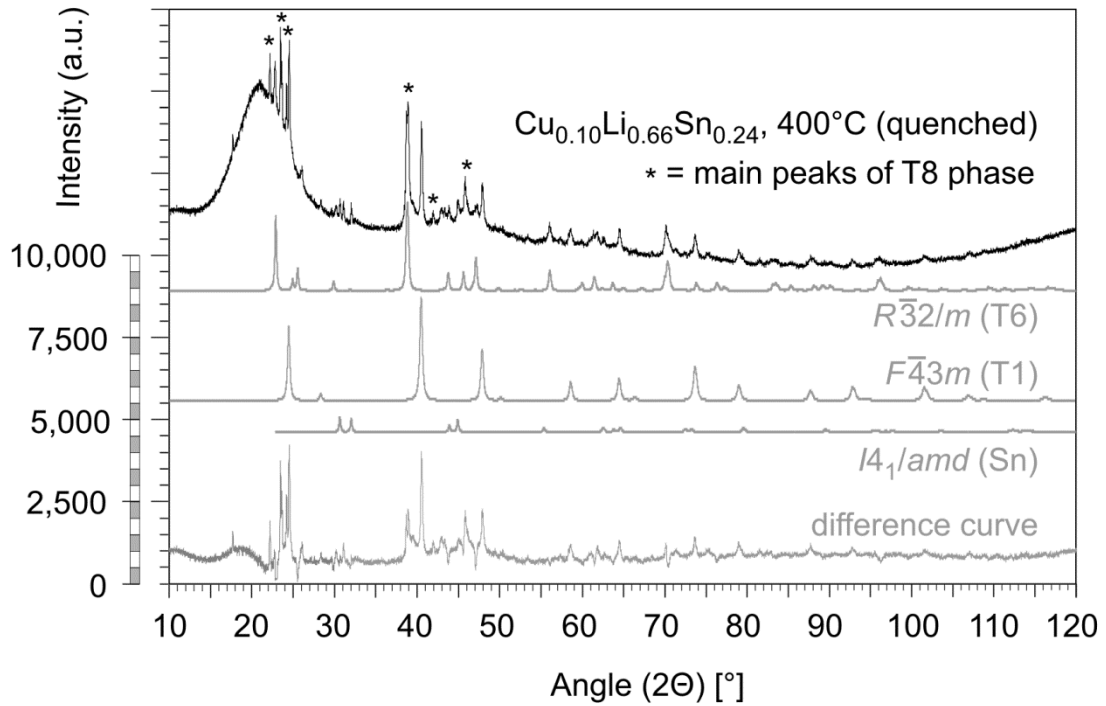
Fig. 7: XRD of sample Cu$_{0.10}$Li$_{0.66}$Sn$_{0.24}$ (# 54), annealed at 400 °C: estimated T8 phase (indicated by *) with (Sn), T1 and T6 phases
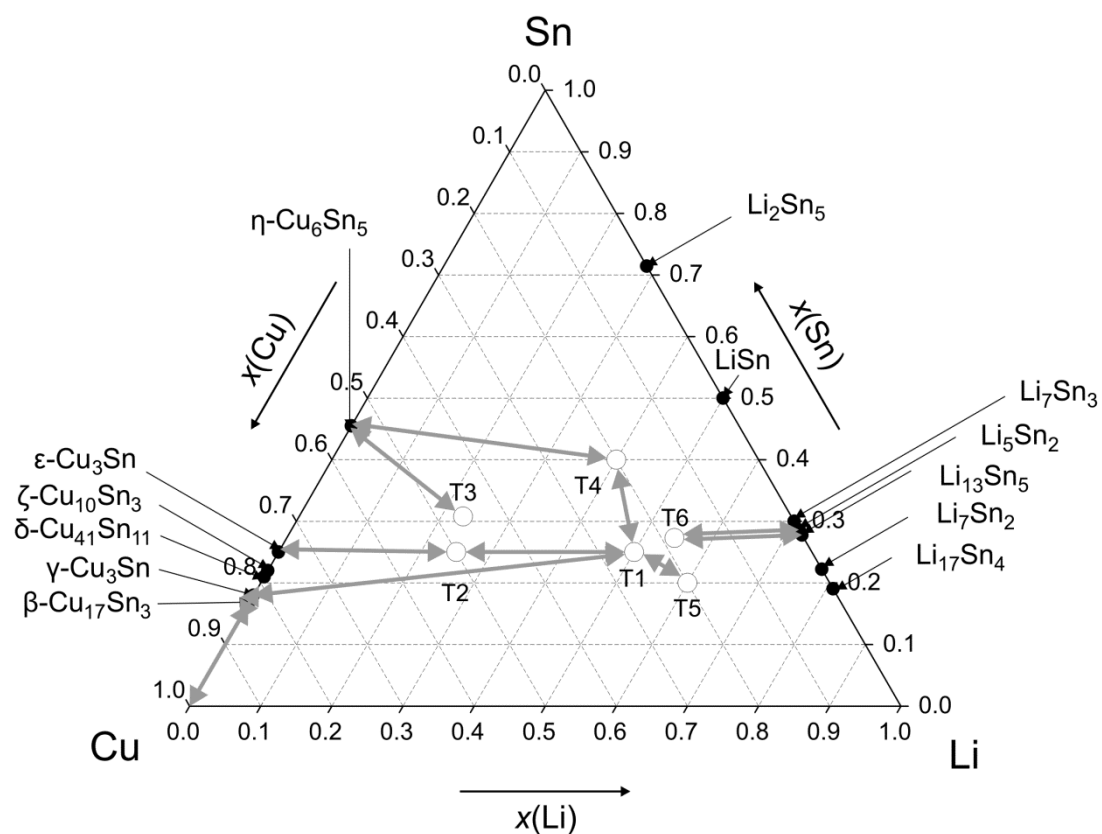
Fig. 8: Relationships between binary phases and known structures of ternary Cu-Li-Sn phases

3.6   Publication #6

The Cu-Li-Sn phase diagram: Isopleths, liquidus projection and reaction scheme

Siegfried Fürtauer[†], Hans Flandorfer[†]

[†]Institute of Inorganic Chemistry – Functional Materials, University of Vienna, Währingerstraße 42, A-1090 Wien

Contributions to this paper:

S. Fürtauer:	Sample preparation and characterization, interpretation, phase diagram development, publication
H. Flandorfer:	General advice and helpful comments, publication and proofreading

Overall contributions of S. Fürtauer to the paper: 90%

Abstract

The Cu-Li-Sn phase diagram was constructed based on XRD and DTA data of 60 different alloy compositions. Eight ternary phases and 14 binary solid phases form 44 invariant ternary reactions, which are illustrated by a Scheil-Schulz reaction scheme and a liquidus projection. Phase equilibria as a function of concentration and temperature are shown along nine isopleths. This report together with an earlier publication of our group provides for the first time comprehensive investigations of phase equilibria and respective phase diagrams. Most of the phase equilibria could be established based on our experimental results. Only in the Li-rich part where many binary and ternary compounds are present estimations had to be done which are all indicated by dashed lines. A stable ternary miscibility gap could be found which was predicted by modelling the liquid ternary phase in a recent work. The phase diagrams are a crucial input for material data bases and thermodynamic optimizations regarding new anode materials for high-power Li-ion batteries.

Introduction

Only few experimental data regarding phase equilibria are available for most of ternary intermetallic systems which contain lithium. The reasons for that are maybe the difficulties and obstacles to prepare and investigate such alloys. This was true for the system Cu-Li-Sn before we started our research which was conducted within the framework of the DFG priority program SPP1473 [1], dedicated to the computational design of new materials for high-power Li-ion batteries. In the meantime, together with our cooperation partners we could establish several new ternary compounds [2-4], four isothermal sections [5], ternary mixing enthalpies [6], and a thermodynamic optimization of the liquid phase [7]. The binary data of Cu-Sn and Li-Sn were taken from recent publications [8, 9], data for Cu-Li refer to an earlier work [10].

The benefit of this work is, besides the fundamental description of a new ternary system[1], the knowledge of equilibrium states for possible materials for the tailored design of Li-

---

[1] Possible metallic systems S: if n = number of applicable metals (n = 65; not considered are nonmetals, noble gases, Tc, elements in 7th period except Ac, Pm and transuranic elements) and d = dimension (unary = 1, binary = 2, ternary = 3,...) is $S = \frac{n!}{(n-d)! \cdot d!} =$

ion battery anodes. Improved cell design using well established materials will not be sufficient for a mandatory enhancement of energy and power density, and thus new materials have to be found. Advanced anode materials, *e.g.* intermetallics, are suggested for the use in such battery applications.

Despite battery performance testing of Cu-Sn alloy anodes, performed by several authors [12-15] who have proposed mechanisms for the lithiation of η´-Cu$_6$Sn$_5$, the understanding of these processes is scarce without detailed knowledge of involved phases, their equilibria and structures. Although, information on equilibrium states is not sufficient to understand and predict battery performance, which is highly influenced by kinetics, phase diagrams are fundamental.

This work on Cu-Li-Sn phase relations together with isothermal sections recently published by the same authors [5] and experimental thermochemical data [6, 7] provides thermodynamic information necessary for a comprehensive assessment and optimization of the respective phase diagram using CALPHAD methods.

Experimental procedure

Sample preparation

Intermetallic samples, which are located mainly along 9 sections across the Gibbs triangle, have been prepared at 60 different compositions from pure elements Cu (99.98 wt. %, wire, Goodfellow, Cambridge, UK), Li (99.8 wt. %, wire, Alfa Aesar, Karlsruhe, Germany) and Sn (99.95 wt. %, ingot, Advent, Oxford, UK). The sample compositions are shown in Fig. 1 together with the 9 cross sections. The Cu-wire was treated in a H$_2$-flow for 5 hours at 300 °C to remove the natural thin oxide layer at the surface. The Li-wire, which was stored originally in mineral oil for oxidation prevention, was cleaned by n-hexane in a supersonic bath. Visible oxidations spots were scraped off with a knife. All manipulations with Li or Li-containing samples were performed in a glove box under Ar atmosphere (< 5 ppm O$_2$ / H$_2$O). Samples have been weighed in thimble-like Ta crucibles, which have been welded with a corresponding lid in an arc furnace. For melting the enclosed metals, the crucibles were put into an induction furnace at 1100 °C. Repetition

---

$\frac{65!}{(65-3)!\cdot 3!} = 43680$ ternary systems; approximately 4000 have been investigated yet [11].

of the melting process twice (only 10 - 20 sec. each to prevent high temperature fatigue of the welding seam) with turning the crucible upside down between the heating steps assured homogenous mixing of the liquid alloys. Then the crucibles were sealed in quartz glass tubes under vacuum. All alloys were annealed consequently in a muffle furnace at 400 °C for several weeks and subsequently at 300, 400, 500 and 600 °C; few of them were annealed also at other temperatures (see Table 1). Especially in case of samples with high Li-contents the Ta sheet became partially permeable for Li vapour. This was evidenced by a darkening of the surrounding quartz glass, which could be explained by a reduction of transparent SiO_2 to brown SiO or related Li-containing silicates. After the heat treatment all samples were quenched in cold water and checked for mass loss. In most cases the mass loss was negligible with respect to the extension of the respective phase fields.

Analytical method: Powder XRD

Ta crucibles were opened in the glove box with a bolt cutter and the alloys have been extracted by squeezing the crucible. The (usually) brittle samples were powdered with a Durit® mortar and fixed with petroleum jelly on a specimen holder consisting of a silicon monocrystal. It was covered with a gastight polycarbonate cap before shuttled out of the glove box. Samples were exposed to Cu-K_α X-ray radiation (40 kV / 40 mA) in a diffractometer equipped with Bragg-Brentano geometry and a Ni filter. Signals were detected by a strip detector. Full-profile Rietveld refinements were applied for phase analyses which are presented in Table 1. Crystallographic information of the binary and ternary phases was listed in [5] recently.

Analytical method: DTA

Approximately 100-150 mg of sample material, which was annealed at 400 °C in order to establish starting equilibrium condition, was filled in Ta crucibles with a flattened bottom. The crucibles were closed with a corresponding lid and welded with an arc furnace. Thermal analysis was done in a single-point DTA instrument, equipped with small alumina discs as spacers between the crucible bottom and the welding bead of the S-type thermocouple. Reference material was a comparable amount of alumina in a second Ta crucible. Temperature calibration was done with pure metals, as Sn, Ag and Au, as well enclosed in Ta crucibles. The furnace program for the measurements was as follows: Fast heating to annealing temperature (20 °C / min up to 400 °C) - equilibration for 30 min - heating with 5 °C / min until 50 K above the estimated liquidus temperature

(however, < 900 °C to prevent leakage of the crucibles) – cooling with 5 °C / min to 100 °C – second heating with 5 °C / min to estimated liquidus temperature – cooling with 5 °C / min to room temperature. Peaks were evaluated with the Netzsch Proteus® software [16], overlapping peaks have been separated by the peak deconvolution tool in the Calisto® software package from AKTS [17]. Characteristic temperatures were determined by evaluation of the peak onset of the respective DTA signals on heating - except liquidus temperatures which correspond to the peak maximum (see Table 2). The estimated error of the temperature measurement is ± 2 K what is relatively high and attributed to the use of Ta crucibles.

Results and discussion

The present work visualizes the Cu-Li-Sn phase diagram, which was constructed based on experimental data. Since there are no such equilibrium phase diagrams for the Cu-Li-Sn system available in literature, it is the first comprehensive description of phase relations for all compositions and temperatures up to 1200 °C and at atmospheric pressure. It is in consistence with four ternary isothermal sections at temperatures between 300 and 600 °C which have been recently published by the authors [5] and considers recent findings of new ternary intermetallic compounds [2-4, 18] and the binary subsystems [7-9, 19]. There is strong experimental evidence for a stable liquid miscibility gap in the ternary system which is discussed in more detail below.

XRD data

60 alloy samples with different compositions have been prepared and annealed at 400 °C and in some cases at various other temperatures. At all 122 samples have been investigated by XRD and the results are listed in Table 1. In most cases the phase analysis showed a consistent picture. Some samples have been annealed between 650 and 750 °C (see Table 1) to check the presence of liquid phase at the respective temperature. This is indicated by the occurrence of non-equilibrium phases from the solidification of liquid phase during quenching. It was the case for samples 23, 25, 51 (annealed at 650 °C), samples 3, 5 (annealed at 700 °C) and sample 23 annealed at 750 °C. The detected equilibrium phases of samples 38, 51 and 55 (all annealed at 650 °C) are in contradiction to the phase equilibria which have been deduced from several other samples. They seem to be shifted towards lower Li-concentrations. This might be caused by Li-losses during sample preparation or by inhomogeneities. Therefore, these samples were not included into the respective isopleths. Samples 44 and 45, both annealed at 200 °C, contain the

phases (Sn) + η + T4. Sample 57 is as well allocated to this three-phase field, and, however, very close to the (Sn) + η–two-phase field; therefore the amount of T4 phase is very low and could not be detected by XRD.

DTA data

The liquidus temperatures (see Table 2) of the samples show a concise picture and could be unified to the construction of the isopleths, Figs. 2-10, and the liquidus projection, Fig. 11. They are indicated by triangle-shaped symbols in the isopleths. Depending on the Li-content the maximum temperature of our DTA runs was chosen to be at 800-900 °C. In case of the samples 4, 7, 8, 10 and 22, which are located in the Cu-rich corner of the phase diagram, the alloys were not totally molten at the maximum. Five samples with very high Sn content show diffuse melting peaks (34, 44, 45, 46, 57) – an exact determination of the peak maxima was difficult or even impossible; therefore these liquidus temperatures were carefully estimated and indicated with a swung dash symbol "~" in Table 2. The liquidus curves in the corresponding isopleths were drawn as dashed lines. Thermal effects below the liquidus are indicated by cross-shaped symbols in the respective isopleths (Figs. 2-10). Most of these thermal effects occurred in more than one sample and could be allocated to invariant reactions which have been listed in Table 3. The evaluation of these reactions is also supported by the phase equilibria of samples annealed at 300, 400, 500, and 600 °C, shown in Table 1 (for the corresponding isothermal sections see Ref. [5]). Some samples, however, show peaks at temperatures, which could not directly be allocated to reaction isotherms or they are at concentrations which are not covered by the reaction isotherms. Temperatures of these heat effects are written in italic in Table 2.

Isopleths

Figs 2-10 represent the 9 isopleths A to I where additional information is given as follows:

- Square symbols illustrate sample compositions at annealing temperatures and correspond to the data given in Table 1.
- Cross-shaped symbols indicate invariant or non-invariant heat effects from DTA signals below the liquidus temperature.
- Triangle-shaped symbols represent liquidus temperatures.
- Circle-shaped symbols indicate binary reacting temperatures from literature.
- Italic numbers designate the sample number according to Tables 1 and 2.

In a first step of construction all available transformation temperatures [7-9, 19] have been plotted along the respective sections. The Cu_2Li_3 phase which was postulated by Gąsior et al. [20] was neglected as discussed in detail by Li et al. [7]. A summary of employed invariant binary reactions is given in Table 4. In a second step of construction, phase equilibria from the isothermal sections at 300, 400, 500, 600 °C [5] and at other temperatures (for all cases see phase analysis by XRD in Table 1) have been included. Due to the lack of microprobe chemical analysis of equilibrium phase compositions, phase field limits had to be estimated. Table 5 summarizes all three-phase equilibria and samples which can be allocated to the associated phase fields. Symbol "x" in the Table indicates that the presence of the phase field at the respective temperature was not directly proven by experiments. However, an assignment was possible regarding adjacent phase fields and results of same alloy compositions annealed at nearby temperatures.

Heat effects of neighbouring samples at similar temperatures were connected with horizontal lines in the isopleth schemes and attributed to invariant reactions. Resulting single-, two- and three-phase fields were constructed strictly respecting the rule of Landau and Palatnik [21]. The single phase fields in Figs. 2-10 are illustrated in dark grey, two-phase fields are shown light grey and three-phase fields are presented in white. All ternary phases were found to be formed peritectically. The peritectic formation temperatures of phases T1-T6 are 720, 745, 458, 585, 732 and 689 °C, respectively (see Table 3). The peritectic formation temperatures of phases T7 and T8 were estimated to be at 693 and 690 °C. In a third step of construction it was verified that each isopleth adapts to other ones along their intersections. In total there are seven intersections involving three isopleths and twelve intersections involving two isopleths; Fig. 1. To keep the amount of prepared alloys within reasonable limits some phase fields or invariant reactions had to be assumed for the construction of isopleths. They are not validated by experiments and therefore drawn as dotted lines in Figs. 2-10 and written in italic in Tables 3. Especially in the Li-rich corner (see isopleths F and I), where five binary Li-Sn phases and at least three ternary phases exist next to each other, phase fields must be very narrow (< 1 at. %) and reliable experimental investigations are impossible regarding the inaccuracy of sample compositions; see section "Sample preparation" and Ref. [5]. The allocation of respective phase fields in this region is estimated and phase transformations could be solely adumbrated by vicinal data and thermodynamic rules. In the Cu-rich corner, several binary Cu-Sn phases make isopleths E and G more complex, especially between 500 °C and liquidus. Generally, in order to show complex regions of isopleths

with a very close sequence of phase fields they are magnified in Figs. 3a, 4a, 4b, 5a, 6a, 7a, 8a, 10a and 10b. For isopleths crossing the liquid miscibility gap mentioned above (all but C and E) the respective phase equilibria could not be established based on our experimental data. These regions are indicated by a question mark.

Liquidus projection

The liquidus projection of the Cu-Li-Sn system is presented in Fig. 11 and is in consistence with all isopleths and liquidus temperatures from DTA and our XRD results. A major experimental limitation is the lack of metallography and phase selective chemical analyses by EPMA due to the instability against air and moisture and the low atomic number of lithium. Therefore it was, *e.g.* not possible to directly identify fields of primary crystallisation from furnace cooled samples.

The primary crystallisation field of (Cu), which is the highest melting phase dominates approximately one third of the liquidus surface, followed by T2 phase, which holds the highest peritectic formation temperature (745 °C) of all ternary phases. The primary crystallisation of T1, T3 and T4 is suggested to be in the direct surrounding. Comparably large primary crystallisation fields are estimated for ε and γ – and a narrower phase field for β which extends far into the centre of the phase diagram. In the Sn-rich corner the dominant primary crystallisation field is that one of the η-phase. The Cu-Sn phases δ, ζ and η´ are formed peritectoidically without involving the liquid phase (*cf.* Table 4) and are therefore the only phases do not show up in the liquidus projection. The ternary phases T5-T8 and most of the binary Li-Sn phases have their primary crystallisation field (Fig. 11a) within the compositional triangle $Cu_{0.4}Li_{0.4}Sn_{0.2} - Li_{0.8}Sn_{0.2} - Li_{0.4}Sn_{0.6}$. As it was difficult to synthesize samples containing only one of the two phases T7 and T8 we assumed only very small regions of primary crystallisation which are shown in detail in Fig. 11a (magnified section of Fig. 11).

The liquidus projection in Fig. 11 shows as well the liquidus isotherms based on our DTA results. It can be observed that the liquidus temperatures mostly descend from the boundary binary systems. Two liquidus valleys, descending towards the Li-corner and towards the Sn-corner, respectively separate the ternary system. Liquidus temperatures of various samples in the Li-rich part clearly indicate a ternary maximum at about 850 °C. There is no experimental indication for the existence of a congruently melting ternary compound. This is supported by the high compound forming tendency in the binary Li-Sn system [9, 24] compared to Cu-Sn [25] and Cu-Li [7]. As a consequence, this maximum can only be caused by a ternary liquid miscibility gap. This assumption is

supported by the assessment of the liquid phase in Li et al. [7]. Similar systems which show a metastable liquid miscibility gap in one of the constituent binaries and a stable one in the ternary are C-Cu-Fe [26, 27] or Al-Cu-Sn [28]. In our case the fields of primary crystallization of Cu, $Li_{17}Sn_4$ and Li_7Sn_2 are very close to each other. Thus we assume an extension of the liquid immiscibility over these three primary crystallization fields. This is similar to the Al-Mg-Sc system [29], which however shows no metastable binary miscibility gap. Accordingly, two ternary monotectic reactions (Em1 and Em2) are proposed based on a wide maximum of the liquidus surface in the Li-rich corner (around $Cu_{0.2}Li_{0.65}Sn_{0.15}$). Each ternary monotectic reaction involves two four-phase equilibria at different liquid compositions, which are connected by a tie-line indicated as solid thin line in Figs. 11 and 11a. Both reactions involve four maxima (m2 – m5) and the solid phases (Cu), $Li_{17}Sn_4$, and Li_7Sn_2. It is noteworthy that for the phase $Li_{17}Sn_4$ two primary crystallisation fields exist. Because the existence and localisation of both reactions are only estimated, the reactions are drawn with dotted lines. Two further maxima (m1 and m6) have to be established to connect the monotectic reactions to adjacent invariant reactions (P8 and U27 in Fig. 11a).

Reaction scheme

The complete reaction scheme of the Cu-Li-Sn system is shown in three temperature intervals (Figs. 12, 13, 14 illustrate reaction schemes until 400 °C, from 400 - 600 °C and higher than 600 °C, respectively). It involves 22 binary (Table 4) and 44 ternary reactions (Table 3), where 14 out of them had to be assumed due to uncertain or missing experimental data. Three unary temperatures for the pure elements, three congruent melting points (compounds $Li_{17}Sn_4$, Li_7Sn_2 and LiSn) and the congruent formation of ε from γ phase are listed in Table 4 but not shown in Figs. 12-14. Two suggested ternary monotectic reactions (Em1: Liq´ → Liq´´ + (Cu) + $Li_{17}Sn_4$ and Em2: Liq´ → Liq´´ + Li_7Sn_2 + $Li_{17}Sn_4$) are located between approximately 700 and 800 °C and involve two different liquid phases Liq´ and Liq´´. Ternary phase fields connected to the maximum points m1-m6 end up in Em1, Em2, P8, and U27. The high temperature part of the reaction scheme above 700 °C (Fig. 14) is dominated by a sequence of peritectic formations of ternary compounds, involving liquid, (Cu) and a fourth phase (745 °C: Liq + (Cu) + β → T2; 732 °C: Liq + (Cu) + $Li_{17}Sn_4$ → T5; 720 °C: Liq + (Cu) + T5 → T1). Phases T6, T7 and T8 are formed at somewhat lower temperatures involving Li-rich phases (693 °C: Liq + Li_7Sn_2 + T5 → T7; 690 °C: Liq + Li_7Sn_2 + T7 → T8; 689 °C: Liq + T1 + T5 → T6). An U-type reaction in the Li-rich region at 703 °C includes the liquid

phase, the congruent melting phases $Li_{17}Sn_4$ and Li_7Sn_2 and the Li-rich ternary phase T5 (U27: Liq + $Li_{17}Sn_4$ → Li_7Sn_2 + T5). A cascade of further U-type reactions, connecting binary Li-Sn compounds and Li-rich ternary compounds T1, T5, T6, T7 and T8 (U17, 20, 21, 23), follows; corresponding heat effects can be compared with Figs. 7a and 10a (magnified sections of isopleths F and I). U24 (680 °C: Liq + T7 → T6 + T8) and U25 (685 °C: Liq + T5 → T6 + T7) are not based on measured DTA effects and had to be estimated from the liquidus projection (Fig. 11a). A central reaction, which is well identified by means of XRD and DTA, is U22 (670 °C: Liq + (Cu) → T1 + T2). At temperatures up to 670 °C, three-phase fields are separated by the dominant two-phase field T1 + T2 (compare isothermal section in [5]); above 670 °C this two-phase field connects (Cu) and Sn-rich liquid. The reaction U22 is present in most isopleths (A-E, G, and H) and maintains an interesting shape of the Liq + (Cu) two-phase region (compare isopleths D, E, H). At 585 °C the phase T4 is formed from Liq, T1 and T2 (P3: Liq + T1 + T2 → T4), which enables several following reactions with adjacent phases T1, T6, Li_7Sn_3, Li_5Sn_2 and LiSn (U12 – U15). The phase T1 occurs in samples 50 and 51 at 400 °C together with T6. The latter one is also present in samples with increased Li-concentrations (#52 and #53) at 600 °C. This requires further reactions between 400 and 500 °C; U7, U8, U10 and U11 at 430, 440, 450 and 460 °C, respectively. They have been included into the reaction scheme even so they are only tentative and therefore drawn with dashed lines (as well as in isopleths F and I). The lowest ternary phase formation temperature is that one of phase T3, which is formed from liquid, T2 and T4 at 458 °C. It is involved in three U-type reactions with binary Cu-Sn phases ε and / or η (U9 at 445 °C: Liq + T2 → ε + T3; U6 at 348 °C: Liq + ε → η + T3; U5 at 328 °C: Liq + T3 → η + T4). The Sn-rich corner is dominated by liquid and T4 phase. Three reactions follow from 321 °C (U4: Liq + LiSn → Li_2Sn_5 + T4) to 220 °C (P1: Liq + Li_2Sn_5 + T4 → (Sn)) and finally to 218 °C (E2: Liq → (Sn) + η + T4). Four reactions take place at temperatures < 200 °C (E1, U1-U3), but except for E1 (180 °C: Liq → (Cu) + (Li) + $Li_{17}Sn_4$) no evident heat effect could be found experimentally. Therefore reactions U1-U3 were estimated based on the vicinal binary reactions e2 (186 °C: η → (Sn) + η´) and p1 (189.1 °C: ε + η → η´) and are indicated using dashed lines. The Cu-rich side is extrapolated from the binary Cu-Sn system into the ternary system. The phase T2 is the dominating one in this region; therefore most reactions including liquid and Cu-Sn phases are connected to T2 (E3-E6, U16, U18 and U26). These ternary reactions occur at temperatures close to the respective binary reactions.

Conclusions and Outlook

Reactions and reaction temperatures between two liquid phases, three unary phases, 14 binary phases and eight ternary phases have been widely clarified by combination of XRD and DTA data. An iterative development of isopleths, isotherms and a liquidus projection, under the consideration of most DTA and XRD results, leads to a consistent description of the phase diagram. The present phase diagram, which is illustrated by nine isopleths, a liquidus projection and a reaction scheme, includes 113 three-phase regions, which are related to 44 ternary invariant reactions. In some parts of the phase diagram, namely in the vicinity of Li-rich binary Li-Sn phases, in some regions close to the Cu-rich binary Cu-Sn phases and at temperatures above 750 and below 200 °C, no clear experimental data were available. Thus assumptions of phase equilibria and reaction temperatures based on adjacent samples had to be made which still require further clarification. Also the existence of the two monotectic ternary reactions Em1 and Em2 should be proved in further investigations. The knowledge of the phase diagram offers the possibility to prepare alloys with predetermined phase composition and microstructure. It is also a valuable reference for a calculated phase diagram, which is usually based on an optimization of thermodynamic data and performed with the CALPHAD approach [30]. An optimization based on this phase diagram and experimental thermochemical data allows the calculation of physicochemical properties for certain regions of the phase diagram, *e.g.* open circuit potentials. These inputs are necessary for a tailored design of materials for application in Li-ion batteries and legitimate fundamental research in the context of applied science.

References

[1]   H.J. Seifert, Karlsruhe Institute of Technology, Materials with New Design for Improved Lithium Ion Batteries. http://www.spp1473.kit.edu. (May 19th, 2016).

[2]   S. Fürtauer, H.S. Effenberger, H. Flandorfer, New intermetallic phases in the Cu-Li-Sn system: The lithium rich phases Li_3CuSn and $Li_6Cu_2Sn_3$, Zeitschrift für Kristallographie - Crystalline Materials, 231 (2016) 79-87.

[3]   S. Fürtauer, H.S. Effenberger, H. Flandorfer, The tin-rich copper lithium stannides: $Li_3Cu_6Sn_4$ and Li_2CuSn_2, Zeitschrift für Kristallographie, 230 (2015) 97-105.

[4]   S. Fürtauer, H.S. Effenberger, H. Flandorfer, $CuLi_2Sn$ and Cu_2LiSn: Characterization by single crystal XRD and structural discussion towards new anode materials for Li-ion batteries, Journal of Solid State Chemistry, 220 (2014) 198-205.

[5]   S. Fürtauer, H. Flandorfer, The Cu-Li-Sn phase diagram: Isothermal sections, Journal of Alloys and Compounds, 682 (2016) 713-722.

[6]   S. Fürtauer, E. Tserenjav, A. Yakymovych, H. Flandorfer, Calorimetric studies of Li-Sn, Cu-Li and Cu-Li-Sn, Journal of Chemical Thermodynamics, 61 (2013) 105-116.

[7]   D. Li, S. Fürtauer, H. Flandorfer, D.M. Cupid, Thermodynamic Assessment of the Cu-Li System and Prediction of Enthalpy of Mixing of Cu-Li-Sn Liquid Alloys, CALPHAD - Computer Coupling of Phase Diagrams and Thermochemistry, 53 (2016) 105-115.

[8]   S. Fürtauer, D. Li, D. Cupid, H. Flandorfer, The Cu-Sn phase diagram, Part I: New experimental results, Intermetallics, 34 (2013) 142-147.

[9]   D. Li, S. Fürtauer, H. Flandorfer, D.M. Cupid, Thermodynamic assessment and experimental investigation of the Li-Sn system, CALPHAD - Computer Coupling of Phase Diagrams and Thermochemistry, 47 (2014) 181-195.

[10]   A.D. Pelton, The Cu-Li (Copper-Lithium) system, Bulletin of Alloy Phase Diagrams, 7 (1986) 142-144.

[11]   G. Effenberg, MSI, Materials Science International Services GmbH, http://www.msiport.com/msi-eureka/products/all-element-systems-abbreviated.html. (May 19th, 2016).

[12]   A. Jansen, J. Clevenger, A. Baebler, J. Vaughey, Variable temperature performance of intermetallic lithium-ion battery anode materials, Journal of Alloys and Compounds, (2011) 4457–4461.

[13]   W. Choi, J.Y. Lee, H.S. Lim, Electrochemical lithiation reactions of Cu_6Sn_5 and their reaction products, Electrochemistry Communications, 6 (2004) 816-820.

[14]   S. Sharma, L. Fransson, E. Sjostedt, L. Nordstrom, B. Johansson, K. Edstrom, A theoretical and experimental study of the lithiation of η´-Cu_6Sn_5 in a lithium-ion battery, Journal of the Electrochemical Society, 150 (2003) A330-A334.

[15]   K.D. Kepler, J.T. Vaughey, M.M. Thackeray, $Li_xCu_6Sn_5$ (0 < x < 13): An intermetallic insertion electrode for rechargeable lithium batteries, Electrochemical and Solid State Letters, 2 (1999) 307-309.

[16]   Proteus NETZSCH Proteus® Software for Thermal Analysis, v. 5.2.1; NETZSCH-Gerätebau GmbH: Selb / Germany, 2011.

[17]   Calisto Calisto Processing ®, v. 1.062; AKTS - Advanced Kinetics and Technology Solutions: Siders / Switzerland, 2011.

[18]   F. Winter, S. Dupke, H. Eckert, U.C. Rodewald, R. Pöttgen, Lithium mobility in the stannides Li_2CuSn_2 and Li_2AgSn_2, Zeitschrift für Anorganische und Allgemeine Chemie, 639 (2013) 2790-2795.

[19]   D. Li, P. Franke, S. Fürtauer, D. Cupid, H. Flandorfer, The Cu-Sn phase diagram part II: New thermodynamic assessment, Intermetallics, 34 (2013) 148-158.

[20]   W. Gąsior, B. Onderka, Z. Moser, A. Dębski, T. Gancarz, Thermodynamic evaluation of Cu-Li phase diagram from EMF measurements and DTA study, CALPHAD - Computer Coupling of Phase Diagrams and Thermochemistry, 33 (2009) 215-220.

[21]   L.S. Palatnik, A.I. Landau, Phase Equilibria in Multicomponent Systems. Holt, Rinehart & Co, New York, 1964.

[22]   J. Sangster, C.W. Bale, The Li-Sn (Lithium-Tin) system, Journal of Phase Equilibria, 19 (1998) 70-75.

[23]   N. Saunders, A.P. Miodownik, The Cu-Sn (Copper-Tin) System, Bulletin of Alloy Phase Diagrams, 11 (1990) 278-287.

[24]   C.J. Wen, R.A. Huggins, Thermodynamic study of the Lithium-Tin system, Journal of the Electrochemical Society, 128 (1981) 1181-1187.

[25]   H. Flandorfer, U. Saeed, C. Luef, A. Sabbar, H. Ipser, Interfaces in lead-free solder alloys: Enthalpy of formation of binary Ag-Sn, Cu-Sn and Ni-Sn intermetallic compounds, Thermochimica Acta, 459 (2007) 34-39.

[26]   N. Bochvar, R. Schmid-Fetzer, E. Semenova, E. Sheftel, MSIT, C-Cu-Fe Ternary Phase Diagram Evaluation, in: G. Effenberg (Ed.) MSI Eureka in SpringerMaterials. MSI Materials Science International Services GmbH, Stuttgart, 2007.

[27]   M. Turchanin, P. Agraval, MSIT, Cu-Fe Binary Phase Diagram Evaluation, in: G.E. (ed.) (Ed.) MSI Eureka in SpringerMaterials. MSI Materials Science International Services GmbH, Stuttgart 2007.

[28]   N. Bochvar, MSIT, Al-Cu-Sn Ternary Phase Diagram Evaluation, in: G. Effenberg (Ed.) MSI Eureka in SpringerMaterials. MSI Materials Science International Services GmbH, Stuttgart, 1992.

[29]   J. Gröbner, R. Schmid-Fetzer, Phase transformations in ternary monotectic aluminum alloys, JOM, 57 (2005) 19-23.

[30]   P.J. Spencer, A brief history of CALPHAD, CALPHAD - Computer Coupling of Phase Diagrams and Thermochemistry, 32 (2008) 1-8.

Table 1: Heat treatment and quenched phases of Cu-Li-Sn samples at annealing temperatures

[1] Samples are ordered with decreasing Cu- and increasing Li-concentration;

[2] Identified phases are ordered with decreasing amount (approximated from Rietveld-refinements);

[3] Corresponding phase fields are ordered systematically (Liq – unary – binary – ternary phases);

* denotes phases, which are only present in traces.

x(Cu)	x(Li)	x(Sn)	Sample No.	Shown in isopleth	Heat treatment	Identified phases [2]	Corresponding phase field [3]	Formed during quenching	Formed during hydro-lysis	Comments
0.80	0.10	0.10	1	C, D, E	400 °C / 27d	(Cu), T2, T1*	(Cu), T1, T2			
0.78	0.02	0.20	2	G	400 °C / 65d	ζ, T2, (Cu)*	(Cu), δ, T2			ζ and δ very similar in XRD
0.78	0.02	0.20	2	G	600 °C / 91d	ζ, δ, T2*	D0$_3$-γ, δ, T2	ζ (from D0$_3$-γ)		
0.70	0.10	0.20	3	E, G	400 °C / 9d	ζ, T2, (Cu)	(Cu), δ, T2			ζ and δ very similar in XRD
0.70	0.10	0.20	3	E, G	700 °C / 22d	ζ, T2, ε	Liq, β, T2	ε, ζ (from Liq, β)		
0.70	0.20	0.10	4	D, H	400 °C / 27d	(Cu), T1	(Cu), T1			
0.70	0.20	0.10	4	D, H	600 °C / 3d	(Cu), T1	(Cu), T1			
0.65	0.10	0.25	5	E	400 °C / 27d	ε, T3, T2*	ε, T2, T3			
0.65	0.10	0.25	5	E	500 °C / 100d	ε, T3, T2*	Liq, ε, T2	T3		

0.65	0.10	0.25	5	E	600 °C / 100d	ε, T2, ζ*, T4*	ε, ζ, T2	T4*		T4 from quenched liquid (minor amount)
0.65	0.10	0.25	5	E	700 °C / 100d	ζ, ε, T2	Liq, β, T2	ε, ζ (from Liq, β)		
0.60	0.10	0.30	6	E	300 °C / 105d	ε, T3, η	ε, η, T3			
0.60	0.10	0.30	6	E	400 °C / 70d	T3, ε, η, (Sn)*, T2*	Liq, ε, T3	(Sn), η, T2		
0.60	0.10	0.30	6	E	500 °C / 65d	ε, T3, η*, (Sn)*	Liq, ε, T2	(Sn), η, T3		Composition shifted to Liq + ε
0.60	0.10	0.30	6	E	600 °C / 65d	ε, T3, η, (Sn)*	Liq, ε, T2	(Sn), η, T3		Composition shifted to Liq + ε
0.60	0.20	0.20	7	C, G, H	400 °C / 21d	T2, (Cu)	T2, (Cu)			
0.60	0.30	0.10	8	D	400 °C / 9d	(Cu), T5, T1	(Cu), T1, T5			
0.60	0.30	0.10	8	D	500 °C / 7d	(Cu), T5, T1	(Cu), T1, T5			
0.57	0.16	0.27	9	-	400 °C / 65d	T2, T3, ε	ε, T2, T3			No isopleth
0.57	0.16	0.27	9	-	600 °C / 91d	T2, ζ, ε, η*, T3*, T4*, (Sn)*	Liq, ε, T2	(Sn), ζ, η, T3, T4		No isopleth
0.55	0.25	0.20	10	G	400 °C / 70d	T1, T2, (Cu)	(Cu), T1, T2			
0.54	0.20	0.26	11	H	500 °C / 35d	T2, T3*	Liq, T2	T3		

0.52	0.20	0.28	12	H	400 °C / 21d	T3, T2, ε	ε, T2, T3			
0.52	0.20	0.28	12	H	500 °C / 35d	T2, δ, T3*, T4*, (Sn)*, η*	Liq, T2	(Sn)*, δ, η*, T3*, T4*		
0.51	0.10	0.40	13	E	300 °C / 122d	η, T3, ε	ε, η, T3			
0.51	0.10	0.40	13	E	400 °C / 21d	ε, T3, T4*, T2*, η*, (Sn)*	Liq, ε, T3	T4*, T2*, η*, (Sn)*		
0.51	0.10	0.40	13	E	500 °C / 35d	ε, η, (Sn), T4*	Liq, ε	(Sn), η, T4*		
0.51	0.10	0.40	13	E	600 °C / 35d	ε, η, T3, (Sn)	Liq, ε	(Sn), η, T3		
0.50	0.18	0.33	14	-	300 °C / 105d	T3, ε, η, (Sn)*	ε, η, T3		(Sn)*	No isopleth
0.50	0.18	0.33	14	-	400 °C / 70d	T3, ε, η, T2*, (Sn)*	Liq, ε, T3	(Sn)*, η, T2*		No isopleth
0.50	0.18	0.33	14	-	500 °C / 65d	T2, δ, ε, T3, η, (Sn)	Liq, ε, T2	(Sn), δ, η, T3		No isopleth
0.50	0.25	0.25	15	C	300 °C / 84d	T2	T2			
0.50	0.25	0.25	15	C	400 °C / 35d	T2	T2			
0.50	0.25	0.25	15	C	600 °C / 84d	T2	T2			
0.47	0.25	0.28	16	-	400 °C / 21d	T2, T3, T4, (Sn)*	T2, T3, T4		(Sn)*	No isopleth
0.47	0.25	0.28	16	-	500 °C / 27d	T2, η, (Sn), T4*	Liq, T2	(Sn), η, T4*		No isopleth
0.47	0.25	0.28	16	-	600 °C / 35d	T2, T4, η*, (Sn)*	Liq, T2	(Sn)*, η*, T4		No isopleth
0.46	0.23	0.31	17	-	400 °C / 70d	T3, T4*	T3, T4			No isopleth
0.46	0.23	0.31	17	-	500 °C / 65d	T2, δ, (Sn)*, η*	Liq, T2	(Sn)*, δ, η*		No isopleth

0.45	0.10	0.45	18	B, E	300 °C / 100d	η, T4, (Sn)	Liq, η, T4	(Sn)		
0.45	0.10	0.45	18	B, E	400 °C / 27d	ε, T3, (Sn), η	Liq, ε, T3	(Sn), η		
0.45	0.45	0.10	19	A, D	400 °C / 27d	(Cu), Li$_{17}$Sn$_4$, (Sn)*	(Cu), Li$_{17}$Sn$_4$		(Sn)*	
0.43	0.43	0.15	20	A	400 °C / 27d	T5, (Cu), T1	(Cu), T1, T5			
0.40	0.20	0.40	21	B, H	300 °C / 100d	T4, η, T3, (Sn)*	η, T3, T4		(Sn)*	
0.40	0.20	0.40	21	B, H	400 °C / 27d	T3, η, (Sn), ε*, T4*	Liq, ε, T3	(Sn), η, T4*		
0.40	0.20	0.40	21	B, H	500 °C / 100d	T2, T4, η, T3*, (Sn)*	Liq, T2	(Sn)*, η, T3*, T4		
0.40	0.40	0.20	22	A, G	400 °C / 56d	T1, (Cu)	(Cu), T1			
0.40	0.40	0.20	22	A, G	600 °C / 3d	T1, (Cu)	(Cu), T1			
0.40	0.50	0.10	23	D	400 °C / 9d	(Cu), Li$_{17}$Sn$_4$, T5, (Sn)*	Liq, (Cu), Li$_{17}$Sn$_4$	(Sn)*, T5		
0.40	0.50	0.10	23	D	650 °C / 2d	(Cu), T5, Li$_{17}$Sn$_4$	Liq, (Cu), Li$_{17}$Sn$_4$	T5		
0.40	0.50	0.10	23	D	750 °C / 4d	Li$_{17}$Sn$_4$, T5, (Cu)	Liq, (Cu), Li$_{17}$Sn$_4$	T5		
0.38	0.30	0.32	24	-	400 °C / 42d	T3, T4, (Sn)*	T3, T4		(Sn)*	No isopleth
0.38	0.30	0.32	24	-	500 °C / 77d	T2, T4, (Sn)*	Liq, T2, T4	(Sn)*		No isopleth
0.38	0.30	0.32	24	-	600 °C / 77d	T2, T4, η, (Sn)	Liq, T2	(Sn), η, T4		No isopleth

0.36	0.36	0.29	25	A	400 °C / 21d	T1, T4, η*, T2*, (Sn)*	T1, T2, T4,		(Sn)*, η*	
0.36	0.36	0.29	25	A	650 °C / 4d	T1, T2, T4, η, (Sn)*	Liq, T1, T2	(Sn)*, η, T4		
0.35	0.40	0.25	26	-	400 °C / 70d	T1	T1			No isopleth
0.33	0.33	0.33	27	A, B, C	400 °C / 70d	T4, T2, T3	T2, T3, T4			
0.33	0.33	0.33	27	A, B, C	500 °C / 65d	T2, T4, η, (Sn)	Liq, T2, T4	(Sn), η		
0.33	0.33	0.33	27	A, B, C	600 °C / 65d	T2, η, (Sn), T4, T1*	Liq, T1, T2	(Sn), η, T4		
0.30	0.20	0.50	28	H	300 °C / 77d	η, T4, (Sn)	Liq, η, T4	(Sn)		
0.30	0.20	0.50	28	H	400 °C / 9d	T3, η, (Sn), ε*	Liq, ε, T3	(Sn), η		
0.27	0.43	0.30	29	-	400 °C / 70d	T4, T1	T1, T4			No isopleth
0.27	0.43	0.30	29	-	650 °C / 3d	T1, T4, η, (Sn)*	Liq, T1	(Sn)*, η, T4		No isopleth
0.27	0.50	0.23	30	-	400 °C / 42d	T1, T5, (Cu)	(Cu), T1, T5			No isopleth
0.25	0.50	0.25	31	B	400 °C / 35d	T1	T1			
0.25	0.50	0.25	31	B	600 °C / 4d	T1, T6, T4	T1, T6	T4		Composition shifted to Liq + T1 + T6
0.25	0.60	0.15	32	-	400 °C / 56d	(Cu), Li$_{17}$Sn$_4$, T5	(Cu), Li$_{17}$Sn$_4$, T5			No isopleth
0.22	0.56	0.22	33	B	400 °C / 54d	T5, T1, (Cu)	(Cu), T1, T5			

0.22	0.56	0.22	33	B	600 °C / 2d	T5, T1, η, (Sn)*, (Cu)*	(Cu), T1, T5		(Sn)*, η	
0.20	0.10	0.70	34	E, I	300 °C / 100d	(Sn), η, T4	Liq, η, T4	(Sn)		
0.20	0.10	0.70	34	E, I	400 °C / 27d	(Sn), η, T4	Liq	(Sn), η, T4		
0.20	0.20	0.60	35	A, H, I	300 °C / 100d	T4, η, (Sn)	Liq, η, T4	(Sn)		
0.20	0.20	0.60	35	A, H, I	400 °C / 27d	T3, T4, η, (Sn), ε*	Liq, ε, T3	(Sn), η, T4		
0.20	0.30	0.50	36	I	300 °C / 105d	T4, η, (Sn)	Liq, η, T4	(Sn)		
0.20	0.30	0.50	36	I	400 °C / 70d	T4, T3, η*, (Sn)*	Liq, T3, T4	(Sn)*, η*		
0.20	0.30	0.50	36	I	500 °C / 65d	T4, (Sn), η	Liq, T4	(Sn), η		
0.20	0.40	0.40	37	C, I	300 °C / 77d	T4, η, (Sn)	Liq, T4	(Sn), η		
0.20	0.40	0.40	37	C, I	400 °C / 70d	T4, η, (Sn)	Liq, T4	(Sn), η		
0.20	0.40	0.40	37	C, I	500 °C / 77d	T4, η, (Sn)	Liq, T4	(Sn), η		
0.20	0.53	0.27	38	I	400 °C / 65d	T6, T1	T6, T7, T8			Composition shifted to T1 + T6
0.20	0.53	0.27	38	-	650 °C / 5d	T6, T1	T6, T7		Phase field shifted to T1 + T6	
0.20	0.55	0.25	39	I	400 °C / 27d	T1, T6, η, (Sn)*	T1, T6, T7	(Sn)*, η		Composition shifted to Liq + T1 + T6

0.20	0.55	0.25	39	I	600 °C / 3d	T1, T6, η, (Sn)*	T1, T6, T7	(Sn)*, η		Composition shifted to Liq + T1 + T6
0.20	0.60	0.20	40	B, G, I	400 °C / 27d	T5, (Cu)	T5, (Cu)			
0.20	0.70	0.10	41	D, I	400 °C / 9d	$Li_{17}Sn_4$, (Cu), (Li)	Liq, (Cu), $Li_{17}Sn_4$	(Li)		
0.20	0.70	0.10	41	D, I	600 °C / 2d	(Li), $Li_{17}Sn_4$, (Cu)	Liq, (Cu), $Li_{17}Sn_4$	(Li)		
0.18	0.55	0.27	42	-	400 °C / 65d	T1, T6, $Li_{13}Sn_5$*, (Sn)*	$Li_{13}Sn_5$, T6, T8		(Sn)*	No isopleth, composition shifted to $Li_{13}Sn_5$ + T1 + T6
0.17	0.67	0.17	43	B	400 °C / 21d	$Li_{17}Sn_4$, (Cu), T5	(Cu), $Li_{17}Sn_4$, T5			
0.15	0.15	0.70	44	A	200 °C / 60d	T4, η, (Sn)	(Sn), η, T4			
0.10	0.10	0.80	45	A, E, F	200 °C / 60d	η, T4, (Sn)	(Sn), η, T4			
0.10	0.20	0.70	46	F, H	300 °C / 100d	T4, (Sn), η	Liq, η, T4	(Sn)		
0.10	0.20	0.70	46	F, H	400 °C / 27d	(Sn), η, T4	Liq	(Sn), η, T4		
0.10	0.30	0.60	47	F	300 °C / 77d	T4, (Sn), Li_2Sn_5, η	Liq, Li_2Sn_5, T4	(Sn), η		
0.10	0.30	0.60	47	F	400 °C / 9d	T4, (Sn), Li_2Sn_5, η	Liq, T4	(Sn), η, Li_2Sn_5		

0.10	0.45	0.45	48	C, F	300 °C / 100d	T4, LiSn, Li_2Sn_5*, η*, (Sn)*	LiSn, Li_2Sn_5, T4		(Sn)*, η*	
0.10	0.45	0.45	48	C, F	400 °C / 27d	T4, η, (Sn), LiSn, Li_2Sn_5*, Li_7Sn_3*, T1*	Liq, LiSn, T4	(Sn), η, Li_2Sn_5*, Li_7Sn_3*, T1*		
0.10	0.45	0.45	48	C, F	500 °C / 100d	T4, LiSn, eta*, Li_2Sn_5*, (Sn)*	Liq, Li_7Sn_3, T6	LiSn, eta*, Li_2Sn_5*, (Sn)*		Composition shifted to Liq + T4
0.10	0.50	0.40	49	F	400 °C / 9d	T1, LiSn, (Sn), η, Li_7Sn_3	LiSn, Li_7Sn_3, T1	(Sn), η		(Sn), η from quenched liquid (minor amount)
0.10	0.50	0.40	49	F	500 °C / 22d	T4, (Sn), Li_7Sn_3, T6*	Liq, Li_7Sn_3, T6	(Sn), T4		
0.10	0.60	0.30	50	F	400 °C / 65d	T1, Li_7Sn_3, $Li_{13}Sn_5$, (Sn)*	Li_7Sn_3, T1	(Sn)*, $Li_{13}Sn_5$		(Sn)*, $Li_{13}Sn_5$ from quenched liquid (minor amount)
0.10	0.60	0.30	50	F	600 °C / 5d	Li_7Sn_3, T1, T4	Liq, Li_5Sn_2, T6	Li_7Sn_3, T4		Composition shifted to Liq + T1
0.10	0.62	0.28	51	F	400 °C / 21d	$Li_{13}Sn_5$, T1, Li_5Sn_2	Li_5Sn_2, $Li_{13}Sn_5$, T1			

0.10	0.62	0.28	51	-	650 °C / 3h	T1, Li$_{13}$Sn$_5$, (Sn)*	Liq, Li$_{13}$Sn$_5$, T8		(Sn)*	Phase field shifted to T1 + Li$_{13}$Sn$_5$
0.10	0.63	0.27	52	F	400 °C / 7d	T6, Li$_{13}$Sn$_5$	Li$_{13}$Sn$_5$, T6, T8			Composition shifted to Li$_{13}$Sn$_5$ + T6 + T8
0.10	0.65	0.25	53	F	400 °C / 34d	T6, T1, Li$_{13}$Sn$_5$*, (Sn)*	Li$_{13}$Sn$_5$, T6, T8	(Sn)*, T1		Composition shifted to Li$_{13}$Sn$_5$ + T1 + T6
0.10	0.65	0.25	53	F	600 °C / 2d	T6, T4, T1, (Sn)*	Li$_{13}$Sn$_5$, T6, T8	(Sn)*, T1, T4		Composition shifted to Liq + T1 + T6
0.10	0.66	0.24	54	F	400 °C / 21d	T6, T1, T8, (Sn)*	Li$_{13}$Sn$_5$, T8			Composition shifted to Li$_{13}$Sn$_5$ + T8
0.10	0.66	0.24	54	F	600 °C / 2d	T6, T1, T8, (Sn)*	Li$_7$Sn$_2$, Li$_{13}$Sn$_5$, T8			Composition shifted to Li$_7$Sn$_2$ + Li$_{13}$Sn$_5$ + T8

0.10	0.70	0.20	55	G, F	400 °C / 9d	(Sn), T7	Li_7Sn_2, $Li_{17}Sn_4$, T5			Composition shifted to Li_7Sn_2 + $Li_{17}Sn_4$ + T5
0.10	0.70	0.20	55	-	650 °C / 4d	T1, T5, T4, (Sn)*	$Li_{17}Sn_4$, T5	T4, (Sn)*		Phase field shifted to Liq + T1 + T5
0.10	0.80	0.10	56	B, D, F	400 °C / 9d	$Li_{17}Sn_4$, (Cu)	Liq, (Cu), $Li_{17}Sn_4$	(Li)		(Li) hardly visible in XRD
0.10	0.80	0.10	56	B, D, F	600 °C / 2d	$Li_{17}Sn_4$, (Cu)	Liq, (Cu), $Li_{17}Sn_4$	(Li)		(Li) hardly visible in XRD
0.05	0.05	0.90	57	A	200 °C / 60d	(Sn), η	(Sn), η, T4			Very low amount of T4
0.05	0.72	0.23	58	-	400 °C / 21d	Li_7Sn_2, $Li_{17}Sn_4$, T1	Li_7Sn_2, T7	T1, T4*, T5		No isopleth, composition shifted to Li_7Sn_2 + $Li_{17}Sn_4$ + T1
0.05	0.75	0.20	59	G	400 °C / 14d	T5, $Li_{17}Sn_4$	$Li_{17}Sn_4$, T5			
0.02	0.49	0.49	60	C	300 °C / 91d	LiSn, T4, Li_2Sn_5, (Sn)*	LiSn, Li_2Sn_5, T4		(Sn)*	
0.02	0.49	0.49	60	C	400 °C / 65d	LiSn, Li_2Sn_5, (Sn), η*, T4*	Liq, LiSn, T4	(Sn), η*, Li_2Sn_5		

Table 2: DTA results of all samples

Thermal effects, which could not directly be considered in isopleths, are in *italic letters*.

x(Cu)	x(Li)	x(Sn)	Sample No.	Shown in isopleth	Heat Treatment [°C]	Thermal effects during heating [°C]	Liq. [°C]
0.80	0.10	0.10	1	C, D, E	27d / 400 °C	745; 747	891
0.78	0.02	0.20	2	G	65d / 400 °C	*534*; 734	741
0.70	0.10	0.20	3	E, G	9d / 400 °C	686; 735; 747	751
0.70	0.20	0.10	4	D, H	27d / 400 °C	725; 738	*
0.65	0.10	0.25	5	E	27d / 400 °C	442; *508; 541; 663; 674;* 730	743
0.60	0.10	0.30	6	E	70d / 400 °C	*209; 325;* 349; 445; *505;* 634; 687	714
0.60	0.20	0.20	7	C, G, H	21d / 400 °C	744	*
0.60	0.30	0.10	8	D	9d / 400 °C	447; 729	*
0.57	0.16	0.27	9	-	65d / 400 °C	215; 436; 738	752
0.55	0.25	0.20	10	G	70d / 400 °C	745	*
0.54	0.20	0.26	11	H	21d / 400 °C	456; 754	763
0.52	0.20	0.28	12	H	21d / 400 °C	*422;* 444; 720	752
0.51	0.10	0.40	13	E	21d / 400 °C	*211; 328;* 349; 447; *504;* 524	645
0.50	0.18	0.33	14	-	70d / 400 °C	211; 326; 446; 455; 653	710
0.50	0.25	0.25	15	C	35d / 400 °C	*531;* 763	774
0.47	0.25	0.28	16	-	21d / 400 °C	457; 549; 727	753
0.46	0.23	0.31	17	-	70d / 400 °C	210; 423; 461; 485; 588; 683	735
0.45	0.10	0.45	18	B, E	27d / 400 °C	216; 332; 346; *527*	582
0.45	0.45	0.10	19	A, D	27d / 400 °C	727; 812	828
0.43	0.43	0.15	20	A	27d / 400 °C	730; 804	833
0.40	0.20	0.40	21	B, H	27d / 400 °C	*219;* 338; 451; 460;	651
0.40	0.40	0.20	22	A, G	56d / 400 °C	*523;* 720; 730	*
0.40	0.50	0.10	23	D	9d / 400 °C	*629; 668; 693;* 827	837
0.38	0.30	0.32	24	-	42d / 400 °C	426; 463; 474; 550; 694	722
0.36	0.36	0.29	25	A	21d / 400 °C	594; *740*	757
0.35	0.40	0.25	26	-	70d / 400 °C	759	770
0.33	0.33	0.33	27	A, B, C	70d / 400 °C	459; *552;* 570; 670	719

0.30	0.20	0.50	28	H	9d / 400 °C	187; 336; 348; 454; 485	538
0.27	0.43	0.30	29	-	70d / 400 °C	599; 709	746
0.27	0.50	0.23	30	-	42d / 400 °C	-	-
0.25	0.50	0.25	31	B	35d / 400 °C	*529*; 690; 721	750
0.25	0.60	0.15	32	-	56d / 400 °C	709; 713; 788	813
0.22	0.56	0.22	33	B	54d / 400 °C	*469*; 717	729
0.20	0.10	0.70	34	E, I	27d / 400 °C	216; ~318; ~370	~380
0.20	0.20	0.60	35	A, H, I	27d / 400 °C	218; 344; 422	450
0.20	0.30	0.50	36	I	70d / 400 °C	212; 330; *431*; 455; 471	530
0.20	0.40	0.40	37	C, I	9d / 400 °C	217; 346; 457; 584; 606	632
0.20	0.53	0.27	38	I	65d / 400 °C	*619*; 660; 707	739
0.20	0.55	0.25	39	I	27d / 400 °C	*520*; 697; 708; 709	736
0.20	0.60	0.20	40	B, G, I	27d / 400 °C	736; 779	782
0.20	0.70	0.10	41	D, I	9d / 400 °C	180; *639; 662; 679*; 687	712
0.18	0.55	0.27	42	-	65d / 400 °C	609; 618; 671; 698	731
0.17	0.67	0.17	43	B	21d / 400 °C	*708*; 732; 837	839
0.15	0.15	0.70	44	A	60d / 400 °C	219	~430
0.10	0.10	0.80	45	A, E, F	60d / 400 °C	221	~350
0.10	0.20	0.70	46	F, H	27d / 400 °C	215; ~380	~390
0.10	0.30	0.60	47	F	9d / 400 °C	218; *299*; 431	471
0.10	0.45	0.45	48	C, F	27d / 400 °C	323; 475; 503; 560	586
0.10	0.50	0.40	49	F	9d / 400 °C	470; 584	599
0.10	0.60	0.30	50	F	65d / 400 °C	507; *589; 596*; 615; 646	678
0.10	0.62	0.28	51	F	21d / 400 °C	618; 645; 681	695
0.10	0.63	0.27	52	F	7d / 400 °C	688	697
0.10	0.65	0.25	53	F	34d / 400 °C	*482*; 690; 700; 709	718
0.10	0.66	0.24	54	F	21d / 400 °C	500; 675; 693; 703; 713	721
0.10	0.70	0.20	55	F, G	9d / 400 °C	*490; 603*; 695; 705; 711	723
0.10	0.80	0.10	56	B, D, F	9d / 400 °C	180; 581; 681	685
0.05	0.05	0.90	57	A	60d / 400 °C	222	~330
0.05	0.72	0.23	58	-	21d / 400 °C	703; 720; 728	752
0.05	0.75	0.20	59	G	14d / 400 °C	718	727
0.02	0.49	0.49	60	C	65d / 400 °C	321; 478	484

*Liquidus temperature was not reached

Table 3: Invariant ternary reactions: Temperatures and reactions in dotted and italic lines are approximated

Temperature [°C]	Reaction	Type / No.	Reaction shown in Isopleth…								
			A	B	C	D	E	F	G	H	I
180	Liq → (Cu) + (Li) + $Li_{17}Sn_4$	E1	x	x		x		x		x	x
187	*η + T4 → (Sn) + η´*	*U1*	*x*	*x*	*x*		*x*	*x*		*x*	*x*
188	*η + T3 → η´ + T4*	*U2*	*x*	*x*	*x*		*x*			*x*	
189	*ε + η → η´ + T3*	*U3*					*x*			*x*	
218	Liq → (Sn) + η + T4	E2	x	x	x		x	x		x	x
220	Liq + Li_2Sn_5 + T4 → (Sn)	P1	x		x		x	x		x	x
321	Liq + LiSn → Li_2Sn_5 + T4	U4		x				x			x
328	Liq + T3 → η + T4	U5	x	x	x		x			x	x
345	*δ → (Cu) + ε + T2*	*E3*				*x*	*x*		*x*		
348	Liq + ε → η + T3	U6	x	x			x			x	x
430	*Li_7Sn_3 + T4 → LiSn + T1*	*U7*						*x*			*x*
440	*Li_5Sn_2 + T6 → $Li_{13}Sn_5$ + T1*	*U8*						*x*			*x*
445	Liq + T2 → ε + T3	U9		x			x			x	
450	*Li_7Sn_3 + T6 → Li_5Sn_2 + T1*	*U10*						*x*			*x*
458	Liq + T2 + T4 → T3	P2	x	x	x					x	x
460	*T4 + T6 → Li_7Sn_3 + T1*	*U11*						*x*			*x*
470	Liq + Li_7Sn_3 → LiSn + T4	U12		x			x				x
476	Liq + T6 → Li_7Sn_3 + T4	U13		x			x				x
503	Liq + Li_5Sn_2 → Li_7Sn_3 + T6	U14		x			x				x
508	γ → (Cu) + δ + T2	E4				x	x		x		
520	Liq + T1 → T4 + T6	U15		x	x						x
540	β → (Cu) + γ + T2	E5				x	x				
580	*ζ → δ + ε + T2*	*E6*					*x*				
585	Liq + T1 + T2 → T4	P3	x	x	x						x
602	*γ + ζ → δ + T2*	*U16*						*x*	*x*		
616	Liq + $Li_{13}Sn_5$ → Li_5Sn_2 + T6	U17						x			x
630	*γ + ε → ζ + T2*	*U18*					*x*		*x*		

634	Liq + γ → ε + T2	U19					x		x		
645	Liq + T8 → Li$_{13}$Sn$_5$ + T6	U20						x			x
659	T5 + T6 → T1 + T7	U21									x
670	Liq + (Cu) → T1 + T2	U22	x	x	x	x	x		x	x	
674	Liq + Li$_7$Sn$_2$ → Li$_{13}$Sn$_5$ + T8	U23						x			
680	*Liq + T7 → T6 + T8*	*U24*									*x*
685	*Liq + T5 → T6 + T7*	*U25*									*x*
685	Liq + β → γ + T2	U26					x		x		
689	Liq + T1 + T5 → T6	P4		x							x
690	Liq + Li$_7$Sn$_2$ + T7 → T8	P5						x			x
693	Liq + Li$_7$Sn$_2$ + T5 → T7	P6						x			x
703	Liq + Li$_{17}$Sn$_4$ → Li$_7$Sn$_2$ + T5	U27						x	x		x
720	Liq + (Cu) + T5 → T1	P7	x	x		x	x		x	x	
732	Liq + (Cu) + Li$_{17}$Sn$_4$ → T5	P8	x	x		x		x	x	x	x
745	Liq + (Cu) + β → T2	P9			x	x	x		x	x	
700-800	*Liq´ → Liq´´ + (Cu) + Li$_{17}$Sn$_4$*	*Em1*									
753-800	*Liq´ → Liq´´ + Li$_7$Sn$_2$ + Li$_{17}$Sn$_4$*	*Em2*									

Table 4: Invariant reactions of the binary subsystems

	Invariant reactions	Reaction type	Temperature [°C]	Ref.
Unary phases	Liq → (βLi)	c1	180.6	[22]
	Liq → (βSn)	c2	231.9681	[22]
	Liq → (Cu)	c3	1084.87	[23]
Cu-Li	Liq → (Cu) + (Li)	e1	180.5	[10]
Cu-Sn	η → (Sn) + η´	e2	186	[23]
	ε + η → η´	p1	189.1	[23]
	Liq → (Sn) + η	e3	227	[23]
	δ → (Cu) + ε	e4	350	[23]
	Liq + ε → η	p2	408	[8]
	γ → (Cu) + δ	e5	518	[8]
	ζ → δ + ε	e7	589	[8]
	β → (Cu) + γ	e6	566	[8]
	γ + ζ → δ	p3	603	[8]
	γ + ε → ζ	p4	641	[8]
	γ → Liq + ε	e8	649	[8]
	ε → γ	c4	676	[23]
	Liq + β → γ	p5	758	[8]
	Liq + (Cu) → β	p6	798	[8]
Li-Sn	Liq → (βLi) + Li$_{17}$Sn$_4$	e9	180.6	[22]
	Liq → Li$_2$Sn$_5$ + (βSn)	e10	214	[22]
	Liq + LiSn → Li$_2$Sn$_5$	p7	327	[9]
	Liq → LiSn	c5	486	[9]
	Liq → Li$_7$Sn$_3$ + LiSn	e11	473	[9]
	Liq + Li$_5$Sn$_2$ → Li$_7$Sn$_3$	p8	509	[9]
	Liq + Li$_{13}$Sn$_5$ → Li$_5$Sn$_2$	p9	698	[9]
	Liq + Li$_7$Sn$_2$ → Li$_{13}$Sn$_5$	p10	724	[9]
	Liq → Li$_{17}$Sn$_4$ + Li$_7$Sn$_2$	e12	752	[9]
	Liq → Li$_{17}$Sn$_4$	c6	758	[9]
	Liq → Li$_7$Sn$_2$	c7	779	[9]

Table 5: Three-phase equilibria in Cu-Li-Sn directly derived from experiments

Phases in three-phase field	Corresponding samples at annealing temperatures				
	300 °C	**400 °C**	**500 °C**	**600 °C**	**Other Temp.**
Liq´ + (Cu) + Li$_{17}$Sn$_4$	x	23, 41, 56	x	41, 56	23 (650 / 750 °C)
Liq´´ + (Cu) + Li$_{17}$Sn$_4$					
Liq + β + T2					3, 5 (700 °C)
Liq + ε + T2			3, 13, 14	6	
Liq + ε + T3		6, 13, 14, 18, 21, 28, 35			
Liq + ε + η		x			
Liq + η + T4	18, 28, 34, 35, 36, 46				
Liq + Li$_{13}$Sn$_5$ + T8					51 (650 °C)
Liq + Li$_2$Sn$_5$ + T4	47				
Liq + Li$_5$Sn$_2$ + T6				50	
Liq + Li$_7$Sn$_3$ + T6			48, 49		
Liq + LiSn + T4		48, 60			
Liq + T1 + T2				27	25 (650 °C)
Liq + T1+ T6				x	
Liq + T2 + T4			24, 27, 36		
Liq + T3 + T4		36			
(Cu) + δ + T2		2, 3	x		
(Cu) + Li$_{17}$Sn$_4$ + T5	x	32, 43	x	x	
(Cu) + T1 + T2	x	1, 10	x	x	
(Cu) + T1 + T5	x	8, 20, 30, 33	x	x	
(Sn) + η + T4					44, 45, 57 (200 °C)
γ + δ + T2				2	
δ + ζ + T2				x	
ε + ζ + T2				5	
ε + η + T3	6, 13, 14				
ε + T2 + T3	x	5, 9, 12			
η + T3 + T4	21				
Li$_{13}$Sn$_5$ + T1 + T6		51			
Li$_{13}$Sn$_5$ + T6 + T8		52, 53		53	
Li$_5$Sn$_2$ + Li$_{13}$Sn$_5$ + T1	x	x			
Li$_5$Sn$_2$ + Li$_7$Sn$_3$ + T1	x	x			
Li$_7$Sn$_2$ + Li$_{13}$Sn$_5$ + T8		54		54	
Li$_7$Sn$_2$ + Li$_{17}$Sn$_4$ + T5	x	x	x	x	
LiSn + Li$_2$Sn$_5$ + T4	48, 60				
LiSn + Li$_7$Sn$_3$ + T1	x	49			

LiSn + T1 + T4	x	x			
T1 + T2 + T4	x	25	x		
T1 + T5 + T7				x	
T1 + T6 + T7	x	39		39	
T2 + T3 + T4	x	16, 24, 27			
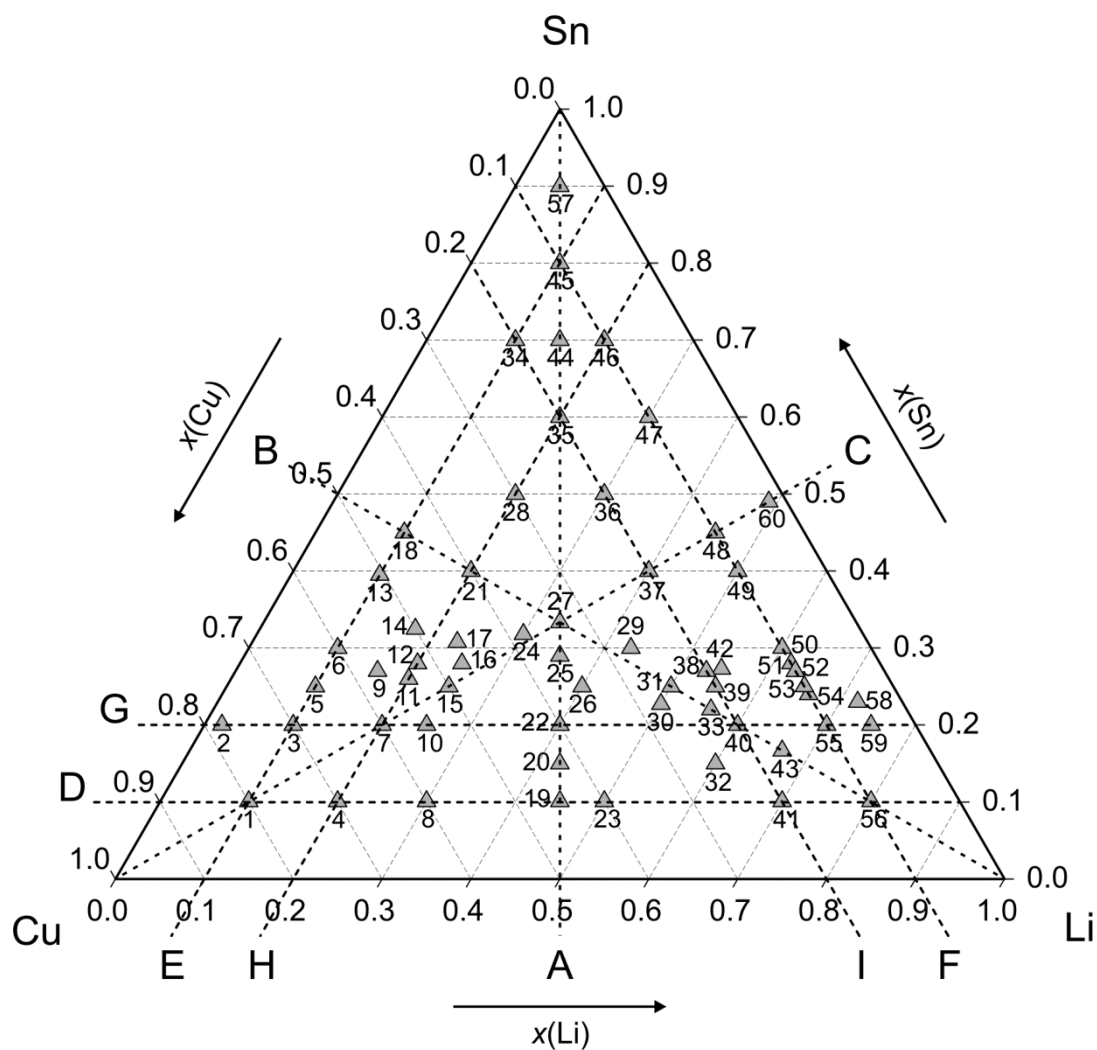
Fig. 1: Sample compositions and isopleth sections (A: $x_{Cu} : x_{Li} = 0.5$; B: $x_{Cu} : x_{Sn} = 0.5$; C: $x_{Li} : x_{Sn} = 0.5$; D: $x_{Sn} = 0.1$; E: $x_{Li} = 0.1$; F: $x_{Cu} = 0.1$; G: $x_{Sn} = 0.2$; H: $x_{Li} = 0.2$; I: $x_{Cu} = 0.2$)

Fig. 2: Isopleth A
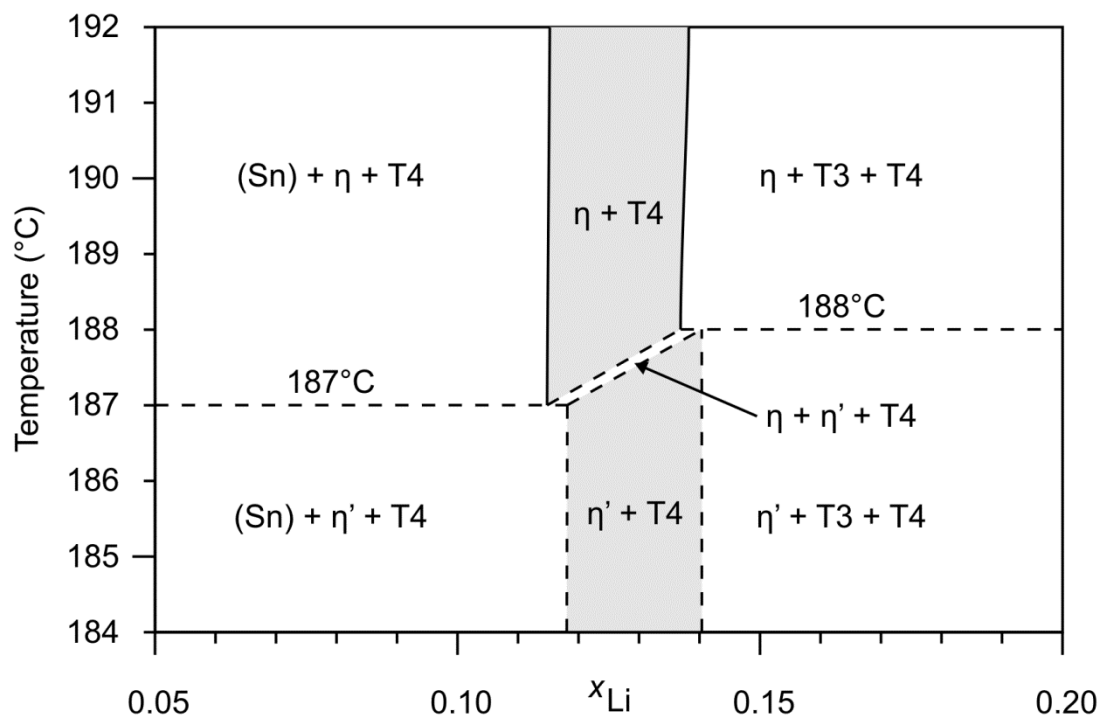
Fig. 3: Isopleth B

Fig. 3a: Isopleth B section from x_{Li} = 0.05 - 0.20 / T = 184 - 192 °C
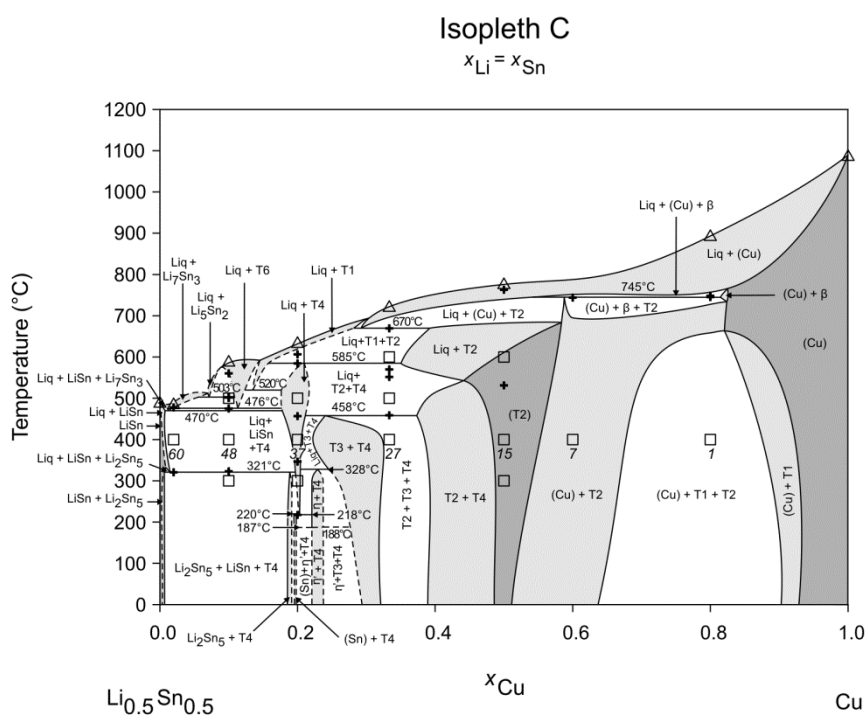
Fig. 4: Isopleth C
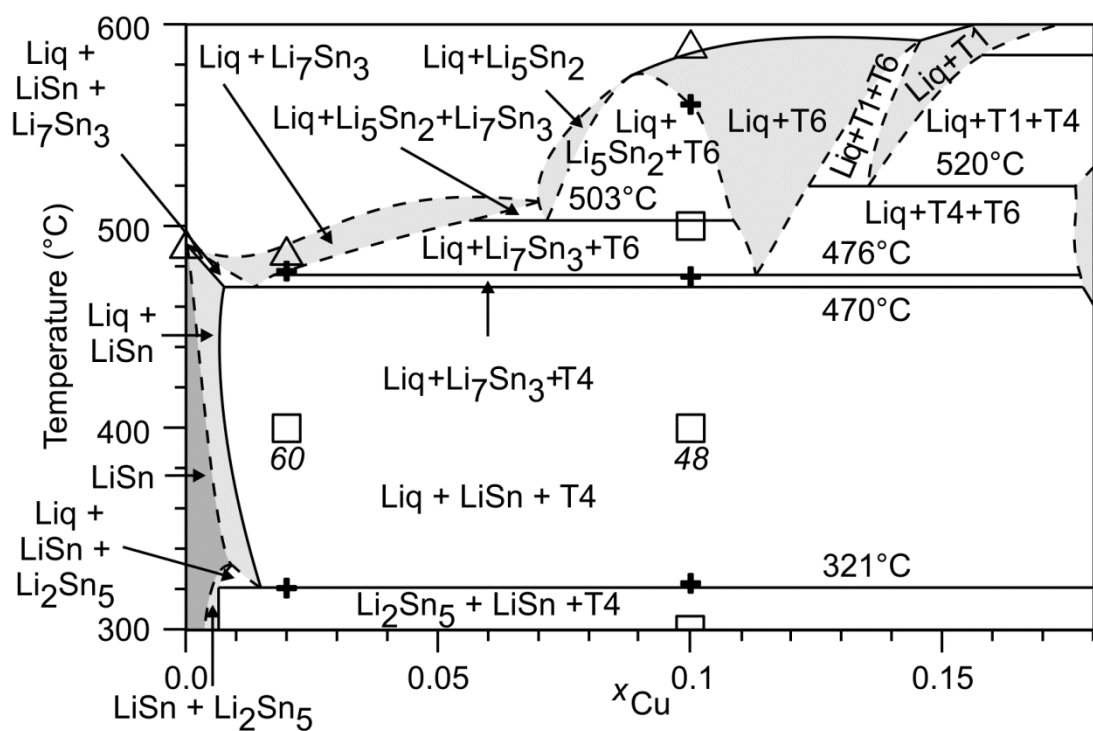
Fig. 4a: Isopleth C section I: x_{Cu} = 0 - 0.18 / T = 300 - 600 °C
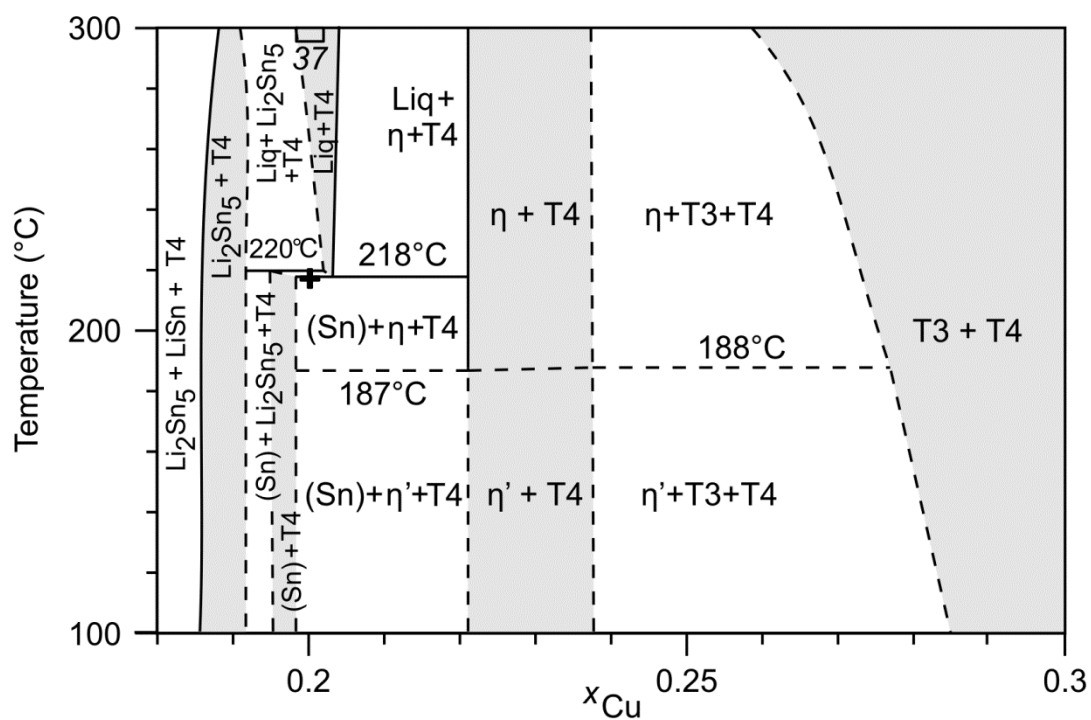
Fig. 4b: Isopleth C section II: x_{Cu} = 0.18 - 0.30 / T = 100 - 300 °C

184
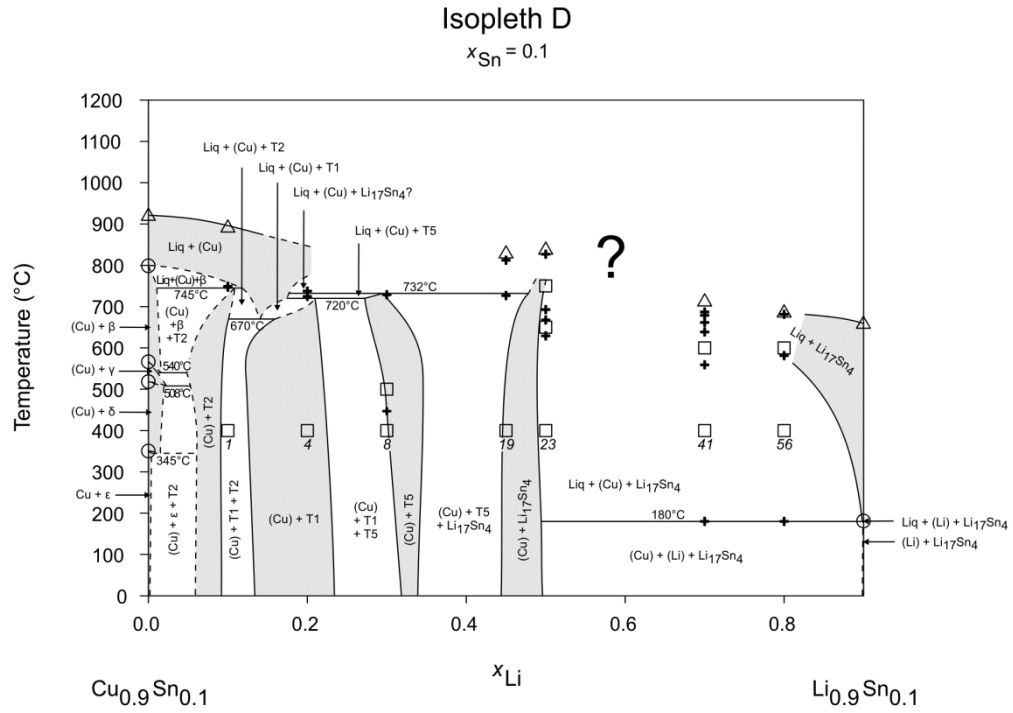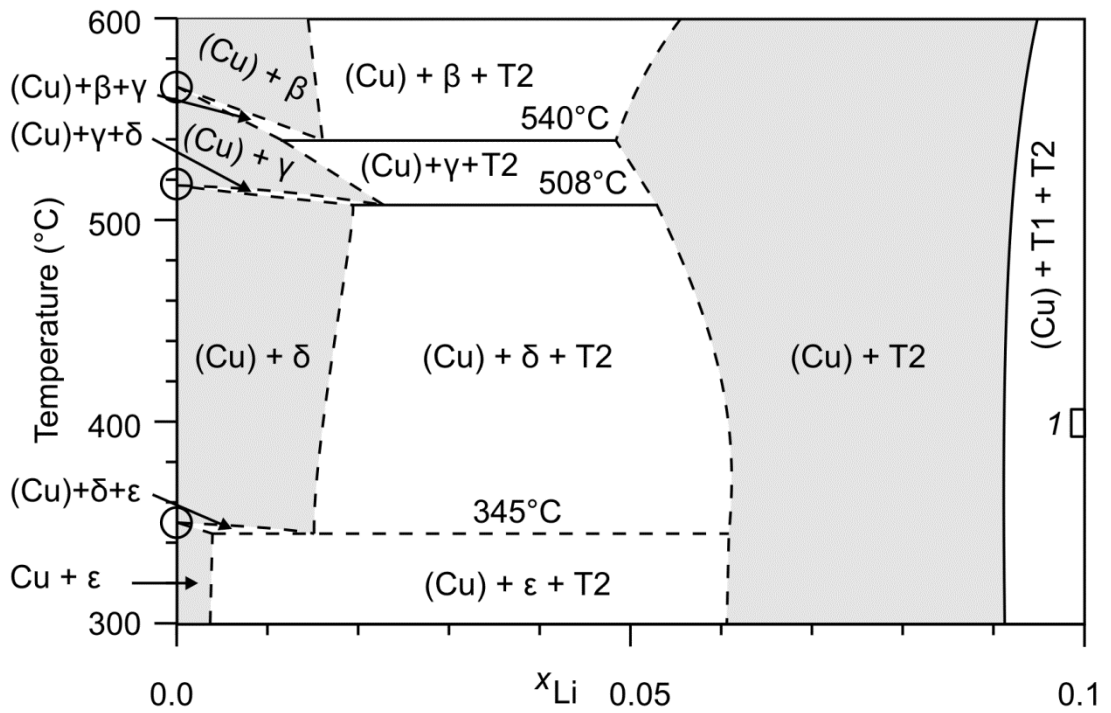
Fig. 5: Isopleth D

Fig. 5a: Isopleth D section from x_{Li} = 0 - 0.10 / T = 300 - 600 °C
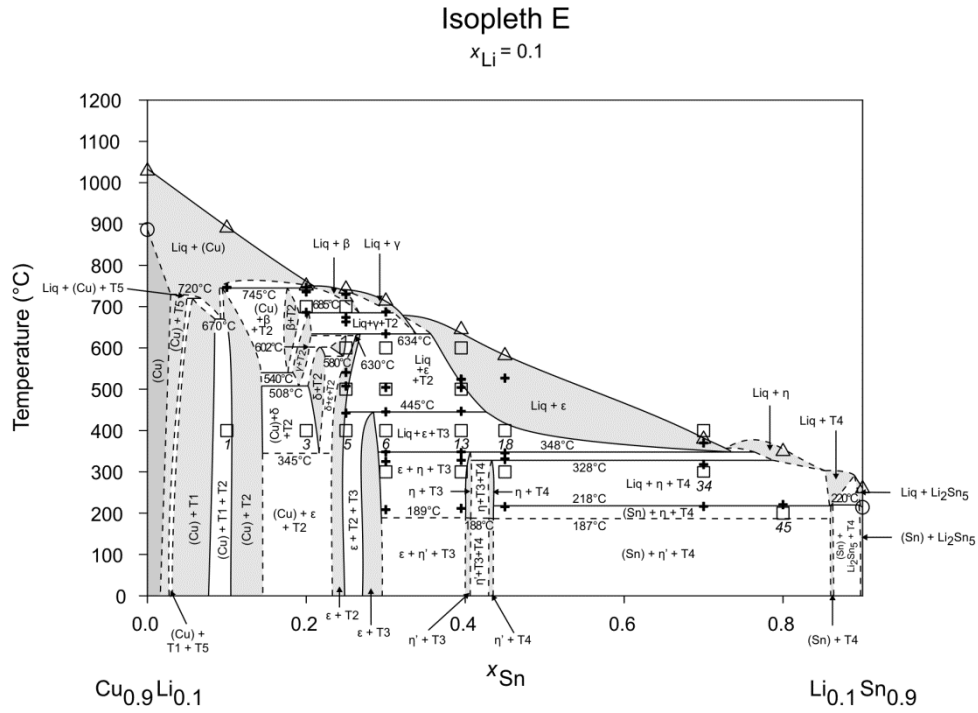
Fig. 6: Isopleth E
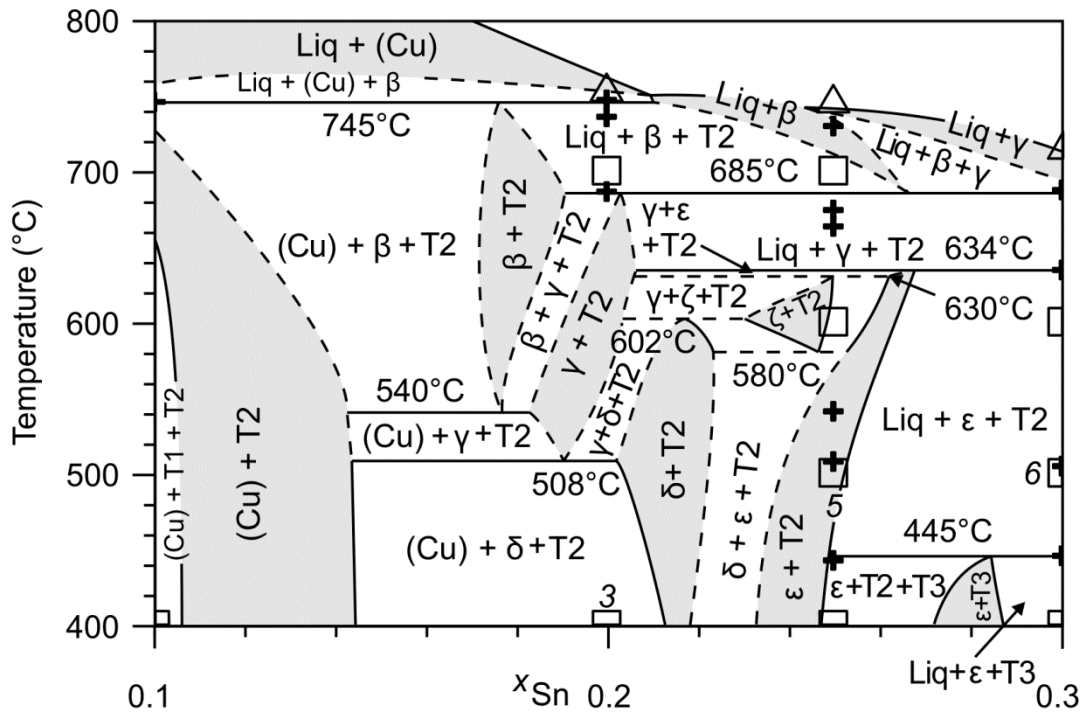
Fig. 6a: Isopleth E section from x_{Sn} = 0.10 - 0.30 / T = 400 - 800 °C

Fig. 7: Isopleth F

Fig. 7a: Isopleth F section from x_{Sn} = 0.20 - 0.40 / T = 400 - 800 °C
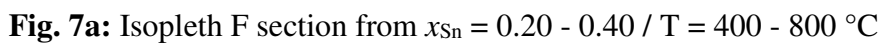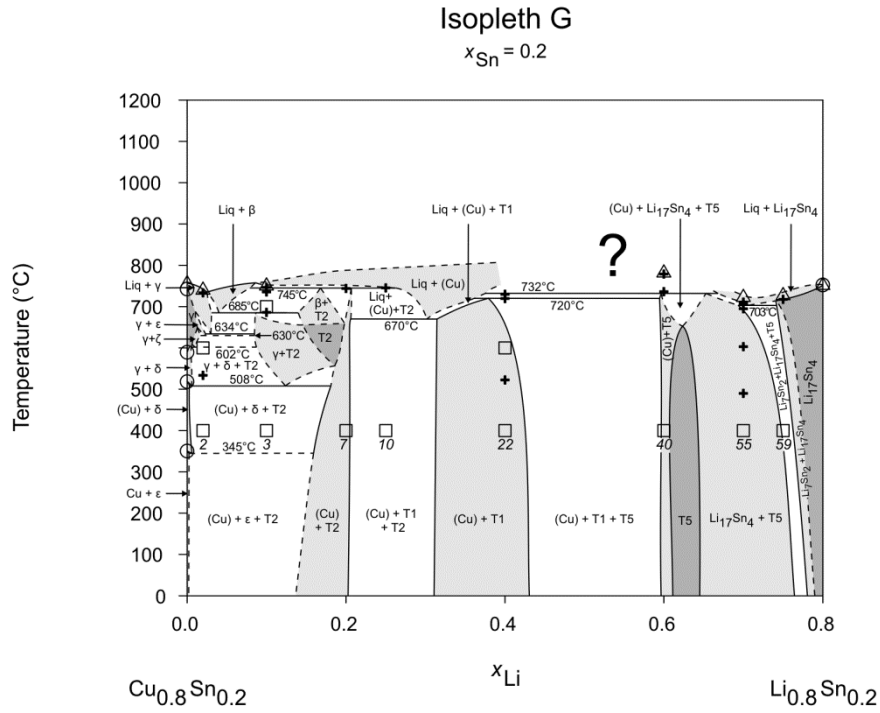
Fig. 8: Isopleth G
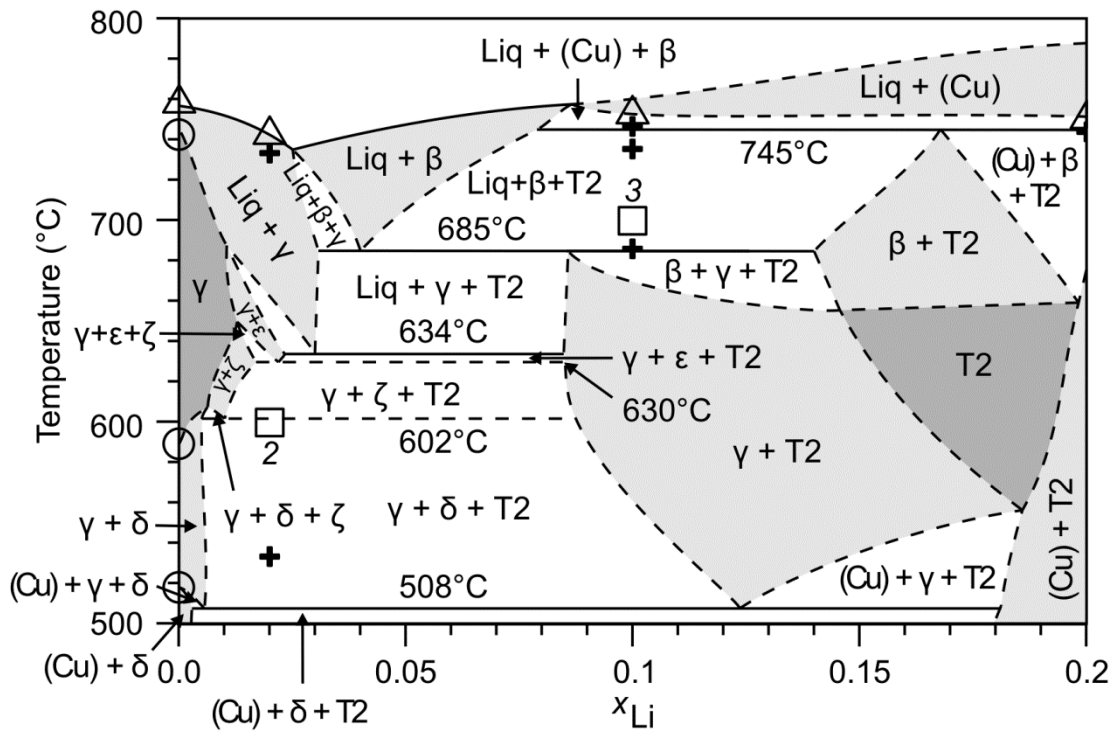
Fig. 8a: Isopleth G section from x_{Li} = 0 - 0.20 / T = 500 - 800 °C
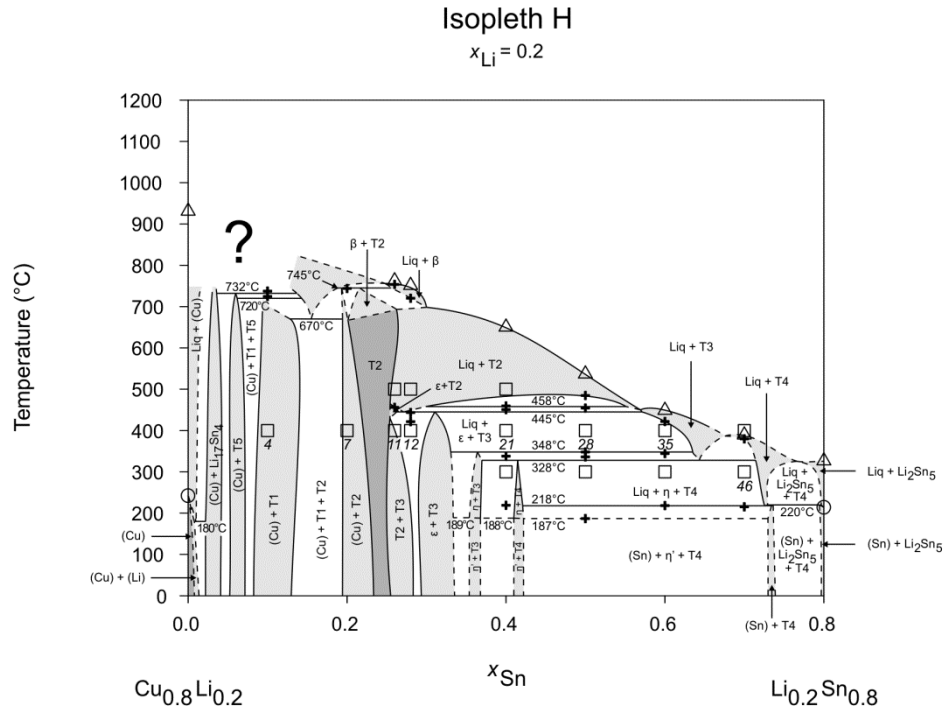
Fig. 9: Isopleth H
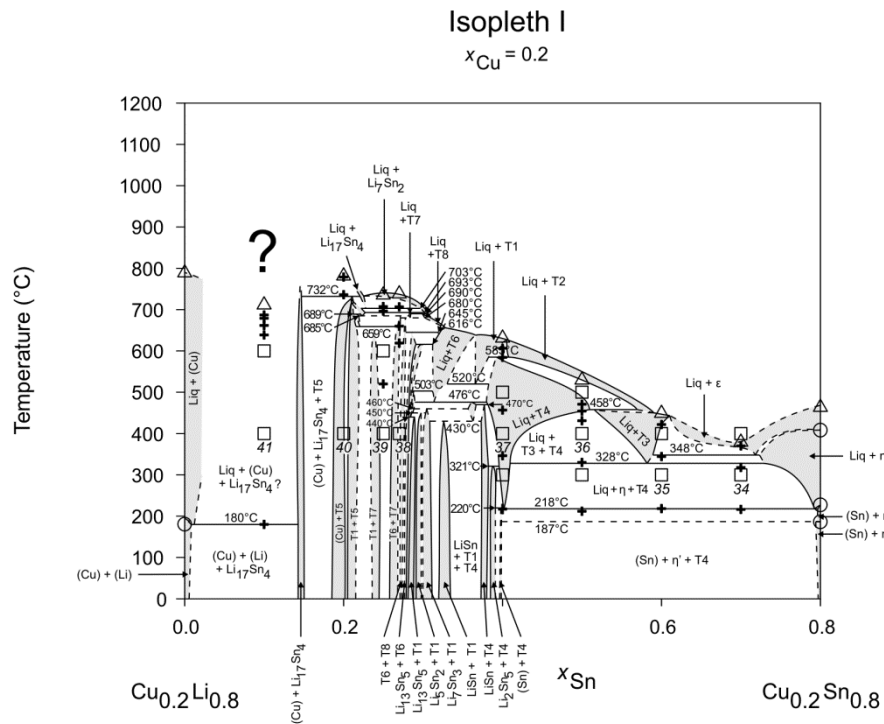
Fig. 10: Isopleth I
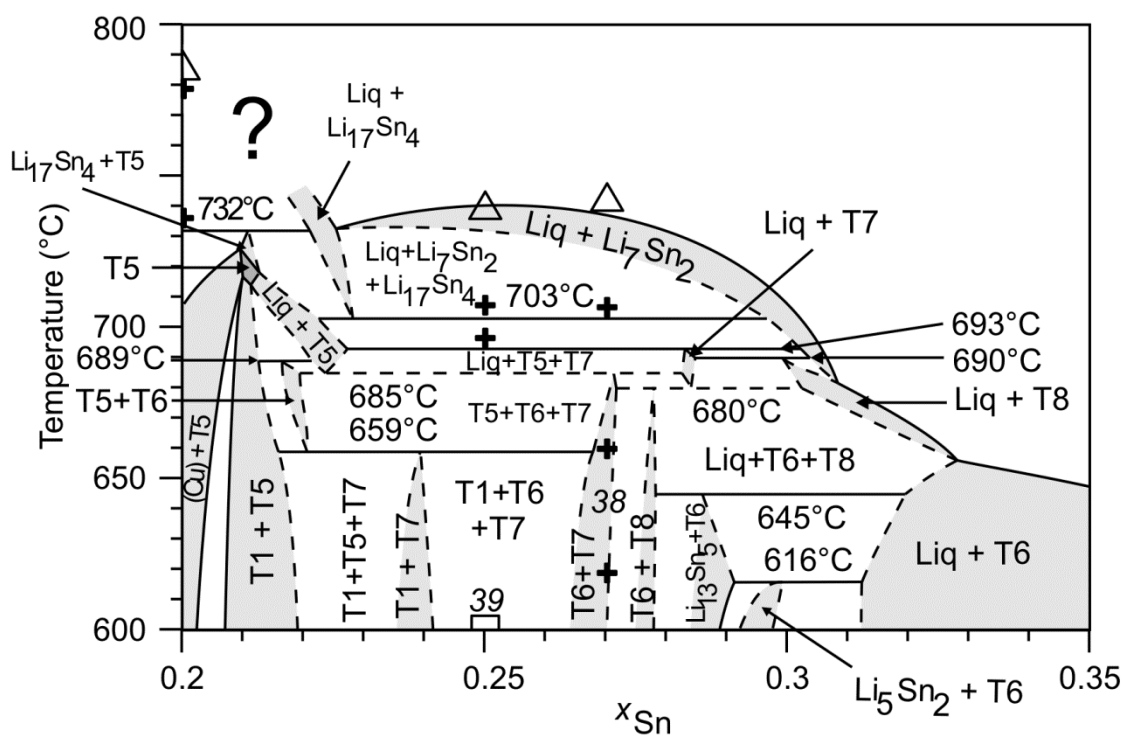
Fig. 10a: Isopleth I section I: x_{Sn} = 0.20 - 0.35 / T = 600 - 800 °C
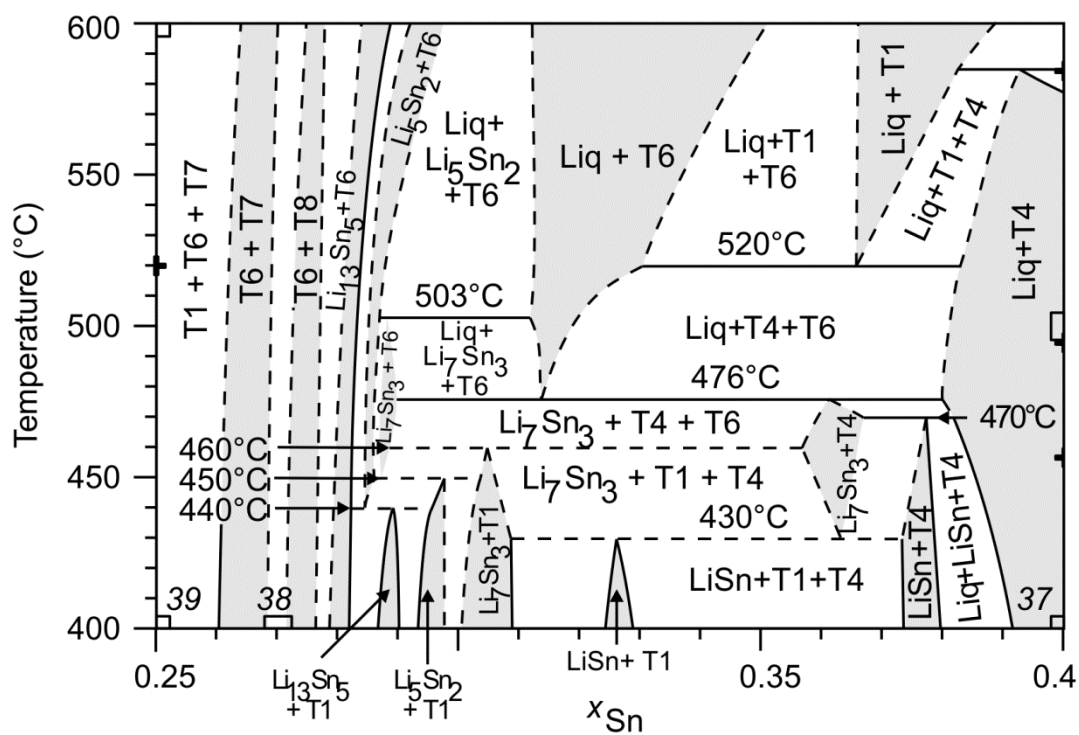
Fig. 10b: Isopleth I section II: x_{Sn} = 0.25 - 0.40 / T = 400 - 600 °C
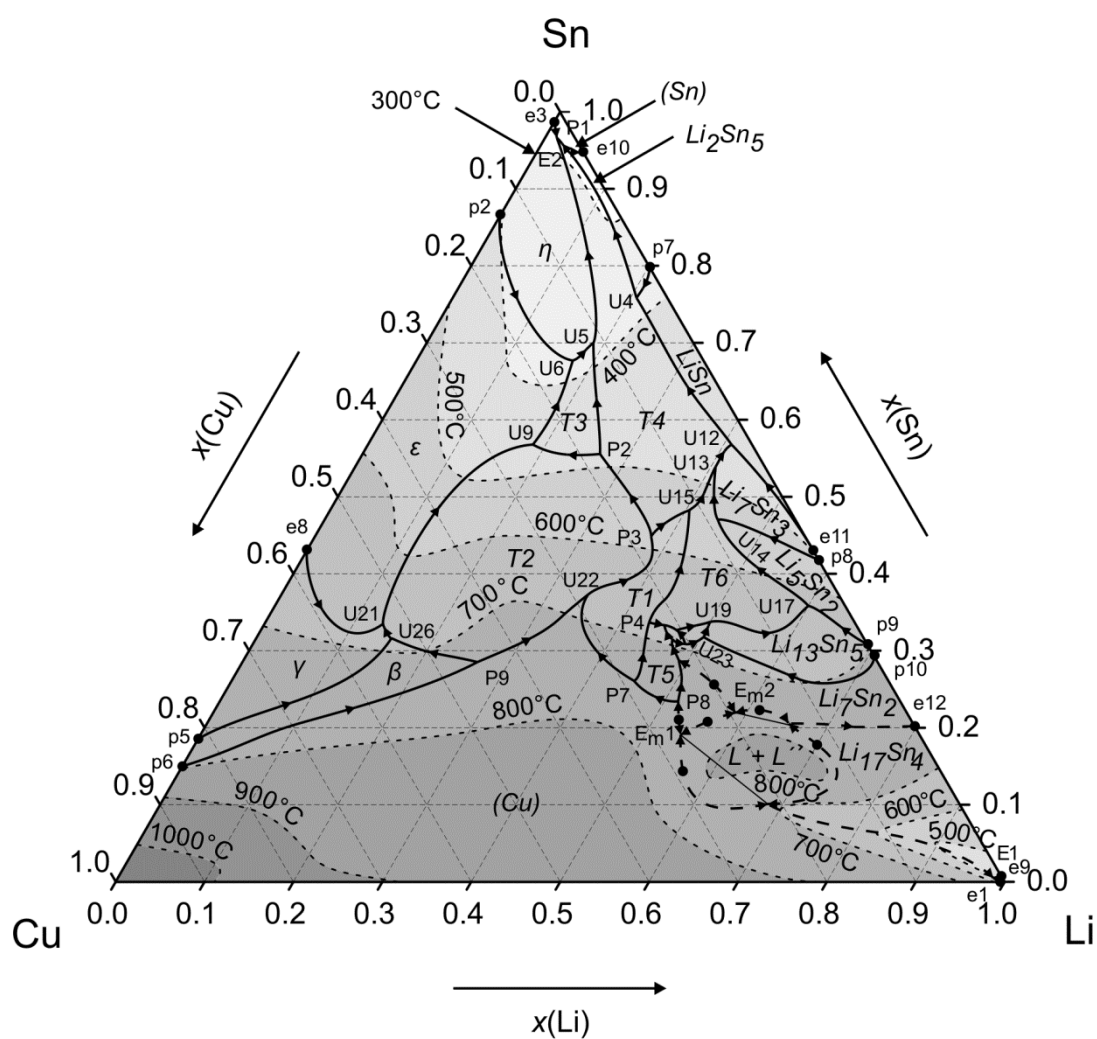
Fig. 11: Liquidus projection
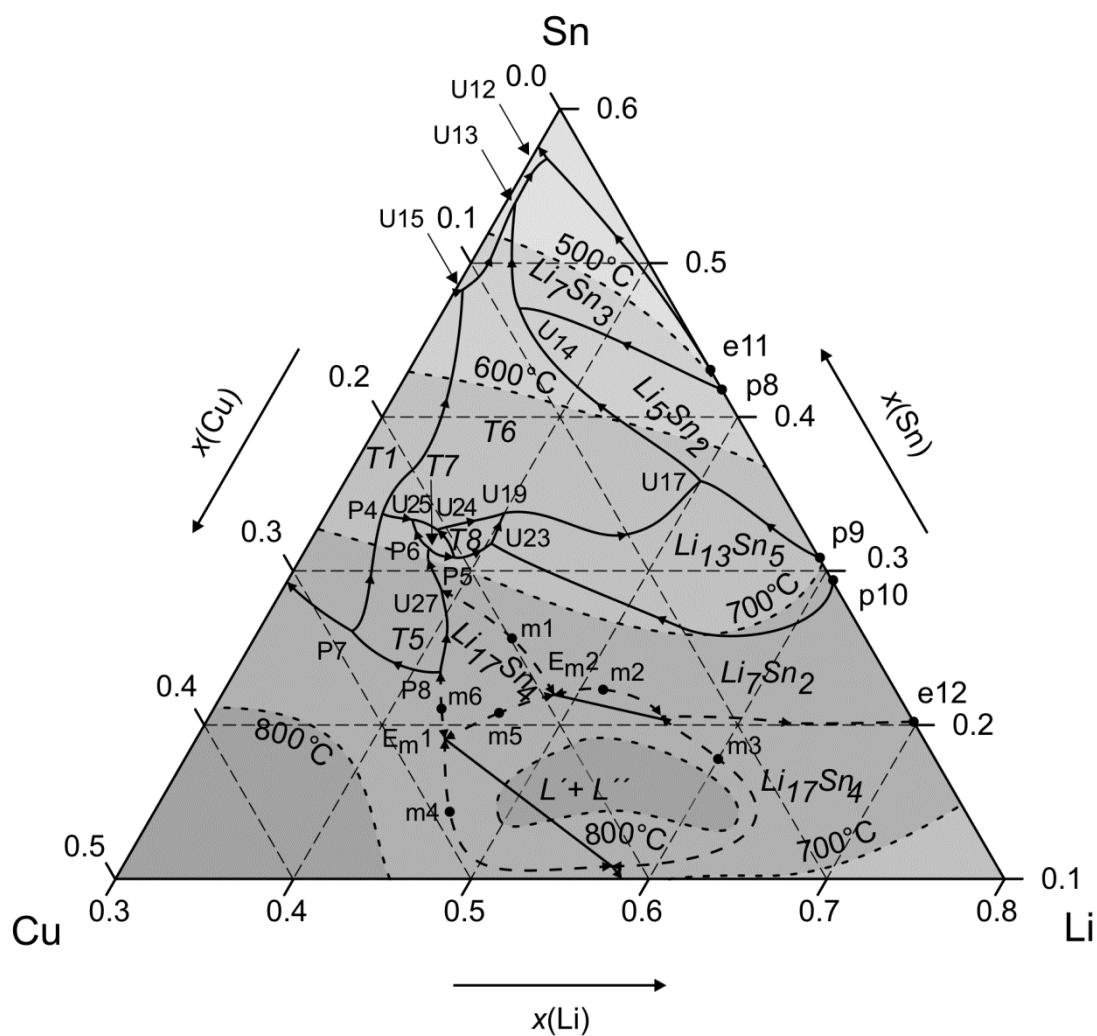
Fig. 11a: Liquidus projection in Li-rich corner
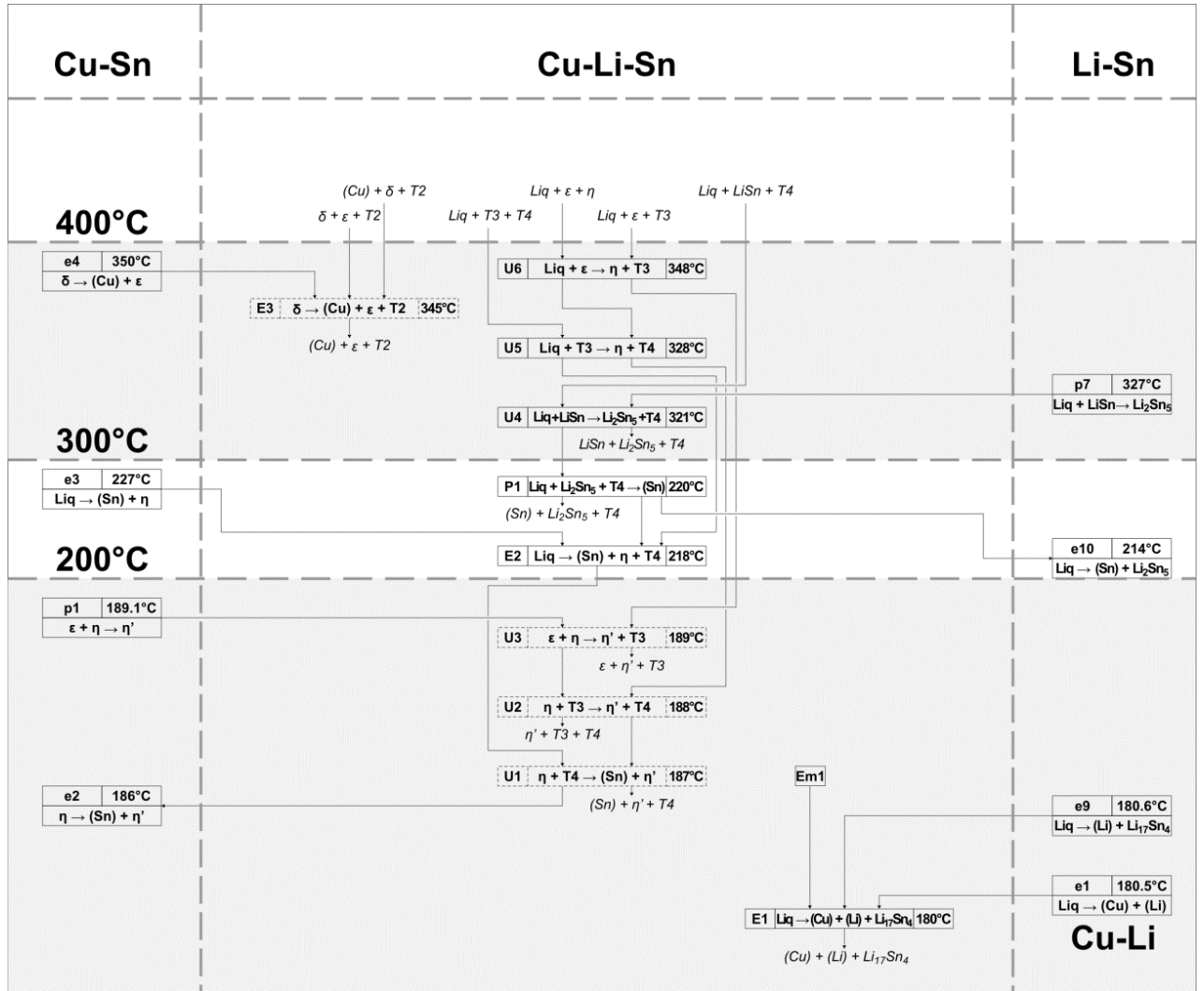
Fig. 12: reaction scheme T < 400 °C
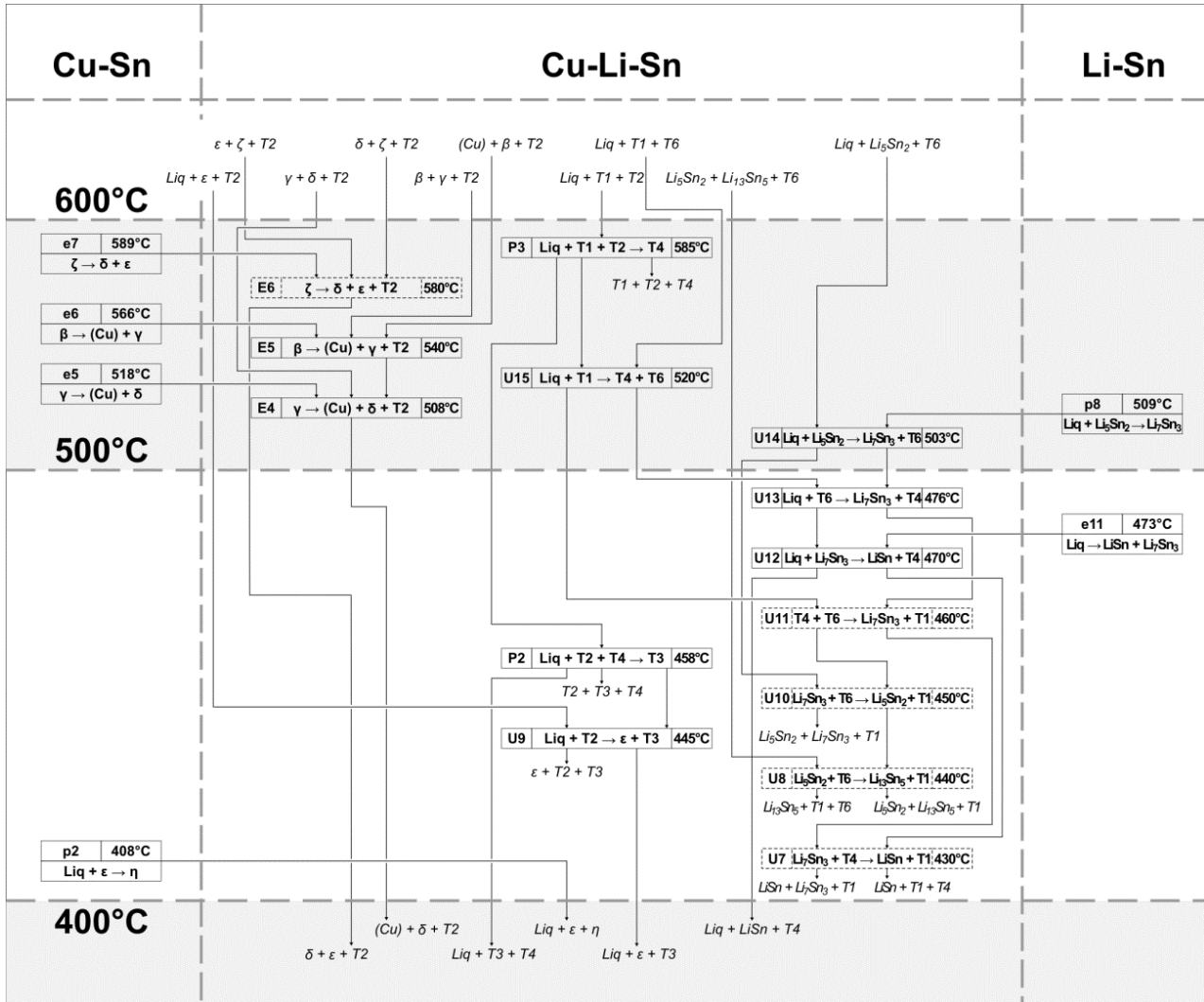
Fig. 13: reaction scheme T = 400 - 600 °C
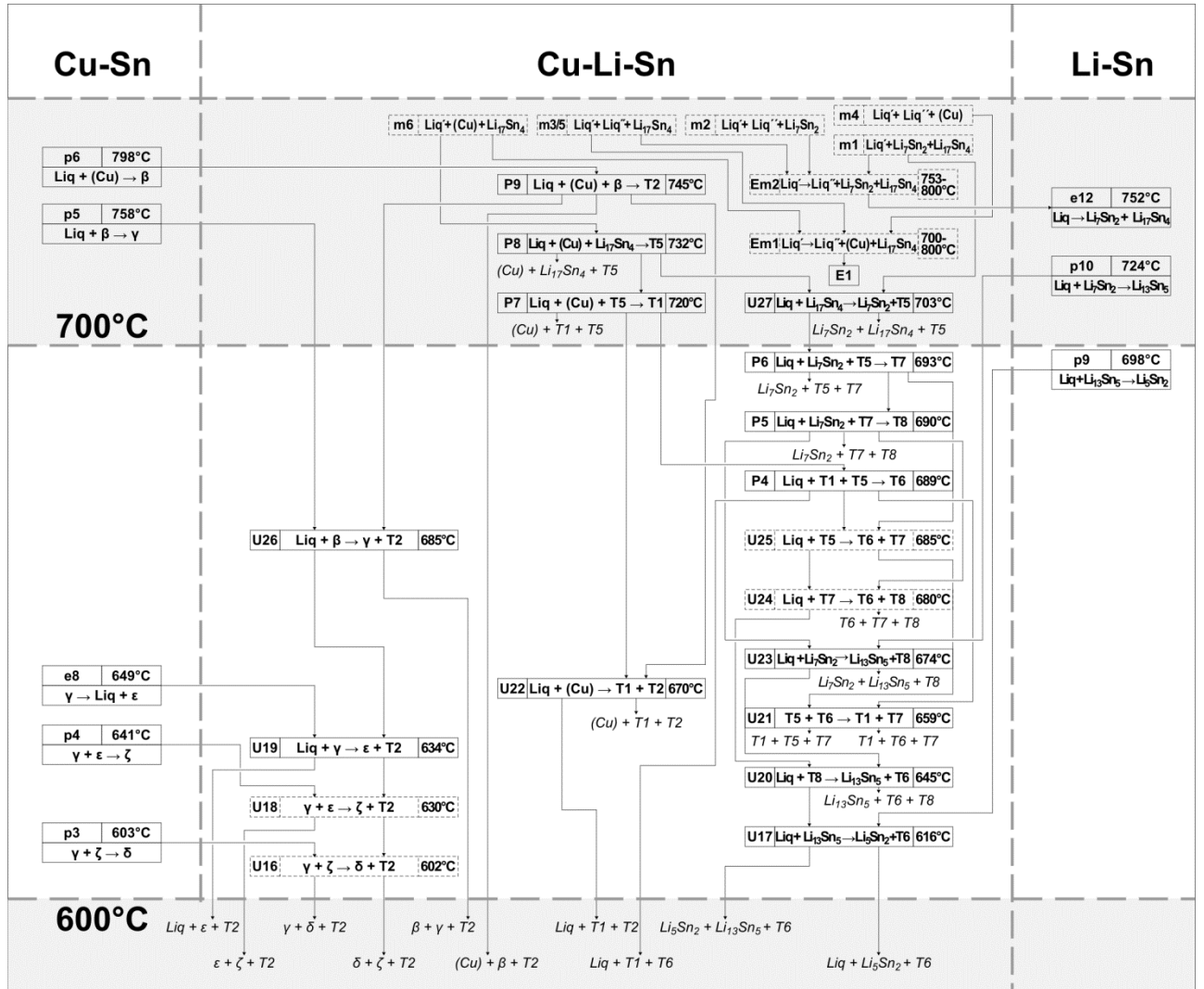
Fig. 14: reaction scheme T > 600 °C

4   Final Conclusions

In the following results from my own experimental work are discussed in detail. Outputs from project cooperation, *e.g.* thermodynamic optimizations or vapour pressure measurements (KEMS), which were achieved solely by our cooperation partners, could be found explicitly in the original publications (see Table 5) and are not part of this discussion.

4.1   Binary systems

4.1.1   Cu-Sn

P-XRD measurements of quenched Cu-Sn samples verified information from literature that the high temperature phases β and γ are not stable at room temperature (publication #9). Moreover, they cannot be quenched but show bulk transformation into the respective LT-phases. For a detailed investigation of phase relations at higher temperature it was necessary to apply HT-PXRD for various samples in the interested phase region. From phase analysis and the trend of lattice parameters a two-phase field involving β and γ could not be verified. Although this was reported already in earlier work [28] most of phase diagram evaluations showed a two-phase field. It was introduced by two authors [28, 29] based on misinterpretation of experimental results and sustained over decades. A higher-order transition between W-type β-phase and BiF_3-type γ-phase was accepted. Depending on temperature and composition, ordering from W- to BiF_3-type compound takes place with increasing tin concentration. Several other reaction temperatures in the Cu-Sn system were slightly revised. These data were used to calculate a self-consistent Cu-Sn phase diagram with a higher-order transformation between W- and BiF_3-structure, based on a four-sublattice model (publication #10).

4.1.2   Cu-Li

Only few and inconsistent literature information was available for Cu-Li. Five Cu-Li samples were prepared and examined with P-XRD and DTA. Results are part of work #16. XRD measurements could neither verify the suggested, but unproved phase Cu_2Li_3 [30] nor the Cu_4Li phase [31]. As a result of additional heat effects in DTA, the thermodynamic description of the calculated Cu-Li phase diagram considers a metastable monotectic reaction, which was also proposed by earlier works [32].

4.1.3 Li-Sn

Publication #11 comprises experimental and theoretical results of the Li-Sn system. Initially this very well investigated system served for the validation of our experimental setup. Our results could reproduce the present literature phase diagram [33] in far extent. 17 samples were prepared and examined with P-XRD and DTA. The phase designation $Li_{22}Sn_5$ [34] was substituted by $Li_{17}Sn_4$ recently derived from neutron diffraction ([35]). Several invariant reaction temperatures were slightly modified. The characters of the invariant reactions involving "Liq + $Li_{17}Sn_4$ + Li_7Sn_2" and "Liq + Li_7Sn_2 + $Li_{13}Sn_5$" were determined by an experimental DTA approach which directly compares alloy samples. The findings were verified by a simulation of the DTA curve. The enthalpy of formation of the phase $Li_{17}Sn_4$ was reinvestigated by solution calorimetry and is in good agreement to the literature data, obtained by EMF measurements [36]. A full assessment of literature and own experimental data leads to a new and self-consistent thermodynamic description of the Li-Sn system. KEMS measurements (publication #12) have been performed on our samples and thermodynamic data obtained were used for the thermodynamic assessment (#11).

4.2 Ternary phases

Before this study was started, the Cu-Li-Sn system comprised two ternary phases (T1 [37-39] and T2 [40]). Both phases could be confirmed and structure determinations based on single crystals are shown in publication #2. During the systematic research in the Cu-Li-Sn system further phases arose: T3, T4 (publication #3, T4 was independently found by Winter et al. [41]), T5 and T6 (publication #4). Crystal structures are listed in Table 6. At least two more ternary phases (T7, T8) occur in the Cu-Li-Sn system – probably at high lithium concentrations and in vicinity to the high-melting intermetallics Li-Sn – but could hitherto not be characterized by SC-XRD.

Besides crystallographic characterization, topological similarities between phases are necessary to understand phase transitions along a composition gradient. Integration of lithium atoms into a crystal lattice potentially forms new intermetallic phases with common structural features; this happens for instance during charging of an anode material. Structural similarities between the various ternary and binary phases in Cu-Li-Sn are shown in Figure 7 and Table 7.

Phase	Stochio-metry	type	Pearson symbol	Space group	No.	a (Å)	b (Å)	c (Å)	β (°)	Ref.
T1	Li_2CuSn	$CuHg_2Ti$	$cF16$	$F\bar{4}3m$	216	6.295	-	-	90	#2
T2	$LiCu_2Sn$	$InPt_2Gd$	$hP8$	$P6_3/mmc$	194	4.3022	-	7.618	90	#2
T3	$Li_3Cu_6Sn_4$	$Li_3Cu_6Sn_4$	$hP13$	$P6/mmm$	191	5.095	-	9.524	90	#3
T4	Li_2CuSn_2	Li_2AuSn_2	$tI20$	$I4_1/amd$	141	4.4281	-	19.416	90	#3
T5	Li_3CuSn	Li_3CuSn	$hP10$	$P6/mmm$	191	4.5769	-	8.461	90	#4
T6	$Li_6Cu_2Sn_3$	$Li_6Cu_2Sn_3$	$hR33$	$R\bar{3}2/m$	166	4.5900	-	30.910	90	#4

Table 6: Investigated ternary phases in Cu-Li-Sn
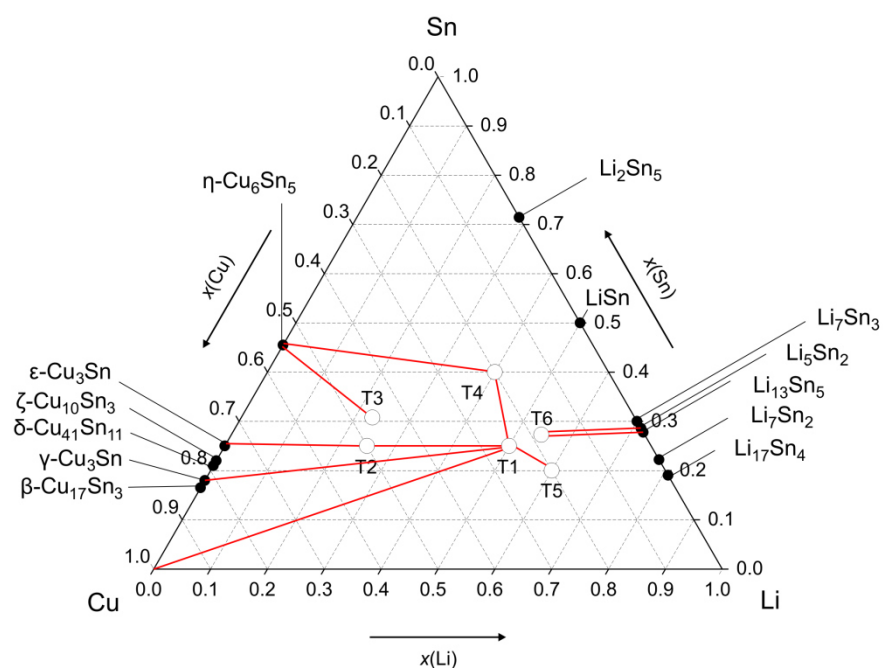
Figure 7: Scheme of structural relationships between phases, composition of phases is stoichiometric

Phase		Structural relationship	Ref.
1	**2**		
(Cu)	T1	fcc (Cu) ($Fm\bar{3}m$): Cu atoms at (0 0 0): T1 phase has eight-fold unit cell, sublattices fcc (Li) (½ ½ ½), fcc (Sn) (¾ ½ ½), fcc (Cu/Li) (½ 0 0), and a corresponding symmetry reduction to $F\bar{4}3m$.	None
γ	T1	Both compounds are based on rock salt structures (γ-phase: Cu- and Sn-atoms; T1 phase: Li- and Sn-atoms), interstitial positions (tetrahedral holes) are filled either with Cu- (γ-phase) or Cu- and mixed Cu/Li-atoms (T1-phase)	#2
ε	T2	Alignment of Cu_2Sn-subunits from ε-phase to hexagonal symmetry and substitution of one Cu- by one Li-atom per formula unit leads to T2-phase	#2
η	T3	Bowl-shaped hexagons form Sn-backbone of η-phase; consecutive shifts of Sn- and Cu-atoms and insertion of Li-atoms result in parallel atom layers (T3-phase)	#3
η	T4	Hexagonal unit cells of η-phase are distorted irregular along in *c*-direction; substitution of Cu- by Li-atoms form T4-phase (tetragonal)	#3
Li_5Sn_2 $Li_{13}Sn_5$	T6	Three kinds of polyhedra form two kinds of layers: distorted octa- and tetrahedra (relation 1:2) form layer A, trigonal prims form layer B. Corners are occupied solely by Sn-atoms, centred atoms are either Li-atoms (binary compounds) or mixed Cu/Li-atoms (T6). Structures differ in the sequence of layers in *c*-direction. Li_5Sn_2 has 6 layers per unit cell (A-B–A-B–A-B), $Li_{13}Sn_5$ constitutes of 5 layers per unit cell (A-B–A-B–A) and T6 has 9 layers per unit cell (A-B-A–A-B-A–A-B-A)	#4
T1	T2	Both phases form honeycomb-shaped structures of Cu- and Sn-atoms: T1 in direction [110], T2 in direction [001]; channels are filled with solely Cu/Li-atoms in T2 (single pile) or with both Li- and Cu/Li-atoms in T1 (two piles, one pile for each kind of atoms).	#2
T1	T4	T1 consists of succeeding layers A (chess pattern Li- and Sn-atoms) and layer B (squared Cu-atoms with face-centred Cu/Li-atoms); T4 consist of layer C (two layers of A with respective shifting of *a*/2) and layer D (layer B with solely squared Cu-atoms).	#3
T1	T5	Different layer sequence in direction [001] for T5 and [111] for T1. Layers A have centred atoms with six vicinal atoms in equal distance; layers B are honeycomb-shaped. T1 has 4 sequencing A layers with …Cu/Li – Li – Cu – Sn…-atoms; T5 has a layer sequence A-B-A-B-A-B with atoms …−Sn−Cu/Li−Cu/Li−Sn−Cu/Li−Cu/Li−…, respectively.	#4

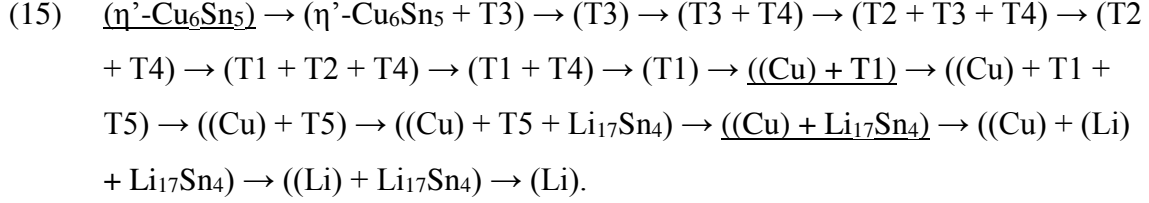**Table 7: List of structural relationships between phases**

4.3 Cu-Li-Sn phase diagram

Publications #5 and #6 are treating the Cu-Li-Sn phase diagram. The first one focuses on four isothermal sections between 300 and 600 °C, which were determined solely by P-XRD technique. The latter one illustrates 9 isopleths, a corresponding liquidus surface, and a Scheil reaction scheme, which has been determined by means of P-XRD and DTA. Besides confirmation of 14 binary compounds in corresponding binary systems, eight additional ternary compounds were found. Structures of six ternary compounds were refined by SC-XRD (see publications #2, #3 and #4). Two ternary compounds (T7 and T8) couldn't yet be structurally characterized, but detected in P-XRD samples. Peritectic formation temperatures of most ternary phases were experimentally determined. The Cu-Li-Sn system consists of 113 three-phase regions, which are linked by 44 ternary reactions. Some reactions were estimated to allow a consistent construction of the Scheil reaction scheme. This concerns the Li-rich corner, reactions related to the high-temperature phases in the Cu-rich corner and low-temperature reactions (< 200 °C). The liquidus projection was constructed based on DTA data of isopleths and corresponding reactions – however, metallographic investigations would be necessary to verify dimensions of primary crystallisation fields. A very special feature of the present phase diagram is a true ternary liquid miscibility gap. It is linked to the metastable miscibility gap in Cu-Li and could be predicted by CALPHAD extrapolations from binary subsystems as shown in publication #16.

Lithium ion batteries with alloy anodes are supposed to operate at temperatures between room temperature and well below 100 °C. To suggest a lithiation path for the most promising anode material η'-Cu_6Sn_5 at room temperature, it has to be estimated from an isothermal section at 300 °C. In the case of Cu_6Sn_5, various authors [5-8] proposed a reaction mechanism, which was found by electrochemical insertion and simultaneous in situ XRD:

(13) $Cu_6Sn_5 + 10\ Li \rightarrow 5\ CuLi_2Sn + (Cu)$

(14) $4\ CuLi_2Sn + 9\ Li \rightarrow Li_{17}Sn_4 + 4\ (Cu)$

This reaction path (see underlined phases in equation (**15**)) is solely based on the thitherto known ternary phases T1 and T2 and can be revised based on our assumptions for low temperature phase relations:

(15) $\underline{(\eta'\text{-}Cu_6Sn_5)} \rightarrow (\eta'\text{-}Cu_6Sn_5 + T3) \rightarrow (T3) \rightarrow (T3 + T4) \rightarrow (T2 + T3 + T4) \rightarrow (T2 + T4) \rightarrow (T1 + T2 + T4) \rightarrow (T1 + T4) \rightarrow (T1) \rightarrow \underline{((Cu) + T1)} \rightarrow ((Cu) + T1 + T5) \rightarrow ((Cu) + T5) \rightarrow ((Cu) + T5 + Li_{17}Sn_4) \rightarrow \underline{((Cu) + Li_{17}Sn_4)} \rightarrow ((Cu) + (Li) + Li_{17}Sn_4) \rightarrow ((Li) + Li_{17}Sn_4) \rightarrow (Li).$

4.4 Calorimetry

Integral enthalpies of mixing at 800 °C (see publication #1) in the Li-Sn system show a minimum at approximately $x_{Sn} = 0.2$. This indicates a strong ordering of the liquid, probably due to formation of Li_4Sn associates. This assumption is supported by the occurrence of several binary compounds in this region (in the solid state at temperatures < 779 °C). Integral mixing enthalpies of the Cu-Li system are predominantly endothermic with weakly negative values at the Cu-rich side.

Experimental and theoretical extrapolation into the ternary system show an exothermic valley along the line $Li_4Sn - Cu_2LiSn$. This is exactly the region where most of the ternary phases occur (T1, T2, T3, T5, T6, T7 and T8).

5   References

1.   Arora, P. and Z.M. Zhang, *Battery separators.* Chemical Reviews, 2004. 104 (10): p. 4419-4462.

2.   Daniel, C., *Materials and processing for lithium-ion batteries.* JOM - The Journal of The Minerals, Metals & Materials Society, 2008. 60 (9): p. 43-48.

3.   Shukla, A.K. and T.P. Kumar, *Materials for next-generation lithium batteries.* Current Science, 2008. 94 (3): p. 314-331.

4.   Whittingham, M.S., *Materials challenges facing electrical energy storage.* MRS Bulletin, 2008. 33 (4): p. 411-419.

5.   Jansen, A., et al., *Variable temperature performance of intermetallic lithium-ion battery anode materials.* Journal of Alloys and Compounds, 2011 (509): p. 4457–4461.

6.   Choi, W., J.Y. Lee, and H.S. Lim, *Electrochemical lithiation reactions of Cu_6Sn_5 and their reaction products.* Electrochemistry Communications, 2004. 6 (8): p. 816-820.

7.   Sharma, S., et al., *A theoretical and experimental study of the lithiation of $\eta´$-Cu_6Sn_5 in a lithium-ion battery.* Journal of the Electrochemical Society, 2003. 150 (3): p. A330-A334.

8.   Kepler, K.D., J.T. Vaughey, and M.M. Thackeray, *$Li_xCu_6Sn_5$ ($0 < x < 13$): An intermetallic insertion electrode for rechargeable lithium batteries.* Electrochemical and Solid State Letters, 1999. 2 (7): p. 307-309.

9.   Seifert, H.J. *Materials with New Design for Improved Lithium Ion Batteries*. May 19th, 2016; Available from: http://www.spp1473.kit.edu.

10.   Spencer, P.J., *A brief history of CALPHAD.* CALPHAD - Computer Coupling of Phase Diagrams and Thermochemistry, 2008. 32 (1): p. 1-8.

11.   Effenberg, G. May 19th, 2016; Available from: http://www.msiport.com/msi-eureka/products/all-element-systems-abbreviated.html.

12.   Bruker-AXS, *Topas*. 1999 / 2000: Billerica / MA.

13.   Wilson, A.J.C., ed. *International Tables for Crystallography*. ed. A.J.C. Wilson. 1992, Kluwer: Dordrecht / NL.

14.   Otwinowski, Z. and W. Minor, *Processing of X-ray diffraction data collected in oscillation mode.* Macromolecular Crystallography, A, 1997. 276: p. 307-326.

15.   Nonius, B.V., *Collect - Data Collection Software*. 1999: Delft / Netherlands.

16.   Sheldrick, G.M., *A short history of SHELX.* Acta Crystallographica Section A, 2008. 64: p. 112-122.

17.   Sheldrick, G.M., *SHELXS 97 - A Program for the Solution of Crystal Structures*, in *University of Göttingen*. 1997: Göttingen.

18.   Sheldrick, G.M., *SHELXL 97 - A Program for Crystal Structure Refinement*, in *University of Göttingen*. 1997: Göttingen.

19.   Dowty, E., *Atoms - A Computer Program for Displaying Atomic Structures*. 2004, Shape Software: Kingsport / TN.

20.   Proteus, *NETZSCH Proteus® Software for Thermal Analysis*. 2011, NETZSCH-Gerätebau GmbH: Selb / Germany.

21.   Calisto, *Calisto Processing ®*. 2011, AKTS - Advanced Kinetics and Technology Solutions: Siders / Switzerland.

22.   Campell, F.C., ed. *Phase Diagrams: Understanding the Basics*. Phase Diagrams: Understanding the Basics. 2012, ASM International. 1-462.

23.   Rhines, F.N., *Phase diagrams in metallurgy - their development and application*. 1956, New York: McGraw-Hill Book Company, Inc.

24. Palatnik, L.S. and A.I. Landau, *Phase Equilibria in Multicomponent Systems*. 1964, New York: Holt, Rinehart & Co.

25. Dinsdale, A., *Thermodynamic data of Unaries*. 2010.

26. Chou, K.C., *A General-Solution Model for Predicting Ternary Thermodynamic Properties.* Calphad-Computer Coupling of Phase Diagrams and Thermochemistry, 1995. 19 (3): p. 315-325.

27. Chou, K.C., et al., *Formalism of new ternary model expressed in terms of binary regular-solution type parameters.* Calphad-Computer Coupling of Phase Diagrams and Thermochemistry, 1996. 20 (4): p. 395-406.

28. Shepherd, E.S. and E. Blough, *The constitution of the copper-tin alloys.* Journal of Physical Chemistry, 1906. 10 (8): p. 630-653.

29. Hoyt, S.L., *On the copper-rich kalchoids (copper-tin-zinc alloys).* Journal of the Institute of Metals, 1913. 10: p. 235-274.

30. Gąsior, W., et al., *Thermodynamic evaluation of Cu-Li phase diagram from EMF measurements and DTA study.* CALPHAD - Computer Coupling of Phase Diagrams and Thermochemistry, 2009. 33 (1): p. 215-220.

31. Old, C.F. and P. Trevena, *Reaction in Copper-Lithium System and Its Implications for Liquid-Metal Embrittlement.* Metal Science, 1981. 15 (7): p. 281-285.

32. Pelton, A.D., *The Cu-Li (Copper-Lithium) system.* Bulletin of Alloy Phase Diagrams, 1986. 7 (2): p. 142-144.

33. Sangster, J. and C.W. Bale, *The Li-Sn (Lithium-Tin) system.* Journal of Phase Equilibria, 1998. 19 (1): p. 70-75.

34. Gladyshevskii, E.I., G.I. Oleksiv, and P.I. Kripyakevich, *New examples of the structural type $Li_{22}Pb_5$.* Soviet Physics, Crystallography (= Kristallografiya), 1964. 9 (3): p. 269-271.

35.   Lupu, C., et al., *X-ray and neutron diffraction studies on "Li$_{4.4}$Sn".* Inorganic Chemistry 2003. 42 (12): p. 3765-3771.

36.   Wen, C.J. and R.A. Huggins, *Thermodynamic study of the Lithium-Tin system.* Journal of the Electrochemical Society, 1981. 128 (6): p. 1181-1187.

37.   Schuster, H.U., D. Thiedemann, and H. Schönemann, *Ternary lithium compounds with formulas of LiMe$_2$X and Li$_2$MeX (Me = Cu, Ag or Au; X = Si, Ge or Sn).* Zeitschrift für Anorganische und Allgemeine Chemie, 1969. 370 (3-4): p. 160-170.

38.   Pauly, H., A. Weiss, and H. Witte, *Crystal structure of ternary intermetallic phases Li$_2$EX (E = Cu, Ag, Au; X = Al, Ga, In, Tl, Si, Ge, Sn, Pb, Sb, Bi).* Zeitschrift für Metallkunde, 1968. 59 (1): p. 47-58.

39.   Schuster, H.U., *Ternäre Lithium-Verbindungen mit Elementen der 4. Hauptgruppe.* Die Naturwissenschaften, 1966. 53 (14): p. 360-361.

40.   Kripyakevich, P.I. and G.I. Oleksiv, *Crystal structure of the compound LiCu$_2$Sn.* Dopovidi Akademiï Nauk Ukraïns'koï RSR, 1970. A (1): p. 63-65.

41.   Winter, F., et al., *Lithium mobility in the stannides Li$_2$CuSn$_2$ and Li$_2$AgSn$_2$.* Zeitschrift für Anorganische und Allgemeine Chemie, 2013. 639 (15): p. 2790-2795.

6 Appendices

6.1 List of figures

6.2 List of tables

6.3 List of equations

6.4 Abbreviations

6.4.1 Authors

Ben	Laszlo Bence
Cup	Damian Cupid
Eff	Herta Silvia Effenberger
Elm	Aicha Elmahfoudi
Fla	Hans Flandorfer
Fra	Peter Franke
Hen	David Henriques
Ips	Herbert Ipser
Li	Dajian Li
Mar	Torsten Markus
Mot	Vladimir Motalov
Ple	Yuriy Plevachuk
Sab	Aziz Sabbar
Tse	Erdenebat Tserenjav
Yak	Andriy Yakymovych

6.4.2 Journals

CALPHAD	CALPHAD
Intermet.	Intermetallics
JALCOM	Journal of Alloys and Compounds
JCT	Journal of Chemical Thermodynamics
JPED	Journal of Phase Equilibria and Diffusion
JSSC	Journal of Solid State Chemistry
MHC	Monatshefte für Chemie
TA	Thermochimica Acta
Zkrist.	Zeitschrift für Kristallographie
Plos One	Plos One

6.4.3 Methods

CALPHAD	Calculation of phase diagrams
DTA	Differential thermal analysis
DSC	Differential scanning calorimetry
EDX	Energy dispersive X-ray spectroscopy
EMF	Electromotive force
HT-PXRD	High temperature powder X-ray diffraction
KEMS	Knudsen effusion mass spectrometry
P-XRD / PXRD	Powder X-ray diffraction
SC-XRD	Single crystal X-ray diffraction
SEM	Secondary electron microscopy

6.4.1 Other abbreviations

LT / HT	Low temperature / high temperature
fcc	Face centred cubic
bcc	Body centred cubic
d	days
m	months
DFG	Deutsche Forschungsgemeinschaft (German Science Fund)
FWF	Fonds wissenschaftlicher Forschung (Austrian Science Fund)

6.5   Scientific contributions

6.5.1   Articles in peer-reviewed journals

#1)   S. Fürtauer, E. Tserenjav, A. Yakymovych, H. Flandorfer, Calorimetric studies of Li-Sn, Cu-Li and Cu-Li-Sn, Journal of Chemical Thermodynamics, 61 (2013) 105-116.

#2)   S. Fürtauer, H. Effenberger, H. Flandorfer. $CuLi_2Sn$ and Cu_2LiSn: Characterization by single crystal XRD and structural discussion towards new anode materials for Li-ion batteries. Journal of Solid State Chemistry, 220 (2014), 198-205.

#3)   S. Fürtauer, H. Effenberger, H. Flandorfer. The tin-rich copper lithium stannides: $Li_3Cu_6Sn_4$ and Li_2CuSn_2. Zeitschrift für Kristallographie – Crystalline Materials, 230 (2015) 97-105.

#4)   S. Fürtauer, H. Effenberger, H. Flandorfer (2015). New intermetallic phases in the Cu-Li-Sn system: The lithium rich phases $CuLi_3Sn$ and $Cu_2Li_6Sn_3$. Zeitschrift für Kristallographie – Crystalline Materials, 231 (2016) 79-87.

#5)   S. Fürtauer, H. Flandorfer (2016). The Cu-Li-Sn phase diagram: Isothermal sections. Journal of Alloys and Compounds, 682 (2016) 713-722.

#6)   S. Fürtauer, H. Flandorfer (2016). The Cu-Li-Sn phase diagram: Isopleths, liquidus projection and reaction scheme. Plos One. *Submitted.*

#7)   A. Elmahfoudi, S. Fürtauer, A. Sabbar, H. Flandorfer, Enthalpy of mixing of liquid systems for lead free soldering: Ni-Sb-Sn system, Thermochimica Acta, 534 (2012) 33-40.

#8)   S. Fürtauer, H. Flandorfer, A new experimental phase diagram investigation of Cu-Sb, Monatshefte für Chemie - Chemical Monthly, 143 (2012) 1275-1287.

#9)   S. Fürtauer, D. Li, D. Cupid, H. Flandorfer, The Cu-Sn phase diagram, Part I: New experimental results, Intermetallics, 34 (2013) 142-147.

#10)   D. Li, P. Franke, <u>S. Fürtauer</u>, D. Cupid, H. Flandorfer, The Cu-Sn phase diagram part II: New thermodynamic assessment, Intermetallics, 34 (2013) 148-158.

#11)   D. Li, <u>S. Fürtauer</u>, H. Flandorfer, D. Cupid. Thermodynamic assessment and experimental investigation of the Li-Sn system. CALPHAD, 47 (2014) 181-195.

#12)   D. Henriques, V. Motalov, L. Bencze, <u>S. Fürtauer</u>, T. Markus. Experimental Thermodynamics of the Li-Sn System by Knudsen Effusion Mass Spectrometry. Journal of Alloys and Compounds, 585 (2014), 299-306.

#13)   Y. Plevachuk, A. Yakymovych, <u>S. Fürtauer</u>, H. Ipser, H. Flandorfer, The Enthalpies of Mixing of Liquid Ni-Sn-Zn Alloys, Journal of Phase Equilibria and Diffusion, 35 (2014) 359-368

#14)   A. Yakymovych, <u>S. Fürtauer</u>, A. Elmahfoudi, H. Ipser, H. Flandorfer, Enthalpy of mixing of liquid Co-Sn alloys. The Journal of Chemical Thermodynamics (2014).

#15)   A. Yakymovych, <u>S. Fürtauer</u>, H. Flandorfer, H. Ipser. Enthalpies of mixing of liquid ternary Co-Li-Sn alloys. Monatshefte für Chemie - Chemical Monthly, 145 (2014) 1697-1706.

#16)   D. Li, <u>S. Fürtauer</u>, H. Flandorfer, D. Cupid. Thermodynamic Assessment of the Cu-Li System and Prediction of Enthalpy of Mixing of Cu-Li-Sn Liquid Alloys: CALPHAD, 53 (2016) 105-115.

#17)   D. Henriques, V. Motalov, L. Bencze, <u>S. Fürtauer</u>, H. Flandorfer, T. Markus. Experimental thermodynamic study of the Cu-Li-Sn System by Knudsen Effusion Mass Spectrometry. Journal of Alloys and Compounds, 687 (2016) 306-311.

6.5.2 Conference presentations

Following conference presentations were held by Siegfried Fürtauer:

(1)   <u>S. Fürtauer</u>, H. Flandorfer, H. Ipser, C. Lengauer. Investigation on the high-temperature-phases of Cu-Sn and Cu-Sb (2010). TOFA 2010 Discussion Meeting on Thermodynamics of Alloys: Porto / Portugal.

(2)   <u>S. Fürtauer</u>, H. Flandorfer. New experimental investigation on Cu-Li-Sn and the constituent binary systems (2012). 26th International Seminar on Heterogeneous Multicomponent Equilibria: Ringberg castle / Germany.

(3)   <u>S. Fürtauer</u>, H. Flandorfer. Thermodynamische Untersuchung von Cu-Li-Sn für neue LIB-Anodenmaterialien (2012). 7. Workshop für Anorganische Chemie in Österreich (WACÖ). Innsbruck / Austria.

(4)   <u>S. Fürtauer</u>, H. Flandorfer. Progress in the investigation of Cu-Li-Sn and the binary constituent systems (2013). 27th International Seminar on Heterogeneous Multicomponent Equilibria: Ringberg castle / Germany.

(5)   <u>S. Fürtauer</u>, H. Flandorfer. Investigation of the Cu-Li-Sn system and the binary constituent systems (2013). TMS 2013 142nd Annual Meeting & Exhibition: San Antonio / USA.

(6)   <u>S. Fürtauer</u>, H. Flandorfer. The Cu-Li-Sn system as new intermetallic anode material for lithium ion batteries (2013). EUROMAT 2013 / European Congress and Exhibition on Advanced Materials and Processes: Sevilla / Spain.

(7)   <u>S. Fürtauer</u>, H. Flandorfer. The Cu-Li-Sn system as new intermetallic anode material for lithium ion batteries (2013). GÖCH Chemietage, Graz / Austria.

(8)   <u>S. Fürtauer</u>, H. Flandorfer. The system Cu-Li-Sn: Phase diagram and thermochemistry (2014). TMS 2014 143rd Annual Meeting & Exhibition: San Diego / USA.

(9)   <u>S. Fürtauer,</u> H. Flandorfer. The Cu-Li-Sn system as promising material for Lithium Ion Batteries (2014). 8. Workshop für Anorganische Chemie in Österreich (WACÖ). Salzburg / Austria.

(10) <u>S. Fürtauer,</u> H. S. Effenberger, H. Flandorfer. Structural features of Cu-Sn, Li-Sn and Cu-Li-Sn alloys: Insertion and transport of lithium (2016). 30th International Seminar on Heterogeneous Multicomponent Equilibria: Ringberg castle / Germany.

6.5.3 Conference posters

Following conference posters were presented by Siegfried Fürtauer:

(1)   <u>S. Fürtauer,</u> H. Flandorfer, H. Ipser. New calorimetric and phase diagram investigations of Cu-Sn (2011). 19. Ulm-Freiberger Kalorimetrietage: Freiberg / Germany.

(2)   <u>S. Fürtauer,</u> H. Flandorfer, H. Ipser. Fachdidaktik Chemie: Fortbildung und Öffentlichkeitsarbeit (2011). 11. Europäischer Chemielehrer/-innenkongress: Klagenfurt / Austria.

(3)   <u>S. Fürtauer,</u> H. Flandorfer, H. Ipser. Phase diagram investigations of Cu-Sn and Cu-Sb (2011). COST MP0602 final meeting: Brno / Czech Republic.

(4)   <u>S. Fürtauer,</u> H. Flandorfer, E. Tserenjav. Investigation of the phase relations in Cu-Li-Sn and the binary constituent systems (2011). EUROMAT 2011 / European Congress and Exhibition on Advanced Materials and Processes: Montpellier / France.

(5)   <u>S. Fürtauer,</u> H. Flandorfer, E. Tserenjav. Investigation of the phase relations in Cu-Li-Sn and the binary constituent systems (2011). GÖCH Chemietage, Linz / Austria.

(6)   S. Fürtauer, H. Flandorfer, E. Tserenjav. Investigation of the phase relations in Cu-Li-Sn and the binary constituent systems (2011). Summer School of the DFG Priority Programme SPP 1473, WeNDeLIB, Marktheidenfeld / Germany.

(7)   S. Fürtauer, H. Flandorfer. Progress in the investigation of Cu-Li-Sn and the binary constituent systems (2012). MSE Materials Science Engineering, Darmstadt / Germany.

(8)   S. Fürtauer, H. Flandorfer. New intermetallic anode materials: Prospects of the Cu-Li-Sn system (2014). TOFA 2014 Discussion Meeting on Thermodynamics of Alloys: Brno / Czech Republic.

(9)   S. Fürtauer, H. Flandorfer. The Cu-Li-Sn system (2015). ECSSC 15: Vienna / Austria.

(10)   S. Fürtauer, H. Flandorfer. The Cu-Li-Sn system (2015). GÖCH Chemietage: Innsbruck / Austria.

6.5.4 Reviews

Siegfried Fürtauer is frequent reviewer of following peer-reviewed Journals:

(1) Journal of Phase Equilibria and Diffusion
(2) Thermochimica Acta
(3) Physica B
(4) Journal of Alloys and Compounds

6.5.5 Miscellaneous

(5) S. Fürtauer. Investigation of relevant phase diagrams for high temperature solder materials: The binary systems Cu-Sn and Cu-Sb (2010). Master Thesis: University of Vienna.

(6) S. Fürtauer, D. Li, D. Henriques, H. Flandorfer. Assessment of Cu-Sn & Cu-Li-Sn for the MSIT database (2012, 2013 and 2016). 26th, 27th and 30th International Seminar on Heterogeneous Multicomponent Equilibria: Ringberg castle/ Germany.

(7) Participation in the WenDeLIB summer schools in Marktheidenfeld / Germany (2011) and Romrod - Alsfeld / Germany (2012).

(8) Participation in the 63rd Lindau Nobel Laureate Meeting (2013) in Lindau / Germany.

(9) Front cover illustration (crystal structure $Li_3Cu_6Sn_4$) in: Zeitschrift für Kristallographie – Crystalline Materials, 230 (2015).

6.6 Epilogue

The present work pays attention to a ternary materials system, Cu-Li-Sn, because its alloys could be interesting for application as lithium storage materials in lithium ion batteries. Challenging, but also very interesting, was the handling of lithium and the preparation of the alloys. Although experience concerning delicate materials and special preparation techniques was available at begin of my studies, the knowledge on how to work with lithium and its alloys was very scarce in our working group. I started with the revision of the binary subsystems Li-Sn and Cu-Li (Cu-Sn was conveniently part of my master thesis), and used that systems as a playground for learning how lithium containing alloys behave and how they could be characterized. Li-Sn is one of the few very well-known lithium intermetallic systems and thus served as a reference for the validation of our methods. It turned out that sample preparation, XRD and DTA analysis could be applied with some restrictions, but a compositional characterization of phases with phase selective spectroscopic methods, like SEM-EDX, was not possible due to the nature of lithium. After the first year I met Prof. Huggins from Stanford, who is an expert in electrochemistry, at the WeNDeLIB summer school 2011 in Marktheidenfeld. He gave a talk about an electrochemical method to determine phase triangulations, the coulometric titration, which was elegant and powerful. The experimental setup seemed to be very simple and is based on an electrochemical deposition of lithium onto a target alloy with succeeding monitoring of the electrochemical potential towards a reference electrode. Each time a new phase forms by lithium insertion, the potential changes in a defined step, which could be used to construct a phase diagram section and allows conclusion on phase stabilities and homogeneity ranges. Nice by-products are electrochemical potentials, which are in direct relation to Gibbs energies, which are very useful for thermodynamic assessments. So, at that time we decided to focus the investigations on coulometric titrations of the ternary Cu-Li-Sn system. However, it turned out very soon that a reliable measurement of electrochemical potentials under the above mentioned conditions is difficult! At a first glance the method seems to be quite simple. However, the respective publications show only a final EMF / x_{Li} curve which cannot be directly measured but constructed from various runs. One should know that measurements are performed at several hundred degrees Celsius, in inert gas atmosphere, with liquid and totally water-free salt melts, and of course with very corrosive and volatile lithium. Lithium attacks ceramic or glassy parts, which have to be used for electric insulation, or, and this is most frustrating, migrates into the melt and foils our idea of electrochemical deposition. After

the application of a current signal the system needs up to several hours until a stable equilibrium signal is established. Several for- and backward titrations are necessary to unambiguously determine the phase boundary concentrations. All these requirements are responsible that successful titrations need elaborate preparations and are very time consuming. I have established electronics and software for control and data acquisition based on National Instruments devices and LabView graphical program suite. As it turned out that successful and reliable measurements in the ternary system need incalculable amount of time I skipped my plans to obsess this method. Instead of I promoted the classic investigation of the phase diagram by XRD and DTA parallel to the coulometric titration project. Interestingly, I found rather quickly several new, unidentified phases. This nice feature was definitely an enrichment of this work! We launched cooperation with Prof. Effenberger of the Institute of Mineralogy and Crystallography in Vienna, and she helped me a lot in depicting single crystals and characterizing the crystal structures of the new phases. In total we examined 6 new ternary phases in addition to the two literature phases which have not been topic of single crystal investigations yet. Two of the new phases are still not characterized because they couldn't be synthesize in sufficient quality. The crystal structure descriptions account for three publications, which constitute a major part of this thesis. After having collected a bundle of XRD and DTA data from many alloy samples, it was possible to evaluate the data set and construct a self-consistent and most probable phase diagram. This took me more than a year of hard brain work – some sketches had to be adapted more than 20 times in an iterative process until most discrepancies were erased. Another approach in phase diagram description would be a direct calculation from an optimized data set based on thermochemical experiments. Obtaining these data is difficult – in many cases they have to be approximated over a wide temperature and concentration range. To support these efforts I have measured enthalpies of mixing at various temperatures in the binary subsystems and the ternary system, as well as enthalpies of formation of intermetallic compounds. Further work will show, if the calculated phase diagram based on thermochemical data fits well with the purely experimental phase diagram, what would be great – but this is another topic and not part of this thesis.

6.7 Abstract (English)

This work is an experimental investigation on the ternary Cu-Li-Sn system and the binary subsystems Cu-Sn, Cu-Li and Li-Sn. It was done within the framework of the DFG priority program "WeNDeLIB" (Materials for the New Design of Li-Ion Batteries). The ternary alloys are interesting materials for improved Li-ion batteries, which could be used for high-power applications as stationary energy storage systems or electro mobility. Despite some lithiation experiments have been already performed with these materials by various authors, the phase relations, particularly the phase diagram, was widely unknown. However, for the design of new Li-ion batteries based on computational methods thermodynamic data for the respective material systems are indispensable.

For this work more than 140 samples from the ternary and constituent binary systems were prepared, annealed at different temperatures and quenched. The phase relations were examined with powder XRD, the reaction and transformation temperatures have been determined by DTA techniques. High-temperature powder XRD was employed to verify the transformations between the non-quenchable high temperature phases of the Cu-Sn system. All binary phase diagrams have been essentially improved and missing phase diagram data was completed.

The complete ternary system was newly investigated, because very scarce literature data was available. In addition to the two known ternary phases, six further ones were identified by powder XRD in which the crystal structures of four phases could be described doing single-crystal XRD. Major phase fields were located by powder XRD, isotherms at 300 °C, 400 °C, 500 °C and 600 °C were established. DTA of all samples together with XRD results revealed a most probable version of the ternary Cu-Li-Sn phase diagram, which is described by nine isopleths, a liquidus surface projection and a corresponding Scheil reaction scheme.

Mixing enthalpies at 500 and 800 °C were measured in the systems Cu-Li, Li-Sn and Cu-Li-Sn by drop calorimetry.

All our results will mandatorily contribute to a high quality thermodynamic assessment of the Cu-Li-Sn system which gives access to the calculation and estimation of various materials properties.

6.8 Abstract (German)

Die vorliegende Arbeit stellt eine experimentelle Untersuchung des ternären Systems Cu-Li-Sn und den zugehörigen binären Randsystemen Cu-Sn, Cu-Li und Li-Sn dar. Sie wurde im Rahmen des Schwerpunktprogrammes "WeNDeLIB" (Werkstoffe mit neuem Design für verbesserte Lithium-Ionen-Batterien) durchgeführt. Die ternären Legierungen sind potentielle Materialien für verbesserte Li-Ionen Akkus, die für Hochenergieanwendungen wie stationäre Energiespeicher oder Elektrofahrzeuge geeignet sind.

Obwohl es diesbezüglich bereits einige wenige konkrete Untersuchungen gab, sind die genauen Phasenverhältnisse, die die Ein- und Auslagerung von Lithium bedingen, noch unzureichend erforscht. Im Speziellen betrifft dies die genaue Kenntnis des Phasendiagramms. Für ein zielgerichtetes Design von verbesserten Li-Ionen Akkus mittels computerunterstützten Verfahren ist eine genaue Kenntnis der thermodynamischen Eigenschaften der zugehörigen Materialsysteme unabdingbar.

In dieser experimentellen Arbeit wurden über 140 binäre und ternäre Legierungsproben hergestellt, bei verschiedenen Temperaturen getempert und anschließend abgeschreckt. Die Phasenverhältnisse wurden mittels Pulverröntgendiffraktometrie untersucht, die Reaktions- und Umwandlungstemperaturen erschlossen sich aus der Differenzthermoanalyse. An gepulverten Cu-Sn Legierungen wurden zusätzlich Hochtemperaturuntersuchungen mittels Röntgendiffraktometrie durchgeführt. Daraus ergaben sich Überlegungen zum Umwandlungsmechanismus der beiden Hochtemperaturphasen, welche aus abgeschreckten Proben nicht isolierbar waren. Alle erwähnten binären Phasendiagramme wurden eingehend überprüft und bisher fehlende experimentelle Informationen ergänzt.

Das komplette ternäre System wurde neu untersucht, da kaum Literatur zu diesem System verfügbar war. Zusätzlich zu den zwei bekannten ternären Phasen wurden sechs weitere mittels Pulverröntgendiffraktometrie entdeckt, die Kristallstrukturen von vier davon konnten mittels Einkristalldaten aufgeklärt werden. Die wichtigsten Phasenfelder im System Cu-Li-Sn wurden mittels Pulverröntgendaten lokalisiert, des Weiteren wurden isotherme Schnitte bei 300 °C, 400 °C, 500 °C und 600 °C beschrieben. Durch Thermoanalyse von allen Proben und Interpretation der aufgetretenen Temperatureffekte, in Kombination mit der Kenntnis der Röntgenstrukturdaten, konnte eine weitgehend vollständige Beschreibung des Phasendiagramms erzielt werden. Dieses wurde in neun

weiteren vertikalen Schnitten, einer Projektion der Schmelzoberfläche sowie eines Reaktionsschemas nach Scheil dargestellt.

Des Weiteren wurden molare Mischungsenthalpien bei 500 und 800 °C von den Systemen Cu-Li, Li-Sn und Cu-Li-Sn mittels Einwurfkalorimetrie gemessen.

Alle diese Ergebnisse sind Ausgangspunkt für eine qualitativ hochwertige thermodynamische Beschreibung des Legierungssystems Cu-Li-Sn und tragen einen wesentlichen Teil dazu bei, dessen Materialeigenschaften berechnen und abschätzen zu können.